Division of Plant and Crop Sciences, School of Biosciences

EVALUATING WHEAT FOR GENETIC VARIATION IN RADIATION USE EFFICIENCY: SCALING TRAITS FROM LEAVES TO CANOPIES

CARLOS ALFREDO ROBLES ZAZUETA

BSc (Hons) Environmental Science Engineering, Instituto Tecnologico de Sonora

MSc Biosciences, Universidad de Sonora

Thesis submitted to the University of Nottingham for the degree of Doctor of Philosophy

February 2022

Abstract

Wheat yields are stagnating or declining in many regions of the planet, requiring efforts to improve the light conversion efficiency, i.e., radiation use efficiency (RUE). RUE is a key trait in plant physiology because it links light capture and primary metabolism with biomass accumulation and yield. High-throughput phenotyping (HTP) was used among a population of field grown wheat with variation in RUE and photosynthetic traits to build predictive models of RUE, biomass and intercepted photosynthetically active radiation (IPAR). The use of remote sensing models predicted RUE with up to 70% accuracy compared to ground truth data. Wheat yield can be defined as the product of solar radiation intercepted throughout the crop cycle, radiation use efficiency and harvest index. Photosynthesis is a central component of RUE but normally measured in the upper layers of the canopy where light conditions are saturating. Significant relationships were found between light saturated photosynthetic rates measured at initiation of booting in the top, middle and bottom layers of the canopy and yield. These findings indicate that there is an opportunity for yield improvement if we consider the requirements of photosynthesis in the middle and bottom layers of wheat canopies where conditions are not light saturating. The study of photosynthesis in the field is constrained by low throughput and lack of integrative measurements at canopy level. Partial least squares regression (PLSR) modelling was used to build predictive models of photosynthetic, biophysical and biochemical traits at the top, middle and bottom layers of wheat canopies. The combined layer model predictions performed better than individual layer predictions. Using HTP allowed us to increase phenotyping capacity 30-fold compared to conventional phenotyping methods and our models can be used to screen varieties for high and low RUE. There is clear consensus in the physiological and breeding communities that improving RUE will be key to boost wheat yield. In the previous years of RUE research little has been explored on the role of root biomass accumulation and its interaction with aboveground biomass accumulation, RUE and yield. Strong positive associations were found between above and belowground biomass accumulation with RUE and root biomass during the vegetative period, and negative

associations between yield components and root biomass accumulation, suggesting there is a coordination between roots and shoot in the vegetative period to maximize growth. However, if too much energy is invested in root biomass this will have an effect in decreasing aboveground biomass during grain filling. More research will be needed to explore new hypothesis in the field that accounts the effect of root biomass in canopy RUE and yield.

Publications

1.- **Robles-Zazueta CA**, Molero G, Pinto F, Foulkes MJ, Reynolds MP, Murchie EH. 2021. Field-based remote sensing models predict radiation use efficiency in wheat. *Journal of Experimental Botany*, 72(10): 3756-3773.

2.- Gibbs JA, McAusland L, **Robles-Zazueta CA,** Murchie EH and Burgess AJ. 2021. A deep learning method for fully automatic stomatal morphometry and maximal conductance estimation. *Frontiers in Plant Science,* 12, 780180.

3.- **Robles-Zazueta CA**, Pinto F, Molero G, Foulkes MJ, Reynolds MP, Murchie EH. 2022. Prediction of photosynthetic, biophysical and biochemical traits in wheat canopies to reduce the phenotyping bottleneck. *Frontiers in Plant Science*, 13, 828451.

Acknowledgments

Table of contents

List of figures

List of tables

Chapter 1 Introduction

1.1 Crop yield threatened by climate change

Crop yield and productivity must increase at least at a rate of 2.4% yearly by 2050 to ensure food security for a population that is growing exponentially and avoid famine in developing countries (Tilman et al., 2011). This will not be an easy task, considering that the International Panel on Climate Change (IPCC) has predicted increases in temperature and extreme events such as heat shocks, fires, formation of more powerful storms and hurricanes and the alteration of precipitation patterns (IPCC, 2014). This will disrupt biogeochemical cycles as previously has been shown for carbon (Reichstein et al., 2013), nitrogen (Galloway et al., 2008) and water cycles (Trenberth et al., 2014).

This disruption of biogeochemical cycles will alter climate patterns, contribute to soil erosion and desertification increasing biotic and abiotic stresses for crops (Xu, 2016). In addition, CO_2 concentration in the atmosphere is increasing at a rate of ~2 ppm $year^{-1}$ and previous studies have suggested that elevated CO_2 concentrations could have the potential to offset environmental stresses through increases in photosynthesis and reduction of transpiration (Ainsworth and Long, 2021; Jägermeyr et al., 2021; Leary et al., 2015; Long et al., 2004). These results need further review as recent studies have indicated that beneficial effects of CO_2 enhancement will be substantially lowered by physiological constraints associated with temperature increases, and there is also a need to increase the extent of this type of experiment under field conditions (Ainsworth et al., 2008; Keenan et al., 2021; Kimball, 2016; Long et al., 2006).

In addition to other factors these changes in climate will result in thermally driven shorter crop cycles, an acceleration of crop development and earlier planting dates which together will cause

a reduction in the total amount of light intercepted by the crop over its life cycle, and in consequence gas exchange and furthermore yield reduction (DaMatta et al., 2010; Driedonks et al., 2016; Kromdijk and Long, 2016). This will have socio-economic repercussions worldwide but most notoriously in developing countries in which the main areas of production of staple crops (wheat, maize and rice) are located (Rajaram et al., 1993).

Wheat (*Triticum aestivum* L.) is one of the 10 most important staple crops in terms of cultivated land and total tonnes of food produced yearly (Table 1.1). Its annual production is estimated in ~765 million tons year^{-1} (FAO, 2021) and provides one fifth of total calories consumed by world population (Reynolds et al., 2012). In the past 50 years, wheat has had a considerable increase in yield, in part because of the Green Revolution where field management practices improved, farmers had access to more technology and breeding took a key role in crop sciences (Richards, 2000). Wheat genotypes developed during the Green Revolution have had an annual increase of ~1% under yield potential conditions and ~3% in stressful environments (Reynolds and Borlaug, 2006).

Table 1.1. First ten crops in terms of global cultivated land. Presented is the average yield and yearly global production. Data are results of 2019 from the Food and Agriculture Organization from the United Nations (FAO) database.

Crop	Cultivated land (km^2)	Average yield (ton ha^{-1})	Global production (M ton year^{-1})
Wheat	2159020	3.55	765.77
Maize	1972043	5.82	1148.5
Rice	1620559	4.66	755.47
Soybean	1205016	2.77	333.67
Barley	511499	31.08	158.98
Sorghum	400747	14.45	57.9
Cotton	386406	21.37	82.59
Canola	340309	20.72	70.51
Bean	330662	8.74	28.9
Millet	316539	8.96	28.37

1.2 Wheat yield progress

Post-Green Revolution gains for wheat are now estimated to be between 0.5%-0.8% year^{-1} (Figure 1.1) but the trend is towards stagnation and, in some cases, already decreasing yields in grain weight per hectare (Valluru et al., 2015). Previous modelling studies of climate change conditions predict a decline of ~6% in wheat yield for every °C degree increment in global mean temperature (Asseng et al., 2015), thus yield gains could stagnate or even decline in the near future (Lobell et al., 2009; Long et al., 2015) representing a threat to world food security.
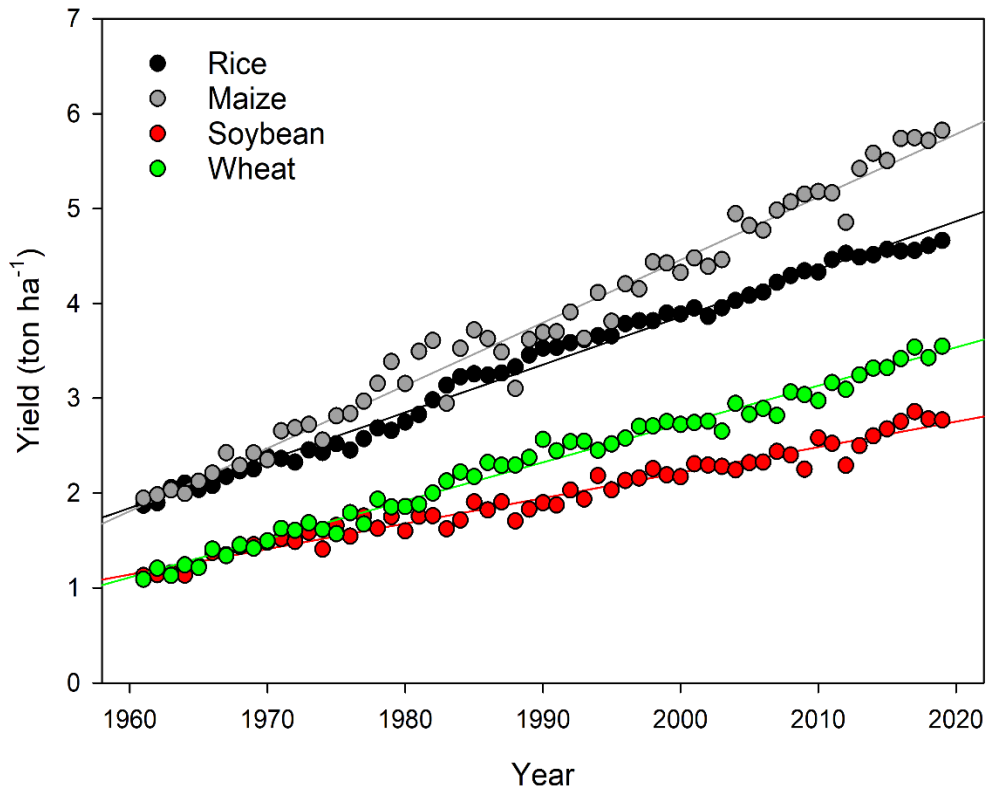
Figure 1.1. Average yearly yields from 1961-2019. Trends show that for these four staple crops, rice, soybean and wheat yields are not increasing at a sufficient rate to ensure food security. Data was retrieved from FAO.

During the Green Revolution, breeding approaches for wheat improvement have had a pivotal role in reducing the gap between farm and theoretical yields. The physiological traits which received most attention was the proportion of total biomass allocated in the grains (harvest index, HI), resistance to diseases such as rust, more efficient partitioning of biomass into harvestable organs resulting in manipulation of source-sink ratios. Finally, to minimize lodging breeders have aimed for thicker stems and shorter plants to reduce the plant centre of gravity and make it more responsive to fertilisation. Canopy architecture has been another area of development with optimization of the leaf area per unit of ground surface (LAI), leaf angle and the preference for genotypes that can stay green for

longer periods during growth cycle (Foulkes et al., 2011; Parry et al., 2011; Reynolds et al., 2012; Richards, 2000; Valluru et al., 2015).

On the other hand, in heat and drought environments, the effort is aimed to improve water use efficiency (the amount of carbon (C) fixed through photosynthesis per molecules of water transpired, WUE). High WUE may be associated with lower stomatal conductance (gs), higher canopy temperatures and reduced photosynthetic capacity thus making it a trait that needs to be studied altogether with other physiological traits to ensure there will be no decreases in gas exchange under optimal growth conditions (Araus et al., 2002; Fischer et al., 1998; Reynolds et al., 1994).

Except for the partitioning traits, most agronomic traits are close to theoretical optimization, and it has been proposed that one of the best options to further increase crop yields (including wheat) will be by improving canopy radiation use efficiency and photosynthetic capacity and efficiency (Evans and Lawson, 2020; Kromdijk and Long, 2016; Lawson et al., 2012; Murchie et al., 2009), but recent reviews in the topic have suggested other avenues such as improving agronomic N use in crops (Sinclair et al., 2019) as well as including less studied plant organs such as spikes, stems and roots to understand its contribution to crop yield (Araus et al., 2021).

1.3 Photosynthesis and radiation use efficiency

More than 90% of biomass produced during a plant lifecycle derives directly from photosynthetic products, reason why future genetic progress in crop yield needs to focus in increasing the conversion rate of PAR to biomass (Long et al.,

2006; Murchie et al., 2009). This conversion ratio is known as radiation use efficiency (RUE) and can be defined as the efficiency of converting light intercepted by the crop into biomass (mass of biomass per units of radiation, g MJ^{-1}) (Murchie and Reynolds, 2013).

One of the first crop scientists who studied this trait was Professor John Monteith, with his work he found that RUE is one of the main drivers of yield, especially under yield potential conditions, when there are no limitations in resource availability (i.e. water and nutrients) and that intercepted rather than incident radiation is critical to understand and compare photosynthesis between different plant species (Monteith, 1977).

Yield is a function of the incident radiation (also known as photosynthetic photon flux density, PPFD), the fraction of intercepted radiation during the growth cycle (ε), RUE and the relationship between grain weight and total crop biomass (harvest index, HI) (Monteith, 1977; Reynolds *et al.*, 2009; Murchie and Reynolds, 2013; Cabrera-Bosquet *et al.*, 2016).

The relationship between RUE and yield is expressed in its simplest form in equation 1:

$$Yield = \sum_{i=1}^{n} PPFD_i \ x \ \varepsilon_i \ x \ RUE_i \ x \ HI \qquad \text{eq. (1)}$$

where n is the duration of crop growth in days, $PPFD_i$ is the incident radiation, ε_i the fraction of incident radiation and RUE_i the radiation use efficiency on the ith day respectively.

Yield can be improved by increasing any of the elements in equation 1, since traits related to HI such as partitioning of carbohydrates into the spikes or traits related to light interception such as leaf area index are close to optimization

(Reynolds et al., 2000b), physiologists and breeders need to focus mainly on RUE related traits and considering relevant reviews on the topic the most important will be increasing the photosynthetic capacity and efficiency, improve canopy architecture and increase the duration of light capture through the introduction of genotypes with "stay green" (Amthor, 2010; Parry et al., 2011; Reynolds et al., 2012; Zhu et al., 2010; Murchie et al., 2018).

1.4 Photosynthesis as a driver for RUE: an overview

Photosynthesis transforms fixed CO_2 into carbohydrates in the chloroplast, a cellular organelle present in eukaryote photosynthetic organisms. Chloroplasts are key for plant growth and development as they do not just fix carbon; they also oversee the synthesis of amino acids, fatty acids, is in charge of immune responses against pathogens, synthesis of pigments such as chlorophyll or carotenoids and responds to environmental stimuli (Pogson et al., 2015).

Inside of the chloroplast, there are green pigments called chlorophylls, essential for photosynthesis as they allow plants and cyanobacteria to absorb energy from sun's radiation. Chlorophyll absorbs light strongly in the blue (~450-495 nm) and red (620-700 nm) while reflecting most of the radiation from the green portion of the electromagnetic spectrum, hence leaves green color (Zhen et al., 2021).

Thus, for photosynthesis to take place plants need to utilize the portion of the electromagnetic spectrum from 400-700 nm although some photosynthesis is driven by wavelengths that can be found above or below this range (Zhen et al., 2021). This area of the electromagnetic spectrum is commonly known as visible

spectrum or photosynthetically active radiation (PAR) (Murchie and Reynolds, 2013; Sinclair and Muchow, 1999).

Once light energy is absorbed by chlorophyll it is converted in the chloroplast into molecules of adenosine triphosphate (ATP) and nicotinamide adenine dinucleotide phosphate (NADPH). This is achieved by the electron transfer reactions in the thylakoid membrane and the transduction of absorbed energy via the chemiosmotic mechanism and ATP synthase (Figure 1.2) (Nobel, 2009). ATP and NADPH are then used to fuel the Calvin Benson cycle within the stroma of the chloroplast.

The Calvin Benson cycle incorporates the enzyme Ribulose-1,5-bisphosphate carboxylase oxygenase (Rubisco), a key limiting step in photosynthesis due to its slow catalytic turnover, its reaction with oxygen which outcompetes CO_2 through photorespiration and its slow activation under light conditions (Bobik and Burch-Smith, 2015). The Calvin Benson cycle generates 3-carbon triose phosphates used to synthesize hexose sugars which are key for metabolic processes fueling growth (Figure 1.2). Hence radiative solar energy is converted into chemical components rich in C that accumulate in plant organs through their life cycle in form of biomass (Pogson et al., 2015). Furthermore, this biochemical process plays a key role in alleviating climate change as atmospheric CO_2 is stored in plant tissues (IPCC, 2014).

Photosynthesis is metabolically complex and requires a high level of regulation and coordination between leaf cells at all orders of complexity. The photorespiratory pathway is an inevitable consequence of Rubisco oxygenation of ribulose-1,5-biphosphate (RuBP) and can result in energetic losses which has

become a target for photosynthesis engineering in the context of crop improvement. Photoprotection refers to a suite of processes that help plants avoid photoinactivation of photosystem II and oxidative stress (Murchie and Niyogi, 2011). This includes the thermal dissipation of excess excitation energy as heat in a process termed non photochemical quenching (NPQ) (Murchie and Ruban, 2020). Stomatal morphology and behaviour are another big component of photosynthesis. It determines the diffusion of gases into the leaf and restricts excessive water loss by coordinating with different organs of the plant (leaves, roots) by sensing through hormones if the soil moisture or ambient humidity might not be high enough to support the water loss cost of photosynthesis (Lambers et al., 2008; Nobel, 2009).
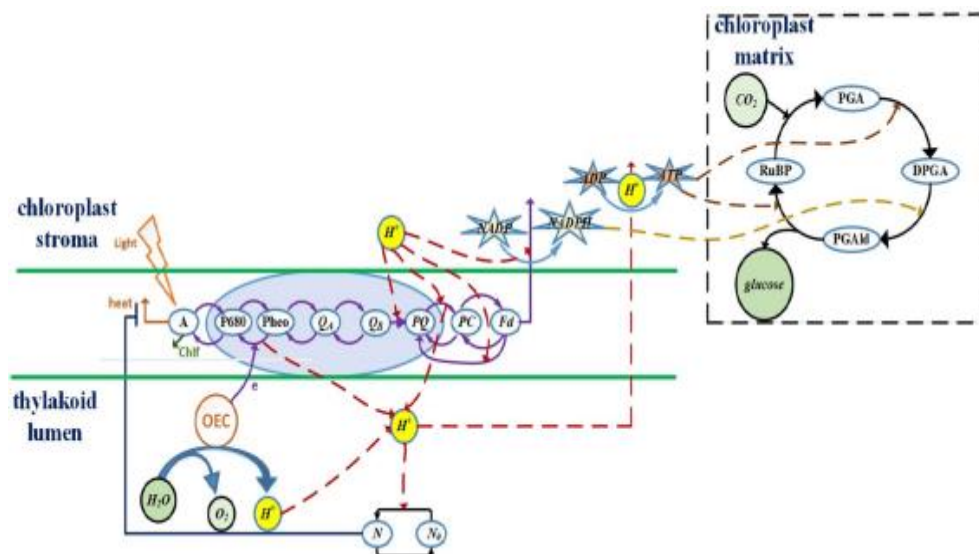
Figure 1.2. Simplified photosynthesis model including light and dark metabolic reactions (i.e. light absorption and glucose formation). Symbols represent: A = Antenna molecules, P680 = Reaction center of PSII with maximum absorption at 680 nm, Pheo = Pheophytin, QA = Primary PSII plastoquinone acceptor, QB = Secondary PSII plastoquinone acceptor, PQ = Plastoquinone, PC = Plastocyanin, Fd = Ferredoxin, OEC = Oxygen evolving complex, PGA = 3-phosphoglycerate, DPGA = Diphosphoglycerate, PGAld = Phosphoglyceraldehyde. Figure from Fu et al., 2020.

1.5 Canopy development, architecture and structure

The role of the photosynthetic source in wheat in driving yield is dependent upon the stage within the canopy development process (Figure 1.3). Carbohydrate accumulation starts from very early growth stages up to senescence of photosynthetic tissues. In the early growth stages (tillering to initiation of booting) it is essential for the plant to capture as much radiation available as possible for rapid growth to form a sufficiently high LAI (3-5) to build up carbohydrate reserves to support a sufficiently large reproductive sink and anchorage/nutrient acquisition root systems. Post anthesis, the sink size and activity become crucial in yield formation, relying on both concurrent photosynthesis and the previously accumulated non-structural carbohydrates reserves in the stems (Saint Pierre et al., 2010). This is important because abiotic stresses during the reproductive process such as heat or drought stress can induce spikelet sterility, accelerate leaf senescence rates and cause a reduction in yield (Moraga et al., 2022). Post anthesis and during grain filling, wheat spikes sink activity shifts the dynamic of canopy photosynthesis, from leaf to spike driven, highlighting the importance of spike photosynthesis (Araus et al., 2021; Molero and Reynolds, 2020; Sanchez-Bragado et al., 2020).

In terms of canopy architecture it has been proposed that pre-anthesis a broad-leaved canopy is preferable to achieve full light interception (~95%) (Reynolds et al., 2000b) whereas post-anthesis flag erect leaves are desired as radiation penetrates easier through the canopy increasing photosynthesis, therefore biomass and yield (Richards et al., 2019).
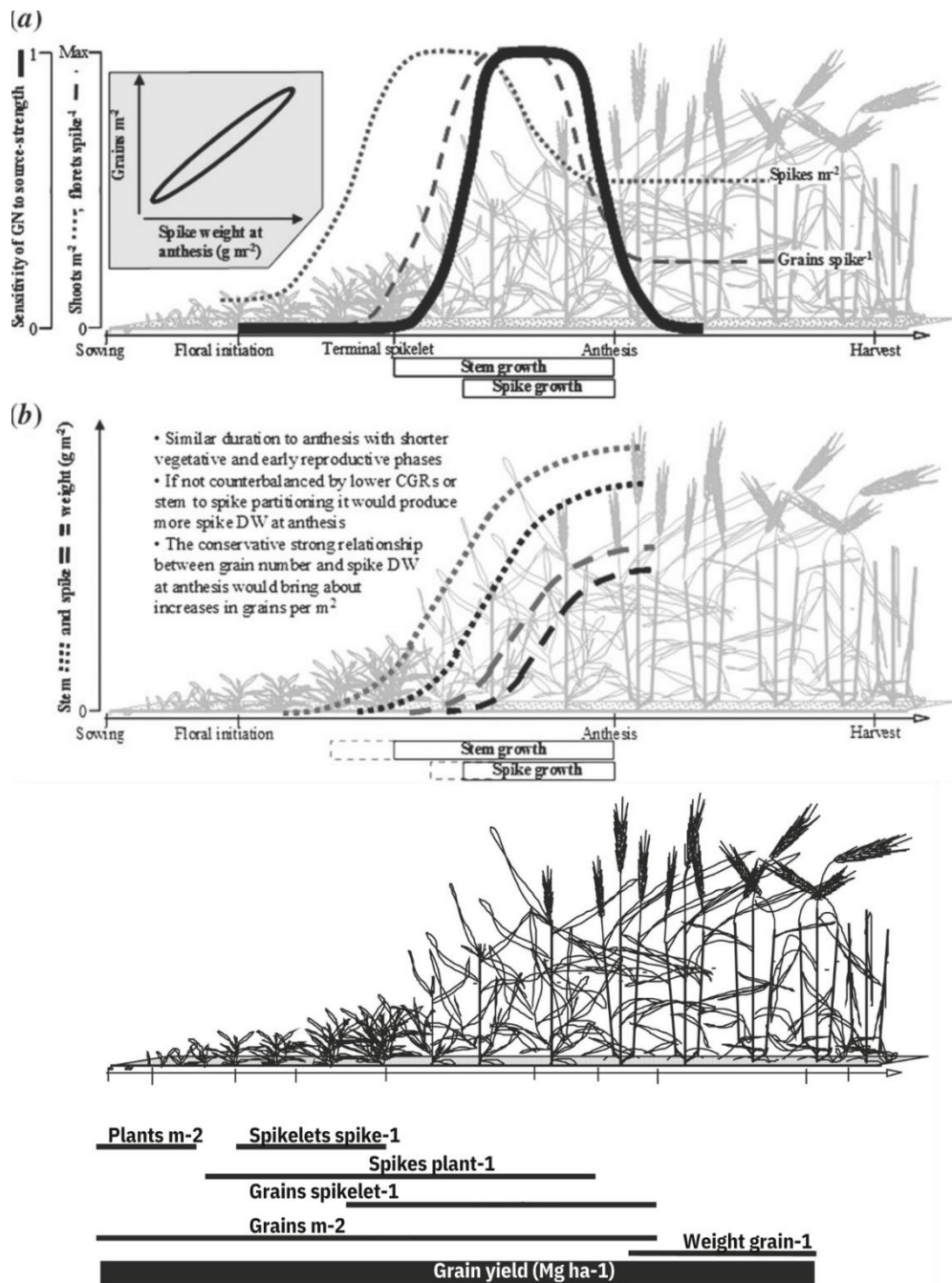
Figure 1.3. Developmental stages in a wheat canopy. During the vegetative stages (emergence-booting) photosynthetic rates, leaf area and stem elongation are at their peak. In grain filling photosynthetic rates are driven by source-sink dynamics caused by the formation of grains, photosynthesis by the spikes and bottom layers of the canopy senescence. Panels a) and b) from Reynolds et al., 2009; bottom panel from Slafer, 2003.

1.6 Options for improving crop photosynthesis

Leaf photosynthesis can be influenced by many traits which can be divided into architectural traits including: leaf angle, curvature, width, length, thickness, plant height, and others (Foulkes and Murchie, 2011) and functional traits such as chlorophyll content, Rubisco and N content, stomatal and mesophyll conductance, adaptation to different light regimes, dissipation of excess heat (i.e. non photochemical quenching, NPQ), respiration, water use efficiency (WUE) and photosynthetic N use efficiency (PNUE) for photosynthesis, the latter two which come at a very high energetic cost for the plant (Hikosaka, 2016; Murchie et al., 2018; Evans and Lawson, 2020). These represent physiological processes and traits that have been receiving attention from the scientific community engaged in photosynthesis improvement to boost crop yield.

It has long been established that crop RUE operates below its theoretical efficiency (Zhu et al., 2008) due to metabolic "losses" that happen at multiple scales which results in reduction in energy conversion to biomass (Murchie, 2017; Reynolds et al., 2012). Then, increasing the photosynthetic capacity of wheat canopies will have several implications on many fields of science requiring interdisciplinary efforts to fulfill it.

One option is to increase Rubisco affinity to CO_2 and catalytic rate to outcompete photorespiration, which reduces photosynthetic efficiency (Sharwood, 2017), this could be achieved by exploiting natural variation in Rubisco properties for example by studying either ancient races or modern genotypes to predict the catalytic variations of Rubisco adaptations under different environments (McAusland et al., 2020; Prins et al., 2016).

Biotechnological approaches include introducing cyanobacterial CO_2 concentrating mechanisms using bicarbonate transporters and microcompartments containing Rubisco called carboxysomes. Furthermore reducing the size of Rubisco molecules can drastically diminish the N requirement of the plant and increase photosynthetic efficiency (Ort et al., 2015) and engineer a photorespiratory bypass pathway in the chloroplast or the peroxisome or by oxidizing the glycolate to CO_2 in the chloroplast (Peterhansel et al., 2013), these strategies have been deemed as an important modification for increasing biomass in C_3 plants such as rice (Shen et al., 2019), arabidopsis (Basler et al., 2016) and camelina (Dalal et al., 2015) but results should be taken with caution as these modifications at cellular level depend on the regulation of other metabolic pathways in conjunction with photorespiration (Xin et al., 2015).

Another option to increase photosynthetic capacity and efficiency, is the bioengineering of C_3 crops with the same carbon concentration mechanisms (Kranz like anatomy) used by C_4 plants that will allow wheat to use radiation more efficiently as currently efficient conversion of solar energy are ~6% for C_4 crops and ~4.6% for C_3 crops (Zhu et al., 2010). This could trigger a more efficient use of water and nitrogen, as well as reducing the inefficiency of photosynthesis due to competition with photorespiration (Long et al., 2015; Ort et al., 2015; Sage et al., 2012; Sage and Stata, 2015).

The duration of light capture is an important characteristic to improve as light availability is highly heterogeneous during different timescales (e.g., seconds, hours, days, months) and these fluctuations regulate the light quality which plants rely on (Murchie and Niyogi, 2011).

Plants developed mechanisms to cope with this variability, for example short-term "memory" light history for changes at seconds or minutes or long-term changes in structure and stoichiometry of the leaves (Retkute *et al.*, 2015). Other mechanisms that can be exploited are shade tolerance and genotypes that could efficiently use the "sun fleck" resource within the canopy (Murchie et al., 2009; Murchie and Reynolds, 2013) as it has been found with understory plants growing in forest floors that sun flecks can represent up to 60% of total daily carbon gains (Niinemets, 2010; Way and Pearcy, 2012).

For these reasons it has been suggested that the selection of wheat genotypes with improved dynamic responses of photosynthesis are important. These include NPQ characteristics such as increased NPQ capacity and acceleration of the relaxation of NPQ under fluctuating light conditions (Hubbart et al., 2018; Kromdijk et al., 2016; Murchie and Lawson, 2013). Furthermore, faster regulation of stomatal aperture under dynamic light will help improve photosynthetic capacity and efficiency (Lawson and Blatt, 2014), particularly now that evidence shows that the responses of photosynthesis and stomatal aperture to dynamic light conditions might be mismatched, and the same goes for steady state conditions (Vialet-Chabrand et al., 2017) which if synchronized could represent an important source of carbon gain for wheat. Moreover, reducing the light harvesting antenna size could improve photosynthetic rates, for several reasons, possibly to avoid saturation of the photosystem I and II complexes but also to improve light distribution within the canopy (Song et al., 2017; Zhu et al., 2010).

Canopy architecture is another avenue for wheat yield improvement. LAI values have reached its optimum for wheat canopies (values between 3-5), but

architecture can still be improved by manipulating leaf width, length and angles in respect to their position in the stem. This will help wheat to adapt quicker from high to low and vice versa light transitions in short time scales (Murchie, 2017; Murchie et al., 2018).

Crop stands with higher LAI and erect leaves have the capacity to intercept more light than ones with flat canopies and evidence is showing higher biomass and yield (Richards et al., 2019). This phenomenon can be explained thanks to Beer's law, which crop scientists have adapted characterizing canopies to estimate the fraction of light absorbed by each stratum of the canopy. In this case erect canopies have a lower extinction coefficient, and this means that light will distribute homogeneously within the canopy and in the opposite flat canopies have a higher extinction coefficient and light will distribute heterogeneously through the canopy (Figure 1.4), with the lower layers receiving ~5-10% of incident radiation (Cabrera-Bosquet et al., 2016; Mantilla-Perez and Fernandez-Salas, 2017; Sinclair and Muchow, 1999; Robles-Zazueta et al., 2022).

To improve yield, canopy architecture needs to be optimised by redistributing nitrogen (N) within the canopy at key growth stages: at initiation of booting to maximize photosynthetic rates and during grain filling to sustain both spike and leaf photosynthesis (Foulkes et al., 2011; Foulkes and Murchie, 2011; Sanchez-Bragado et al., 2020) and by selecting stay-green genotypes to keep green tissues (i.e. physiologically active) close to physiological maturity (Parry et al., 2011; Pinto et al., 2016; Thomas and Ougham, 2014). Finally, manipulations of other organs of the canopy such as spikes and stems has been addressed recently and findings suggest that spikes can play a major role in CO_2 uptake as bottom and middle layer leaves start to senesce (Sanchez-Bragado et al., 2014; Molero and

Reynolds, 2020) and stem photosynthesis might be an important target to improve canopy photosynthesis (Simkin et al., 2020).

If all these goals stated above are achieved and photosynthetic capacity, efficiency and stomatal dynamics are improved wheat yields can increase more than 50% compared to actual yield rates (Reynolds et al., 2009).
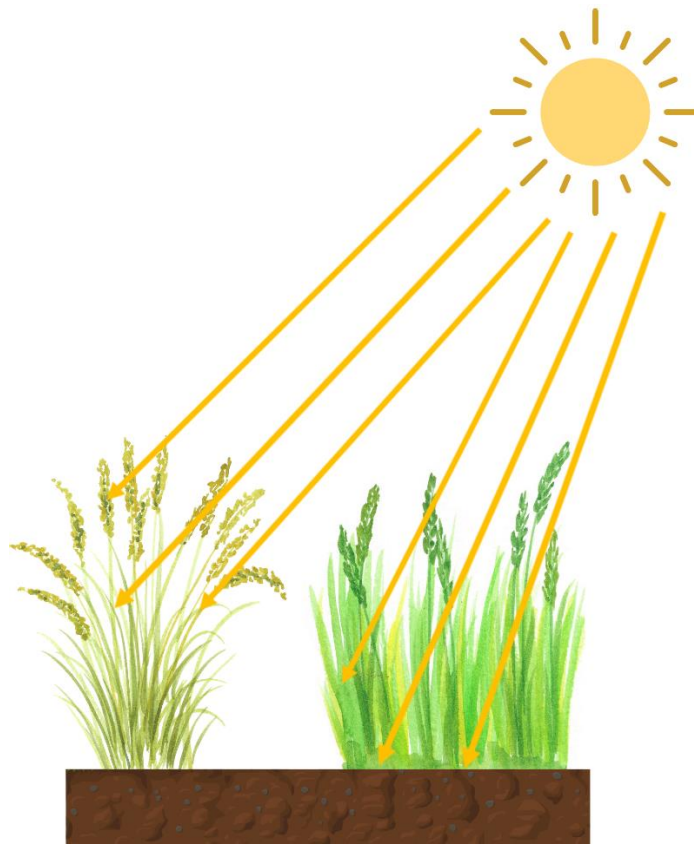
Figure 1.4. Diagram depicting the concept of light distribution within a canopy. On the left side (darker plants) a floppy wheat canopy is represented where LAI is at optimal values (3-5) and there is a high extinction coefficient which reduces the amount of light that penetrates to the lower strata of the canopy. In the right side (brighter plants), an erect canopy with smaller LAI and upright leaves is represented. A smaller extinction coefficient and higher light penetration through the canopy is expected in this type of canopies which are characterized by zones of high productivity at the top and medium productivity in the bottom layers with leaves adapted to dynamic light conditions and delayed senescence rates.

1.7 Plant phenotyping

A phenotype can be defined as the manifestation of traits that result from the interaction between an organism and the environment where it develops (Mahner and Kary, 1997).

From this point of view, we can define plant phenotyping as methodologies used to measure physiological or structural traits such as plant growth, resource use efficiency, gas exchange, architecture, organ stoichiometry, partitioning of assimilates into plant organs and others, at different spatiotemporal scales (from organs to canopies and from seconds to years), with an emphasis for non-invasive technologies (Fiorani and Schurr, 2013)

To achieve higher yields, phenotyping needs to be improved at the same pace genotyping has done in the era of "omics" (Poland et al., 2012), to reduce the bottleneck in phenotyping, phenomes and genomes need to be studied at the same time scales and accelerate the screening process (Cabrera-Bosquet et al., 2012; Reynolds and Langridge, 2016; Reynolds et al., 2020; Tester and Landridge, 2010).

Several authors have recently addressed the term "phenomics" (or high-throughput plant phenotyping, HTP) which can be defined as the use of novel methodologies which include —but is not restricted to— remote sensing, programming, data mining, ecophysiology and imaging techniques that allow phenotyping in a multi-dimensional matrix with different developmental stages and environmental scenarios (Araus and Cairns, 2014; Fiorani and Schurr, 2013; Furbank and Tester, 2011).

Examples of tools used for HTP purposes are manual measurements of chlorophyll fluorescence for rapid assessment of photosynthetic parameters such as quantum yield or chlorophyll fluorescence responses to dynamic light (Table 1) (Baker, 2008; Murchie and Lawson, 2013), canopy temperature measurements (Flexas et al., 2012) or infrared imaging to relate to *gs* (McAusland et al., 2013). More recently the use of chlorophyll fluorescence and sun induced fluorescence (SIF) has been used to estimate canopy photosynthesis (Pinto et al., 2020) and field measurements of spectral reflectance have become the new gold standard for HTP of traits such as photosynthesis, *gs*, WUE, accumulation of biomass, biochemical and biophysical leaf traits (Cotrozzi and Couture, 2020; Garbulsky et al., 2011; Heckmann et al., 2017; Robles-Zazueta et al., 2022; Silva-Pérez et al., 2018) and recently RUE and biomass at canopy scale (Robles-Zazueta et al., 2021; Tewes and Schellberg, 2018).

The scales and tools used to monitor crops using remote sensing can vary in price and complexity, but the most common ones are unmanned aerial vehicles (UAV), phenomobiles, field spectroradiometers and satellites (e.g. MODIS Terra, MODIS Aqua, LANDSAT missions, AVHRR). From these tools UAVs, phenomobiles and field spectroradiometers combine precision, speed and are easy to handle and coupled with a variety of sensors with different spectral resolutions (e.g. RGB, NDVI, red edge, near infrared, multi or hyperspectral, and thermal) (Sankaran et al., 2015) have become cheaper are paving the way as a useful tool in crop phenotyping programs (Araus and Cairns, 2014; Bendig et al., 2012).

These tools work mainly by two different approaches, active sensing and passive sensing. Active sensors tools emit a light pulse at different wavelengths of the

electromagnetic spectrum (often referred as bands), while passive sensors do not emit these pulses. Both active and passive sensors measure the signal that comes back after it had interacted with an object (i.e. clouds, vegetation, water, soil, or a mix of different objects) (Turner et al., 2003).

The spectral resolutions of these measurements can vary depending on spectral resolution of the instrument, but usually range between 300-2500 nm (Table 1.2). For example, the most common vegetation index, the normalised difference vegetation index (NDVI) which is calculated with the reflectance from the bands located in the near infrared and red electromagnetic spectrum (R_{800}-R_{680}/R_{800}+R_{680}), has been used to study plant growth, canopy greenness, biomass dynamics and the amount of absorbed photosynthetically active radiation (APAR) (Pask et al., 2013; Tattaris et al., 2016). Other areas of the spectra with physiological relevance are the near infrared (700-1100) for photosynthesis and biomass accumulation, the shortwave infrared (1300-2500) for biochemical and biophysical traits (Robles-Zazueta et al., 2022).

The use of HTP will be necessary for more accurate and rapid phenotyping of large wheat populations in order to speed up screening and increase genetic gains, and to upscale physiological traits related to RUE (Furbank et al., 2019). This trait is difficult to measure in large populations because it involves destructive sampling at different growth stages, requires hard labour and resources and in case of harvest sampling error yield data can be compromised.

Table 1.2. Most common measured physiological traits in breeding programs. Measurements are divided in conventional methods (low throughput, CM) and novel methods (high throughput, HTP).

	Measurement type		Temporal resolution		Spatial resolution		Wavelength	Applications	Knowledge frontier	References
Trait	CM	HTP	CM	HTP	CM	HTP				
Plant biomass, yield	Destructive sampling on key growth stages, yield components	Vegetation indices, RGB imagery, Light Detection and Radar data (LIDAR)	Low	High	Whole plants	Canopy	RGB (400-700 nm), Near Infrared (NIR) (700-850 nm), Red Edge (680-730 nm)	Aboveground biomass estimation, canopy greenness, growth monitoring	Root biomass estimation, increase the accuracy of biomass estimation, estimation of yield components	(Cabrera-Bosquet et al., 2011; Fiorani and Schurr, 2013; Robles-Zazueta et al., 2021; Sankaran et al., 2015; Tattaris et al., 2016; Ustin and Gamon, 2010; White et al., 2012)
Canopy architecture (height, leaf structure, canopy	Manual measurements using measuring tape, biomass	RGB imagery, light detection and ranging data (LIDAR measurements),	Low to high	High	Whole plants, canopy	Whole plants, canopy	RGB (400-700 nm), Near Infrared (NIR) (700-850 nm),	Aboveground biomass, resource capture by the crop (carbon,	Estimation of RUE using remote sensing, reconstruction of canopies in	(Burgess et al., 2017a; Burgess et al., 2017b; Cabrera-Bosquet et al., 2016; Hämmerle and Höfle, 2016; Müller-

| density, LAI, light interception), RUE | harvest and light interception measurements, measurement of leaf width and length, sceptometer | multispectral and hyperspectral imagery, 3D canopy reconstruction using RGB cameras, stereo imaging, kinnect sensor | | | | | Hyperspectral (300-2500 nm) | light, nitrogen, water), leaf length, width and angle | the field to estimate light interception, photosynthesis and biomass,

Root architecture, manipulation of canopy architecture to increase resource capture | Linow et al., 2015; Paulus et al., 2014; Pound et al., 2017; Robles-Zazueta et al., 2021) |
| Phenology: Emergence, heading, flowering, senescence, greenness | Visual assessment using the Zadoks growth scale, use of low-cost RGB cameras | RGB imagery using photogrammetry, hyperspectral imagery and spectral ground data to calculate vegetation indices related to plant greenness and senescence | Medium | High | Canopy | Canopy | RGB (400-700 nm), Near Infrared (NIR) (700-850 nm), Hyperspectral (300-2500 nm) | Nutrition and water management, pests and diseases control | Develop stay-green genotypes to increase photosynthesis and biomass without compromising other yield components, | (Lopes and Reynolds, 2012; Pinto et al., 2016; Sadeghi-Tehran et al., 2017) |

| Gas exchange traits: Net CO_2 assimilation, stomatal conductance, transpiration, chlorophyll fluorescence, pigments | Infrared gas analyzer (IRGA), Leaf porometer, Canopy temperature, Canopy reflectance, Fluorometer | Sun-Induced Fluorescence (SIF), Hyperspectral UAV and ground data, Thermal imagery, Scale Invariant Feature Transform (SIFT) | Low (few samples at key phenological stages) to medium (measurements every week) | Low to high | Organ (i.e. leaves or spikes) | Canopy | Chlorophyll fluorescence at 760 nm, Hyperspectral (300-2500 nm) | Net CO_2 assimilation at leaf, canopy and ecosystem levels, circadian rhythm in plants to see how they use light during the whole day, machine learning to estimate photosynthesis | reduction of the timeframe between booting and anthesis stages to increase yield Integration of methods from leaves (gas exchange) to ecosystem (eddy covariance and satellite data), integration through modelling of RUE, NUE and WUE | (Babar et al., 2006; Baldocchi, 2014; Blackburn, 2007; Garbulsky et al., 2011; Guo and Trotter, 2004; Li et al., 2010; Meroni et al., 2009; Ollinger, 2011; Peñuelas et al., 2011; Pinto et al., 2017; Silva-Pérez et al., 2018; Tindall et al., 2015; Zhu et al., 2004; Furbank et al., 2021) |

1.8 Hypothesis

1. The main components of RUE are biomass and intercepted radiation by the canopy. Based on this we hypothesize that predictive models using reflectance data collected at a canopy level will be more accurate than models using reflectance data at leaf level due to a better representation of canopy processes.

2. To improve RUE and yield it has been implied that photosynthetic rates need to increase. Canopy architecture plays a role in the distribution of light within wheat canopies. We expect genotypes with erect flag leaves and broadened middle and bottom leaves to have higher RUE and yield compared to erect genotypes which usually have smaller leaf area.

3. Models derived from rapid measurements of multiple layers of the canopy will produce better predictions than models created just with individual leaf layers, due to the unknown trait variability caused by a gradient from top to bottom of wheat canopies.

4. Competition between shoot and roots for resources will affect source-sink ratios, harvest index and ultimately yield. Therefore, we expect that greater root biomass accumulation will have an antagonist effect over aboveground traits, especially shoot biomass accumulation, harvest index and yield.

1.9 Objectives

1.9.1 Main objective

Implement a high-throughput phenotyping approach based on field and remote sensing techniques to estimate RUE and photosynthetic traits at leaf and canopy scales and understand which canopy layer is more important for yield improvement while enabling rapid screening of wheat lines in a large population panel (PS Tails) for the purpose of rapid genetic improvement and breeding.

1.9.2 Specific objectives

1. Measure physiological traits related to RUE and photosynthesis in the field at leaf and canopy scale in a high biomass wheat panel under yield potential conditions.

2. Predict RUE, biomass and intercepted PAR with HTP techniques based on vegetation indices and partial least squares regressions modelling to alleviate the phenotyping bottleneck of these traits.

3. Define which layer or combination of canopy layers can explain the largest variability of RUE and yield to aid in the selection of appropriate photosynthetic screening traits.

4. Build predictive models of photosynthetic, biophysical and biochemical traits and explore the use of these predictions as means to select wheat genotypes for higher RUE.

5. Analyse root biomass accumulation and its relationship with physiological and agronomical traits to improve our understanding of the link between root and shoot physiology and RUE.

Chapter 2 Field based remote sensing models predict radiation use efficiency in wheat

Carlos A. Robles-Zazueta[1,2], Gemma Molero[2,3], Francisco Pinto[2], M. John Foulkes[1], Matthew P. Reynolds[2], Erik H. Murchie[1*]

[1]Division of Plant and Crop Science, School of Biosciences, University of Nottingham, LE12 5RD, UK.

[2]Global Wheat Program, International Maize and Wheat Improvement Center (CIMMYT), carretera Mexico-Veracruz km 45, El Batan, Texcoco, Mexico C. P. 56237.

[3]KWS Momont Recherche, 7 rue de Martinval, 59246 Mons-en-Pevele, France.

Author contribution:

Conceptualization of the project: Carlos A. Robles-Zazueta, Gemma Molero, Francisco Pinto, Matthew P. Reynolds and Erik H. Murchie.

Investigation, data curation and formal analysis: Carlos A. Robles-Zazueta.

Methodology: Carlos A. Robles-Zazueta, Gemma Molero, Francisco Pinto, M. John Foulkes, Matthew P. Reynolds and Erik H. Murchie

Original draft: Carlos A. Robles-Zazueta and Erik H. Murchie.

Review and editing: Carlos A. Robles-Zazueta, Gemma Molero, Francisco Pinto, M. John Foulkes, Matthew P. Reynolds and Erik H. Murchie.

Funding acquisition: Gemma Molero, Matthew P. Reynolds and Erik H. Murchie.

Project management: Erik H. Murchie and Matthew P. Reynolds.

*Author for correspondence: erik.murchie@nottingham.ac.uk

Abstract

Wheat yields are stagnating or declining in many regions, requiring efforts to improve the light conversion efficiency, i.e. radiation use efficiency (RUE). RUE is a key trait in plant physiology because it links light capture and primary metabolism with biomass accumulation and yield, but its measurement is time consuming and this has limited its use in fundamental research and large scale physiological breeding. In this study, high-throughput phenotyping (HTP) approaches were used among a population of field grown wheat with variation in RUE and photosynthetic traits to build predictive models of RUE, biomass and intercepted photosynthetically active radiation (IPAR). Three approaches were used: best combination of sensors, canopy vegetation indices and partial least square regression. The use of remote sensing models predicted RUE with up to 70% accuracy compared to ground truth data. Water indices and NDVI are the better options to predict RUE, biomass and IPAR, and indices related to NPQ (PRI) and senescence (SIPI) are better predictors for these traits at the vegetative and grain filling stages respectively. These models will be instrumental to explain canopy processes, improve crop growth, yield modelling, and potentially be used to predict RUE in different crops or ecosystems.

Keywords: *Radiation Use Efficiency, high-throughput phenotyping, wheat*, *hyperspectral reflectance, vegetation indices, partial least square regression, physiological breeding*

2.1 Introduction

Staple crop yields must increase by at least at a rate of 2.4% per year to ensure food security for a growing population, dietary changes and expanding use of biofuels (Foley et al., 2011; Ray et al., 2013). Recent studies suggest that yield gains for staple crops are on average 1.2%-1.3% year^{-1} therefore it will not be sufficient to meet 2050 food demands (Ray et al., 2012). Moreover, climate change predictions of future environmental conditions suggest crops will be subjected to higher temperatures, flooding, drought and shifts in precipitation patterns which will affect development, primary metabolic events, biomass accumulation and yield (Porter et al., 2014; Asseng et al., 2015; Garatuza-Payan et al., 2018). The socio-economic repercussions will be felt worldwide but mostly in low-income countries (Rajaram et al., 1993) and the challenge of raising staple crop yields is one of the main goals for the scientific community in this century (Bailey-Serres et al., 2019).

2.1.1 Avenues for wheat yield improvement

Wheat (*Triticum aestivum* L.) is one of the most important staple crops and its annual production is estimated to be ~770 million tonnes year^{-1} (FAOSTAT, 2020). Physiological approaches for wheat improvement have had a pivotal role in reducing the gap between field and theoretical yields. So far, the main physiological traits improved in wheat have been reduction in plant height to minimize lodging, the partitioning of biomass into the grain and optimisation of leaf area index (LAI) (Foulkes et al., 2011; Parry et al., 2011; Reynolds et al., 2012). It has been proposed that to further increase yield it will be necessary to

improve photosynthesis and the conversion rate of photosynthetically active radiation (PAR) to biomass by the canopy (Long et al., 2006; Murchie et al., 2009, 2018; Zhu et al., 2010). This conversion rate is known as radiation use efficiency (RUE) and is defined as the biomass (dry weight) generated per unit absorbed radiation, (g MJ^{-1}) (Monteith, 1977).

Under yield potential conditions, yield has been defined as a function of incident PAR, the fraction of intercepted radiation during the crop cycle (FPAR, ε), RUE and the relation between grain dry weight and aboveground dry biomass (HI) (Reynolds et al., 2005). This is expressed in equation 1:

$$Yield \ = \ \int_{i=1}^{n} PAR_i \ x \ FPAR_i \ x \ RUE_t \ x \ HI \qquad \text{eq. (1)}$$

Where n is the day when a genotype reaches physiological maturity, PAR_i is the incident radiation in the ith day, $FPAR_i$ the fraction of incident radiation absorbed of the ith day, RUE_t the radiation use efficiency of the crop cycle and HI the harvest index.

Theoretically yield could be improved by increasing any of the elements from equation 1 but since traits related to harvest index and light interception are close to optimum, the focus to increase yield should be shifted on improving RUE (Amthor, 2010; Zhu et al., 2010; Parry et al., 2011). Due to the complexity of RUE being the product of many underlying processes that are sensitive to the environment and the fact that measuring it is labour and cost intensive, its potential for increasing yield it is not currently exploited in wheat breeding programs. Therefore, it is necessary to develop high throughput methods to measure and predict RUE for field research and breeding purposes.

2.1.2 Importance of radiation use efficiency in the context of yield improvement

The importance of RUE in plant physiology resides in the association of RUE and yield, as RUE alone can explain ~40% of its variability and it can help us to elucidate the roles of light capture and key plant processes of leaf biochemistry that drives biomass and yield (Hubbart et al., 2018; Molero et al., 2019). Evidence from FACE experiments suggest that there is room for RUE improvement that could be driven by leaf photosynthesis (Ainsworth and Long, 2005, 2021) and it has been suggested that even small increases in these two traits will have a major impact in wheat yield if HI can be maintained to modern levels (Parry et al., 2011). In contrast with the negative correlation existing between aboveground biomass measured at different growth stages and HI (Aisawi et al., 2015; Molero et al., 2019; Sierra-Gonzalez et al., 2021), no negative associations were observed between HI and RUE measured in the vegetative stages and across the whole crop cycle (Molero et al., 2019). Hence, increasing RUE is a promising strategy to achieve further genetic gains in yield without penalising HI.

In order to measure RUE in a crop canopy it is necessary to harvest aboveground biomass for at least two points in time, which is time consuming and can compromise the accuracy of yield measurements in the remaining plot area. Especially if several harvests throughout the crop cycle are needed this becomes a big issue for breeding programs. However, this may be solved using non-invasive phenotyping techniques.

2.1.3 Phenotyping of radiation use efficiency and its components

High-throughput phenotyping (HTTP) refers to the use of novel non-invasive techniques to measure physiological and agronomical traits (e.g., plant growth, biomass accumulation, gas exchange, canopy architecture, organ stoichiometry, grain yield) combining multidisciplinary knowledge that allows plant phenotyping at different spatio-temporal (seconds to years) and hierarchical scales (cells to canopies) (Furbank and Tester, 2011; Fiorani and Schurr, 2013; Tardieu et al., 2017; Araus et al., 2018; Reynolds et al., 2020).

Optical remote sensing techniques are among the most widely used for HTP. This data usually ranges from 350-2500 nm encompassing areas of the visible (400-700 nm), near infrared (NIR, 700-1350 nm), red edge (680-730 nm) and shortwave infrared (1350-2500 nm) spectrum (Gamon et al., 2019). Hyperspectral data have been used mainly in two ways: spectral indices (also known as vegetation indices, VI) calculated from relations between reflectance at specific wavelengths and physiological traits (Penuelas et al., 1997; Blackburn, 1998; Cabrera-Bosquet et al., 2011) and by using the whole spectra as an individual data point to predict traits of interest (e.g. leaf N and C content, CO_2 assimilation, respiration, maximum velocity of Rubisco carboxylation, electron transport rate, leaf mass and specific leaf areas) using statistical methods such as partial least square regression (PLSR) (Serbin et al., 2014; Yendrek et al., 2017; Silva-Pérez et al., 2018; Coast et al., 2019; Fu et al., 2020). The advantage of these two approaches is that hundreds or thousands of lines can be screened without the need of destructive and time-consuming field sampling. Moreover, as HTP technologies become cheaper, crop physiologists and

breeders will be able to study complex traits more cost effectively (Reynolds *et al.*, 2020).

Previous studies have predicted yield in wheat and rye (Montesinos-López et al., 2017; Galán et al., 2020), aboveground biomass in wheat, rice, rye and barley (Babar et al., 2006; Gnyp et al., 2014; Marshall and Thenkabail, 2015; Galán et al., 2020) and RUE in maize (Tewes and Schellberg, 2018) using optical remote sensing approaches, but to date there is not such an effort to predict RUE in the field using a HTP physiological breeding approach for wheat. The impact of predicting a multicomponent trait like RUE with a HTP approach in field conditions would be very high for physiological breeding programs while its full implementation would be very feasible in medium term (Furbank et al., 2019; Roitsch et al., 2019).

2.2 Hypothesis

Our hypothesis is that prediction models using canopy reflectance data will be more accurate than models using a different combination of sensors (which include leaf reflectance), due to a better representation of canopy processes.

2.3 Objectives

The objectives of this study are the prediction of RUE, biomass and intercepted PAR (IPAR) with HTP techniques based on vegetation indices and partial least squares regression models to define which approach will help more to alleviate the phenotyping bottleneck of these traits.

2.4 Materials and methods

2.4.1 Wheat population

Spring bread wheat cultivars were chosen from the 'Photosynthesis Respiration Tails' (PS Tails) trial which consisted of 80 genotypes including advanced line material coming from the High Biomass Association Panel (HiBAP) from CIMMYT. This germplasm is characterized by their high aboveground biomass and for containing lines with contrasting RUE expression and has breeding value as it represents material that breeders use for their crosses for yield potential (for further information of HiBAP see Molero et al., (2019)). For this study a subset of 11 genotypes (Table 2.1) was selected based on RUE at the vegetative and grain filling stages, yield, HI, flag leaf photosynthesis and plant height to consider different levels of productivity and contrasting canopy architecture. This selection was made using data available from the 2016/2017 field season at CIMMYT's experimental station (Molero, unpublished data).

The 11 lines were studied in three consecutive field seasons (2017/2018, 2018/2019 and 2019/2020 from now on referred to as Y1, Y2 and Y3 respectively). Experiments were carried out at CIMMYT's Campo Experimental Norman E. Borlaug (CENEB) field station in Ciudad Obregon, Sonora, Mexico (27° 23' 46'' N, 109° 55' 42'' W, 38 mamsl) during the spring wheat growth season that encompasses early December-early May.

Table 2.1. Reference ID, cross name, average days to initiation of booting (DTInB), days to anthesis (DTA), days to physiological maturity (DTPM), intercepted PAR, aboveground biomass and radiation use efficiency measured at different growth stages for the wheat genotypes studied. ~Genotypes studied only in Y2 and Y3.

ID	Cross name	DTInB	DTA	DTPM	IPARE40	IPARInB	IPARA7	IPARPM	BME40	BMInB	BMA7	BMPM	RUE_E40InB	RUE_InBA7	RUE_preGF	RUE_GF	RUE_Total
1	KRICHAUFF~	60	77	119	224.39	365.82	543.27	833.56	188.47	466.32	978.38	1348.94	1.75	2.91	2.33	1.21	1.61
2	W15.92/4/PASTOR//HXL7573/2*BAU/3/WBLL1	59	74	113	230.22	359.2	524.44	762.38	217.14	515.19	905.55	1210.31	2.21	2.3	2.11	1.26	1.55
3	KUKRI	64	79	117	232.446	405.17	575.98	836.45	196.14	569.52	1075.3	1319.4	2.06	3.08	2.52	1.04	1.62
4	MUNAL #1	65	80	116	226.94	406.3	565.17	804.02	199.21	558.62	998.14	1235.51	1.87	2.8	2.27	0.85	1.51
5	JANZ~	60	73	116	229	371.49	534.41	822.75	190.05	497.99	893.31	1260.97	2.08	2.39	2.21	1.41	1.57
6	CHEWINK #1	62	80	118	233.53	385.28	567.81	843.43	186.36	517.53	994.67	1319.23	2.02	2.57	2.32	1.12	1.62
7	SOKOLL//PUB94.15.1.12/WBLL1	60	75	116	232.73	375.19	551.88	833.83	211.96	495.62	943.88	1390.22	1.92	2.58	2.28	1.55	1.77
8	PUB94.15.1.12/FRTL/5/CROC_1/AE.SQUARROSA(205)//	59	74	116	230.92	368.04	538.45	824.21	214.35	551.04	1027.9	1445.18	2.26	2.71	2.56	1.43	1.8

#	Genotype																
9	BORL95/3/PRL/SARA//TSI/VEE#5/4/FRET2 C80.1/3*QT4118//KAUZ/RAYON/3/2*TRCH/7/CMH79A.955/4/AGA/3/4*SN64/CNO67//INIA66/5/NAC/6/RIALTO/8/WBLL1*2/KURUKU	64	80	120	230.75	409	576.06	870.62	205.15	607.09	1127.2	1416.93	2.11	2.77	2.55	1.15	1.68
10	QUAIU*2/KINDE	58	74	114	223.5	346.8	522.34	759.87	206.70	517.04	987.58	1345.11	2.35	2.59	2.44	1.37	1.72
11	BORLAUG100 F2014⁻	59	74	115	228	357.51	525.58	791.4	202.45	444.28	953.7	1259.33	1.65	2.86	2.35	1.19	1.57
	Mean	61	76	116	229.31	377.26	547.76	816.59	201.64	521.84	989.59	1322.83	2.03	2.69	2.36	1.23	1.64
	H^2	0.91	0.92	0.84	0	0.88	0.92	0.76	0	0.48	0.57	0.7	0.23	0	0.25	0.46	0.6
	G	***	***	***	ns	***	***	***	ns	ms	*	**	ns	ns	ns	ms	*
	Y	***	***	***	***	*	***	***	ns	ns	ns	**	*	ns	ns	ns	***
	GxY	***	***	***	ns	*	ns	*	**	*	ns	*	ns	ns	ns	ns	ms

BM_E40: biomass 40 days after emergence, BM_InB: biomass at initiation of booting, BM_A7: biomass 7 days after anthesis, BM_PM: biomass at physiological maturity, IPAR_E40: accumulated intercepted PAR 40 days after emergence, IPAR_InB: accumulated intercepted PAR at initiation of booting, IPAR_A7: accumulated intercepted PAR 7 days after anthesis, IPAR_PM: accumulated intercepted PAR at physiological maturity, RUE_E40InB: RUE from the period of 40 days after emergence to initiation of booting calculated with APAR, RUE_InBA7: RUE from the period of initiation of booting to 7 days after anthesis calculated with APAR, RUE_preGF: RUE pre grain filling calculated with APAR, RUE_GF: RUE grain filling calculated with APAR, RUE_Total: RUE of the whole crop cycle calculated with APAR. ms: marginally significant (0.1>p>0.05), * = significant at $p<0.05$, ** = significant at $p<0.01$, *** = significant at $p<0.001$, ns: not significant. H^2 = Heritability, G = Genotype, Y = Environment, GxY = Interaction genotype by environment.

2.4.2 Field conditions

Experimental design was a randomised complete block design with three replications in raised beds, two beds per plot (bed width = 0.8 m) and two rows per bed (row width = 0.2 m) in 4 m x 1.6 m plots in Y1 (plot area = 6.4 m^2). For Y2, the same experimental design was used but the number of replications was increased to four, and plot length increased to 5 m x 1.6 m, increasing the area (plot area = 8 m^2). In Y3, irrigation system was changed to optimise the water use and reduce lodging in the experimental station and a drip irrigation system was put in place. Randomised complete block design was used with the same replications and plot area as Y2 but the plants were sown as six row plots with 15 cm between rows on the flat with drip irrigation.

Sowing dates were December 5th 2017, December 6th 2018 and December 18th 2019 for Y1, Y2 and Y3 respectively. Emergence dates were December 12th 2017, December 12th 2018 and December 26th 2019 (Y1, Y2 and Y3 respectively). Harvest dates were May 8th 2018, April 30th 2019 and May 13th 2020 (Y1, Y2 and Y3 respectively). Seed rate was ~250 g m^{-2} in the three years. Irrigation was applied four times during the crop cycle in approximate 25-day intervals (pre sowing, 25, 50, 75, 100 days after emergence). Plants were grown under optimal conditions in the field with pests, weed control and fertilisation to avoid limitations to yield. In Y1 fertilization was applied in the form of urea (200 kg N ha^{-1}) 25 days after emergence (DAE). For Y2 fertilization was divided in 100 kg N ha^{-1} 25 DAE and another 100 kg N ha^{-1} 58 DAE. Finally for Y3, 100 kg N ha^{-1} were applied 30 DAE and 50 kg N ha^{-1} 50 DAE; 50 kg P ha^{-1} were applied in the three cycles when the first application of N was made.

Phenology was scored according to the Zadoks growth scale for cereals (Zadoks et al., 1974). The growth stages recorded were initiation of booting (GS41), anthesis (*GS*65) and physiological maturity (GS87) when 50% of the shoots in the plot reached each stage. Meteorological data from a nearby station to the experimental site was collected for the whole crop cycle, thermal time and accumulated PAR were calculated for the growth stages where biomass was collected (Table 2.1).

2.4.3 Ground truth traits

2.4.3.1 Light interception

The percentage of light intercepted (LI) was measured using a linear ceptometer (AccuPAR LP-80, Decagon Devices, Pullman, WA, USA) at 40 days after emergence (canopy closure), GS41 and GS65 + 7 days. Incident, reflected and transmitted PAR through the canopy were measured around 11 am-1 pm when clear skies and low wind velocity conditions prevailed following phenotyping protocols (Pask *et al.*, 2013). The following equation was used to calculate the percentage of LI by the canopy:

$$LI\ (\%) = \frac{PAR_i - PAR_r - PAR_g}{PAR_i - PAR_r}\ x\ 100 \qquad \text{eq. (2)}$$

where LI (%) is the percentage of light intercepted by the canopy, PAR_i, PAR_r and PAR_g are the incident, reflected and transmitted PAR respectively.

LI (%) was used to estimate the amount of intercepted PAR (IPAR) by the canopy in the same growth stages where aboveground biomass was harvested.

2.4.3.2 Aboveground biomass

Aboveground biomass was harvested at four key developmental growth stages: canopy closure (40 days after emergence, 40DAE), initiation of booting (GS41), initiation of the grain filling period (GS65 + 7 days) and physiological maturity (GS87).

At 40DAE biomass was harvested in 0.4 m^2 (25 cm for each bed in the plot) and at GS41 and GS65 + 7d biomass was harvested in 0.8 m^2 (50 cm for each bed in the plot). Biomass harvests were made leaving 25 cm (40 DAE) and 50 cm (GS41, GS65 + 7 days) at the northern side of the plots to reduce border effects in subsequent harvests. All fresh biomass was weighed and a subsample of 50 shoots was weighted and dried in an oven at 70 °C for 48 h and dry weight was recorded. At GS87, biomass was calculated from the measurement of yield components. For every growth stage the aboveground biomass was calculated as follows:

$$Aboveground\ biomass\ =\ Subsample\ dry\ weight\ x\ \frac{Total\ fresh\ weight\ x\ Harvested\ Area}{Subsample\ fresh\ weight} \qquad \text{eq. (3)}$$

2.4.3.3 Radiation use efficiency

RUE was estimated from the slope of the linear regression between aboveground biomass and the corresponding accumulated IPAR during the determined growth period (Monteith, 1977). Incoming radiation from a nearby meteorological station was used to calculate the accumulated PAR by multiplying irradiance x 0.45 to convert it to PAR.

RUE observations in this study are presented for five different growth periods: canopy closure to GS41 (RUE_E40InB), GS41 to GS65 + 7d (RUE_InBA7),

pre-grain filling stage (40 DAE to GS65 + 7d, RUE_preGF), grain filling stage (GS65 + 7d to GS87, RUE_GF) and RUE of the crop cycle which comprises the period from canopy closure to physiological maturity (40 DAE to GS87, RUE_Total). For RUE_GF and RUE_Total a correction factor was used to account for intercepted radiation during the last 25% (in days) of the grain filling period when canopy leaves start to senesce based on a light interception model (Reynolds *et al.*, 2000b). Calculations were made as follows:

$$RUE\_E40InB \ = \ \frac{(BM\ GS41 - BM\ E40)}{(Acc\ IPAR\ GS41 - Acc\ IPAR\ E40)} \qquad \text{eq. (4)}$$

$$RUE\_InBA7 \ = \ \frac{(BM\ GS65 + 7d - BM\ GS41)}{(Acc\ IPAR\ \ GS65 + 7d - Acc\ IPAR\ GS41)} \qquad \text{eq. (5)}$$

$$RUE\_preGF \ = \ \frac{(BM\ GS65 + 7d - BM\ E40)}{(Acc\ IPAR\ GS65 + 7d - Acc\ IPAR\ E40)} \qquad \text{eq. (6)}$$

$$RUE\_GF \ = \ \frac{(BM\ GS87 - BM\ GS65 + 7d)}{[(DTA + 25\%\ grain\ filling\ days) - (Acc\ IPAR\ GS65 + 7d)] + [(Acc\ IPAR\ GS87) - (DTA + 25\%\ grain\ filling\ days)]} \qquad \text{eq. (7)}$$

$$RUE\_Total \ = \ \frac{(BM\ GS87 - BM\ E40)}{Acc\ IPAR\ GS87 + \{(Acc\ IPAR\ GS87) - [(Acc\ IPAR\ GS87) - (DTA + 25\%\ grain\ filling\ days)] - Acc\ IPAR\ E40\}} \qquad \text{eq. (8)}$$

2.4.4 Remote sensing measurements

Remote sensing data was collected above the canopy and throughout the layers of the canopy (flag, second and third leaves). Chlorophyll content (SPAD) was measured with a SPAD-502 meter (Konika Minolta, Japan), canopy temperature (CT) was measured using an infrared thermometer (LT 300, Sixth Sense, USA) and Normalized Differenced Vegetation Index (NDVI) was measured using a Green Seeker (Trimble, USA) from canopy closure to late grain filling at least once a week described by (Pask et al., 2013).

Hyperspectral reflectance was measured using a field spectroradiometer with a spectral range from 350-2500 nm with a 3 nm spectral resolution in the visible-

near infrared (VNIR) and 10 nm resolution in the shortwave infrared (SWIR) spectrum equipped with an optic fibre with a field of view of 25° (ASD Field Spec ® 3, Boulder, CO, USA). Reflectance was measured at 0.5 m at the nadir of the canopy with a pistol grip (ASD Field Spec ® 3, Boulder, CO, USA) under clear sky conditions and when low wind speeds were predominant to make sure we were collecting the signal from the canopy instead of soil or vegetation/soil mixed signals. Six data points were collected at each plot and then averaged to obtain the reflectance of each plot.

Leaf reflectance was measured using a leaf clip equipped with a halogen bulb as light source (ASD Field Spec ® 3, Boulder, CO, USA). Healthy leaves were clipped in the middle portion and measurements were taken for flag, second and third leaves in one fertile shoot per plot. The first measurement was taken at GS41 and the last at GS75. Both canopy and leaf reflectance data were averaged to get representative values from the vegetative period (40 DAE to GS55) and the grain filling period (GS65 to GS75). Reflectance measurements were made between 10 am-2 pm where the Sun is close to its zenith at this latitude.

2.4.5 Data analysis

Adjusted means from each year were calculated for the ground truth and remote sensing traits as well was the predictions from PLSR using the linear model from package lme4 (R Core Team, 2016) with the guide user interface META-R v 6.04 (Alvarado et al., 2020) as follows:

$Y_{ijk} = \mu + Rep_i + \varepsilon_{ijk}$ eq. (9)

Where Yijk is the ground truth or remote sensing trait, μ is the mean effect, Rep$i$ is the effect of the ith replicate, and εijk is the error associated with the ith replication.

If statistically significant differences were not found between genotypes, vegetation indices were adjusted with phenology from GS41 for vegetative period averages and phenology from GS65 for grain filling period averages as covariates. Phenotypic correlations between RUE and remote sensing traits (SPAD, CT, NDVI Green Seeker and vegetation indices) were calculated using Pearson product-moment correlations and a threshold was established to select only VI with statistically significant phenotypic correlations ($p<0.05$).

2.4.5.1 Vegetation Indices

After field sampling, average reflectance collected above the canopy and the leaves from each plot was processed using View Spec Pro software (Analytical Spectral Devices Inc., Boulder, CO, USA). These values were later used to calculate different VI available from the literature (Li et al., 2010; Garbulsky et al., 2011; Ollinger, 2011; Pask et al., 2013) and Index Database (https://www.indexdatabase.de/) using R Studio (R Core Team, 2016). In table 2 are shown the VI which correlated significantly with RUE, biomass and IPAR, and that were used for building the predictive models.

Table 2.2. Common remote sensing physiological traits found to correlate with radiation use efficiency, biomass and intercepted PAR during the three field seasons measured in this study. Vegetation indices were calculated with data collected with an ASD Field Spec hyperspectral radiometer and when stated Green Seeker sensors, infrared thermometer and SPAD meter were also used to collect data.

Trait	Meaning	Equation	Physiological relevance	Reference
CT	Canopy Temperature	N/A	Stomatal conductance, transpiration, root water uptake	Reynolds et al., 1994
CRI	Carotenoid Reflectance Index	$(1/R510)-(1/R550)$	Carotenoid content	Steddom et al., 2003
CUR	Curvature Index	$(R675*R690)/R683^2$	Diurnal variation of chlorophyll fluorescence, Fv/Fm	Zarco-Tejada et al., 2000
EVI	Enhanced Vegetation Index	$2.5[(R900-R680)/(R900+6*R680-7.5*R475+1)]$	Photosynthetic capacity, canopy greenness without saturation problems	Huete et al., 2002
GI	Green Index	$R554/R677$	Canopy greenness, yield	Smith et al., 1995

GNDVI-1	Green Normalized Differenced Vegetation Index-1	R810-[(R510+R561)/2]/R810+[(R510+R561)/2]	Canopy greenness, photosynthetic capacity, N status	Gitelson and Merzlyak, 1997
J	Maximum electron transport rate	Partial least square regression modelling	Leaf e^- transport rate	Silva-Pérez et al., 2018
NDVI	Normalized Differenced Vegetation Index	(R800-R680)/(R800+R680)	Chlorophyll content, canopy greenness, photosynthetic capacity, energy absorption	Tucker, 1979
NDVIGS	Normalized Differenced Vegetation Index measured with a Green Seeker sensor	(R800-R680)/(R800+R680)	Chlorophyll content, canopy greenness, photosynthetic capacity, energy absorption	Tucker, 1979
NDWI	Normalized Differenced Water Index	(R860-R1240)/(R860+R1240)	Canopy water content	Gao, 1996
NDWI-2	Normalized Differenced Water Index-2	(R970-R850)/(R970+R850)	Canopy water content	Babar et al., 2006
NDWI-3	Normalized Differenced Water Index-3	(R970-R920)/(R970+R920)	Canopy water content	Babar et al., 2006

NDWI-4	Normalized Differenced Water Index-4	(R970-R880)/(R970+R880)	Canopy water content	Babar et al., 2006
NPCI	Normalized Pigments Chlorophyll ratio Index	(R680-R430)/(R680+R430)	Canopy water and N status	Penuelas et al., 1994
OSAVI	Optimized Soil Adjusted Vegetation Index	(1+0.16)(R800-R670)/(R800+R670+0.16)	Chlorophyll content and canopy greenness reducing the effect of soil interference	Daughtry et al., 2000
PRI	Photochemical Reflectance Index	(R531-R570)/(R531+R570)	Carotenoid content, xanthopyll cycle, gas exchange, non-photochemical quenching	Penuelas et al., 1995
PSSRa	Pigment Specific Simple Ratio of chlorophyll a	R800/R675	Chlorophyll a content	Blackburn, 1998
PSSRb	Pigment Specific Simple Ratio of chlorophll b	R800/R650	Chlorophyll b content	

RARSa	Ratio Analysis of Reflectance Spectra of chlorophyll a	R675/R700	Chlorophyll a content	Chapelle et al., 1992
RARSb	Ratio Analysis of Reflectance Spectra of chlorophyll b	R675/(R650*R700)	Chlorophyll b content	Blackburn, 1998
RGR	Red Green Ratio	(R612+R660)/(R510+R560)	Red pigments and chlorophyll content	Steddom et al., 2003
rNDVI	Red edge Normalized Difference Vegetation Index	(R750-R705)/(R750+R705)	Chlorophyll content, canopy greenness, photosynthetic capacity, energy absorption	Sims and Gamon, 2002
SAVI	Soil Adjusted Vegetation Index	[(R800-R680/R800+R680+0.75)](1+0.75)	Chlorophyll content and canopy greenness without soil interference	Huete, 1988
SIPI-1	Structure Insensitive Pigment Index-1	(R800-R445)/(R800-R680)	Carotenoid and chlorophyll content	Penuelas et al., 1995
SIPI-2	Structure Insensitive Pigment Index-2	(R800-R435)/(R415-R435)	Plant senescence related to stress	Pask et al., 2013
SPAD	N/A	N/A	Plant chlorophyll content	Pask et al., 2013

44

SR-1	Simple Ratio-1	R800/R680	Canopy greenness and chlorophyll content	Sims and Gamon, 2002
TCARI	Transformed Chlorophyll Absorption Reflectance Index	$3[(R700-R670)-0.2(R700-R550)](R700/R670)$	Canopy greenness, chlorophyll content, gas exchange reducing the effect of soil and non-photosynthetic components	Haboudane et al., 2002
$TCARI_{705,750}$	Transformed Chlorophyll Absorption Reflectance Index calculated with reflectance from 705 and 750 nm	$3[(R750-R705)-0.2(R750-R550)(R750/R705)]$	Canopy greenness, chlorophyll content, gas exchange reducing the effect of soil and non-photosynthetic components	Wu et al., 2008
VARI	Visible Atmospherically Resistant Index	$(R560-R660)/(R560+R660-R459)$	Canopy coverage	Steddom et al., 2003
V_{cmax}/N_{area}	Maximum velocity of Rubisco carboxilation/N content based on leaf area	Partial least square regression modelling	Photosynthetic N use efficiency	Silva-Pérez et al., 2018
WI	Water Index	R900/R970	Canopy water content	Penuelas et al., 1997

2.4.5.2 Partial Least Square Regression

Averaged reflectance spectral data of each plot collected above the canopy was post-processed to remove spurious data in areas of the spectra where negative or higher than 1 value were present. Spectral reflectance from 350-1800 nm and 1951-2450 nm were then used to predict RUE, biomass and IPAR using the Principal Component and Partial Least Squares Regression package (pls) in R (Mevik and Wehrens, 2007) following the method proposed in (Serbin et al., 2014).

While building the models 80% of the dataset was used as training data and 20% was used as test data to validate the PLSR models. The number of components used in the models was based on the smallest root mean square error in the cross-validation stage (RMSEP-CV) and smallest prediction of the residual sum of squares (PRESS) from the training dataset. After these steps, PLSR modelling generates loadings and scores which are used to generate regression coefficients and intercepts for each individual wavelength and thus the model can be build multiplying those values against each wavelength reflectance value. The regression coefficient (R^2), the model bias and the relative error of prediction were considered to evaluate and compare the models.

2.4.5.3 Linear models

To build the linear models using the best combination of sensors (*bcs*) and vegetation indices measured above the canopy (*cVI*), best subset regression was used with RUE, biomass and IPAR of the different growth stages as dependent variables and the remote sensing traits as independent variables using the

software Sigma Plot 13.0 (Systat Software Inc., San Jose, CA, USA). These linear models assume an association between the dependent and independent variables as follows:

$$y = b_0 + b_1x_1 + b_2x_2 + b_3x_3 + \ldots b_ix_i \qquad \text{eq. (10)}$$

Where y is the dependent variable, x the independent variable and b the regression coefficients.

To compare the predictive ability of the models presented in this study a set of criteria was considered such as the regression coefficient (R^2), the variance inflation factor (VIF) to avoid multicollinearity between the variables used to predict RUE or biomass and the root mean square error (RMSE), calculated as follows:

$$RMSE = \sqrt{\frac{\sum(X_i - Y_i)^2}{n}} \qquad \text{eq. (11)}$$

Where X_i are the predicted values, Y_i the observed values and n the total number of observations.

2.5 Results

2.5.1 Accumulated IPAR
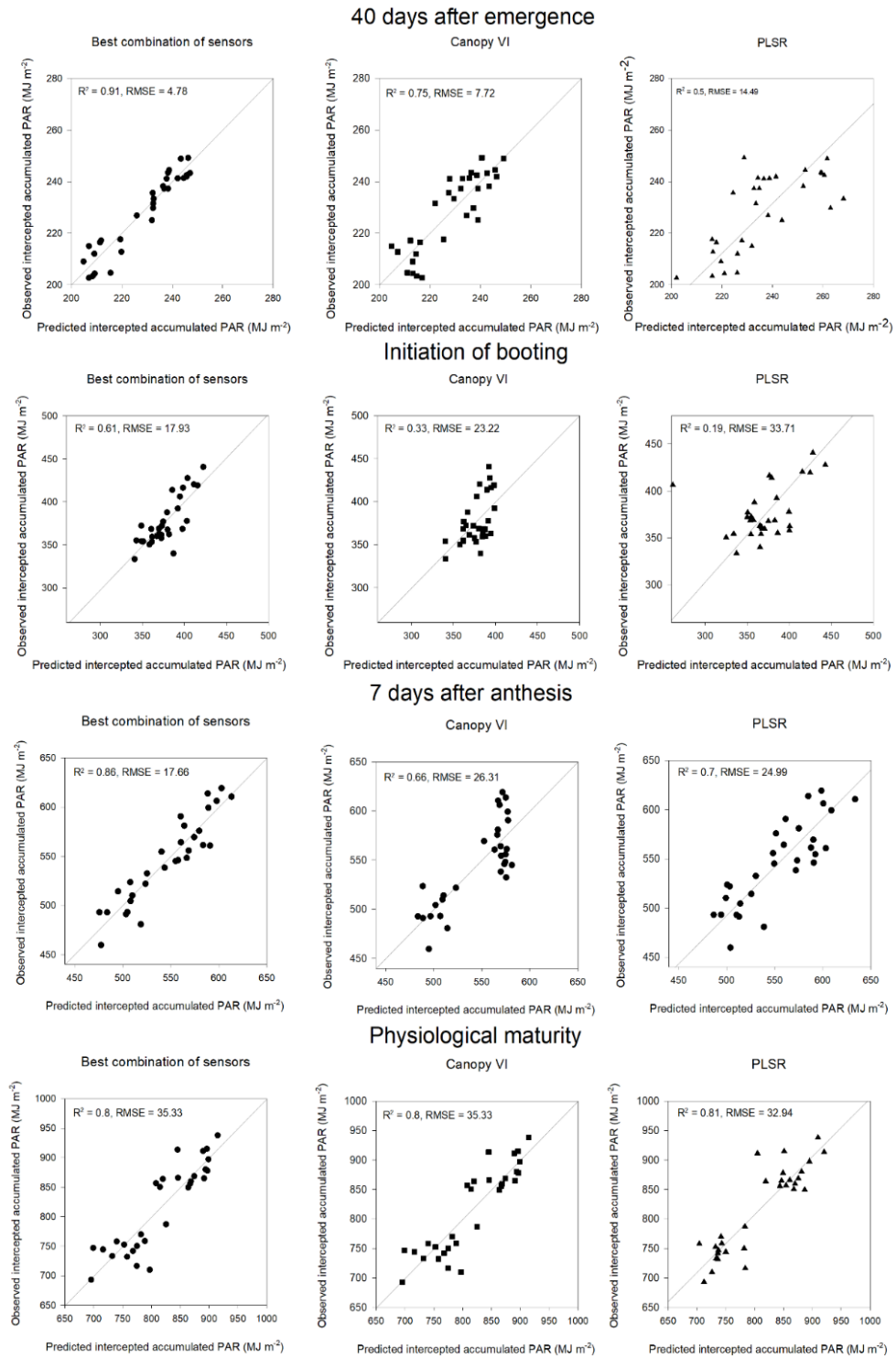
Figure 2.1. Intercepted accumulated PAR predictions with the different approaches used. Left panels represent predictions using the best combination of sensors (*bcs*), middle panel are predictions using vegetation indices derived from canopy reflectance (*cVI*) and the right panels represent predictions made with partial least square regression (PLSR).

IPAR_E40_*bcs* was predicted using a linear combination of CTvg and NDVIGSvg. This model had the best performance of all methods and growth stages for this trait with $R^2 = 0.91$ and RMSE of 4.78 MJ m^{-2}. In contrast, IPAR_E40_*cVI* was best predicted using NDWI-3 from the vegetative period and model performance was $R^2 = 0.75$ and RMSE of 7.72 MJ m^{-2}. With PLSR modelling the lowest $R^2 = 0.5$ and highest prediction error RMSE = 14.49 MJ m^{-2} were found for IPAR_E40 (Figure 2.1).

IPAR_InB_*bcs* was predicted using NDVIGSvg and PRIvg measured at the canopy level. Model performance was the lowest for this trait with $R^2 = 0.61$ and RMSE = 17.93 MJ m^{-2} (Table 2.3). IPAR_InB_*cVI* predictions were worse than IPAR_InB_*bcs*, but they were made only using the Optimised Soil Adjusted Vegetation Index (OSAVI) from the vegetative period with $R^2 = 0.33$ and RMSE = 23.22 MJ m^{-2}. PLSR predictions were poor when the canopy was not fully closed, and we hypothesise that this could be due to mixed reflectance from leaves and soil affecting IPAR predictions with this method (Figure 2.1).

IPAR_A7_*bcs* predictions were made using CTgf, PRIvg, GNDVI-1gf, and NDWI-4gf with $R^2 = 0.86$ and RMSE = 17.66 MJ m^{-2}. Two of these remote sensing traits are related to canopy water content, transpiration and plant water uptake (canopy temperature and NDWI-4) and one is related to LAI and canopy greenness (GNDVI-1) (Table 2.3, Figure 2.1). Predictions with *cVI* were made using PRI from the vegetative period and rNDVI from the grain filling period, model statistics were $R^2 = 0.66$ and RMSE = 26.31 MJ m^{-2}. PLSR predictions were better than *cVI* with RMSE = 24.99 MJ m^{-2} and $R^2 = 0.7$ (Figure 2.1).

IPAR_PM_*bcs* and IPAR_PM_*cVI* predictions were made using the same remote sensing traits, PRIvg, SAVIvg and SIPI-1gf, $R^2 = 0.8$ and RMSE = 35.33 MJ m^{-2} (Table 3). PLSR predictions at physiological maturity performed the best in comparison to the other growth stages for this method with $R^2 = 0.8$ and RMSE = 32.94 MJ m^{-2}. IPAR_PM can certainly be predicted by either of the three methods proposed here and obtain similar results (Figure 1).

2.5.2 Biomass

The best estimation of BM_E40_*bcs* resulted from the linear model using J$_{max}$ modelled in the third leaf during the vegetative period (JTLvg) with $R^2 = 0.2$ and RMSE = 24.53 g m^{-2}, whereas the linear combination of WI, NDVI and SAVI from the vegetative growth period resulted in the best estimations for and BM_E40_*cVI* with $R^2 = 0.17$ and RMSE = 25.83 g m^{-2} (Table 2.3). PLSR predictions at this growth stage performed worse compared to the other methods with $R^2 = 0.02$ and RMSE = 52.91 g m^{-2} (Figure 2.2). The use of leaf reflectance measurements to predict biomass at this growth stage performed better than predictions using canopy reflectance.

BM_InB_*bcs* was predicted using a combination of VIs measured above the canopy (NDWI-4canvg), flag leaf (GIFLvg) and third leaf (TCARITLvg). The model performance was $R^2 = 0.42$ and RMSE = 53.35 g m^{-2} (Table 2.3, Figure 2.2). BM_InB_*cVI* predictions were made with NDWI-4 and TCARI measured at the vegetative period ($R^2 = 0.34$, RMSE = 55.8 g m^{-2}). PLSR predictions were the worst of the three methods at GS41 having less accuracy and the highest error with $R^2 = 0.19$ and RMSE = 82.12 g m^{-2} (Figure 2.2).

50

BM_A7_*bcs* was predicted using PRI measured above the canopy during the vegetative period and in the flag leaf during the grain filling period (PRIcanvg, PRIFLgf). Model performance was $R^2 = 0.32$ and RMSE = 76.92 g m^{-2} (Figure 2.2). BM_A7_*cVI* was predicted using PRI from the vegetative period (PRIcanvg). Predictions were less accurate ($R^2 = 0.18$, RMSE = 83.18 g m^{-2}) compared to *bcs* but it was noteworthy that for both linear methods PRI was the common index used (Figure 2.2, Table 2.3) and PLSR predictions performed worst compared to the other methods ($R^2 = 0$, RMSE = 98.38 g m^{-2}) (Figure 2.2).
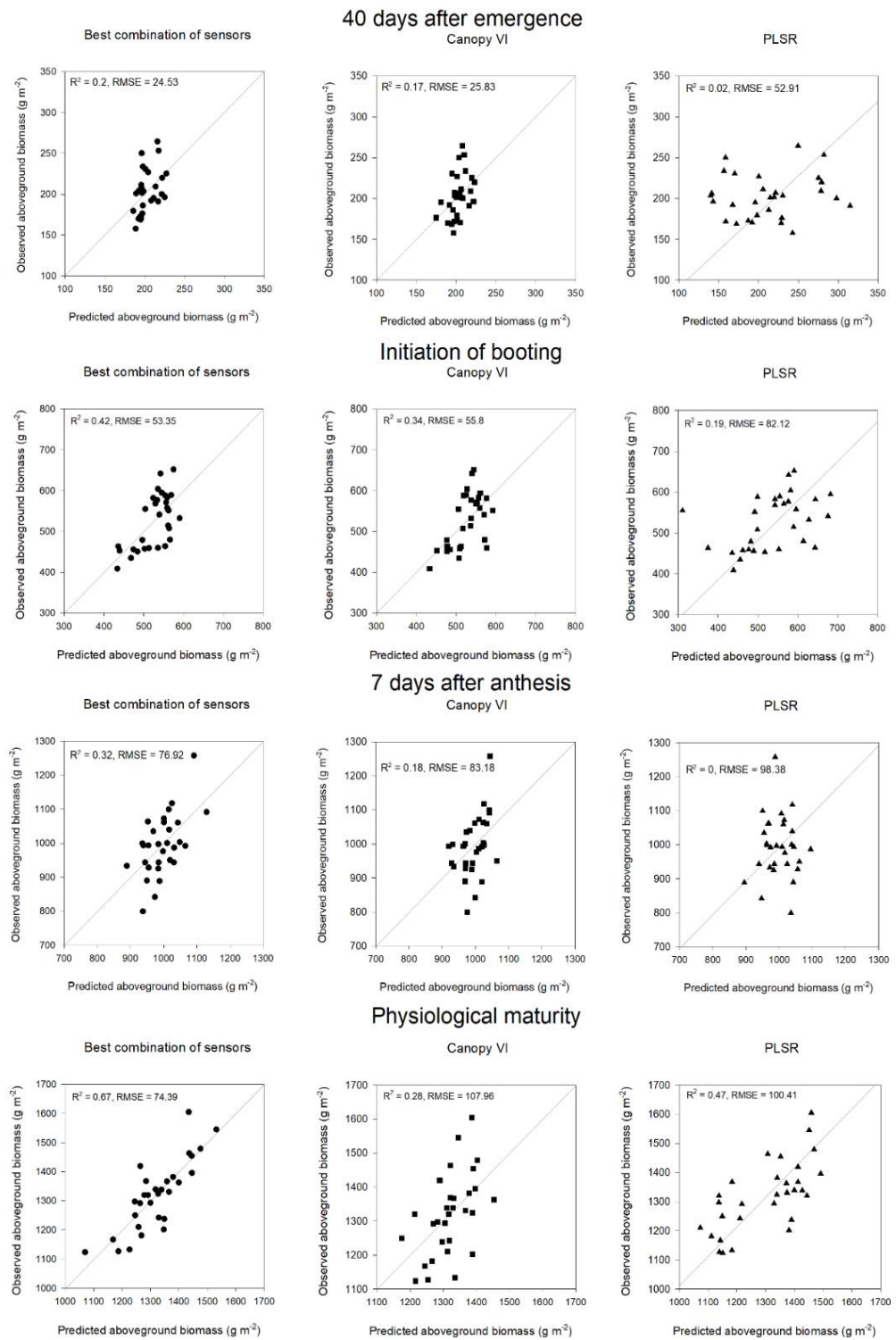
Figure 2.2. Aboveground biomass predictions with the different approaches used. Left panels represent predictions using the best combination of sensors (*bcs*), middle panel are predictions using vegetation indices derived from canopy reflectance (*cVI*) and the right panels represent predictions made with partial least square regression (PLSR).

2.5.3 Radiation use efficiency
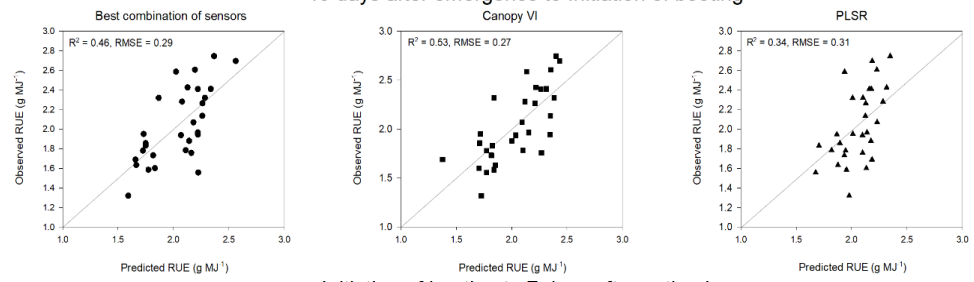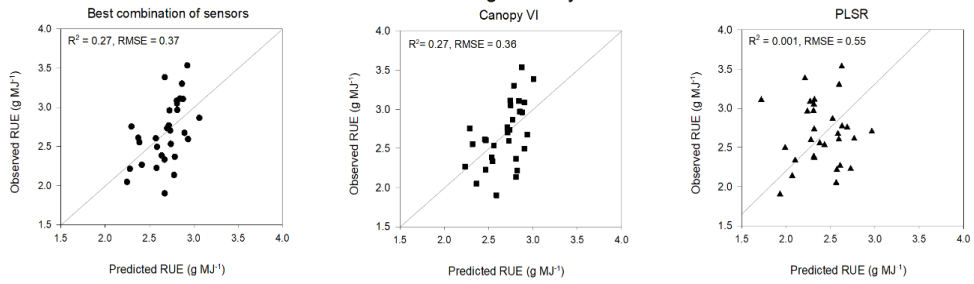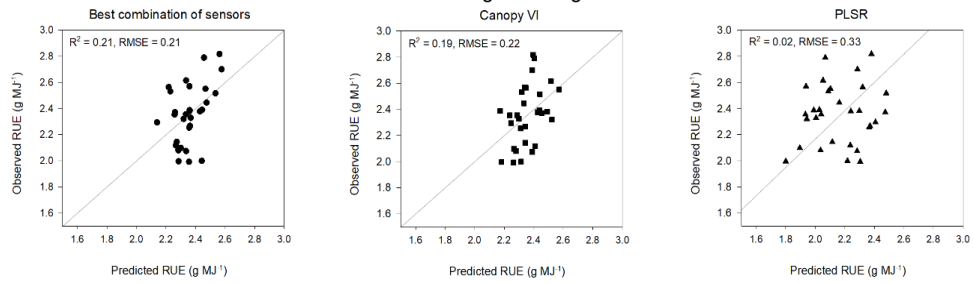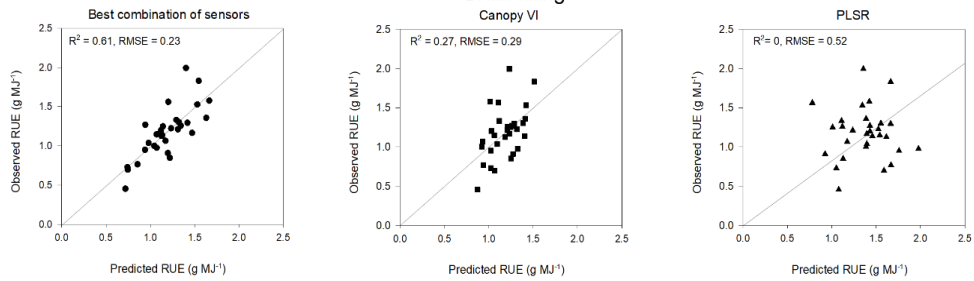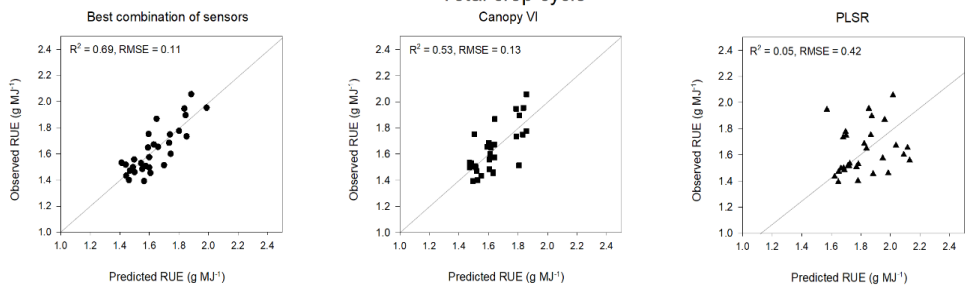
Figure 2.3. Radiation use efficiency predictions with the different approaches used. Right panels represent predictions using the best combination of sensors (*bcs*), middle panel are predictions using vegetation indices with canopy reflectance (*cVI*) and the left panels represents predictions made with partial least square regression (PLSR).

BM_PM_*bcs* predictions were the most accurate of the three methods at physiological maturity with $R^2 = 0.67$ and RMSE = 74.39 g m^{-2} (Table 2.3). BM_PM_*cVI* was predicted using pigment indices, these predictions were the least accurate of this growth stage for any method with $R^2 = 0.28$ and RMSE = 107.96 g m^{-2}. PLSR predictions were more accurate than *cVI* with $R^2 = 0.47$ and RMSE = 100.41 g m^{-2} (Figure 2.2).

From 40 days after emergence to initiation of booting (RUE_E40InB_*bcs*) was predicted using water and chlorophyll indices (Table 2.3), predictions with this method at this growth stage were less accurate in comparison to the other methods $R^2 = 0.29$ and RMSE = 0.46 g MJ^{-1} (Figure 2.3). RUE_E40InB_*cVI* predictions were the best at this growth stage ($R^2 = 0.53$ and RMSE 0.27 g MJ^{-1}. Vegetation indices used for this method were related to chlorophyll (PSSRbvg) and water content (WIvg). PLSR model performed better than *bcs* at this growth stage ($R^2 = 0.34$, RMSE = 0.31 g MJ^{-1}) (Figure 3), but in general in all the traits predicted in this study PLSR modelling produced less accurate results compared to *bcs* or *cVI* models (Figure 2.3, Table 2.3).

RUE_InBA7_*bcs* was predicted using NDWI-3 measured above the canopy, EVI and TCARI$_{705}$ at the third leaf (NDWI-3canvg, EVITLvg, TCARI$_{705}$TLvg). RUE_InBA7_*cVI* was predicted using NDWI-3 and EVI measured at the vegetative period. Both models performed the same with $R^2 = 0.27$ and RMSE = 0.37 g MJ^{-1} (Table 2.3) and were better compared to PLSR estimations $R^2 = 0$ and RMSE = 0.55 g MJ^{-1} (Figure 2.3).

RUE_preGF_*bcs* was predicted using the chlorophyll content of the third leaf measured with a SPAD meter (Table 2.3). The model estimations with this

method resulted in poor estimations with $R^2 = 0.21$ and RMSE = 0.21 g MJ^{-1} (Figure 2.3) but in return this model is the easiest to build as only uses measurements from a sensor very easy to deploy in the field. RUE_preGF_*cVI* model performance was similar to *bcs* (Table 2.3) with $R^2 = 0.19$ and RMSE = 0.22 g MJ^{-1}. All RUE predictions with *bcs* method at the vegetative period (RUE_E40InB, RUE_InBA7, RUE_preGF) were predicted with traits related to chlorophyll content in the bottom of the canopy. PLSR estimations were the worst of the three methods with $R^2 = 0.02$ and RMSE = 0.33 g MJ^{-1} (Figure 2.3).

RUE_GF_*bcs* estimations were the best with $R^2 = 0.61$ and RMSE = 0.23 g MJ^{-1} but also was the model that used most variables which can reduce the applicability on field conditions (Table 2.3). RUE_GF_*cVI* estimations were outperformed by the *bcs* model but we found a trend at grain filling where VI related to chlorophyll content and gas exchange were used to predict IPAR and biomass (Table 2.3). PLSR predictions at grain filling were the worst for any model at any given growth stage with $R^2 = 0$ and RMSE = 0.52 g MJ^{-1} (Figure 3).

RUE_Total_*bcs* predictions were made with NDWI-2 measured above the canopy, CUR from the second leaf measured on the vegetative stage, and NPCI from the third leaf measured during the grain filling period (NDWI-2canvg, CURSLvg, NPCITLgf) (Table 2.3). Our results show the predictions with *bcs* model at physiological maturity were the most accurate of any growth stages/methods used ($R^2 = 0.69$, RMSE = 0.11 g MJ^{-1}) for RUE, in comparison RUE_Total_*cVI* had lower accuracy in the predictions but similar RMSE ($R^2 = 0.53$, RMSE = 0.13 g MJ^{-1}), which indicates that RUE predictions could be done

faster just by using VI at the canopy scale and results will not differ much from

the *bcs* method.

Table 2.3. Models used to predict radiation use efficiency, biomass and PAR interception at the different growth stages measured in this study. Two models are presented for each trait, the first is the best combination of sensors (*bcs*) and the second hyperspectral measurements at the canopy level (*cVI*). bv = 10 best values from each trait.

Trait	Model	R^2	Adj. R^2	RMSE	R^2_bv	RMSE_bv
RUE_E40InB	$-9.347 + 12.906WIcanvg - 4.004NDVITLvg - 0.795TCARITLvg$	0.46	0.4	0.29	0.02	0.26
	$-15.443 - 0.0674PSSRb\_vg + 16.469WI\_vg$	0.53	0.5	0.27	0.31	0.28
RUE_InBA7	$-1.791 + 13.247NDWI\text{-}3canvg + 4.721EVITLvg + 6.656TCARI_{705}TLvg$	0.27	0.19	0.37	0.45	0.28
	$7.543 + 28.717NDWI\text{-}3\_vg - 3.123EVI\_vg$	0.27	0.22	0.36	0.17	0.35
RUE_preGF	$0.47 + 0.0446SPADTLvg$	0.21	0.18	0.21	0.53	0.16
	$19.762 + 0.0389CRI\_vg - 22.547NDVI\_vg + 10.455NDWI\_vg + 53.698PRI\_vg$	0.19	0.06	0.22	0.01	0.25
RUE_GF	$-2.523 - 10.05VARIcanvg - 4.661RARSacangf + 16.258SIPI\text{-}1TLvg + 1.17GITLgf - 0.0112JFLgf - 0.0401Vc_{max}/N_{area}SLvg$	0.61	0.51	0.23	0.55	0.18
	$3.886 - 79.296PRI\_vg - 0.675GI\_gf$	0.27	0.22	0.29	0.01	0.36
RUE_Total	$5.972 - 15.681NDWI\text{-}2canvg - 5.458CURSLvg + 2.21NPCITLgf$	0.69	0.65	0.11	0.85	0.05

	$0.845 + 0.992RGR\_gf$	0.53	0.51	0.13	0.23	0.15
BM_E40	$294.202 - 0.394JTLvg$	0.2	0.17	24.53	0.01	31.07
	$56.67 + 610.986WI\_vg - 844.888NDVI\_vg + 308.836SAVI\_vg$	0.17	0.07	25.83	0.09	31.4
BM_InB	$89.423 - 220.49NDWI\text{-}4canvg + 213.15GIFLvg - 344.448TCARITLvg$	0.42	0.35	53.35	0.09	56.14
	$-206.393 - 7575.28NDWI\text{-}4\_vg + 737.072TCARI\_vg$	0.34	0.29	55.8	0.03	64.26
BM_A7	$435.468 + 14412.02PRIcanvg + 9039.943PRIFLgf$	0.32	0.27	76.92	0.31	85.28
	$696.304 + 15902.35PRI\_vg$	0.18	0.15	83.18	0.38	88.51
BM_PM	$361.694 + 98.526PSSRaFLvg + 106.66RARSbSLvg - 1.52SIPI\text{-}2SLvg - 135.394SR\text{-}1TLvg$	0.67	0.62	74.39	0.38	77.12
IPAR_E40	$674.582 - 44.419CRI\_vg + 43.295PSSRa\_vg - 2.543SIPI2\_vg$	0.28	0.2	107.96	0.08	84.68
	$289.723 - 9.158CTvg + 168.407NDVIGSvg$	0.91	0.9	4.78	0.05	4.02

58

	$80.287 - 2056.97NDWI\text{-}3\_vg$	0.75	0.74	7.72	0.34	6.68
IPAR_InB	$26.039 + 306.267NDVIGSvg + 6808.693PRIcanvg$	0.61	0.58	17.93	0.4	17.49
	$-500.416 + 1051.142OSAVI\_vg$	0.33	0.31	23.22	0.09	28.59
IPAR_A7	$-875.05 + 36.048CTgf + 6718.306PRIcanvg + 509.163GNDVI\text{-}1cangf - 2997.16NDWI\text{-}4cangf$	0.86	0.84	17.66	0.63	15.57
	$618.021 + 6935.272PRI\_vg - 33.644rNDVI\_gf$	0.66	0.63	26.31	0.24	29.22
IPAR_PM	$40.181 + 12435.71PRIcanvg + 1050.561SAVIcanvg - 201.546SIPI\text{-}1cangf$	0.8	0.78	35.33	0.11	28.02
	$40.181 + 12435.71PRI\_vg + 1050.561SAVI\_vg - 201.546SIPI1\_gf$	0.8	0.78	35.33	0.11	28.02

Abbreviations: E40InB = 40 days after emergence to initiation of booting period, InBA7 = Initiation of booting to 7 days after anthesis period, preGF = pre grain filling period (40 days after emergence to 7 days after anthesis), GF = Grain filling period (7 days after anthesis to physiological maturity), Total = crop cycle, E40 = 40 days after emergence, InB = Initiation of booting, A7 = 7 days after anthesis, PM = Physiological maturity, RMSE = Root Mean Square Error, %var = percentage of variability between observed traits and predictions, can = measurement at canopy level, FL = measurement at the flag leaf, SL = measurement at the second leaf, TL = measurement at the third leaf.

2.6 Discussion

RUE is a key trait that underpins crop productivity due to its close relation with photosynthesis, biomass accumulation and yield and it is of great interest in breeding for higher yield potential (Murchie et al., 2009; Reynolds et al., 2012; Hubbart et al., 2018; Molero et al., 2019; Joynson et al., 2021). However, its complex nature caused by the interaction of several physiological processes affecting it at different growth stages and the difficulty to screen it in large field trials has not allowed physiologists and breeders to fully implement HTP approaches to predict it (Furbank et al., 2019). In this study a HTP approach is proposed and validated with ground truth data collected during three field growth cycles by combining different remote sensing techniques using hyperspectral reflectance to calculate vegetation indices and PLSR to develop statistical models that provide the flexibility to be tested in large wheat populations in yield potential conditions. Eventually this can be extended to populations grown under different environmental conditions (e.g. heat, drought and nutrient deficiency stresses) or in other important crops such as rice, barley, or rye.

The implementation of this methodology can reduce drastically the time and manual labour needed to measure RUE and its components. Field aboveground biomass harvests and ceptometer measurements take time and cost more resources than implementing a HTP method to assess RUE components and there is an opportunity to reduce the experimental error caused by different people sampling in the same experiment. If the data produced with these models coupled with UAV imaging plus a pipeline for data extraction and upscaling could shift the narrative in physiological breeding as genetic gains for this trait are not often seen due to its phenotyping bottleneck.

2.6.1 Physiological mechanisms underlying bcs and cVI models

Our models indicate that at the vegetative period, which encompasses the phenological stages from canopy closure to anthesis, two water indices (WI, NDWI) and NDVI were used to build models to predict RUE, biomass or IPAR (Figure 4). Water indices have been associated with biomass accumulation in wheat with very strong phenotypic correlations at the vegetative stages of booting and heading (Babar et al., 2006) which is within the period of our measurements for the vegetative stage. NDVI is an index that has been related to gas exchange capacity, N content, biomass and even yield by using canopy greenness as a proxy, as well as indicator of IPAR in the green tissues (termed as PAR_{green}) and this has been reported in several studies for perennial and annual plants (Gamon et al., 1995; Hatfield and Prueger, 2010; Tattaris et al., 2016; Duan et al., 2017; Hinojo-Hinojo and Goulden, 2020). Water indices are more sensitive to variations in LAI than NDVI, this means that during the vegetative period where LAI is larger in comparison to the grain filling stage in wheat (Calderini et al., 1997), water indices can be a better option than to predict RUE, biomass and IPAR than NDVI.

We suggest to use water indices over NDVI to predict biomass to reduce the confounding effects once the canopy closes and NDVI reaches values close to 0.9, which causes saturation of NDVI. In a physiological-breeding context this becomes a problem because during the vegetative stages there are not big differences between the phenological development of different wheat genotypes and the genotypic differences in NDVI might be negligible due to higher LAI at this growth period, while evidence indicate water indices correlate well with

biomass and most importantly are able to capture genotypic differences at GS41 (Babar et al., 2006; Prasad et al., 2009; Gutierrez et al., 2010).

During the grain filling period (GS65 to GS79) the common VIs to predict RUE and its components were PRI and SIPI. The relationship between PRI and RUE indicates that if PRI increases RUE will increase as well (higher PRI lower non photochemical quenching, NPQ), this implies that there could be a source limitation or source-sink co-limitation in these genotypes at grain filling (Acreche et al., 2009). PRI has been related to photosynthetic processes such as the xanthophyll cycle, NPQ, chlorophyll fluorescence, carotenoids/chlorophyll ratio and RUE measured at leaf and ecosystem scales. These photosynthetic processes play a key role for fast annual growth plants such as rice and wheat as it can increase productivity through biomass accumulation and photosynthetic rates by enhancing photoprotection in high-light environments by limiting photoinhibition (Hubbart et al., 2018), preventing the over-reduction of PSII and regulating the electron transport factors that can help optimise field CO_2 assimilation (Murchie and Ruban, 2020).
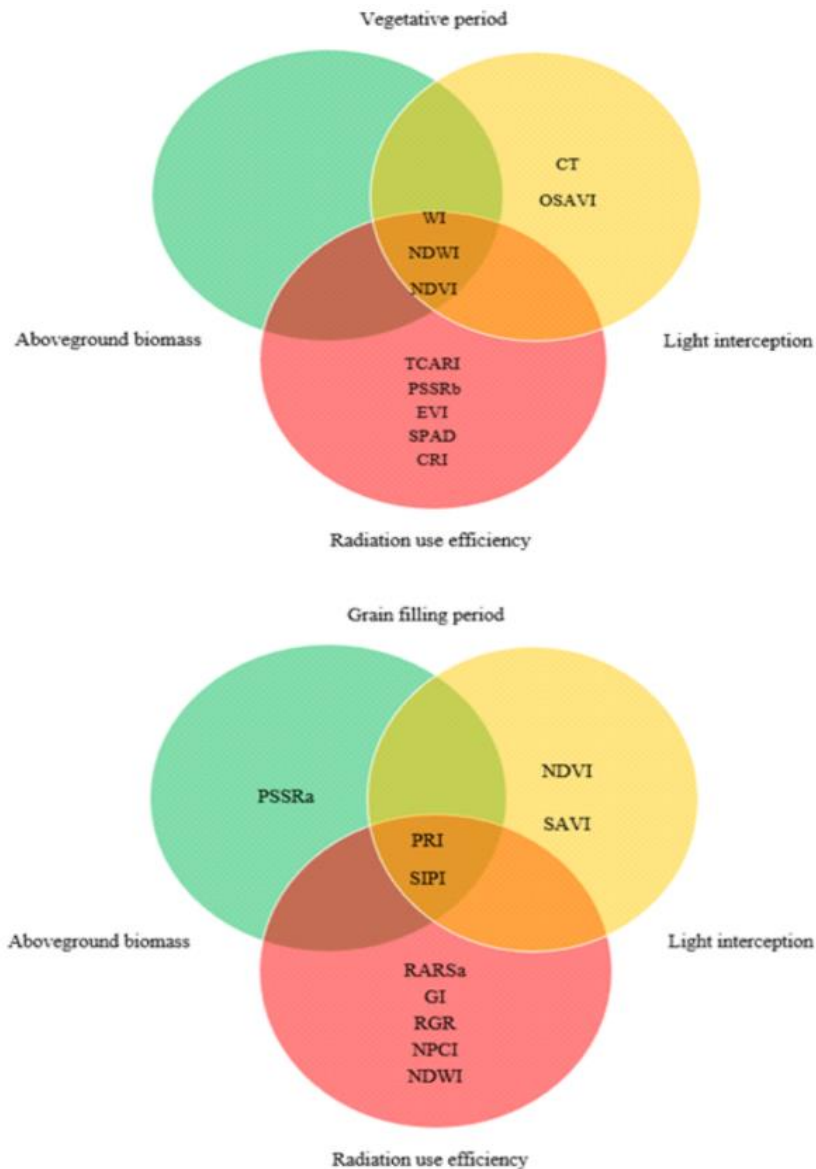
Figure 2.4. Venn diagram highlighting the correlation between remote sensing traits with aboveground biomass (green circle), light interception (yellow circle) and radiation use efficiency (red circle) during the vegetative (canopy closure to 7 days after anthesis) and grain filling period (7 days after anthesis to physiological maturity). Interactions represent remote sensing traits that correlate with various physiological traits.

Regressions of PRI with RUE have been found to be consistent across leaves, canopies and ecosystems with R^2 ranging from 0.4-0.75 (Garbulsky *et al.*, 2011). In wheat, using PRI alone was not enough to predict RUE or light use efficiency (LUE) due to drastic reduction in canopy chlorophyll content when the

senescence period starts (Wu *et al.*, 2010), but our results show that using PRI combined with VI that accounts chlorophyll content (VARI, RARSa, GI) and canopy senescence (SIPI) can improve the model predictions as shown in RUE_GF_*bcs* compared to RUE_GF_*cVI* (Table 3).

The activation of NPQ causes the reduction of long-term photosynthetic capacity particularly in top and middle parts of the canopy in erect genotypes where light availability can exceed the needs of photosynthesis. In addition, leaves in the lower part of the canopy should have rapid responses to changes in light caused by sun position through the day and wind movement (Murchie and Niyogi, 2011). Efficiently disengaging photoprotective NPQ during changes from high to low light is a mechanism that has been demonstrated to increase plant biomass up to 20% in tobacco compared to plants without this ability (Kromdijk et al., 2016). Additionally, slow responses of photosynthesis to increasing light could cost up to 21% of CO_2 assimilation in wheat (Taylor and Long, 2017).

Then it will be possible to increase RUE by designing a new wheat ideotype with a "smart canopy" for wheat with erect flag leaves to allow light penetration to lower (and usually shaded) parts of the canopy and to avoid light saturation, similarly to what has been proposed for sorghum canopies (Mantilla-Perez et al., 2020). Evidence found in wheat canopies indicate that erectophile genotypes can have up to 11% higher biomass and 24% higher yields compared to planophile genotypes (Richards et al., 2019) therefore, the addition of erectophile genotypes and the use of remote sensing models that correlate NPQ and PRI can become important in wheat physiological breeding to increase RUE, biomass and yield, especially because wheat is grown under contrasting light environments across different latitudes which still leaves the door open to optimise these traits.

The structural insensitive pigment index (SIPI) is correlated with the chlorophyll content and rate of senescence of the canopy. The use of this index in our models imply that canopies that can stay greener for longer periods of time will benefit from higher biomass and IPAR accumulation and increase RUE rates in the later stages of the crop cycle, where remobilisation of nutrients to the grains, optimal N distribution through the canopy and yield formation are critical (Foulkes and Murchie, 2011; Sinclair and Rufty, 2012). It has been suggested that developing canopies which can stay greener for longer periods of time will be one of the keystones for yield improvement in future warmer climates (Lopes and Reynolds, 2012). Although in this study models fitted better using SIPI instead of NDVI or SPAD measurements, which are usually the traits used for stay-green, this could suggest that VI related to chlorophyll or other pigment content could potentially be used interchangeably to score senescence which is closely correlated to IPAR (Figure 2.4).

2.6.2 Partial least square regression models

To our knowledge this is the first study where predictions of RUE, biomass and IPAR in field grown wheat are made with PLSR modelling. Previous attempts to predict genetic variation in physiological traits with this method have been made mostly at leaf scale considering only top of the canopy leaves. Traits such as A_{max}, gs, V_{cmax}, J_{max}, have been predicted successfully with R^2 of 0.49, 0.34, 0.74, 0.7, respectively in spring wheat (Silva-Pérez et al., 2018), V_{cmax} ($R^2 = 0.89$), J_{max} ($R^2 = 0.93$) and N leaf content per mass basis ($R^2 = 0.89$) on aspen and cotton (Serbin et al., 2012); V_{cmax} ($R^2 = 0.65$), N leaf content ($R^2 = 0.96$) and chlorophyll content ($R^2 = 0.85$) in maize (Yendrek et al., 2017), leaf dark

respiration (R^2 = 0.5-0.63), leaf N content (R^2 = 0.91) and LMA (R^2 = 0.75) (Coast et al., 2019).

Predictions of traits mentioned above at leaf level were more accurate in comparison to our predictions of RUE or biomass where in some cases no associations between predictions and observations were found, especially during the grain filling period (Figure 2.3, R^2 = 0). Our hypothesis for this poor performance of PLSR models is that RUE and biomass accumulation are more complex physiological processes in the hierarchical scale of yield than gas exchange in single leaf layers or organ stoichiometry, as these two might be affected by more physiological traits happening within the canopy, plus the effects of root physiology, biomass accumulation at different growth stages during the crop cycle and mixed signals from different canopy layers and vegetation plus soil. Most of the studies have used sunlit leaf measurements from the top of the canopy to upscale whole canopy physiological processes assuming that top layer is representative of the whole canopy (Gara et al., 2019). This is not true, especially in crop canopies where there is a very dynamic light environment caused by wind, gaps due to planting methods, poor stand establishment, lodging, pest and disease effects or even biomass harvests. The dynamic light environment can influence photosynthetic rates from leaves lower in the canopy and this could reduce or boost biomass accumulation and therefore RUE (Murchie et al., 2018).

This highlights the importance of using measurements which integrate the whole canopy instead of just the sunlit part of the canopy and in future studies the use of punctual reflectance measurements instead of averages might result in better PLSR predictions for the traits presented in this study. Arguments can be made

that measuring leaf reflectance from the different layers of the canopy could be used instead of measuring reflectance above the canopy to represent the canopy optical properties, but in a HTP physiological breeding context this would take much more time in the field than collecting ground truth data, negating the benefits of the methods and might not be worth doing as our results show that *cVI* models perform similarly to *bcs* models in most of the growth stages (Figure 2.5).
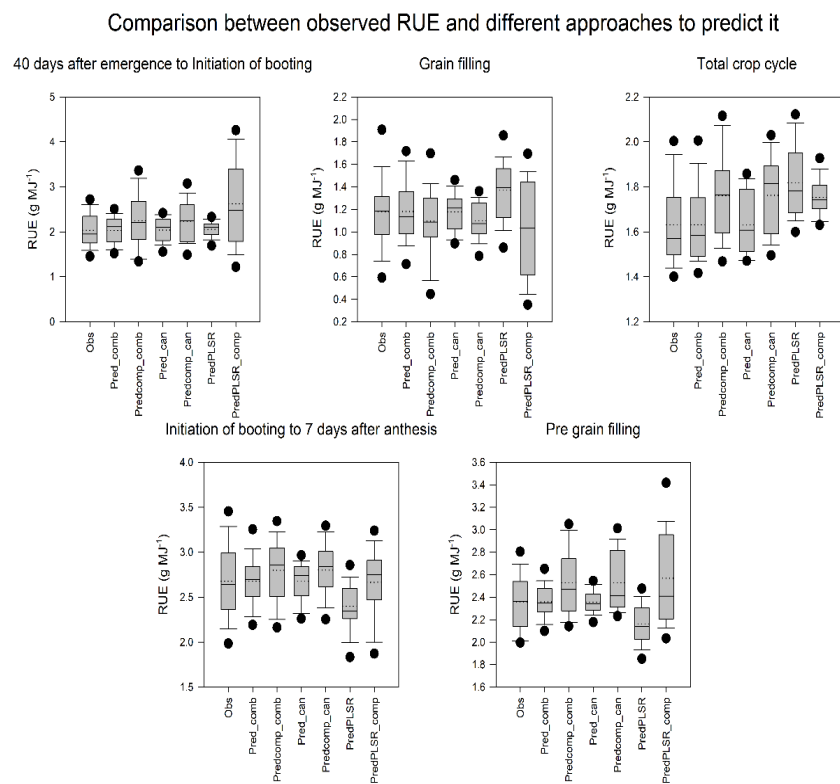
Figure 2.5. Comparison of the approaches to build the models used to predict radiation use efficiency in the different growth stages measured in the crop cycle. From left to right: Obs = ground truth data, Pred_comb = predictions with the best combination of sensors, Predcomp_comb = predictions with the estimated components from the best combination of sensors, Pred_can = predictions with vegetation indices calculated from canopy reflectance, Predcomp_can = predictions with the estimated components calculated with vegetation indices from canopy reflectance, PredPLSR = predictions with partial least squares regression with canopy reflectance and PredPLSR_comp = predictions with the estimated components calculated with partial least squares regression from canopy reflectance.

Models built using VIs from the literature were the most accurate predictors of RUE, biomass and IPAR in most of the growth stages (Figure 5). We suggest predicting RUE directly instead of estimating it from its components since predictions of biomass, IPAR carry their own source of error and then predicting RUE from those increases the error prediction further (Table 2.3). Using the models built with canopy VIs allowed us to capture the highest accuracy predicted values of RUE, biomass and IPAR indicating genotypes that could perform the best without increasing measurement time in the field, as measuring all the leaves from the canopy could have entailed, underlining the applicability of these models in physiological breeding programs.

2.7 Conclusions

2.7.1 Should we rely on remote sensing for studies of growth analysis?

This is the first effort to predict RUE in a HTP field based physiological breeding context in wheat with data collected across three different crop cycles. The approaches to predict RUE and its components showed acceptable level of accuracy (53% in the vegetative growth stage, 61% during grain filling and 69% considering the whole crop cycle) but we recognize that models can be improved by increasing the number of genotypes or including data from different environments. The models presented in this study have major implications for physiological breeding as improving C fixation through RUE represents the baseline to increase crop yields. We acknowledge that using remote sensing models cannot fully replace the collection of ground truth data but it can considerably reduce the amount of time (i.e. from 3 days of field work and lab

sample processing to 45 minutes measuring hyperspectral reflectance in the field) and resources spent especially on big trials where hundreds of lines could be screened in a matter of hours and be used in QTL or GWAS studies to bridge the gap between phenomics and genomics. In addition, the present approach could help to predict RUE and biomass in experiments where biomass sampling is not possible due to plot size (<1 m) typically used to select plant genetic resources in pre-breeding programs. Finally, the models built with data collected at leaf and canopy scale in this study can be used to refine C cycle models built with satellite imagery data and increase the link between remote sensing platforms to understand C cycle dynamics at the regional scale better.

Chapter 3 Contribution to yield of wheat photosynthesis at different canopy layers

Carlos A. Robles-Zazueta[1,2*], Gemma Molero[2,3], Francisco Pinto[2], Matthew P. Reynolds[2], Erik H. Murchie[1*]

[1]Division of Plant and Crop Sciences, School of Biosciences, University of Nottingham, Sutton Bonington Campus, Leicestershire, LE12 5RD, United Kingdom.

[2]Global Wheat Program, International Maize and Wheat Improvement Center (CIMMYT), carretera Mexico-Veracruz km 45, El Batan, Texcoco, Mexico. CP 56237.

[3]Current address: KWS Momont Recherche, 7 rue de Martinval, 59246 Mons-en-Pevele, France.

*Authors for correspondence: carlos.robleszazueta@nottingham.ac.uk, erik.murchie@nottingham.ac.uk

Abstract

Yield (grain weight) can be defined as the product of solar radiation intercepted throughout the crop cycle, radiation use efficiency (biomass accumulated per unit radiation intercepted, RUE) and harvest index. Photosynthesis is a central component of RUE but normally measured in the upper layers of the canopy where radiation is highest. Here we hypothesize that measurements made within the middle and bottom layers of wheat canopies will be key to understand the link between canopy photosynthesis and yield. The objectives of this study were to measure photosynthesis throughout the canopy to study the relationship of gas exchange with biomass, RUE and yield; and define which layer or combination of layers have a higher contribution to grain yield at different growth stages. Significant relationships were found between photosynthetic rates measured at saturating light (A_{sat}) and yield. A_{sat} at initiation of booting measured at the top ($R^2 = 0.33$, $p<0.1$), middle ($R^2 = 0.49$, $p<0.05$) and bottom ($R^2 = 0.44$, $p<0.05$) layers of the canopy resulted in positive relationships. When measured 7 days after anthesis, the strongest relationship was found between A_{sat} measured in the top leaf and yield ($R^2 = 0.62$, $p<0.001$). These findings indicate that there is an opportunity for yield improvement if we consider the requirements of photosynthesis in the middle and bottom layers of the canopy where light conditions are more dynamic.

Keywords: *canopy photosynthesis, leaf photosynthesis, yield improvement, physiological breeding, RUE*

3.1 Introduction

Wheat (*Triticum aestivum* L.) is the most widely grown crop worldwide accounting for ~30% of all sown area for cereals and ~ 40% of total cereal exports at 118 million tonnes (FAO, 2021). Increasing wheat yield is jeopardized by shifts in climate patterns which will cause wheat to be subjected to severe heat and extreme cold events more often in the largest producing regions of the planet (Langridge and Reynolds, 2021). The challenge of increasing wheat yield, without increasing cultivation area, coupled with the threats posed by climate change represent one of the toughest challenges' humanity will face this century.

3.1.1 Yield as a product of canopy photosynthesis

From a physiological standpoint, wheat yield is the product of the photosynthesis of the different layers of the canopy, the spikes and stems (Araus et al., 2021). Agronomically speaking yield can be defined as the product of radiation intercepted throughout the crop cycle, the efficiency of plants to convert radiation into biomass (i.e. radiation use efficiency, RUE) and the proportion grain weight in regard to biomass weight at physiological maturity (i.e. harvest index, HI) under yield potential conditions (Slafer, 2003; Murchie et al., 2009; Reynolds et al., 2012).

Recent reviews have asserted that increasing photosynthesis will be one of the best avenues to increase crop yield, including wheat (Horton, 2000; Long et al., 2004; Murchie et al., 2009, 2018; Zhu et al., 2010; Lawson et al., 2012; Reynolds et al., 2012; Faralli and Lawson, 2019; Evans and Lawson, 2020; Furbank et al., 2020; Simkin et al., 2020; and references therein), because leaf photosynthesis

is the primary source for carbohydrate accumulation in plants for most part of the growth cycle. However there are not clear indications of the association of photosynthesis and yield and empirical evidence has been contradictory (Table 3.1).

This could be explained because the majority of studies relating photosynthesis with source (biomass, RUE) or sink (yield) traits have mainly focused on short term measurements of light saturated photosynthesis in the sunlit layer of the canopy, usually the flag leaf in cereals and considering photosynthesis measurements only in flag leaves may not allow us to fully exploit both the genetic variability and the full phenotypic range of photosynthesis for yield improvement (Murchie et al., 2018). Measuring only in flag leaves has been justified in the past due to finding of associations between photosynthesis with high yielding varieties (Fischer et al., 1998), the lack of automated light sources of infrared gas analysers (IRGA) in the past and the low throughput of these measurements in the field. The emergence of high-throughput methods and the importance of coupling photosynthesis with growth analysis measurements justify the measurement of the different canopy layers.

Furthermore, there is a lack of studies coupling traditional growth analysis (relative growth rate, biomass accumulation) with canopy photosynthesis, as previous studies have focused mostly on wheat flag leaves (Pinto et al., 2017) or occasionally spike photosynthesis (Molero and Reynolds, 2020) but to date no study has tried to dissect different leaf layers within the canopy and their relationship to yield in field conditions.

3.1.2 Photosynthesis and light distribution within canopies

Yield formation is a product of the integral of photosynthesis from different leaf positions within the canopy, each of which are exposed to different micro-environmental conditions. Canopy photosynthesis models partially consider this (e.g. WIMOVAC, APSIM, CAPTS; Casadebaig et al., 2016; Song et al., 2017; Wang et al., 2019) and it has long been suggested that photosynthetic traits from bottom layers of the canopy could have a large role in improving biomass accumulation and yield in wheat and rice (Burgess et al., 2019; Foo et al., 2020; Salter et al., 2020). However, our empirical understanding of this function beyond models of canopy photosynthesis is very limited.

Light is extinguished from the top to the bottom of the canopy in an exponential fashion which is normally aligned with both N content and leaf photosynthetic capacity (Hirose, 2005; Hikosaka, 2016). Lower canopy layers are characterized by low irradiance which can be subjected to light levels close to compensation point alternating with brief periods of high light availability. High photosynthetic productivity could therefore arise from efficient acclimation to low light (e.g. low respiration rates) and the efficient exploitation of these periods of high light (Kromdijk et al., 2016). Additionally, it has been shown that bottom layers of canopies not only support photosynthesis but acts as a N sink which can be remobilized to the upper leaves and grains during grain filling when light interception in this layer is limited by senescence (Lemaire et al., 2007) and this has been confirmed by ray tracing modelling coupled to 3D canopy reconstructions (Burgess et al., 2016; Townsend et al., 2018).

It will be important to fully understand the physiological mechanisms of adjustment and regulation (acclimation) of wheat photosynthetic machinery to

different light levels, temperature and N distribution, factors which can be highly heterogeneous within a canopy. One of the most important light adjustment mechanisms is the response to sun flecks, which are transitions from low to high light conditions in matter of seconds or minutes characterized by an increase of direct or diffuse radiation, especially at bottom layers of the canopy (Porcar-Castell and Palmroth, 2012), and represent an important light resource as they can boost photosynthesis rates (Pearcy, 1990; Murchie and Niyogi, 2011) if they are sufficiently frequent (Burgess et al., 2018).

3.1.3 Photosynthesis relationship with plant growth

As mentioned previously, the relationship between gas exchange traits (including light saturated photosynthetic CO_2 assimilation [A_{sat}], stomatal conductance [gs] and dark respiration [R_d]) and yield are inconsistent (Table 3.1). This may be due to a number of factors including the role of dynamic photosynthesis responses, phenology and source-sink interactions. Carmo-Silva et al., (2017) found a strong link with HI and yield when flag leaf assimilation was measured at 1000 µmol m^{-2} s^{-1}, which in tropical or subtropical latitudes are the upper end of radiation levels expected to be measured in the middle layer of wheat canopies, and in comparison, flag leaf A_{sat} did not correlate with HI or yield. These results could explain why even though genetic variation in photosynthetic capacity has been found under field conditions (Driever et al., 2014) no consistent relationships are yet to be described in most studies which focus only in A_{sat} at the top layer. Even though there have been previous efforts of addressing canopy photosynthesis in the field specially with modelling or flux chambers (Zhu et al., 2012; Song et al., 2016; Wu et al., 2018) these studies have

not explored the importance of each individual leaf layer and their contribution to important agronomic traits such as biomass or yield.

3.2 Hypothesis

It has been stated that the best route to improve RUE and yield photosynthetic rates need to increase. Canopy architecture plays a role in the distribution of light within wheat canopies. We expect genotypes with erect flag leaves and broadened middle and bottom leaves to have higher RUE and yield compared to erect genotypes which usually have smaller leaf area. Therefore, we hypothesize that photosynthetic rates from the middle and bottom layers of wheat canopies will be key to understand the link between canopy photosynthesis, light distribution and yield.

3.3 Objectives

Due to the absence of studies considering different layers of the canopy and the lack of understanding of the role of individual wheat canopy layers for biomass accumulation, RUE and yield; the objectives of this study were to define which layer or combination of canopy layers can explain the variation in biomass, RUE and yield to aid in the selection of photosynthetic traits and improve our understanding of the interaction between canopy architecture and light distribution with yield.

Table 3.1. Relationships between gas exchange traits (CO_2 assimilation under light saturating conditions [A_{sat}], stomatal conductance [gs] and dark respiration [R_d]) with yield, and aboveground biomass. YP: Yield potential, F: Field, AE [CO_2]: Atmospheric and elevated [CO_2], GC: Growth chamber, DNT: Different N treatments, D: Drought, HNT: High night temperature, WW: Well-watered. Where the study did not specifically look for links between A_{sat}, gs or R_d with biomass and/or yield the tool WebPlotDigitizer (http://arohatgi.info/WebPlotDigitizer) was used to extract the values and calculate the regression coefficient between the variables. When not specified, the photosynthetic measurements were done in the uppermost leaf at the specific growth stage measurement took place.

Trait	Yield	Biomass_PM	Crop	Environment	Reference
A_{sat}	$r^2 = 0.33$, $p<0.1$ (top layer at InB)	$r^2 = 0$ (top layer at InB)	Wheat	YP (F)	This study
	$r^2 = 0.49$, $p<0.05$ (middle layer InB)	$r^2 = 0.18$ (middle layer InB)			
	$r^2 = 0.44$, $p<0.05$ (bottom layer InB)	$r^2 = 0.07$ (bottom layer InB)			
	$r^2 = 0.62$, $p<0.001$ (top layer at A7)	$r^2 = 0.02$ (top layer at A7)			
	$r^2 = 0.07$ (middle layer A7)	$r^2 = 0.25$ (middle layer A7)			
	$r^2 = 0.26$ (bottom layer A7)	$r^2 = 0.05$ (bottom layer A7)			
	$r^2 = 0.3$, $p<0.1$ (canopy InB)	$r^2 = 0.23$ (canopy InB)			
	$r^2 = 0.19$ (canopy A7)	$r^2 = 0$ (canopy A7)			
	$r^2 = 0.4$, $p<0.01$	$r^2 = 0.37$, $p<0.01$	Cassava	YP (F)	El-Sharkawy et al., (1990)
	$r^2 = 0.35$, $p<0.01$ (panicle initiation WW)	$r^2 = 0.32$, $p<0.01$ (panicle initiation WW)	Sorghum	YP and D (F)	Peng et al., (1991)
	$r^2 = 0.86$, $p<0.01$ (mid-development WW)	$r^2 = 0.83$, $p<0.01$ (mid-development WW)			
	$r^2 = 0.53$, $p<0.01$ (head exertion WW)	$r^2 = 0.46$, $p<0.01$ (head exertion WW)			
	$r^2 = 0.74$, $p<0.001$ (avg WW)	$r^2 = 0.67$, $p<0.001$ (avg WW)			
	$r^2 = 0.25$, $p<0.05$ (panicle initiation D)	$r^2 = 0.36$, $p<0.05$ (panicle initiation D)			
	$r^2 = 0.44$, $p<0.01$ (mid-development D)	$r^2 = 0.55$, $p<0.01$ (mid-development D)			
	$r^2 = 0.13$ (head exertion D)	$r^2 = 0.15$ (head exertion D)			
	$r^2 = 0.5$, $p<0.001$ (avg D)	$r^2 = 0.66$, $p<0.001$ (avg D)			
	$r^2 = 0$ (WW)	$r^2 = 0.01$ (WW)	Wheat	YP and D (F)	Wada et al., (1994)
	$r^2 = 0.4$, $p<0.01$ (D)	$r^2 = 0.53$, $p<0.01$ (D)			
	$r^2 = 0.13$ (pre-anthesis)	$r^2 = 0.25$ (pre-anthesis)	Wheat	YP (F)	Gent (1995)
	$r^2 = 0.84$, $p<0.001$ (post-anthesis)	$r^2 = 0.74$, $p<0.001$ (post-anthesis)			
	$r^2 = 0.85$, $p<0.05$	$r^2 = 0.07$	Wheat	YP (F)	Fischer et al., (1998)
	$r^2 = 0$		Wheat	YP (F)	Lu et al., (1998)
	$r^2 = 0.28$, $p<0.05$	$r^2 = 0.64$, $p<0.01$	Wheat	YP (F)	Gutiérrez-Rodríguez et al., (2000)

$r^2 = 0.73$, $p < 0.01$	$r^2 = 0.36$, $p < 0.01$	Wheat	YP (F)	Reynolds et al., (2000a)
$r^2 = 0.52$, $p < 0.001$ (mid-stem elongation)	$r^2 = 0.03$ (mid-stem elongation)	Wheat	YP (F)	Jiang et al., (2003)
$r^2 = 0.31$, $p < 0.05$ (late stem elongation)	$r^2 = 0.01$ (late stem elongation)			
$r^2 = 0.19$, $p < 0.1$ (heading)	$r^2 = 0.13$ (heading)			
$r^2 = 0.44$, $p < 0.01$ (anthesis)	$r^2 = 0.01$ (anthesis)			
$r^2 = 0.28$, $p < 0.05$ (soft dough)	$r^2 = 0$ (soft dough)			
$r^2 = 0.04$ (hard dough)	$r^2 = 0.01$ (hard dough)			
$r^2 = 0.3$, $p < 0.05$ (cycle average)	$r^2 = 0.03$ (cycle average)			
	$r^2 = 0.99$, $p < 0.001$ (ambient CO_2)	Rice	AE [CO_2]	Sakai et al., (2006)
	$r^2 = 0.99$, $p < 0.001$ (elevated CO_2)			
	$r^2 = 0.04$	Wheat	YP (F)	Chytyk et al., (2011)
$r^2 = 0.42$, $p < 0.01$ (grain filling)		Wheat	YP (F)	Zheng et al., (2011)
$r^2 = 0.12$	$r^2 = 0.07$	Wheat	YP (F)	Driever et al., (2014)
	$r^2 = 0.23$	Wheat	YP (GC)	Pang et al., (2014)
$r^2 = 0.56$, $p < 0.05$ (heading, WW)		Wheat	YP and D (F)	Sun et al., (2014)
$r^2 = 0.01$ (3 days after anthesis, WW)				
$r^2 = 0.26$ (20 days after anthesis, WW)				
$r^2 = 0.49$ (heading, D)				
$r^2 = 0$ (3 days after anthesis, D)				
$r^2 = 0.12$ (20 days after anthesis, D)				
$r^2 = 0.49$ (jointing)	$r^2 = 0.02$ (jointing)	Wheat	YP (F)	Chen and Hao (2015)
$r^2 = 0.01$ (anthesis)	$r^2 = 0.15$ (anthesis)			
$r^2 = 0.34$ (grain filling)	$r^2 = 0.05$ (grain filling)			
$r^2 = 0.23$ (average)	$r^2 = 0.07$ (average)			
$r^2 = 0.38$ (WW high N)	$r^2 = 0.02$ (WW high N)	Wheat	DNT (GC)	Barbour and Kaiser, (2016)
$r^2 = 0.19$ (D high N)	$r^2 = 0.86$ (D high N)			
$r^2 = 0.42$ (WW adequate N)	$r^2 = 0.01$ (WW adequate N)			
$r^2 = 0$ (D adequate N)	$r^2 = 0$ (D adequate N)			
$r^2 = 0.98$ (average)	$r^2 = 0.89$ (average)	Rice	DNT (F)	Huang et al., (2016)
$r^2 = 0.93$ (moderate N); $r^2 = 0.98$ (high N)	$r^2 = 0.86$ (moderate N)			

	$r^2 = 0.92$ (high N)			
$r^2 = 0.01$ (spike, heading)	$r^2 = 0.18$ (spike, heading)	Wheat	YP (GH)	Zhou et al., (2016)
$r^2 = 0.28$ (flag leaf, heading)	$r^2 = 0.38$ (flag leaf, heading)			
$r^2 = 0.76$ (spike, grain filling)	$r^2 = 0.91$ (spike, grain filling)			
$r^2 = 0.2$ (flag leaf, heading)	$r^2 = 0.14$ (flag leaf, heading)			
$r^2 = 0.39$ (spike, average)	$r^2 = 0.55$ (spike, average)			
$r^2 = 0.24$ (flag leaf, average)	$r^2 = 0.26$ (flag leaf, average)			
$r^2 = 0.75$, $p<0.001$ (pre-anthesis)	$r^2 = 0.63$, $p<0.001$ (pre-anthesis)	Wheat	DNT (F)	Gaju et al., (2016)
$r^2 = 0.76$, $p<0.001$ (post-anthesis)	$r^2 = 0.59$, $p<0.001$ (post-anthesis)			
$r^2 = 0$ (A_{sat})	$r^2 = 0$	Wheat	YP (F)	Carmo-Silva et al., (2017)
$r^2 = 0.27$, $p<0.05$ (A_{Q1000}, pre-anthesis)				
$r^2 = 0.27$, $p<0.05$ (A_{Q1000}, post-anthesis)				
$r^2 = 0.55$ (400 ppm CO_2)	$r^2 = 0.81$ (400 ppm CO_2)	Wheat	YP (GC)	Driever et al., (2017)
$r^2 = 0.43$ (1300 ppm CO_2)	$r^2 = 0.6$ (1300 ppm CO_2)			
$r^2 = 0.08$ (A_{Q1800}, pre-anthesis)	$r^2 = 0.37$, $p<0.05$	Wheat	YP (GH)	Pennachi et al., (2018)
$r^2 = 0.08$ (A_{Q1000}, pre-anthesis)				
$r^2 = 0.08$ (A_{Q500}, pre-anthesis)				
$r^2 = 0.08$ (A_{Q250}, pre-anthesis)				
$r^2 = 0.05$ (A_{Q100}, pre-anthesis)				
$r^2 = 0.03$ (A_{Q1800}, post-anthesis)				
$r^2 = 0.04$ (A_{Q1000}, post-anthesis)				
$r^2 = 0.03$ (A_{Q500}, post-anthesis)				
$r^2 = 0.01$ (A_{Q250}, post-anthesis)				
$r^2 = 0.01$ (A_{Q100}, post-anthesis)				
$r^2 = 0.39$ (spike, average)				
$r^2 = 0.24$ (flag leaf, average)				
$r^2 = 0.23$ (HNT)	$r^2 = 0.27$ (HNT)	Wheat	HNT and YP (GC)	Impa et al., (2019)
$r^2 = 0.03$ (control)	$r^2 = 0.54$ (control)			
$r^2 = 0.9$, $p<0.01$		Rice	YP (F)	Chen et al., (2020)
$r^2 = 0.12$ (spike)		Wheat	YP (F)	Molero and Reynolds (2020)
$r^2 = 0.17$ (flag leaf)				
$r^2 = 0.64$, $p<0.05$ (spike photosynthesis)	$r^2 = 0.9$, $p<0.01$ (spike photosynthesis)	Wheat	YP (GH)	Elazab et al., (2021)

			Crop	Trait	Reference
	$r^2 = 0.36$ (flag leaf photosynthesis)	$r^2 = 0.33$ (flag leaf photosynthesis)			
gs	$r^2 = 0.04$ (top layer at InB) $r^2 = 0.05$ (middle layer InB) $r^2 = 0$ (bottom layer InB) $r^2 = 0.01$ (top layer at A7) $r^2 = 0$ (middle layer A7) $r^2 = 0.07$ (bottom layer A7) $r^2 = 0.04$ (canopy InB) $r^2 = 0.01$ (canopy A7)	$r^2 = 0.05$ (top layer at InB) $r^2 = 0.14$ (middle layer InB) $r^2 = 0.07$ (bottom layer InB) $r^2 = 0.21$ (top layer at A7) $r^2 = 0.52$, $p<0.01$ (middle layer A7) $r^2 = 0.21$ (bottom layer A7) $r^2 = 0.03$ (canopy InB) $r^2 = 0.34$, $p<0.1$ (canopy A7)	Wheat	YP (F)	This study
	$r^2 = 0.03$	$r^2 = 0.01$	Cassava	YP (F)	El-Sharkawy et al., (1990)
	$r^2 = 0.85$, $p<0.001$	$r^2 = 0.01$	Wheat	YP (F)	Fischer et al., (1998)
	$r^2 = 0.86$, $p<0.001$		Wheat	YP (F)	Lu et al., (1998)
	$r^2 = 0.28$, $p<0.05$	$r^2 = 0.58$, $p<0.01$	Wheat	YP (F)	Gutiérrez-Rodríguez et al., (2000)
	$r^2 = 0.72$, $p<0.01$	$r^2 = 0.45$, $p<0.01$	Wheat	YP (F)	Reynolds et al., (2000a)
	$r^2 = 0.53$, $p<0.001$ (mid-stem elongation) $r^2 = 0.24$, $p<0.05$ (late stem elongation) $r^2 = 0.27$, $p<0.05$ (heading) $r^2 = 0.26$, $p<0.05$ (anthesis) $r^2 = 0.21$ (soft dough) $r^2 = 0.12$ (hard dough) $r^2 = 0.27$, $p<0.05$ (cycle average)	$r^2 = 0.09$ (mid-stem elongation) $r^2 = 0.24$, $p<0.05$ (late stem elongation) $r^2 = 0.01$ (heading) $r^2 = 0.07$ (anthesis) $r^2 = 0$ (soft dough) $r^2 = 0.01$ (hard dough) $r^2 = 0.07$ (cycle average)	Wheat	YP (F)	Jiang et al., (2003)
		$r^2 = 0.25$ (jointing) $r^2 = 0$ (flowering) $r^2 = 0.01$ (grain filling) $r^2 = 0.08$ (average)	Wheat	YP (F)	Chytyk et al., (2011)
	$r^2 = 0.48$, $p<0.01$		Wheat	YP (F)	Zheng et al., (2011)
		$r^2 = 0.78$	Wheat	YP (F)	Pang et al., (2014)
	$r^2 = 0.77$, $p<0.05$ (jointing) $r^2 = 0.08$ (anthesis) $r^2 = 0.04$ (grain filling)	$r^2 = 0.25$ (jointing) $r^2 = 0$ (anthesis) $r^2 = 0.01$ (grain filling)	Wheat	YP (F)	Chen and Hao (2015)

			Crop		Reference
	$r^2 = 0$ (average)	$r^2 = 0.08$ (average)			
	$r^2 = 0.01$ (WW high N)	$r^2 = 0.3$ (WW high N)	Wheat	DNT (GC)	Barbour and Kaiser (2016)
	$r^2 = 0.51$ (D high N)	$r^2 = 0.93$ (D high N)			
	$r^2 = 0.78$ (WW adequate N)	$r^2 = 0.07$ (WW adequate N)			
	$r^2 = 0$ (D adequate N)	$r^2 = 0.01$ (D adequate N)			
	$r^2 = 0.39$, $p<0.05$ (pre-anthesis)	$r^2 = 0.39$, $p<0.05$ (pre-anthesis)	Wheat	DNT (F)	Gaju et al., (2016)
	$r^2 = 0.37$, $p<0.05$ (post-anthesis)	$r^2 = 0.34$, $p<0.05$ (post-anthesis)			
	$r^2 = 0$	$r^2 = 0$	Wheat	YP (F)	Carmo-Silva et al., (2017)
	$r^2 = 0.05$ (gs_{Q1800}, pre-anthesis)				Pennacchi et al., (2018)
	$r^2 = 0.04$ (gs_{Q1000}, pre-anthesis)				
	$r^2 = 0.04$ (gs_{Q500}, pre-anthesis)				
	$r^2 = 0.04$ (gs_{Q250}, pre-anthesis)				
	$r^2 = 0.04$ (gs_{Q100}, pre-anthesis)				
	$r^2 = 0.03$ (gs_{Q1800}, post-anthesis)				
	$r^2 = 0.03$ (gs_{Q1000}, post-anthesis)				
	$r^2 = 0.03$ (gs_{Q500}, post-anthesis)				
	$r^2 = 0.03$ (gs_{Q250}, post-anthesis)				
	$r^2 = 0.03$ (gs_{Q100}, post-anthesis)				
R_d	$r^2 = 0$	$r^2 = 0.02$	Wheat	YP (F)	Reynolds et al., (2000a)
		$r^2 = 0.91$, $p<0.001$ (ambient CO_2)	Rice	AE [CO_2]	Sakai et al., (2006)
		$r^2 = 0.92$, $p<0.001$ (elevated CO_2)			
		$r^2 = 0.25$	Wheat	YP (F)	Chytyk et al., (2011)
	$r^2 = 0.05$ (spike, heading)	$r^2 = 0$ (spike, heading)	Wheat	YP (F)	Zhou et al., (2016)
	$r^2 = 0.46$ (spike, grain filling)	$r^2 = 0.22$ (spike, grain filling)			
	$r^2 = 0.26$ (spike, average)	$r^2 = 0.11$ (spike, average)			
	$r^2 = 0.42$ (high night temp)	$r^2 = 0.65$ (high night temp)	Wheat	HNT and YP (GC)	Impa et al., (2016)
	$r^2 = 0.4$ (control)	$r^2 = 0.44$ (control)			
	$r^2 = 0.69$, $p<0.05$ (spike respiration)	$r^2 = 0.62$ (spike respiration)	Wheat	YP (GH)	Elazab et al., (2021)
	$r^2 = 0.45$ (flag leaf respiration)	$r^2 = 0.07$ (flag leaf respiration)			

3.4 Materials and methods

3.4.1 Field studies

Eleven spring bread wheat genotypes selected from the Photosynthesis Respiration Tails (PS Tails) panel from the International Maize and Wheat Improvement Center (CIMMYT) were grown at CIMMYT's field station Campo Experimental Norman E. Borlaug (CENEB) in Ciudad Obregón, Sonora, México (27° 23' 46'' N, 109° 55' 42'' W, 38 mamsl). The genotypes were studied in three consecutive field seasons (2017-2018, 2018-2019, 2019-2020, referred hereafter as Y1, Y2 and Y3). Eight genotypes were studied in Y1 and three genotypes were added for Y2 and Y3. The selection criteria were their contrasting RUE expression at vegetative and grain filling stages, grain filling flag leaf photosynthesis rates, yield, HI and canopy height. Further information of the genotypes used in this study can be found in Robles-Zazueta et al., (2021). Mean temperature of the growing season (December-April) for the three years was 17.43 °C with average rainfall of 20.27 mm and incident PAR of 8.08 MJ m^{-2}.

3.4.2 Experimental design

A randomised complete block design with three and four replicates per genotype with two beds per plot (Y1 and Y2, respectively), and four replicates per genotype with six rows one bed plots (Y3) was used. Sowing dates were December 5th 2017, December 6th 2018 and December 18th 2019 for Y1, Y2 and Y3 respectively. Emergence dates were December 12th 2017, December 12th 2018 and December 26th 2019 (Y1, Y2 and Y3 respectively). Harvest dates were

May 8th 2018, April 30th 2019 and May 13th 2020 (Y1, Y2 and Y3 respectively). Seed rate was ~250 g m^{-2} for the three years. Irrigation was applied four times after emergence during the crop cycle in approximate 25-day intervals (pre sowing, 25, 50, 75, 100 days after emergence). Plants were grown under optimal conditions in the field with pests, weed control and fertilisation to avoid limitations to yield. In Y1 fertilization was applied in the form of urea (200 kg N ha^{-1}) 25 days after emergence (DAE). For Y2 fertilization was divided in 100 kg N ha^{-1} 25 DAE and another 100 kg N ha^{-1} 58 DAE. Finally, for Y3 100 kg N ha^{-1} were applied 30 DAE and 50 kg N ha^{-1} 50 DAE; 50 kg P ha^{-1} were applied in the three cycles when the first application of N was made.

3.4.3 Phenology

Phenological stages were scored visually according to the Zadoks growth scale for cereals (Zadoks et al., 1974). Growth stages recorded were canopy closure (~40 days after crop emergence, E40), initiation of booting (GS41, InB), heading (GS55, H), anthesis (GS65, A) and physiological maturity (GS87, PM).

3.4.4 Canopy architecture

Canopy height was measured at E40, InB, H, A7 and PM at the south, north and middle areas of each bed using a measuring tape attached to a 1.5 m stick, then six values per plot were averaged. From H onwards canopy height was measured from the base of the stem to the tip of the spike without considering the awns. Leaf width and length were measured at InB and A7 with a ruler.

At A7 a method was developed to measure leaf angles with respect to the ligule, leaf curvature measured at the point where the leaf bends, and distance from the stem to the tip of the leaves. Leaf angle and curvature were measured in flag, second and third leaves with a protractor and distance from stem to tip of the leaves using a ruler. Spike and awn length were measured in six shoots per plot following field phenotyping protocols (Pask et al., 2013).

Light interception (LI) was measured using a ceptometer (AccuPAR LP-80, Decagon Devices, Pullman, WA, USA). LI was measured at E40, InB and A7 to calculate the light intercepted and extinction coefficient by the canopy. Incident, reflected and transmitted PAR through the canopy were measured from 11 am-1 pm when clear skies and low wind velocity conditions prevailed. The following equation was used to calculate the percentage of LI by the canopy:

$$LI\ (\%) = \frac{PAR_i - PAR_r - PAR_g}{PAR_i - PAR_r}\ x\ 100 \qquad \text{eq. (1)}$$

where LI (%) is the percentage of light intercepted by the canopy, PAR_i, PAR_r and PAR_g are the incident, reflected and transmitted PAR respectively.

Extinction coefficient was calculated based on Beer's law modified by Monsi and Saeki to study plant canopies (Hirose, 2005) as follows:

$$k = -ln\frac{PAR_g}{\frac{PAR_i}{LAI}} \qquad \text{eq. (2)}$$

where ln is the natural logarithm, PAR_g the transmitted PAR, PAR_i the incident PAR and LAI the leaf area index of the canopy.

Twelve shoots were randomly selected for biomass partitioning where plant organs were separated from stem, green area of flag, second, third and remaining

(below third leaf) leaves partitioning at InB and A7. Leaf green areas were measured using a leaf area meter (LI 3100C, Licor Biosciences, Lincoln, NE, USA). Finally, samples were dried in an oven for 2 days at 70°C, weighed and data was used to calculate the leaf area index (LAI) as follows:

$$LAI = \frac{Green\ leaf\ lamina\ area}{\#\ stems\ m^2} \qquad \text{eq. (3)}$$

Finally, at A7, peduncle, internode 2 and 3 length were measured with a ruler in the stems from the shoots used for biomass partitioning.

3.4.5 Measurement of source traits

Aboveground biomass was sampled following Robles-Zazueta et al., (2021). Samples of biomass at InB, 7 days after anthesis (A7) and PM were collected. Biomass harvests were made in 0.4 m^2 (40 days after emergence) and 0.8 m^2 (InB, A7), leaving 25 and 50 cm respectively at the northern side of the plots to reduce border effects in subsequent biomass samplings. All fresh biomass was weighed, and a subsample of 50 shoots was weighted and dried in an oven at 70 °C for 48 h, to record dry weight and measure LAI. For biomass at PM, calculations were made from the measurement of yield components. For every growth stage, the aboveground biomass was calculated according to Pask et al., (2013):

$$Aboveground\ biomass = Subsample\ DW \times \frac{Total\ FW \times Harvested\ area}{Subsample\ FW} \qquad \text{eq. (4)}$$

RUE was estimated from the slope of the linear regression between accumulated aboveground biomass and the corresponding accumulated intercepted PAR during the determined growth period (Monteith, 1977). Incoming radiation from

a nearby meteorological station was used to calculate the accumulated PAR multiplying irradiance by 0.45 to convert it to PAR and ceptometer (AccuPAR LP-80, Decagon, Pullman, WA, USA) measurements were used to correct the accumulated radiation for the fraction of absorbed PAR of each genotype using the same approach as Robles-Zazueta et al., (2021).

Gas exchange was measured with an infrared gas analyzer (IRGA, Licor 6400 XT, Licor Biosciences, Lincoln, NE, USA) at InB (Y1 and Y2) and A7 (Y1, Y2, Y3). Spot measurements (A_{sat}) were made on healthy plants using the leaf chamber fluorometer (6400-40 Licor Biosciences, Lincoln, NE, USA) in order to replicate environmental conditions from the study site (1800 µmol m^{-2} s^{-1} PAR, 28 °C for block temperature). Leaf chlorophyll content was measured using a SPAD-502 meter (Konika Minolta, Japan).

Measurements were taken in the flag (top of the canopy), second (middle of the canopy) and third leaves (bottom of the canopy) in two main shoots per plot as indicated in Robles-Zazueta et al., (2022) and then upscaled to canopy level. Measurements were performed between 10:00-15:00 as this timeframe has been found to maximize the stability and accuracy of the measurements (Evans and Santiago, 2014).

A_{sat} was upscaled to canopy level by multiplying each layer A_{sat} values by its corresponding LAI. A_{sat} rates were assumed for all canopy layers due to methodological reasons to simplify phenotyping in the field and find if light saturating photosynthesis which occurs in different occasions during the day in middle and bottom canopy layers can explain the relation with gas exchange and yield.

In this study, spike and stem photosynthesis was not measured therefore was not considered in our estimations of canopy photosynthesis. Calculations were made as follows:

$$\text{Canopy Photosynthesis} = \sum(A_{sat}\text{FL x LAI FL}) + (A_{sat}\text{SL x LAI SL}) + (A_{sat}\text{TL x LAI TL}) \qquad \text{eq. (5)}$$

Where A_{sat} is CO_2 assimilation under light saturated conditions (1800 µmol m^{-2} s^{-1} PAR), LAI is leaf area index, and FL, SL, TL are flag leaf, second leaf and third leaf respectively.

Water soluble carbohydrate (WSC) content was measured in stems and spikes of 12 randomly selected shoots at A7. Samples were dried in an oven at 70 °C for 48 hours and then milled for lab colorimetry analysis following the protocol in Pask et al., (2013).

3.4.6 Measurement of sink traits

When the genotypes reached PM, 50 shoots were randomly harvested from each plot and dried in an oven at 70 °C for 48 hours. Then the spikes were threshed to separate the grains from the rest of biomass and the harvest index was calculated as follows:

$$Harvest\ index\ (HI) = \frac{Grain\ dry\ weight}{Biomass\ dry\ weight} \qquad \text{eq. (6)}$$

Yield was sampled in the field using an automated harvest machine (LD 350, Wintersteiger AG, Austria) and plot length was measured before yield was measured to consider the plot area lost from previous biomass harvests Pask et al., (2013). From the yield sample, a subsample was collected to be processed in

the lab to measure grain moisture content, calculate the thousand grain weight (TGW), number of grains per spike (GSP), grains m^{-2} (GM2), and afterwards the grain weight per spike (GWSP) and the number of spikes m^{-2} (SM2) was calculated. Yield was calculated according to Pask et al., (2013):

$$Yield = \left(\frac{Plot\ yield\ \left(\frac{Dry\ weight\ yield\ subsample}{Fresh\ weight\ yield\ subsample}\right)+Grain\ dry\ weight_{50\ shoots}}{Area\ harvested}\right) \quad \text{eq. (7)}$$

3.4.7 Statistical analysis

Bilinear unbiased estimators (BLUEs) were calculated for each trait by analysing data collected in the three years using the general linear model with META-R v6.04 (Alvarado et al., 2020). Days to GS41 and GS65, were used as covariates to correct the physiological traits for phenological variation at the vegetative and grain filling periods, respectively only when they were significant. To calculate BLUEs the following equation was used:

$$Y_{ijkl} = \mu + Env_i + Rep_j(Env_i) + Gen_l + Env_i\ x\ Gen_l + Cov + \varepsilon_{ijkl} \quad \text{eq. (8)}$$

Where Y_{ijkl} is the trait of interest, μ is the mean effect, Env_i is the effect of the ith environment, Rep_j is the effect of the jth replicate within the ith environment, Gen_l is the effect of the lth genotype, Env_i x Gen_l are the effects of the ith environment and lth genotype interaction, Cov is the effect of the covariate and ε_{ijkl} is the error associated with the environment i, replication j, kth incomplete block and lth genotype.

Broad sense heritability (H^2) across the three years was calculated as follows:

$$H^2 = \frac{\sigma_g^2}{\sigma_g^2 + \frac{\sigma_{ge}^2}{nEnv} + \frac{\sigma_e^2}{(nEnv\ x\ nreps)}} \quad \text{eq. (9)}$$

Where σ_g^2 is the genotype error variance, σ_e^2 is the environment error variance, σ_{ge}^2 is the genotype x environment interaction error variance, nEnv is the number of environments and nreps the number of replicates.

3.5 Results

Table 3.2. Physiological traits measured in the field study at canopy level. Data presented is the mean (standard deviation) from 8 genotypes studied in three years plus 3 more genotypes studied two years, minimum, maximum, least significant differences (LSD), coefficient of variation (CV), heritability (H^2) and the statistical differences caused by genotypes (G), years of data collection (Y) or the interaction between GxY. * = significant at $p<0.05$, ** = significant at $p<0.01$, *** = significant at $p<0.001$, ms = marginally significant ($0.1>p>0.05$), ns = no statistical significance.

Trait	Mean (SD)	Minimum	Maximum	LSD	CV	H^2	G	Y	GxY
Sink									
Yield (g m^{-2})	622.6 (30.82)	571.53	649.12	51.36	5.31	0.57	*	ns	**
HI	0.47 (0.018)	0.436	0.499	0.02	4.96	0.86	***	***	ns
TGW (g)	43.11 (1.66)	36.24	47.98	2.88	6.33	0.91	***	***	ns
GSP (# spike^{-1})	49.12 (4.37)	38.34	55.53	5.79	12.69	0.84	***	*	ns
GWSP (g spike^{-1})	2.11 (0.17)	1.39	2.4	0.26	11	0.91	***	*	ns
GM2 (grains m^{-2})	14604.68 (972.02)	11963.71	16314.09	1777.86	8.13	0.78	***	***	**
SM2 (spikes m^{-2})	303.41 (32.71)	269.4	420.8	40.25	12	0.91	***	*	ns
Source									
BM_E40 (g m^{-2})	201.64 (33.92)	186.36	217.15	52.57	16.67	0	ns	ns	**
BM_InB (g m^{-2})	521.84 (60)	444.28	607.09	98.08	13.4	0.48	ms	ns	*
BM_A7 (g m^{-2})	989.59 (126.72)	893.31	1127.18	137.86	14.23	0.57	*	ns	ns
BM_PM (g m^{-2})	1322.83 (90.55)	1210.31	1445.18	131.68	7.12	0.7	**	**	*
RUE_preGF (g MJ^{-1})	2.36 (0.36)	2.111	2.56	0.39	17.26	0.25	ns	ns	ns
RUE_GF (g MJ^{-1})	1.23 (0.5)	0.85	1.55	0.49	41.01	0.46	ms	ns	ns
RUE_Total (g MJ^{-1})	1.64 (0.14)	1.51	1.8	0.19	8.97	0.6	*	***	ms
Canopy A$_{sat}$_InB (µmol m^{-2} s^{-1})	110.26 (24.79)	84.57	130.97	48.92	21.51	0.15	ns	ns	ns
Canopy A$_{sat}$_A7 (µmol m^{-2} s^{-1})	90.09 (30.87)	75.55	116.94	35.3	35.59	0.05	ns	ns	ns
WSC_stems (g m^{-2})	122.91 (34.63)	72.31	168.9	64.05	34.04	0.64	**	ns	**
WSC_spikes (g m^{-2})	39.24 (12.79)	27.84	49.62	18.74	38.49	0.55	*	ns	ns
Architecture									
Height_E40 (cm)	36.97 (1.65)	34.62	38.87	2.97	4.09	0.72	**	***	ns
Height_InB (cm)	65.34 (3.41)	60.67	74.39	10.31	4.97	0.36	ns	**	***
Height_H (cm)	82.74 (3.58)	75.14	89.41	7.97	6.37	0.8	***	***	ns

Height_A7 (cm)	99.61 (3.84)	90.64	106.12	10.05	4.25	0.71	**	ns	*
Height_PM (cm)	110.77 (2.06)	100.91	116.99	3.35	1.92	0.94	***	***	**
Internode 2 (cm)	21.25 (0.81)	19.82	23.39	1.43	3.63	0.84	***	ns	***
Internode 3 (cm)	13.77 (0.54)	10.54	15.92	1.08	4.3	0.95	***	***	***
Peduncle (cm)	38.42 (1.34)	35.07	42.73	2.84	4.05	0.81	***	***	***
Spike (cm)	11.44 (0.4)	9.3	12.94	0.74	3.76	0.94	***	ns	***
Awns (cm)	6.27 (0.36)	4.84	6.84	0.35	5.92	0.97	***	***	ns
Shoots_E40 (# m^{-2})	805.38 (123.45)	710.39	928.65	128.12	16.98	0.74	***	ns	ns
Shoots_InB (# m^{-2})	534.65 (88.27)	429.91	697.84	91.31	17.77	0.85	***	***	ns
Shoots_A7 (# m^{-2})	454.02 (62.92)	373.66	604.8	71.47	16.66	0.88	***	ns	ns
LI_E40 (%)	89.57 (3.78)	87.14	91.28	4.6	4.77	0	ns	*	ns
LI_InB (%)	96.4 (1.84)	92.81	98.62	3.51	2.45	0.49	ms	ms	ns
LI_A7 (%)	97.7 (0.9)	96.77	98.51	1.2	1.15	0.49	ms	**	ns
LAI_InB	7.04 (1.22)	5.97	8.77	1.73	18.83	0.54	*	*	ms
LAI_A7	5.35 (0.84)	4.38	6.23	1.22	19.05	0.41	ms	ns	ns
k_InB	0.46 (0.09)	0.38	0.54	0.13	19.95	0.21	ns	*	*
k_A7	0.78 (0.15)	0.67	0.91	0.16	16.66	0.56	*	ms	ns
Phenology									
InB (days)	60.77 (0.96)	58.36	64.59	2.17	1.84	0.91	***	***	***
H (days)	71.03 (0.92)	68.16	74.83	2.37	1.31	0.92	***	***	***
A7 (days)	76.29 (1.15)	73.07	80.27	2.52	1.61	0.92	***	***	***
PM (days)	116.4 (1.01)	113.33	119.65	2.4	1.01	0.83	***	***	***

HI: harvest index, TGW: thousand grain weight, GSP: grains per spike, GWSP: grain weight per spike, GM2: grains per m^{-2}, SM2: spikes per m^{-2}, LI: light interception, LAI: leaf area index, k: extinction coefficient, RUE_preGF: radiation use efficiency from pre grain filling period, RUE_GF: radiation use efficiency from grain filling period, RUE_Total: radiation use efficiency from the whole crop cycle, BM: aboveground biomass, WSC: water soluble carbohydrates.

Table 3.3. Physiological traits measured in the field study in the different canopy layers. Data presented is the mean from the field experiments from the three years, minimum, maximum, least significant differences (LSD), coefficient of variation (CV), heritability (H^2) and the statistical differences caused by genotypes (G), years of data collection (Y) or the interaction between GxY. * = significant at $p<0.05$, ** = significant at $p<0.01$, *** = significant at $p<0.001$, ms = significant at $p<0.1$, ns = no statistical significance, T = Top layer of the canopy, M = Middle layer of the canopy, B = Bottom layer of the canopy. [+]Data collected in two years of study.

Initiation of booting

Trait	Minimum			Mean			Maximum			LSD			CV			H^2			G			Y			GxY		
	T	M	B	T	M	B	T	M	B	T	M	B	T	M	B	T	M	B	T	M	B	T	M	B	T	M	B
A_{sat}	21.1	21.6	12.4	25.6	26.9	15.9	28.6	30.4	19.3	4.98	9.19	8.51	12.91	19.68	25.64	0.37	0.09	0	ns	ns	ns	ns	ns	ns	ns	ns	ms
LAI	1.3	1.56	1.54	1.53	1.73	1.75	2.03	2.04	2.05	0.48	0.42	0.33	24.8	19.9	20.1	0.6	0.3	0.5	*	ns	*	*	ns	ms	ms	ns	ns
Length	20.73	27.9	30.6	24.12	30.44	32.68	29.23	33.82	36.04	3.23	4.15	3.82	8.2	6.14	6.28	0.9	0.5	0.4	***	ms	ns	ms	ns	ns	***	***	***
Width	1.7	1.44	1.33	1.91	1.62	1.42	2.1	1.73	1.51	0.11	0.12	0.1	5.08	5.17	5.69	0.9	0.7	0.5	***	**	*	ns	**	ms	**	ns	
LI	35.93	29.7	6.73	44.9	35.17	10.4	53.31	41.43	14.03	17.8	12.9	7.92	20.3	24.9	53.8	0	0	0	ns	ns	ns	***	***	***	**	ns	ns
SPAD	44.12	46.3	43	45.77	48.12	45.26	49.01	50.5	47.56	3.53	2.31	2.71	5.07	3.89	6.25	0.4	0.7	0.6	ns	***	*	ns	**	*	**	ns	ns

7 days after anthesis

Trait	Minimum			Mean			Maximum			LSD			CV			H^2			G			Y			GxY		
	T	M	B	T	M	B	T	M	B	T	M	B	T	M	B	T	M	B	T	M	B	T	M	B	T	M	B
A_{sat}	19.4	12	7.2	22	16.7	10.2	24.5	19.5	13	12.9	19.7	25.6	19	25.1	39.4	0.4	0.7	0.5	ms	***	*	**	**	**	ns	ns	ns
LAI	1.13	1.67	1.75	1.43	2.31	2.14	1.76	2.75	2.54	0.42	0.86	0.78	10.1	23	36	0.6	0.4	0	*	ns	ns	ns	***	***	ms	ns	ns
Angle[+]	43.06	34	45.1	91.95	76.03	75.44	109.4	100.4	94.88	42.8	39.2	59.6	23.1	19.2	30	0.5	0.7	0	*	**	ns	***	**	ms	**	***	***
Curvature[+]	27.44	27.6	49.1	44.97	63.31	64.69	85.69	90.94	88	69.4	46.3	57.8	74.5	42.6	45.3	0	0.4	0	ns	ns	ns	ms	ms	ns	***	**	ms
Distance[+]	16.06	17.4	19.7	19.35	22.17	22.7	22.01	24.99	25.71	7.35	5.31	5.79	12.9	12.7	18.2	0	0.5	0.2	ns	ms	ns	ns	ms	ns	***	*	ns
Length[+]	23.18	28.4	30.7	27.47	31.19	33.34	24.4	29.68	31.65	3.27	2.95	3	9.03	7.86	7.38	0.9	0.6	0.7	***	*	**	ns	ns	ns	ns	ns	ns[+]
Width[+]	1.81	1.53	1.39	2.04	1.68	1.54	1.9	1.54	1.38	0.19	0.22	0.14	5.17	8.06	7.76	0.9	0.6	0.8	***	*	**	ns	ns	**	ms	ns	ns
LI	27.68	22.8	7.81	34.8	27.1	9.62	42.62	31.5	14.37	11.7	8.97	6.69	30.2	33.2	59	0.3	0	0	ns	ns	ns	ns	**	ns	ns	ns	ns
SPAD	47.83	47	40.8	50.6	49.3	44.43	53.18	52.11	47.94	2.06	1.91	2.97	4.01	4.18	7.21	0.9	0.9	0.8	***	***	***	***	ns	ms	ns	ns	ns

A_{sat}: photosynthesis rate at light saturating conditions, LAI: leaf area index, LI: percentage of light intercepted, Curvature: leaf curvature where the leaf starts to bend, Distance: distance from stem to tip of the leaf.

3.5.1 Agronomic traits

Grain yield across years was 622.6 ± 30.8 g m^{-2} and H^2 was 0.57 (Table 3.2). Yield component traits (HI, TGW, GSP, GM2 and SM2) showed highly statistically significant differences among genotypes with high H^2 estimates (0.78-0.91). RUE during the vegetative period (RUE_preGF) ranged from 2.11-2.56 g MJ^{-1} and was higher compared to RUE from grain filling (RUE_GF, 0.85-1.55 g MJ^{-1}) or RUE encompassing the whole crop cycle (RUE_Total, 1.51-1.8 g MJ^{-1}). However, H^2 estimates for RUE_preGF (0.25) were lower than RUE_GF and RUE_Total (0.46 and 0.6, respectively). Differences among genotypes were identified for RUE_GF and RUE_Total at $p<0.1$ and $p<0.05$, respectively (Table 3.2). Aboveground biomass ranged from 201.64 ± 33.92 g m^{-2} in E40 to 1322.83 ± 90.55 g m^{-2} in PM. The highest variability of any growth stage was found at PM, with differences between genotypes and across years ($p<0.01$) but in general the sink traits varied more between genotypes and years than the source traits and H^2 was increasing along the growth stages, with medium to high heritability found at A7 (H^2 = 0.57) and PM (H^2 = 0.7) (Table 3.2).

Differences in canopy architecture, stem and spike architecture were found in all growth stages, except for plant height at A7 (Table 3.2). LAI only showed genetic variability at canopy (Table 3.2) and layer level at InB (Table 3.3) but no differences were found at A7. Similarly, statistically significant differences were found in leaf angles measured in the top and middle layers of the canopy (Table 3.3). Despite the differences in canopy architecture and light distribution, the canopies in all the genotypes studied captured the same amount of light in all the growth stages studied (Table 3.2).

3.5.2 Leaf and canopy light saturating photosynthesis

Canopy photosynthetic rates ranged from 84.57 µmol m^{-2} s^{-1} to 130.97 µmol m^{-2} s^{-1} at InB and 75.55 µmol m^{-2} s^{-1} to 116.94 µmol m^{-2} s^{-1} at A7. No statistically significant differences were found (Table 3.2). A similar trend was found for A_{sat} from individual layers at InB with no significant differences found between genotypes within the canopy layers (Table 3.3). In our study, both canopy and layer photosynthesis rates were higher at InB and decreased at A7. At InB the highest A_{sat} rates were found in the middle layer (26.91 µmol m^{-2} s^{-1}) and top layer rates were statistically similar (25.58 µmol m^{-2} s^{-1}) with the lowest A_{sat} rates found at the bottom layer (15.95 µmol m^{-2} s^{-1}). In contrast to InB, at A7 statistically significant differences were found within layers (middle and bottom), with a decreasing trend in A_{sat} rates from top (21.99 µmol m^{-2} s^{-1}) to bottom layers (10.19 µmol m^{-2} s^{-1}) of the canopy with medium to high H^2 estimates (0.5-0.7) (Table 3.3).

3.5.3 RUE, biomass and yield relation with photosynthesis

Overall, the relationship between RUE measured in the different growth periods and A_{sat} measured at different layers of the canopy was very poor both for A_{sat} measured during InB and A7. A_{sat} measured in the top of the canopy at InB only correlated slightly significant with RUE_GF (Figure 3.1, top panel). When A_{sat} was measured at A7 the relationship with RUE improved (RUE_preGF and top A_{sat}, $p<0.1$; RUE_GF and middle A_{sat}, $p<0.1$) but still were not statistically significant (Figure 3.1, bottom panel).
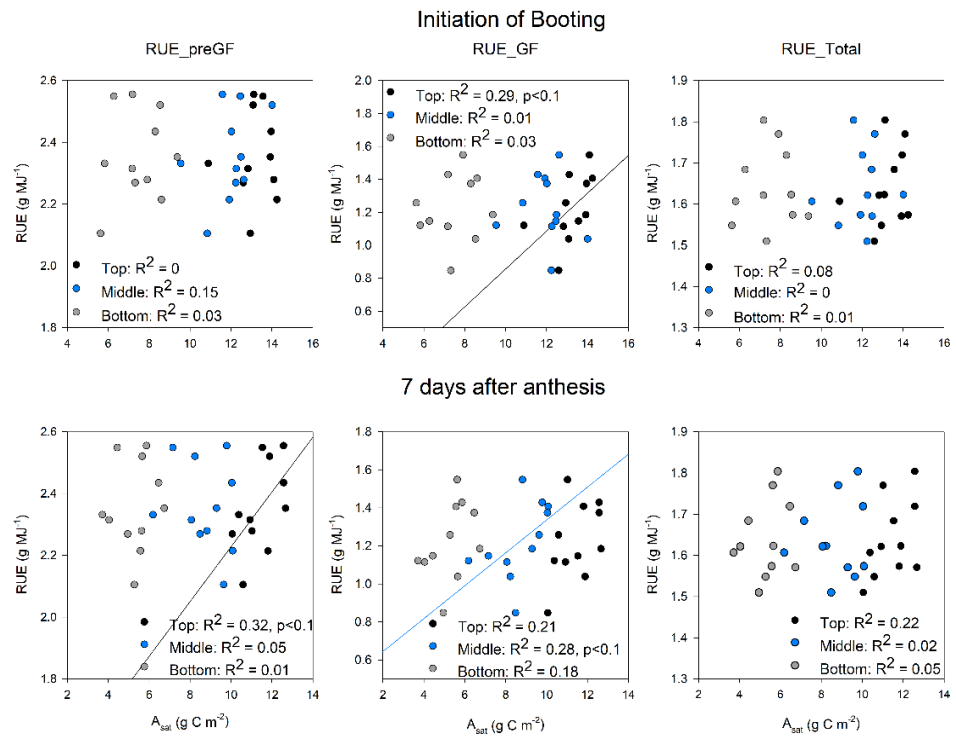
Figure 3.1. Linear regressions between radiation use efficiency (RUE) and the integral of CO_2 assimilation at light saturating conditions (A_{sat}) measured at different layers of the canopy from initiation of booting (top panels) and 7 days after anthesis (bottom panels). Black dots: Top of the canopy, blue dots: middle of the canopy, grey dots: bottom of the canopy. Lines represent significant linear regressions.

When combining different layers of the canopy the relationship between RUE and A_{sat} significantly improved compared to using individual layers. RUE_preGF correlated significantly with the top + middle layer combination ($R^2 = 0.37$, $p<0.05$) and a marginally significant relationship was found when the three canopy layers were considered ($R^2 = 0.32$, $p<0.1$) (Figure 2, top panel). No significant relationships between RUE_GF and RUE_Total with the layer A_{sat} combinations measured at InB were observed (Figure 3.2, top panel). Different A_{sat} layer combinations measured at A7 correlated better with RUE.

A significant association between RUE_preGF and A_{sat} was found when top + bottom layers were combined ($R^2 = 0.42$, $p<0.05$), middle + bottom layers with

RUE_GF (R^2 = 0.42, p<0.05) and top + bottom layers had a marginally significant link with RUE_Total (R^2 = 0.3, p<0.1) (Figure 3.2, bottom panel).
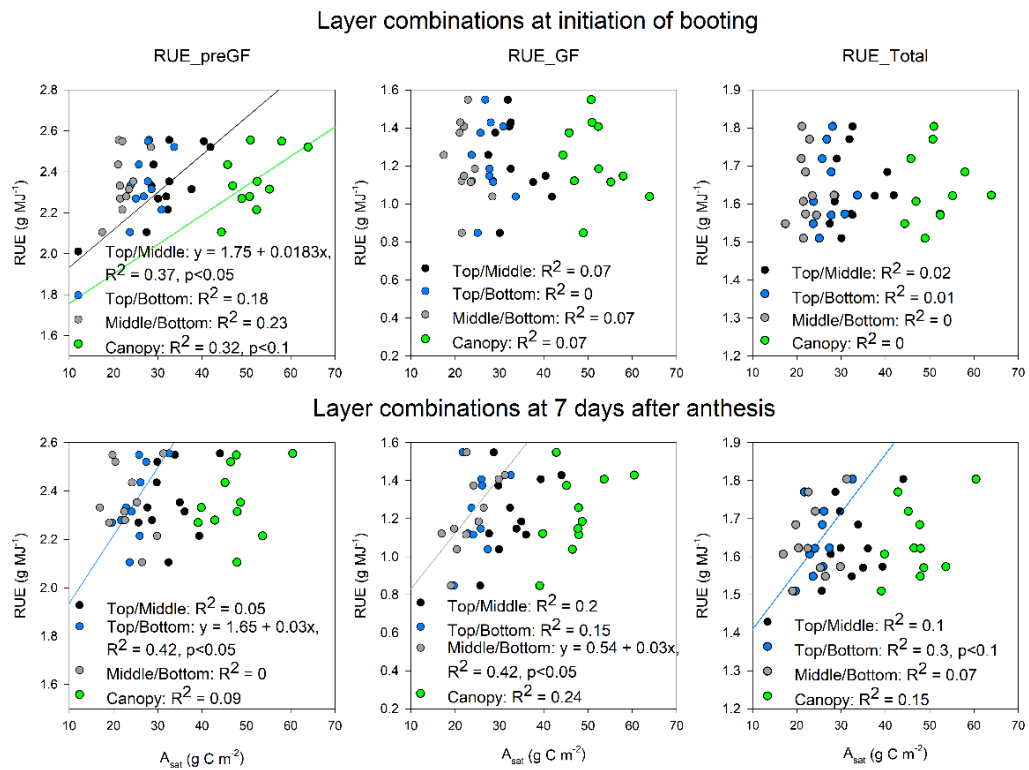
Figure 3.2. Linear regressions between radiation use efficiency (RUE) and the integral of CO_2 assimilation at light saturating conditions (A_{sat}) measured by combining different layers of the canopy in initiation of booting (top panels) and 7 days after anthesis (bottom panels). Black dots: Top and middle, blue dots: top and bottom, grey dots: middle and bottom, green dots: top, middle and bottom. Lines represent significant linear regressions.
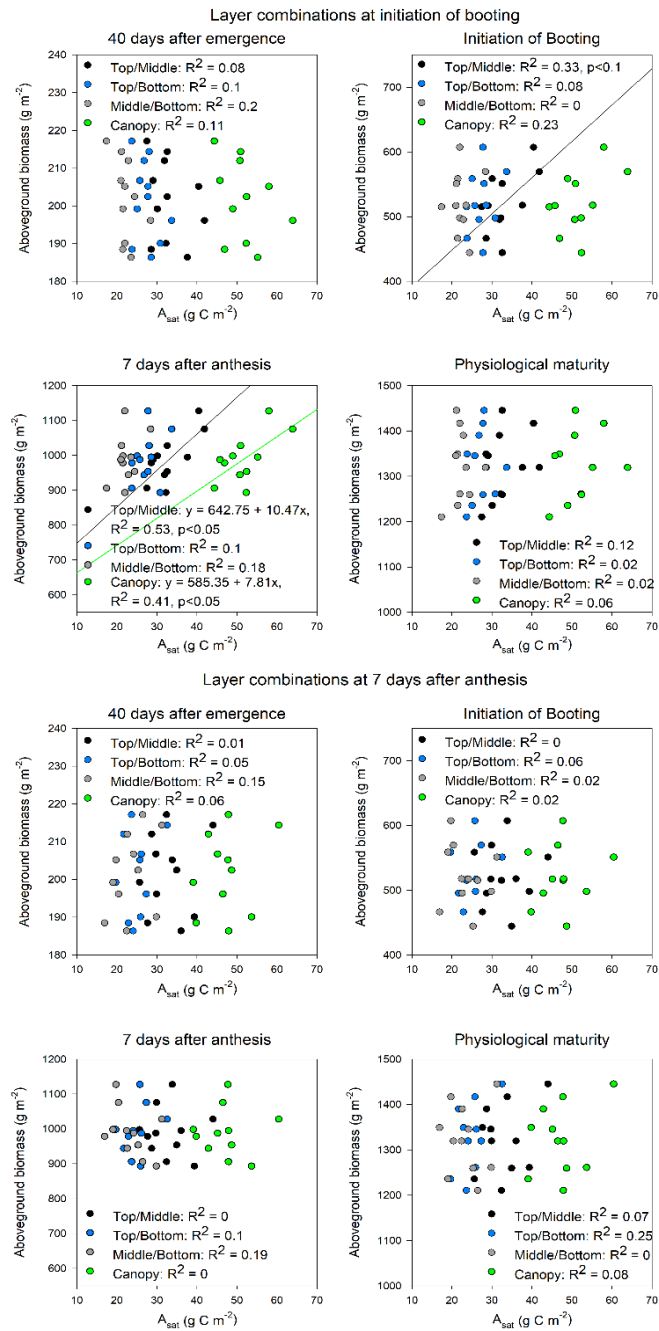
Figure 3.3. Linear regressions between aboveground biomass and CO_2 assimilation at light saturating conditions measured by combining different layers of the canopy in initiation of booting (panels 1-4) and 7 days after anthesis (panels 5-8). Black dots: Top and middle, blue dots: top and bottom, grey dots: middle and bottom, green dots: top, middle and bottom. Lines represent significant linear regressions.

With the combination of different canopy layers, a marginal significant relation was found between biomass and A_{sat} from the top + middle layers at InB ($R^2 = 0.33$, p<0.1). The combinations of top + middle ($R^2 = 0.53$, p<0.05) and whole canopy ($R^2 = 0.41$, p<0.05) resulted in positive associations with biomass at A7 (Figure 3.3, top panels). For A_{sat} at A7, no significant relationships with biomass at any growth stage were found, but when combining different layers, the top + bottom and middle + bottom layers with biomass from PM showed a weak positive relationship ($R^2 = 0.25$) (Figure 3.3, bottom panels), which was in line with the findings for RUE and A_{sat}.
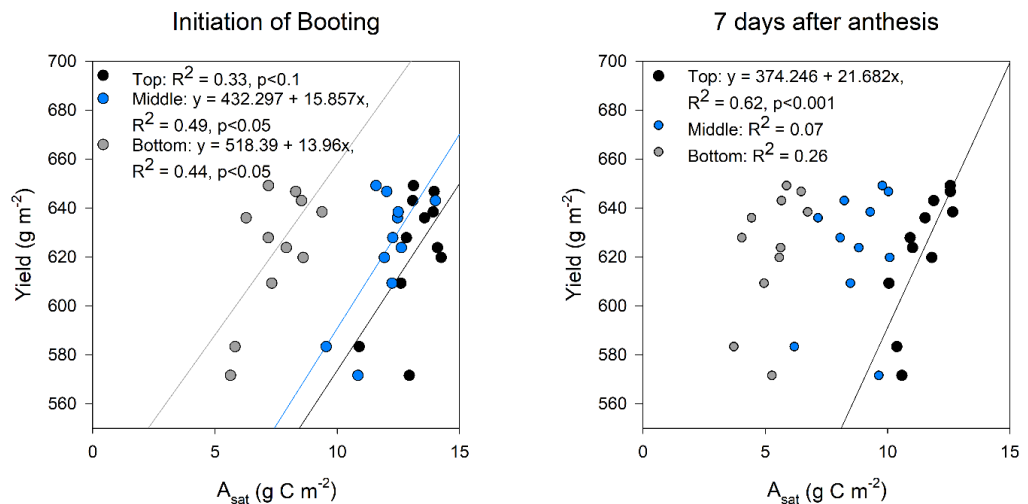
Figure 3.4. Linear regressions between grain yield and CO_2 assimilation at light saturating conditions at initiation of booting (left panel) and 7 days after anthesis (right panel). Black dots: top, blue dots: middle, grey dots: bottom. Lines represent significant linear regressions.

Significant relationships were found between photosynthetic rates both at InB and A7 with yield. A_{sat} at InB from the top ($R^2 = 0.33$, p<0.1), middle ($R^2 = 0.49$, p<0.05) and bottom ($R^2 = 0.44$, p<0.05) layers of the canopy produced positive relationships (Figure 3.4, left panel). The strongest association found in this

study was between top A_{sat} at A7 and yield ($R^2 = 0.62$, p<0.001) (Figure 3.4, right panel).
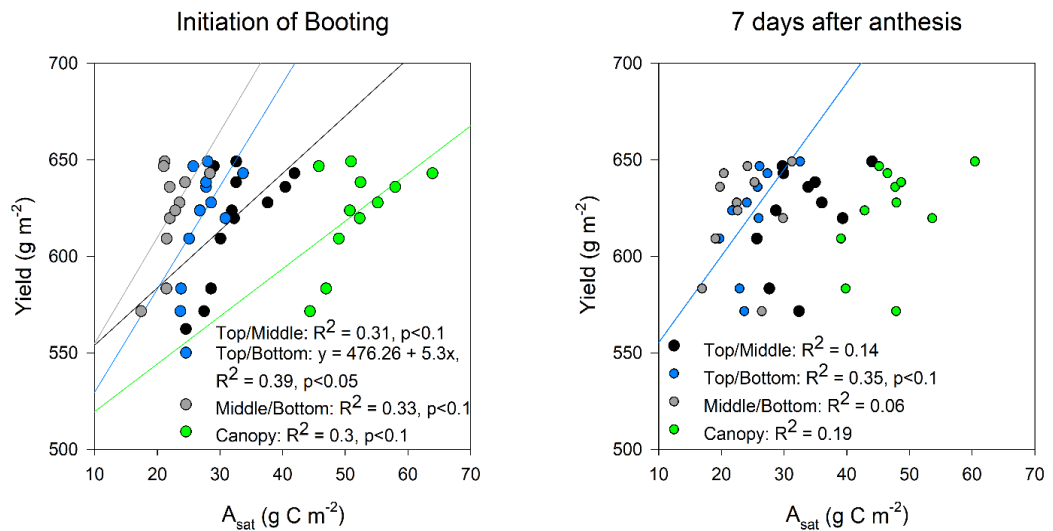
Figure 3.5. Linear regressions between grain yield and CO_2 assimilation at light saturating conditions measured by combining different layers of the canopy in initiation of booting (left panel) and 7 days after anthesis (right panel). Black dots: top and middle layer, blue dots: top and bottom layer, grey dots: middle and bottom layer. Lines represent significant linear regressions.

Using a combination of canopy layers did not improve the relationships found compared to the ones established with individual layers neither at InB nor A7. Top + middle ($R^2 = 0.31$, p<0.1), middle + bottom ($R^2 = 0.33$, p<0.1) and all the canopy layers combined ($R^2 = 0.3$, p<0.1) had a marginally significant relationship with yield. Top + bottom layers ($R^2 = 0.39$, p<0.05) was the only combination where we found a significant link between yield and A_{sat} from InB (Figure 3.5, left panel). For A7, only top + bottom ($R^2 = 0.35$, p<0.1) had positive relationship with yield (Figure 3.5, right panel).

3.6 Discussion

This is the first study to consider the impact of photosynthesis at discrete layers of wheat canopies on biomass, RUE and yield in wheat; as well as the combined impact of different layer combinations. This work also explores the reasons why there is not a clear consensus in the literature for the presumably necessary relationship between photosynthesis and performance traits. Furthermore, comparisons between different layer combinations were explored to examine if the relationship between these traits with photosynthesis improves and be able to suggest which canopy layers could be added for future screening efforts by identifying lines with optimised photosynthesis along the canopy.

Our results suggest that the relationship between yield, biomass and RUE with leaf photosynthesis has not been consistent due to the lack of integration of different canopy layers and studies that address the role of above and belowground respiration and C allocation, the micro-environmental conditions in which plants are grown and the different phenological stages where these relationships have been studied.

3.6.1 RUE, biomass and yield improvement: why there is a lack of consensus?

Our results indicate that phenology has a great influence on the strength of the relationships found between performance traits and photosynthesis. The lack of genotypic differences at InB could be explained by the influence of canopy architecture as all the studied genotypes intercepted the same amount of light in this growth stage because these cultivars are subject to light saturating conditions

in the top and possibly middle layer of the canopy. In contrast, at A7 moderate H^2 and genotypic differences found highlight that photosynthetic rate for middle and bottom canopy layers could be added in breeding pipelines to improve yield in the future as it complies with the selection criteria of traits to be included in pre-breeding programmes (Reynolds et al., 2020). Thus, enhancing canopy architecture to optimise light distribution has to be a priority to boost middle and bottom layer photosynthetic rates.

Previous studies that have explored the association between source and sink traits with photosynthesis have focused on flag leaves (wheat, rice) or top of the canopy leaves (cassava and sorghum) and there is a range of environments (yield potential, drought, different N fertilisation rates, glasshouse and growth chamber) that influence the source-sink ratios of plants, which adds a confounding effect to the study of these relationships.

In our study, A_{sat} from the middle layer of the canopy both at InB and A7 were best associated with genotypic differences in biomass at PM (r^2 = 0.18, 0.25, respectively) because flag leaves are subjected to light saturating conditions for most of the crop cycle. The relationship with biomass in our study is within the range of previous studies for sorghum at panicle initiation (r^2 = 0.32) (Peng et al., 1991), pre-anthesis in wheat (r^2 = 0.25) (Gent, 1995), but smaller than the relationships presented for wheat grown in the field under drought (Wada et al., 1994) and heat stress conditions (Gutiérrez-Rodríguez et al., 2000; Reynolds et al., 2000a), contrasting N fertilisation regimes (Huang et al., 2016) and wheat grown under different N levels at pre and post-anthesis (Gaju et al., 2016).

On the other hand, yield and A_{sat} relationship is more established than the biomass and A_{sat} relationship (Table 3.1). In our study photosynthetic rates at InB in every layer measured had significant relationship with yield (Table 3.1). Very strong associations were found in field grown sorghum under drought and irrigation especially in the mid-development stage ($r^2 = 0.86$, $p<0.01$; $r^2 = 0.83$, $p<0.01$, for yield potential and drought, respectively) (Peng et al., 1991) and for wheat measured at the vegetative stage differences between the relationships under yield potential and drought stress conditions were strongly contrasting ($r^2 = 0$, $r^2 = 0.4$, $p<0.01$, respectively) (Wada et al., 1994).

For most of field trials that previously reported relationships between yield and photosynthesis, the strongest relationships were found at grain filling (Gent, 1995; Fischer et al., 1998; Reynolds et al., 2000a; Zheng et al., 2011; Gaju et al., 2016), similar to our findings. This evidence suggests that yield improvement in wheat has come hand in hand with increments in A_{sat} and *gs*, because selection of new varieties with greater biomass is thought to inadvertently come with greater gas exchange rates. This indicates that it will be easier to find wheat varieties with higher yield if photosynthetic rates and stomatal conductance are high during grain filling.

In contrast to field trials, when plants were studied in controlled settings the strongest relationships were found (Table 3.1). Examples of this findings are rice grown under elevated [CO_2] (Sakai et al., 2006), wheat grown under drought and high N fertilisation rates (Barbour and Kaiser, 2016). Spike photosynthesis in wheat grown with optimum irrigation in a glasshouse showed contrastingly better relationship with yield (Zhou et al., 2016; Elazab et al., 2021) compared to spike photosynthesis measured in the field under yield potential (Molero and

Reynolds, 2020); and a similar trend was found for flag leaf A_{sat} and A_{max} when wheat was grown in growth chambers (Driever et al., 2017) versus when the same genotypes were studied in the field (Driever et al., 2014).

From the abovementioned examples it is clear that the range of growing conditions plants are subjected have a clear effect on the relationship between yield and photosynthesis. Since photosynthetic traits can be environmental, time specific and developmental stage dependant (Flood et al., 2016), this needs to be considered when screening lines in different environments if yield is to be boosted. Plants developing in controlled environments typically have higher growth rates, higher leaf N concentration (key for photosynthesis) and smaller leaf area which affect the plant source-sink balance (Poorter et al., 2016) and could explain the better relationships found in controlled settings compared to the field (Table 3.1).

3.6.2 Canopy photosynthesis as a driver of yield improvement

Our results indicate that preferential improvement in the middle and bottom layers of canopy photosynthesis are most likely to boost yield due to the strong positive associations between photosynthesis and yield, especially at InB. However, given that these results were derived under light saturated conditions at all canopy layers, modifications on canopy architecture might be needed to improve light penetration through middle and bottom layers (e.g. erect leaves, increasing lower internode length, smaller LAI at the top and larger LAI at the bottom of the canopy) which can potentially translate to higher plants, but recent evidence suggest that is not necessarily the case (Rivera-Amado et al., 2020).

It has been suggested that exploiting the genetic variation in biomass (Aisawi et al., 2015) and RUE (Joynson et al., 2021) can be an important avenue for yield improvement, and furthermore help to understand the genetic basis of physiological traits related source (e.g. LAI, partitioning, photosynthesis, chlorophyll content within the canopy) and the improvement of yield (Molero et al., 2019). Nevertheless, if physiological variables do not show a relationship with growth analysis, RUE or yield new physiological traits will not be introduced in breeding pipelines.

In this study we established that including middle and bottom layers of the canopy to physiological studies, can help us to find genotypes with higher RUE rates, biomass and yield, as relationships of photosynthesis with RUE, biomass and yield, and *gs* with biomass were found (Table 3.1). Recent research has found mixed results about yield being source or sink limited, with indications that increments in grain filling source capacity including higher LAI and spike or leaf photosynthesis will improve yield (Rivera-Amado et al., 2020). On the other hand, Quintero et al., (2018) found that increasing the sink size will boost wheat yield. These mixed results suggest a source-sink co-limitation of yield; therefore, it will be paramount to increase canopy photosynthesis with an emphasis on middle and bottom layer at InB to allow plants to have greater photoassimilates reserves stored in the stems when remobilization starts at grain filling and leaf senescence at the bottom of the canopy diminishes the overall photosynthetic rates.

3.7 Conclusions

To our knowledge, this is the first effort to include different layers of the canopy to the study of the relationships between source and sink traits with gas exchange. Our results indicate that the growth stage where measurements take place are crucial to understand better the link between photosynthesis and yield. Even though it is highlighted in this study that measuring middle and bottom layers of the canopy can help us understand this link, it is noteworthy that flag leaf photosynthesis is the preferred method to phenotype gas exchange because of its simplicity and the lack of HTP methods. Therefore, the development of HTP methods, for example based on optical remote sensing will increase the feasibility of including middle and bottom layer phenotyping into breeding pipelines for large trial screenings by allowing us to predict gas exchange traits quickly as shown by Robles-Zazueta et al., (2022).

Discrepancies in the literature related to the relationship between photosynthetic traits and yield or biomass appear to be related to differences in growing conditions that still obscure these relationships. Future studies should consider measuring different wheat genotypes in multi-environmental trials coupled with high-throughput phenotyping of different canopy layers with modelling approaches that consider the addition of spike and stem photosynthesis in at least one vegetative and one reproductive stage to catch the variability caused by phenology, environmental and management conditions where wheat is grown.

Chapter 4 Prediction of photosynthetic, biophysical and biochemical traits in wheat canopies to reduce the phenotyping bottleneck

Carlos A. Robles-Zazueta[1,2*], Francisco Pinto[2], Gemma Molero[2,3], M. John Foulkes[1], Matthew P. Reynolds[2], Erik H. Murchie[1*]

[1]Division of Plant and Crop Sciences, School of Biosciences, University of Nottingham, Sutton Bonington Campus, Leicestershire, LE12 5RD, United Kingdom.

[2]Global Wheat Program, International Maize and Wheat Improvement Center (CIMMYT), carretera Mexico-Veracruz km 45, El Batan, Texcoco, Mexico. CP 56237.

[3]Current address: KWS Momont Recherche, 7 rue de Martinval, 59246 Mons-en-Pevele, France.

Author contribution:

Conceptualization of the project: Carlos A. Robles-Zazueta, Francisco Pinto, Gemma Molero, Matthew P. Reynolds and Erik H. Murchie.

Field experimental design: Carlos A. Robles-Zazueta, Francisco Pinto, Gemma Molero.

Investigation, data curation and formal analysis: Carlos A. Robles-Zazueta.

Methodology: Carlos A. Robles-Zazueta and Francisco Pinto.

Original draft: Carlos A. Robles-Zazueta.

Review and editing: Carlos A. Robles-Zazueta, Francisco Pinto, Gemma Molero, M. John Foulkes, Matthew P. Reynolds and Erik H. Murchie.

Funding acquisition: Francisco Pinto, Gemma Molero, Matthew P. Reynolds and Erik H. Murchie.

Project management: Matthew P. Reynolds and Erik H. Murchie.

*Authors for correspondence: carlos.robleszazueta@nottingham.ac.uk, erik.murchie@nottingham.ac.uk

Abstract

To achieve food security, it is necessary to improve radiation use efficiency (RUE) and yield through the enhancement of canopy photosynthesis to increase the availability of assimilates for the grain, but its study in the field is constrained by low throughput and lack of integrative measurements at canopy level. In this study, partial least squares regression (PLSR) was used with high-throughput phenotyping (HTP) data in spring wheat to build predictive models of photosynthetic, biophysical and biochemical traits for the top, middle and bottom layers of wheat canopies. The combined layer model predictions performed better than individual layer predictions with significance as follows for photosynthesis: $R^2 = 0.48$, RMSE = 5.24 μmol m^{-2} s^{-1}; stomatal conductance: $R^2 = 0.36$, RMSE = 0.14 mol m^{-2} s^{-1} and transpiration: $R^2 = 0.39$, RMSE = 1.42 mmol m^{-2} s^{-1}. The predictions of these traits from PLSR models upscaled to canopy level compared to ground truth data were statistically significant at initiation of booting ($R^2 = 0.3$, $p<0.05$; $R^2 = 0.61$, $p<0.001$; $R^2 = 0.29$, $p<0.05$) and 7 days after anthesis ($R^2 = 0.15$, $p<0.05$; $R^2 = 0.65$, $p<0.001$) except for transpiration. Using HTP allowed us to increase phenotyping capacity 30-fold compared to conventional phenotyping methods. This approach can be adapted to screen breeding progeny and genetic resources for RUE and improve our understanding of wheat physiology by adding different layers of the canopy to physiological modelling.

Keywords: *canopy photosynthesis, high-throughput phenotyping, PLSR, physiological breeding, RUE, yield improvement*

4.1 Introduction

4.1.1 Looking for yield improvement through the photosynthesis lens

Increasing crop biomass and radiation use efficiency (RUE; dry weight biomass produced per unit radiation intercepted) through the enhancement of photosynthesis has been presented as one of our best options to improve staple crop yields (Evans and Lawson, 2020). Multiple lines of evidence suggest that increased photosynthesis would stimulate higher yields and moreover there is room for improvement within existing crop systems (Zhu et al., 2010; Slattery et al., 2013; Kromdijk et al., 2016; South et al., 2019; Ainsworth and Long, 2021).

Most of the yield gains achieved in wheat (*Triticum aestivum* L.) from the Green Revolution came through the provision of the necessary resources for crop growth (i.e. water, nutrients, pest control) and the introduction of reduced height (*Rht*) genes to increase harvest index (HI; proportion of biomass allocated in the grains) and plant structural integrity thereby making it more responsive to irrigation and nutrients while reducing the risk of lodging (Reynolds et al., 2012). Currently, pre-breeding efforts in wheat are focused in improving traits such as aboveground biomass, light interception, HI and RUE (Molero et al., 2019). Some of these traits are close to optimum, HI (close to 0.6) and light interception (canopies intercepting ~95% of light), whereas RUE and biomass have a high potential for improvement. Therefore, increasing wheat photosynthesis has become a primary goal to increase yield (Murchie et al., 2009).

Biomass and RUE have increased in some wheat lines serendipitously without direct selection of RUE or photosynthetic traits. It has been suggested that RUE

improvements in wheat needs to be addressed through changes in leaf or spike photosynthesis (Carmo-Silva et al., 2017; Molero and Reynolds, 2020; Sanchez-Bragado et al., 2020) as previous studies have found a significant relationship between genetic variation in flag leaf light-saturated photosynthesis rates (A_{sat}) and stomatal conductance (*gs*) with yield (Fischer et al., 1998; Gutiérrez-Rodríguez et al., 2000; Reynolds et al., 2000a; Gaju et al., 2016) and aboveground biomass (Reynolds et al., 2000a; Gaju et al., 2016) at pre and post-anthesis growth stages. However, recent studies have failed to find a clear link between single leaf photosynthesis or *gs* with yield (Driever et al., 2014; Silva-Pérez et al., 2020).

In chapter 3, we identified that middle and bottom layers of wheat canopy can be a great option to exploit the photosynthetic phenotypic range for yield improvement but to fully exploit genetic variation in existing germplasm we need to develop high-throughput plant phenotyping (HTP) methods for faster assessment of photosynthetic-related traits and also find ways in which measurements of leaf or canopy photosynthesis will meaningfully correlate with canopy biomass and RUE to accelerate genetic yield gains.

4.1.2 Canopy photosynthesis modelling

Photosynthesis field research in wheat has been relatively slow in comparison to the study of other traits such aboveground biomass accumulation, light interception, RUE or leaf and canopy pigment content despite the latter requiring heavy manual labour in the field. This is a consequence of several factors that hinder accurate and representative estimations of photosynthetic traits under

field conditions which are mostly related to the complexity of photosynthesis as a trait. These include the time it takes to measure a leaf in the field for maximum assimilation rate under light saturating conditions per leaf (A_{sat}, ~15-25 min), the impracticality and low throughput techniques for measuring more complex photosynthetic traits such as induction, CO_2 or light concentration curves (A/C_i, A/Q curves), and the confounding effect of crop phenology. Moreover, photosynthesis is typically measured in flag leaves which are usually exposed to light saturating conditions for most of the day and thus not representing the environmental conditions found across the whole canopy (Murchie et al., 2018).

Photosynthesis research gained a lot of interest after the seminal work from Farquhar et al., (1980). Since then methodologies were developed to measure, upscale to canopy level ("big leaf" models) and model photosynthesis considering mainly sunlit leaves, assuming that its rates would change with light intensity, penetration and distribution, N content and leaf angles (Farquhar, 1989) with this modelling approach being applied in natural ecosystems (De Pury and Farquhar, 1997) and C_3 and C_4 crop systems upscaling information from individual leaves to canopy level (Yin and Struik, 2009; Wu et al., 2019). Given that prediction of canopy photosynthesis is improved with knowledge of photosynthesis at multiple canopy leaf layers by contemplating resource differences in each layer, methodologies emerged to increase the spatio-temporal scales over which measurements can be made. Photosynthetic reactions can now be measured at cellular, leaf and plant level with low to medium throughput phenotyping techniques (Murchie et al., 2018), and at ecosystem scale using sensors mounted on micrometerological stations (Baldocchi, 2003) and estimate biome photosynthesis using chlorophyll fluorescence information collected from

satellite sensors as a proxy of productivity (Farquhar et al., 2001; Parazoo et al., 2014; Duveiller and Cescatti, 2016; Zhang et al., 2016). Although these are exciting methodologies used for photosynthesis research, the latter examples are not easy to deploy in wheat breeding programs as hundreds of lines are grown in plots placed next to each other and upscaling information from leaves to plots can be hard due to the spatial scale mismatch in these methods which can vary from mm^2 to km^2.

4.1.3 High-throughput phenotyping of photosynthetic, biophysical and biochemical traits

There have been various investigations to assess photosynthetic related traits at multiple canopy levels such as A_{sat}, RUE, the fraction of absorbed photosynthetically active radiation (fAPAR), maximum velocity of Rubisco carboxylation (V_{cmax}), electron transport rate (J_{max}), non-photochemical quenching (NPQ) and other chlorophyll fluorescence parameters have been assessed in glasshouse studies coupled with 3D reconstructions using ray tracing modelling in wheat (Townsend et al., 2018), rice (Burgess et al., 2016; Foo et al., 2020), maize (Cabrera-Bosquet et al., 2016), pearl millet, bambara groundnut (Burgess et al., 2017) and arabidopsis (Retkute et al., 2015) in different canopy layers. Under field conditions, A_{sat} measurements have been made with a custom made sensor (OCTOflux) which allowed the user to increase the phenotypic capabilities ~4-7 times compared to conventional IRGAs (infrared gas analyser) by measuring 8 leaves at a time (Salter et al., 2018), A_{sat} measurements made in the top and bottom layers of wheat canopies (Salter et al., 2020), modelling with light response curves coupled with eddy covariance flux estimations of gross

primary productivity (GPP) (Hoyaux et al., 2008) and through image spectroscopy used to measure photochemical efficiency in wheat and maize (Pinto et al., 2016).

While these studies have shown that it is possible to estimate canopy photosynthesis through modelling, it has usually required laborious and complex manual measurements. Some have been used only in controlled environmental conditions or have not been tested in a HTP context limiting their use for physiological breeding. Additionally, these techniques are hard to deploy in the field, especially in breeding programs where hundreds of plots are grown in close proximity with limited space to manoeuvre large phenotyping equipment.

Recently, optical remote sensing techniques have gained attention due to the possibility of measuring hundreds or thousands of lines without the need of destructive sampling and in a small fraction of time compared to conventional phenotyping methods. Spectral data collected in the field has been used to calculate spectral indices or the full reflectance signature of an area of the electromagnetic spectrum usually ranging from 350 to 2500 nm to predict physiological traits at leaf or canopy scales (Ollinger, 2011; Gamon et al., 2019; Robles-Zazueta et al., 2021). Among the methods using the full spectral range, partial least squares regression (PLSR) modelling has become the gold standard for HTP modelling of physiological traits such as leaf A_{sat}, V_{cmax}, J_{max}, dark respiration, leaf C, N and chlorophyll content, protein, sugars, leaf mass area and specific leaf area (Serbin et al., 2012; Silva-Pérez et al., 2018; Coast et al., 2019; Burnett et al., 2021; Furbank et al., 2021). However, most of the studies have focused in measurements of sunlit leaves at the top of the canopy, this highlights the need for studies that include different layers to integrate the whole canopy.

4.2 Hypothesis

Our hypothesis is that models derived from rapid measurements of multiple layers of the canopy will produce better predictions than models created with individual leaf layers, due to unknown trait variability caused by a gradient from top to bottom of the canopy.

4.3 Objectives

The objectives of this study are to predict photosynthetic, biophysical and biochemical traits using PLSR modelling, to compare the measurements of A_{sat}, gs and transpiration with PLSR predictions and to explore the use of these predictions as means to select wheat genotypes for higher RUE.

4.4 Materials and methods

4.4.1 Plant material and experimental design

Spring bread wheat cultivars chosen from the Photosynthesis Respiration Tails (PS Tails) panel from the International Maize and Wheat Improvement Center (CIMMYT) were grown at CIMMYT's Campo Experimental Norman E. Borlaug (CENEB) field station in Ciudad Obregon, Sonora, Mexico (27° 23' 46'' N, 109° 55' 42'' W, 38 mamsl) during the spring wheat growth season that encompasses early December-early May.

A subset of 8 cultivars and advanced lines were studied in year 1 (Y1) and three more lines were added years 2 and 3 (Y2, Y3) to have a total of 11 lines. Germplasm from this panel is characterized by contrasting RUE expression at vegetative and grain filling stages, high aboveground biomass and these lines are used for their promising high yield potential.

The experimental design was a randomised complete block design with three replicates in raised beds and two beds per plot (Y1), same experimental design but four replications per genotype in Y2 and Y3. Sowing dates were December 5th 2017, December 6th 2018 and December 18th 2019 for Y1, Y2 and Y3 respectively. Emergence dates were December 12th 2017, December 12th 2018 and December 26th 2019 (Y1, Y2 and Y3 respectively). Harvest dates were May 8th 2018, April 30th 2019 and May 13th 2020 (Y1, Y2 and Y3 respectively). Seed rate was ~250 seeds m^{-2} in the three years. Irrigation was applied four times during the crop cycle in approximate 25-day intervals (pre sowing, 25, 50, 75, 100 days after emergence). Plants were grown under optimal conditions in the field with pests, weed control and fertilisation to avoid limitations to yield. In

Y1 fertilization was applied in the form of urea (200 kg N ha^{-1}) 25 days after emergence (DAE). For Y2 fertilization was divided in 100 kg N ha^{-1} 25 DAE and another 100 kg N ha^{-1} 58 DAE. Finally, for Y3 100 kg N ha^{-1} were applied 30 DAE and 50 kg N ha^{-1} 50 DAE; 50 kg P ha^{-1} were applied in the three cycles when the first application of N was made.

Phenology was scored according to the Zadoks growth scale for cereals (Zadoks et al., 1974). The growth stages recorded were initiation of booting (GS41, InB), anthesis (GS65, A) and physiological maturity (GS87, PM) when 50% of the shoots in the plot reached a particular stage. Meteorological data from a nearby station to the experimental site were collected for the whole crop cycle and accumulated PAR was calculated for the growth stages where biomass was collected.

4.4.2 Aboveground biomass and biophysical traits

Aboveground biomass was sampled following Robles-Zazueta et al., (2021). Samples of biomass at InB, A7 and PM were collected. Biomass harvests were made in 0.4 m^2 (40 days after emergence) and 0.8 m^2 (InB, A7), leaving 25 and 50 cm respectively at the northern side of the plots to reduce border effects in subsequent biomass samplings. All fresh biomass was weighed, and a subsample of 50 shoots was weighed and dried in an oven at 70 °C for 48 h, to record dry weight. For biomass at PM, calculations were made from the measurement of yield components. For every growth stage, the aboveground biomass was calculated according to Pask et al., (2013):

$$\text{Aboveground biomass} = \text{Subsample DW} \times \frac{\text{Total FW} \times \text{Harvested area}}{\text{Subsample FW}} \qquad \text{eq. (1)}$$

At InB and A7, 12 shoots were randomly selected for biomass partitioning. In the lab, plant organs were separated in stems, flag, second, third and remaining leaves in GS41 and the same organs plus spikes in GS65 + 7d. After partitioning, leaf areas were measured using an area meter (LI 3100C, Licor Biosciences, Lincoln, NE, USA). Finally, samples were dried in an oven for 2 days at 70°C, weighted and data was used to calculate the leaf area index (LAI), specific leaf area (SLA) and leaf mass area (LMA) as follows:

$$\text{LAI} = \frac{\text{Green leaf lamina area}}{\text{\# stems m}^2} \qquad \text{eq. (2)}$$

$$SLA = \frac{Leaf\ green\ area}{Leaf\ dry\ mass} \qquad \text{eq. (3)}$$

$$LMA = \frac{Leaf\ dry\ mass}{Leaf\ green\ area} \qquad \text{eq. (4)}$$

4.4.3 Radiation use efficiency

RUE was estimated from the slope of the linear regression between accumulated aboveground biomass and the corresponding accumulated intercepted PAR during the determined growth period (Monteith, 1977). Incoming radiation from a nearby meteorological station was used to estimate the accumulated PAR multiplying irradiance by a factor of 0.45 to convert it to PAR and ceptometer (AccuPAR LP-80, Decagon, Pullman, WA, USA) readings were used to correct the accumulated radiation for the fraction of absorbed PAR by each genotype following the same procedure explained in length in chapter 2 (Robles-Zazueta *et al.* 2021).

4.4.4 Photosynthetic and chlorophyll measurements

Spot measurements of A_{sat}, *gs*, transpiration (E), the maximum efficiency of PSII photochemistry under light conditions (F_v'/F_m') and photosystem II quantum yield (ΦPSII) were made using an IRGA (Licor 6400 XT, Licor Biosciences, Lincoln, NE, USA) at InB (Y1 and Y2) and A7 (Y1, Y2, Y3) coupled with the leaf chamber fluorometer (6400-40 Licor Biosciences, Lincoln, NE, USA).

Photosynthetic measurements were made at the flag (top of the canopy), second (middle of the canopy) and third (bottom of the canopy) leaves in two healthy shoots per plot with light conditions set at 1800 µmol m^{-2} s^{-1} PAR and leaves were acclimated for ~15-20 min until steady state was reached. Chlorophyll content was measured using a SPAD-502 meter (Konika Minolta, Japan) in the same leaves where photosynthesis was measured (Pask et al., 2013).

Measurements were performed between 10:00-15:00 as this timeframe has been found to maximize the stability and accuracy of the measurements (Evans and Santiago, 2014). Then CO_2 assimilation (A_{sat}), stomatal conductance (*gs*) and transpiration (E) were upscaled from leaves to canopy level by multiplying each individual layer value by the LAI of its corresponding layer. This is an adaptation of the protocol for upscaling C and N content proposed by Gara et al., (2019). Calculations are shown in equations 5 and 6:

$$\text{Canopy Photosynthesis} = \sum(A_{sat}FL \times LAI\ FL) + (A_{sat}SL \times LAI\ SL) +$$

$$(A_{sat}TL \times LAI\ TL) \qquad \qquad \text{eq. (5)}$$

$$\text{Canopy Transpiration} = \sum(E\ FL \times LAI\ FL) + (E\ SL \times LAI\ SL) +$$

$$(E\ TL \times LAI\ TL) \qquad \qquad \text{eq. (6)}$$

Where A_{sat} is CO_2 assimilation, E is transpiration, LAI is leaf area index, and FL, SL, TL are flag leaf, second leaf and third leaf respectively.

For *gs*, an average of the three layers of the canopy was estimated to obtain a *gs* pooled value of the canopy to assess if average *gs* of any leaf in the canopy correlated better with the traits of interest.

4.4.5 Total C and N content

Flag, second and third leaf samples from each genotype were collected from the field to obtain the total C and N content at GS41 and GS65 + 7d in Y1 and Y2. Leaf samples were dried in an oven at 70 °C for 48 h, then finely grounded, weighted and analysed with the dry combustion Dumas method using an elemental analyser (Flash 2000, Thermo Scientific, Waltham, MA, USA).

4.4.6 Leaf hyperspectral reflectance

Hyperspectral reflectance was collected on the adaxial sides of the same leaves were gas exchange data was collected. Measurements were made using a leaf clip equipped with a halogen bulb light source (ASD Field Spec® 3, Boulder, CO, USA). Reflectance was measured in the flag, second and third leaves at the same growth stages as photosynthesis measurements, making sure there were not water or dust particles in the leaves to avoid noisy readings and were collected between 10:00-15:00.

4.4.7 Statistical analysis

Leaf spectral reflectance (350-2500 nm) collected at the three positions of the canopy was used to predict the photosynthetic, biophysical and biochemical traits using the PLSR method (Serbin et al., 2012; Serbin et al., 2014) using the pls package from R Studio (Mevik and Wehrens, 2007). Before constructing the models, outliers of the traits measured were removed ($\pm 3 \sigma$) and the dataset was divided for training (70%) and validation (30%). A jackknife resampling test with 1000 iterations was done to estimate the variance and model bias. Then the number of components used was defined by the smallest root mean square error from the cross validation stage (RMSEP CV) in conjunction with the smallest prediction of the residual sum squares from the training model. After the validation process, regression coefficients and intercepts were generated and multiplied by the reflectance value of each individual wavelength to predict the abovementioned traits (Serbin et al., 2014; Silva-Pérez et al., 2018).

The models were built based on two approaches: individual layers and all canopy layers combined. The size of the training and validation dataset and statistical parameters used to evaluate the models is presented in Table 4.1. Then results were compared to define which approach was better to predict the physiological traits based on the regression coefficient (R^2), root mean square error (RMSE) and the model bias (Table 4.1). Furthermore, variable importance in projection (VIP) scores for each physiological trait were calculated to define which areas of the electromagnetic spectrum carry significant weight for the model construction, where values >1 represent areas of higher importance comparted to values <1.

Table 4.1. Statistical parameters used to build the PLSR models. The lowest RMSEP CV was used to select the ideal number of components. NT: Datapoints used for training dataset, NV: Datapoints used for validation dataset, RMSEP CV: root mean square error from cross validation, NC: Number of components, R^2T: Determination coefficient from test model, R^2V: Determination coefficient from validation model, RMSE_V: root mean square error from validation, Bias_V: Validation model bias.

Trait	Layer	NT	NV	RMSEP CV (Trait units)	NC	R^2T	R^2V	RMSE_V (Trait units)	Bias_V (%)
A_{sat}	Top	157	69	4.47	10	0.23	0.11	4.96	-0.78
	Middle	155	67	4.51	11	0.48	0.34	6.6	1.28
	Bottom	146	64	4.65	10	0.16	0.07	5.82	0.54
	Combined	525	198	5.19	15	0.46	0.48	5.24	-0.32
gs	Top	155	67	0.14	5	0.11	0.17	0.16	0.004
	Middle	149	64	0.14	5	0.29	0.37	0.15	-0.01
	Bottom	155	69	0.14	5	0.28	0.22	0.15	0.019
	Combined	460	199	0.14	13	0.34	0.36	0.14	0.005
E	Top	157	69	1.31	8	0.05	0.15	1.35	0.09
	Middle	155	69	1.45	6	0.34	0.39	1.56	0.54
	Bottom	156	69	1.37	7	0.28	0.37	1.42	0.27
	Combined	471	204	1.26	20	0.39	0.39	1.42	-0.05
F_v'/F_m'	Top	151	66	0.03	12	0.27	0.36	0.04	0.008
	Middle	154	67	0.03	10	0.03	0.18	0.81	-0.81
	Bottom	152	67	0.04	6	0	0.1	0.05	-0.13
	Combined	458	199	0.04	14	0.16	0.17	0.05	-0.003
ΦPSII	Top	157	69	0.03	12	0.49	0.29	0.04	0.0037
	Middle	154	64	0.04	8	0.43	0.52	0.04	0.001
	Bottom	145	63	0.03	12	0.26	0.56	0.04	-0.004
	Combined	458	198	0.04	14	0.57	0.57	0.04	-0.003
SPAD	Top	150	66	2.08	5	0.61	0.63	2.2	-0.03
	Middle	155	68	1.99	10	0.24	0.24	1.56	0.54
	Bottom	152	69	2.88	3	0.07	0.04	2.79	-0.25
	Combined	460	198	2.4	13	0.47	0.48	2.48	0.217
Total C	Top	89	40	1.3	8	0.38	0.3	1.9	-0.922
	Middle	85	39	1.71	1	0.05	0.03	1.86	-0.48
	Bottom	84	37	1.73	3	0.06	0.02	1.95	0.175
	Combined	260	114	0.66	27	0.33	0.35	1.5	0.15
Total N	Top	90	40	0.11	20	0	0	0.62	0.093
	Middle	88	39	0.38	6	0.35	0.3	0.56	0.0714
	Bottom	87	38	0.38	9	0.44	0.31	0.53	0.0082
	Combined	266	116	0.44	8	0.3	0.38	0.49	0.008
SLA	Top	153	67	3.74	3	0.03	0.17	4.18	0.033
	Middle	122	54	2.92	10	0.11	0.01	3.66	0.354
	Bottom	136	59	3.07	13	0.57	0.63	4.38	-0.241
	Combined	413	178	4.38	6	0.31	0.32	5.23	-0.117
LMA	Top	150	65	0.01	3	0.07	0.05	0.01	-0.0013
	Middle	119	52	0.01	2	0.01	0.01	0.01	-0.002
	Bottom	134	60	0	14	0.49	0.56	0.01	-0.0001
	Combined	450	195	0.01	14	0.49	0.46	0.01	-0.0013
LAI	Top	149	64	0.34	7	0.02	0.06	0.36	0.078
	Middle	129	57	0.34	4	0.05	0.03	0.42	-0.057
	Bottom	126	56	0.31	7	0.11	0.06	0.47	-0.1916
	Combined	430	186	0.45	13	0.12	0.28	0.44	-0.0241

Bilinear unbiased estimators (BLUEs) were calculated for each trait measured on the field using the general linear mixed model with META-R v 6.04 (Alvarado et al., 2020). Physiological traits were adjusted using the days to initiation of booting as a covariate for traits measured during the vegetative stage and days to anthesis for traits measured during the grain filling stage. For the analysis combined across the three years, the following model was used:

$$Y_{ijkl} = \mu + Env_i + Rep_j(Env_i) + Gen_l + Env_i \ x \ Gen_l + Cov + \varepsilon_{ijkl} \qquad \text{eq. (7)}$$

Where Y_{ijkl} is the trait of interest, μ is the mean effect, Env_i is the effect of the ith environment, Rep_j is the effect of the jth replicate, Gen_l is the effect of the lth genotype, Env_i x Gen_l are the effects of the ith environment and the environment x genotype interaction, Cov is the effect of the covariate and ε_{ijkl} is the error associated with the environment i, replication j, kth incomplete block and lth genotype. In this study the term environment refers to the individual year where data was collected (Y1, Y2 or Y3) therefore three environments were analysed.

Broad sense heritability (H^2) across environments was calculated as follows:

$$H^2 = \frac{\sigma_g^2}{\sigma_g^2 + \frac{\sigma_{ge}^2}{nEnv} + \frac{\sigma_e^2}{(nEnv \ x \ nreps)}} \qquad \text{eq. (8)}$$

Where σ_g^2 is the genotype error variance, σ_e^2 is the environment error variance, σ_{ge}^2 is the genotype x environment interaction error variance, nEnv is the number of environments and nreps the number of replicates.

Finally, in order to compare our estimations of A_{sat}, gs and E with the predictions from PLSR models, we used the equations generated from the validation models and calculated BLUEs of the predicted A_{sat}, gs, E and LAI to upscale these predictions to a canopy level.

4.5 Results

4.5.1 Canopy layer position and phenological effects on photosynthetic traits

Photosynthetic traits were greater in the middle leaf layer of the canopy than the top layer in InB and strong statistical differences were found between the middle and bottom layers of the canopy, with greater A_{sat}, *gs* and E rates in the middle layer (Table 4.2). With exception of total C content, statistically significant differences between layers were found in all the physiological traits measured in this study. Similarly, differences between growth stages were strongly significant for all the traits. This highlights the importance of considering adding data from different phenological stages to build more robust models that could predict these traits at any given point in time of the wheat growing season (Table 4.2).

Our results showed that genetic variation of the main photosynthetic traits within individual leaf layers was not found (Table 4.3), however statistically significant differences were found between layers, growth stages, and the interaction layer x growth stage (Table 4.2). Additionally, no significant differences were found by the genotype x position and genotype x environment x position interactions (Table 4.2). Most of the traits showed a lower H^2 at InB compared to A7. For photosynthetic traits, H^2 was higher in the middle layer, except for *gs* which showed the highest H^2 at the bottom of the canopy (Table 4.2).

4.5.2 Predicting photosynthetic, biophysical and biochemical traits with hyperspectral reflectance

Fv'/Fm' was the photosynthetic trait with the smallest accuracy prediction of all, both for the separated (Top: $R^2 = 0.36$, Middle: $R^2 = 0.18$, Bottom: $R^2 = 0.1$) and combined layers approach ($R^2 = 0.17$) (Figure 4.1A and Figure 4.1D, respectively). On the other hand, ΦPSII and SPAD predictions were traits with a great relation between observations and predictions with both approaches. In the case of ΦPSII, the middle and bottom layer of the canopy were crucial to improve model accuracy, while the top layer had a smaller regression value (Figure 4.1B); this was opposite to SPAD predictions where the top layer of the canopy had the highest relationship, therefore the most influence, on model accuracy (Figure 4.1C, upper panel). In the case of these three traits, we found that the two approaches produced similar regressions between observations and predictions, but in the case of Fv'/Fm' the combined layer approach was better (Figure 4.1, bottom panels).
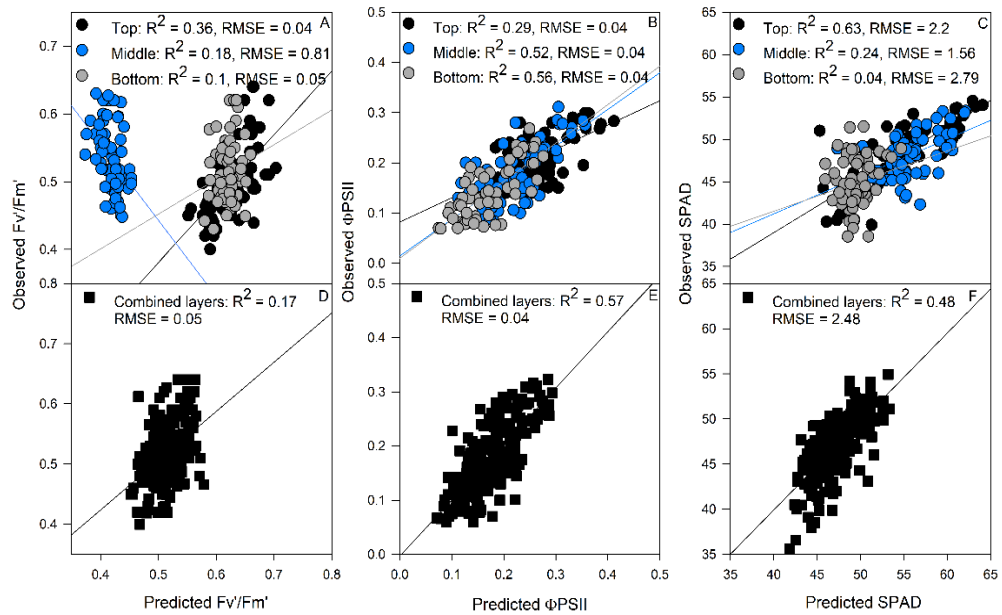
Figure 4.1. Validation results of PLSR models predicting Fv'/Fm' (A), ΦPSII (B) and SPAD (C) by separating each layer of the canopy (top panels) and predictions of Fv'/Fm' (D), ΦPSII (E) and SPAD (F) combining all layers of the canopy (black squares). Black dots: top of the canopy, blue dots: middle of the canopy, grey dots: bottom of the canopy.

Total C (%) and N (%) predictions were poor compared to the photosynthetic traits, possibly due to a smaller sampling size compared to the other traits predicted (Table 4.1) and the experimental conditions where N was not a limiting factor coupled with low genetic variability as only eleven genotypes were studied (Table 4.3), could have had an effect on the low predictions of these two traits. The top layer produced best predictions for C content (Figure 4.2A, $R^2 = 0.3$, RMSE = 1.9), whilst the middle and bottom layers were more important for N content predictions (Figure 4.2B, $R^2 = 0.3$, p<0.001 and $R^2 = 0.31$, p<0.001, respectively). When all the layers were combined, predictions were better than separating the layers for both traits with RMSE of 1.5% and 0.49% for C and N prediction, respectively (Figure 4.2A and 4.2B, bottom panels). N content decreased from top to bottom of the canopy, but C content was equally distributed through the canopy. Both traits had the smallest H^2, which suggests

these traits are highly dependent on field management, environmental conditions and sampling size (Table 4.3).
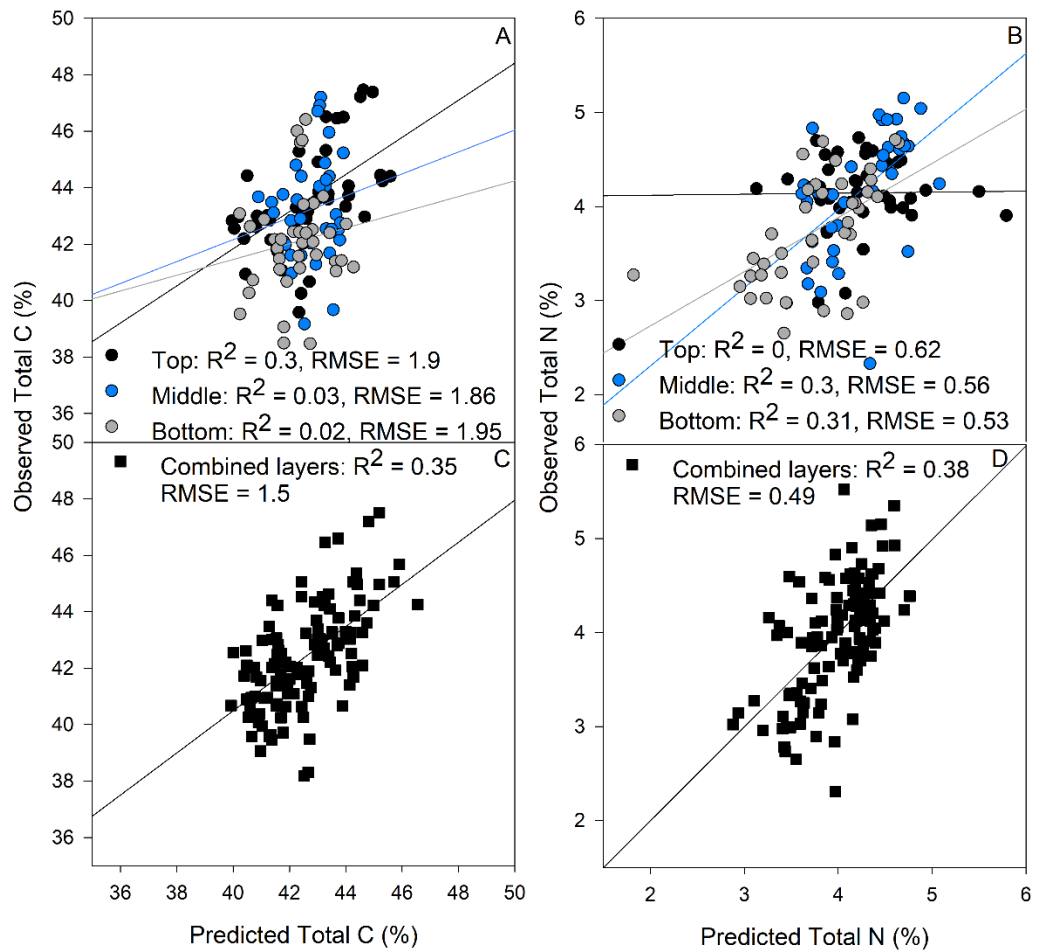
Figure 4.2. Validation results of PLSR models predicting total carbon (A) and nitrogen (B) content by separating each layer of the canopy (top panels) and predictions of total carbon (C) and nitrogen (D) combining all layers of the canopy (black squares). Black dots: data collected at the top of the canopy, blue dots: data collected at the middle of the canopy, grey dots: data collected at the bottom of the canopy.

Table 4.2. Mean ± standard deviation values of canopy traits measured in this study. T = Top, M = Middle, B = Bottom represent the layer of the canopy where the measurement was taken. * = p<0.05, ** = p<0.01, *** = p<0.001, ms = 0.1>p>0.05, ns = no significance.

Trait	Initiation of booting			7 days after anthesis			L	GxL	EnvxL	GxEnvxL	GS	LxGS	GSxEnv	LxGSxEnv
	T	M	B	T	M	B								
A_{sat}	25.5±3.07	26.9±4.7	15.9±4.12	22±3.96	16.7±3.98	10.1±3.7	***	ns	ms	ns	***	***	ns	ns
gs	0.39±0.12	0.46±0.15	0.34±0.14	0.32±0.09	0.25±0.09	0.15±0.06	***	ns	ms	ns	***	***	ns	ns
E	4.9±1.08	5.57±1.13	4.44±1.29	4.19±0.9	3.42±0.91	2.26±0.85	***	ns	ms	ns	***	***	***	ns
F_v'/F_m'	0.47±0.03	0.52±0.03	0.5±0.027	0.52±0.03	0.54±0.03	0.51±0.03	***	ns	*	ns	***	***	***	ns
ΦPSII	0.31±0.02	0.31±0.037	0.26±0.04	0.25±0.029	0.22±0.029	0.17±0.03	***	ns	ns	ns	***	***	***	ns
LAI	1.53±0.33	1.73±0.33	1.75±0.34	1.43±0.3	2.31±0.62	2.14±0.54	***	ns	***	ns	***	***	***	***
C	44.5±1.49	44.2±1.61	42.6±1.64	40.4±2.15	41.1±4.16	43.4±5.55	ns	ns	ms	ns	***	***	ns	**
N	4.4±0.34	4.6±0.4	4.2±0.47	4±0.48	3.7±0.64	3.6±0.8	**	ns	ns	ns	***	ns	ns	**
SLA	19.8±3	20.4±2.15	24.2±1.92	17.6±2.27	37.4±5.04	31.9±3.83	***	ns	***	ns	***	***	***	***
LMA	0.05±0.01	0.05±0.005	0.04±0.004	0.06±0.01	0.04±0.004	0.04±0.005	***	ns	***	ns	***	***	***	***
SPAD	45.8±2.16	48.1±1.71	45.3±2.34	50.6±1.93	49.3±2.18	44.4±2.78	***	ns	*	ns	***	***	***	***

L: Layer, GxL: Genotype x Layer, EnvxL: Environment x Layer, GxEnvxL: Genotype x Environment x Layer, GS: Growth Stage, LxGS: Layer x Growth Stage, GSxEnv: Growth Stage x Environment, LxGSxEnv: Layer x Growth Stage x Environment.

Table 4.3. Heritability, statistical differences by genotype, environment and the interaction genotype by environment of the measured traits at initiation of booting and 7 days after anthesis. * = p<0.05, ** = p<0.01, *** = p<0.001, ms = 0.1>p>0.05, ns = no significance.

| | Initiation of booting | | | | | | | | | | | | 7 days after anthesis | | | | | | | | | | | |
| | H^2 | | | G | | | Env | | | GxEnv | | | H^2 | | | G | | | Env | | | GxEnv | | |
Trait	T	M	B	T	M	B	T	M	B	T	M	B	T	M	B	T	M	B	T	M	B	T	M	B
A_{sat}	0.37	0.09	0	ns	ns	ns	ns	ns	ns	ns	ns	ms	0.43	0.73	0.54	ms	***	*	**	**	**	ns	ns	ns
gs	0.26	0	0	ns	ns	ns	ns	ns	ns	ns	**	*	0.47	0.65	0.73	ms	**	**	**	***	**	**	*	ns
E	0	0	0	ns	ns	ns	ns	ns	ns	*	**	*	0.47	0.77	0.73	ms	***	***	**	**	**	ns	ns	ns
F_v'/F_m'	0.34	0.7	0	ns	**	ns	*	**	ns	ns	ns	ns	0.36	0.26	0.7	ns	ns	**	**	*	**	ns	ms	*
ΦPSII	0	0	0	ns	ns	ns	*	**	**	ms	ms	ns	0.69	0.71	0.42	**	**	ms	***	***	***	ns	ms	ns
LAI	0.56	0.32	0.54	*	ns	*	*	ns	ms	ms	ns	ns	0.58	0.35	0.03	*	ns	ns	ns	***	***	ms	ns	ns
C	0	0	0.07	ns	ns	ns	ns	ns	ns	ns	*	ns	0	0	0	ns	ns	ns	ns	ns	ns	ns	ns	ns
N	0.11	0.07	0	ns	ns	ns	*	ns	ns	ns	*	*	0.51	0	0	ns	ns	ns	ns	ns	ns	ns	ms	ns
SLA	0.17	0.62	0.07	ns	*	ns	**	***	***	ns	ns	ns	0.12	0.33	0	ns	ns	ns	***	***	***	*	ns	**
LMA	0.36	0.76	0.23	ns	***	ns	**	***	***	*	ns	ns	0.29	0.1	0.16	ns	ns	ns	***	***	***	ns	ns	***
SPAD	0.36	0.74	0.6	ns	***	*	ns	**	*	**	ns	ns	0.87	0.86	0.81	***	***	***	***	ns	ms	ns	ns	ns

H^2: Heritability, G: Genotype, Env: Environment, GxEnv: Genotype x Environment.

The bottom layer predictions were more accurate than top and middle layers for the biophysical traits. Predictions at the bottom for SLA were $R^2 = 0.63$, p<0.001, for LMA were $R^2 = 0.56$, p<0.001, and for LAI were $R^2 = 0.06$, p<0.1 (Figure 4.3A, 4.3B and 4.3C, respectively). When combining the three layers the results were similar for LMA and better for LAI predictions, but in the case of SLA the separated layer model produced predictions (Figure 4.3D, 4.3E and 4.3F, respectively). These results comply with our field observations as narrower smaller leaves at the top layer and broader, larger leaves at the middle and bottom layers of the canopy were found (Table 4.2).
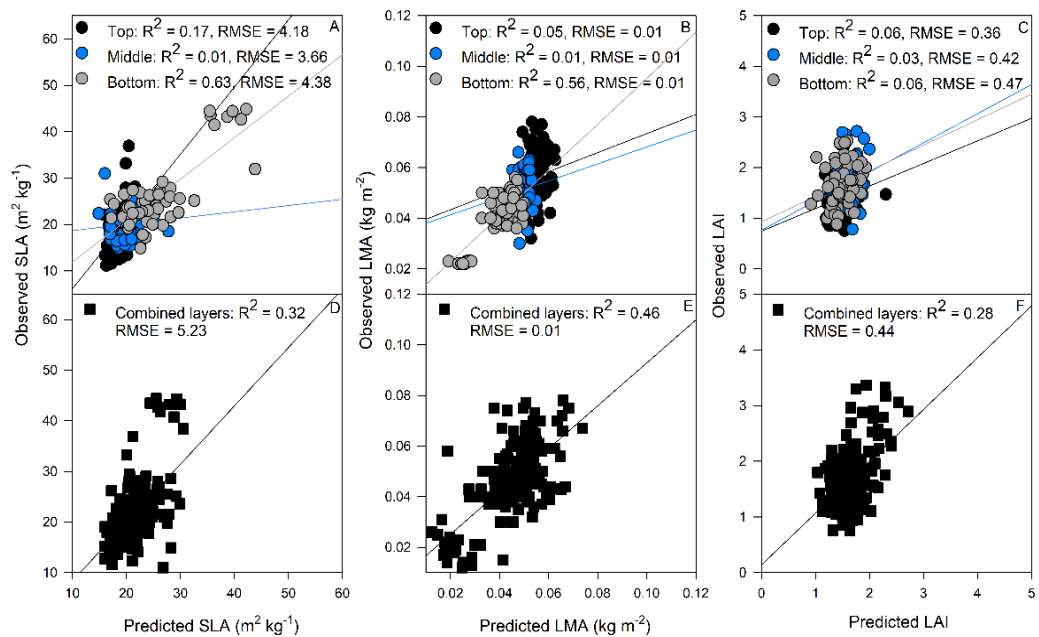
Figure 4.3. Validation results of PLSR models predicting specific leaf area (SLA) (A), leaf mass area (LMA) (B) and leaf area index (LAI) (C) by separating each layer of the canopy (top panels) and predictions of SLA (D), LMA (E) and LAI (F) combining all layers (bottom panels, black squares). Black dots: data collected at the top of the canopy, blue dots: data collected at the middle of the canopy, grey dots: data collected at the bottom of the canopy.

Our results indicate that photosynthetic traits prediction was better using the combined layer approach rather than estimating the traits separated (Figure 4.4), except for E where the two approaches yielded similar results (Figure 4.4C and

Figure 4.4F). A_{sat} predictions from the combined model had RMSE of 5.24 µmol

m^{-2} s^{-1} (Figure 4.4D), *gs* RMSE of 0.14 mol m^{-2} s^{-1} (Figure 4.4E) and

transpiration RMSE of 1.42 mmol m^{-2} s^{-1} (Figure 4.4F). For these three traits the

middle layer had more importance for model accuracy (Figure 4.4, upper

panels).
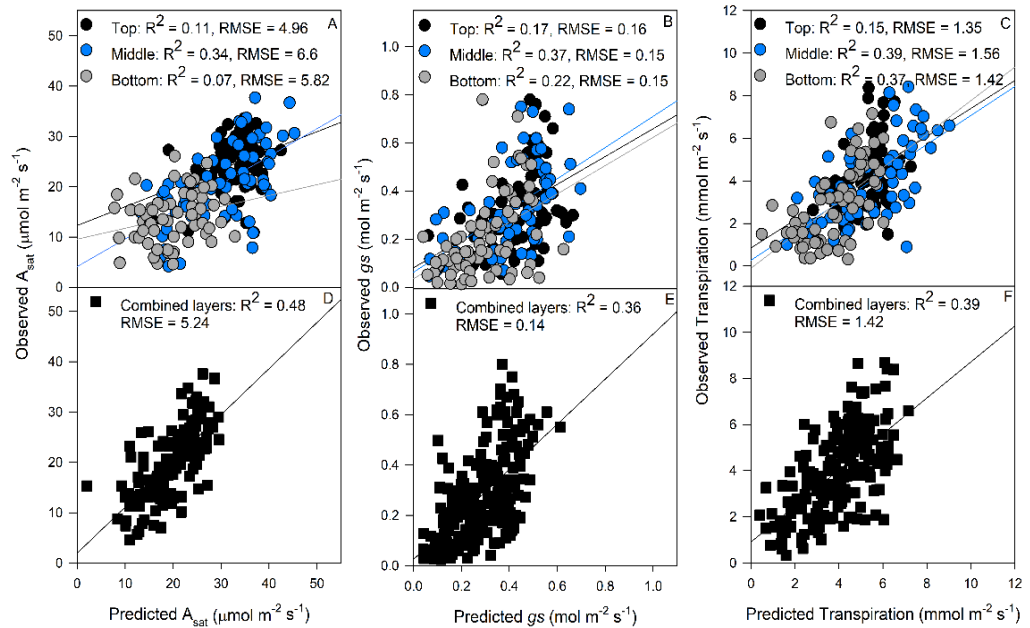
Figure 4.4. Validation results of PLSR models predicting A_{sat} (A), *gs* (B) and E (C) by separating each layer of the canopy (top panels) and predictions of A_{sat} (D), *gs* (E) and E (F) combining all layers (bottom panels, black squares). Black dots: data collected at the top of the canopy, blue dots: data collected at the middle of the canopy, grey dots: data collected at the bottom of the canopy.

Variable importance in projection (VIP) scores were calculated to find spectrum

areas with most importance in the model building. We found three main areas

with greatest importance in the building of the photosynthetic, biophysical and

biochemical models at 350-369 nm, 527-575 nm and 671-750 nm. These three

peaks correspond to an area of the spectrum known as visible near infrared

(VNIR) which has relevance for gas exchange, canopy greenness, water content,

biophysical and biochemical traits such as the ones from this study. After smaller

peaks in the shortwave infrared region (SWIR), spectral wavelengths above 1436 nm lacked importance for the predictive model building (VIP scores <1) (Figure 4.5).
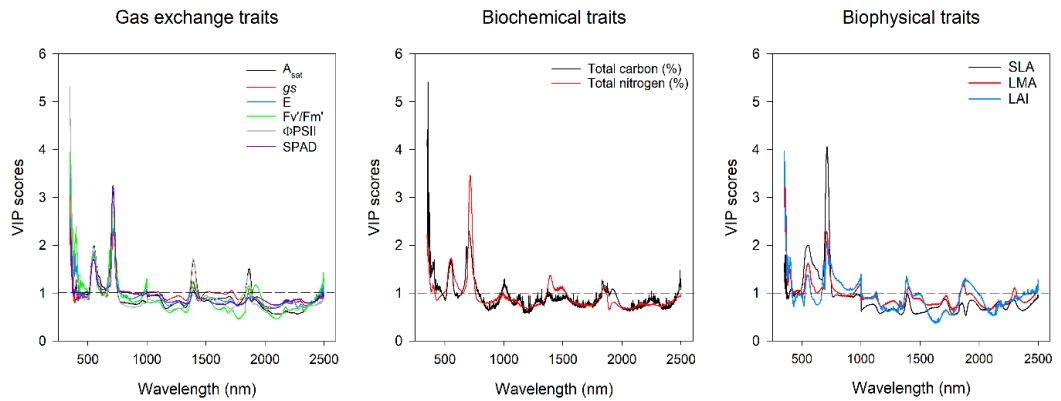
Figure 4.5. Variable importance in projection plot of gas exchange, biochemical and biophysical traits of the models built with all the canopy layers combined. Y axis represent the variance importance score where values >1 represent wavelengths with greater weight for the model predictions. X axis represent the wavelength (nm). Physiological traits are represented by different colours in each plot as indicated in the figure legends.

4.5.3 Photosynthetic predictions and their relationship with RUE

The prediction accuracy for canopy A_{sat} at InB was better ($R^2 = 0.3$, $p<0.05$) than predictions at A7 ($R^2 = 0.15$, $p<0.05$) (Figure 4.6). Canopy E had a similar trend as canopy A_{sat} predictions with better predictions found at InB ($R^2 = 0.61$, $p<0.001$) compared to predictions at A7 ($R^2 = 0.06$) (Figure 4.6). For averaged gs, our results showed statistical significant relationships between ground truth data and predictions both at InB ($R^2 = 0.29$, $p<0.05$) and A7 ($R^2 = 0.65$, $p<0.001$) (Figure 4.6).
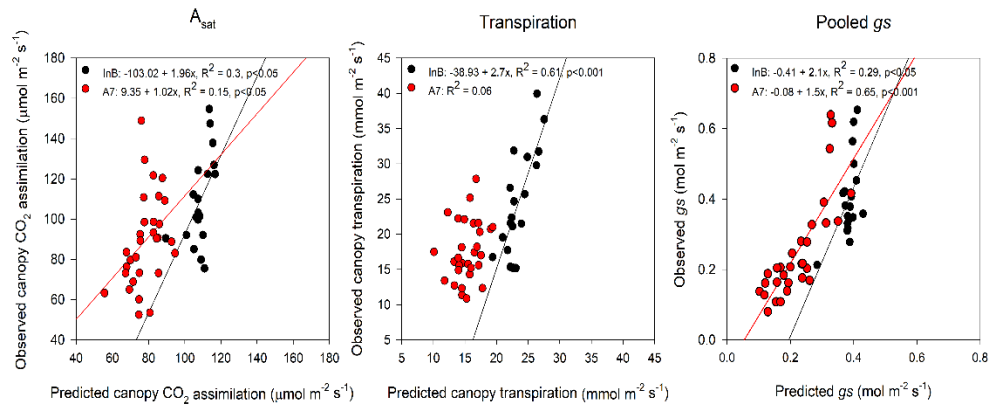
Figure 4.6. Comparison between observations and predictions of canopy assimilation, transpiration and stomatal conductance. Black dots represent data from initiation of booting and red dots from 7 days after anthesis. Data shown are the observed vs predicted BLUEs in 2 years of study (InB, n = 19) and 3 years of study (A7, n = 30).

The positive associations between RUE from canopy closure to InB (RUE_E40InB) with predicted canopy A_{sat} from InB ($R^2 = 0.22$, p<0.05) and A7 ($R^2 = 0.35$, p<0.001) were statistically significant. We found a marginally significant association between canopy A_{sat} predictions at A7 and RUE_InBA7 ($R^2 = 0.13$, p<0.1). No significant relationships were found for RUE_preGF, but a link between RUE_GF and canopy A_{sat} A7 was found ($R^2 = 0.16$, p<0.05). Finally, the link found between RUE of the whole crop cycle (RUE_Total) and canopy A_{sat} predictions was positive and the strongest of any growth stage ($R^2 = 0.37$, p<0.01 for InB; and $R^2 = 0.41$, p<0.001 for A7) (Figure 4.7).

Predicted pooled *gs* at InB correlated significantly with RUE_E40InB ($R^2 = 0.12$, p<0.05) and RUE_Total ($R^2 = 0.28$, p<0.05). For predictions at A7 significant relations were found with RUE_InBA7 ($R^2 = 0.19$, p<0.05), RUE_preGF ($R^2 = 0.13$, p = 0.05) and RUE_Total ($R^2 = 0.3$, p<0.01). Marginally significant associations were also found at RUE_GF ($R^2 = 0.1$, p<0.1) (Figure 4.8). Finally, for most of the growth stages where RUE and predicted canopy A_{sat} and *gs* were associated these relationships were positive.
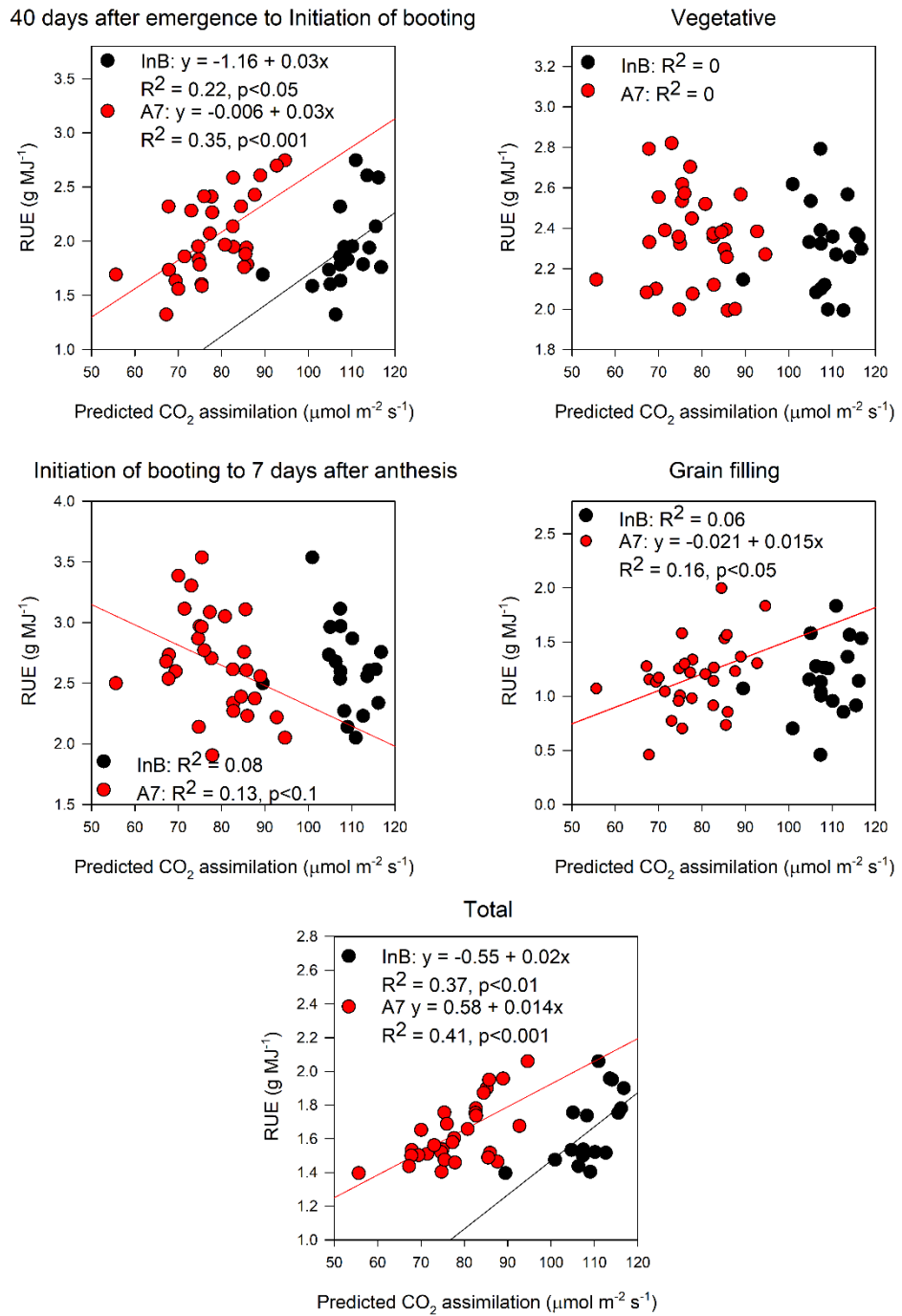
Figure 4.7. Relationship between radiation use efficiency measured at different growth stages and predictions of canopy photosynthesis retrieved using partial least squares regression. Black dots represent data from initiation of booting and red dots from 7 days after anthesis. Data shown are the observed vs predicted BLUEs in 2 years of study (InB, n = 19) and 3 years of study (A7, n = 30).
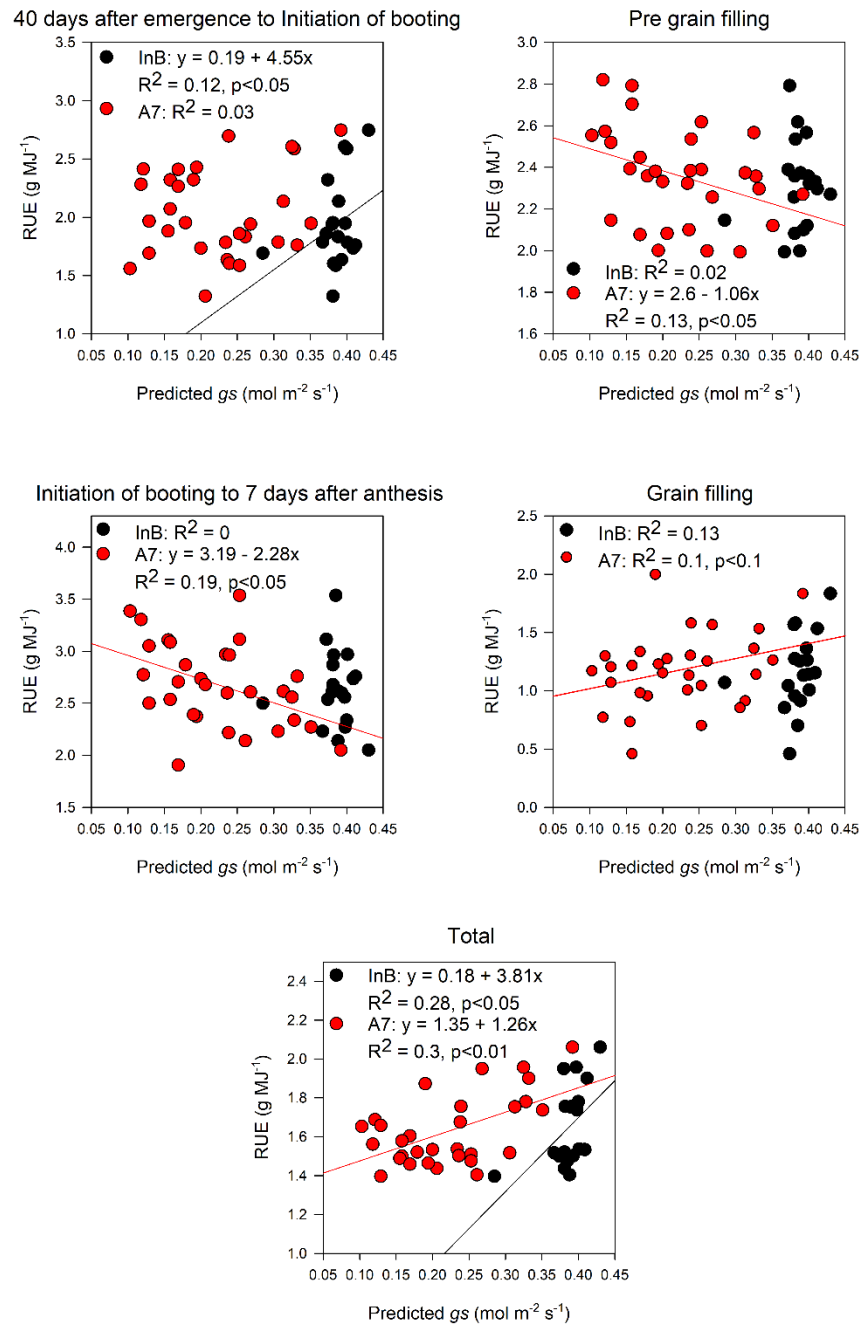
Figure 4.8. Relationship between radiation use efficiency measured at different growth stages and predictions of canopy average stomatal conductance retrieved using partial least squares regression. Black dots represent data from initiation of booting and red dots from 7 days after anthesis. Data shown are the observed vs predicted BLUEs in 2 years of study (InB, n = 19) and 3 years of study (A7, n = 30).

4.6 Discussion

Natural variation of photosynthetic traits has not been fully exploited in breeding programs, representing a crucial untapped resource fundamental to increase wheat yields (Molero and Reynolds 2020). Mainstreaming photosynthetic traits into breeding pipelines has been limited by the lack of methods to quantify them in a HTP context under field conditions.

Leaf and canopy hyperspectral reflectance measurements have largely been acknowledged as proxies with the potential to quantify different photosynthetic, biophysical and biochemical traits at HTP (Silva-Pérez et al., 2018; Ely et al., 2019; Meacham-Hensold et al., 2020). Previous studies combining spectral reflectance and PLSR modelling to predict physiological traits have mostly focused on sunlit leaves at the top of the canopy, and thus they may not be representative of the whole canopy. In contrast, our models were developed to predict physiological traits within the canopy during the vegetative and grain filling wheat stages.

Our approach showed that the best predictions were achieved when the three layers of the canopy were combined compared to using individual layers for most traits measured. The results in this study add relevance to measurement of physiological traits not only in the top layer of wheat canopies but highlight middle and bottom layers as they showed higher H^2, improved the accuracy of the models and can provide robust information to find wheat genotypes that could adapt better to light gradients and exploit them in order to increase canopy photosynthesis.

The use of the leaf clip attached to the field spectroradiometer allowed us to perform comfortably measurements at the top and middle layers of the canopy, but at the bottom layer measurements became hard to do. Therefore, new spectroradiometer alternatives which are lighter and easier to deploy in field conditions should be considered to improve bottom layer phenotyping as this is still necessary to measure lower parts of the canopy as UAVs are only able to collect data from the top layer of the canopy.

4.6.1 Biochemical and biophysical traits

Compared to previous studies our predictions of %C and %N are the lowest reported to date (R^2 = 0.35, 0.38 for C and N, respectively) and besides LAI, SLA and Fv'/Fm' these traits also showed low R^2 compared to the other traits predicted (Table 4.1). We hypothesize that this could be due to the variability of these traits within the canopy layers and across growth stages. In particular, significant differences between layers, growth stages and the interaction of these two factors plus a decreasing trend for %N across both the layers and growth stages was found (Table 4.2). In other studies predicting N traits, regressions between observations and predictions were very high, including N per leaf mass (R^2 = 0.7, 0.89, 0.97, 0.91) in wheat, aspen, cotton and temperate forest trees (Serbin et al., 2012; Serbin et al., 2014; Silva-Pérez et al., 2018; Coast et al., 2019). Predictions of %C and %N were high for tobacco (R^2 = 0.75, 0.76 respectively) when a larger portion of the spectra was used (500-2400 nm) compared to canopy level (R^2 = 0.74, 0.66) hyperspectral camera measurements with a smaller spectral range (500-900 nm) (Meacham-Hensold *et al.* 2020), for the average of predictive models including tomato, cucumber, soybean and

poplar (R^2 = 0.95, 0.92; Ely *et al.*, 2019) and wheat (R^2 = 0.94; Ecarnot *et al.*, 2013)

The importance of measuring N content in plant leaves comes from the fact that N is defined as an important resource required in large quantities for the photosynthetic machinery, and its distribution within plant canopies has often been described to follow a gradient (from higher to lower content) in relation to the position of the leaf, following the same pattern as light distribution, gradients of chlorophyll a:b and Rubisco (Evans 1993; Hikosaka 2016). This distribution pattern has an effect on canopy architecture as leaves with high N content are characteristic of canopies with higher SLA and this was found in the middle layer of the canopy in this study (Table 4.2). Leaves with higher N content tend to be thicker and have larger mesophyll surfaces to arrange the chloroplasts, remobilize N to the grain and regulate the use of Rubisco (Moreau *et al.* 2012). In general, the N predictions were very poor, especially at high leaf N levels (4-6%). This can be explained due to the management conditions in our experimental site, where full irrigation and high N availability can contribute to the relative high N values and lack of genetic variability in the flag leaf, additionally the high levels of N in flag leaves might have contributed to the lack of genetic variation in A_{sat} amongst genotypes in the top layer of the canopy.

The results from individual layers and whole canopy predictions indicate that the growth stage where measurements are taken is key to build the predictive models, in this case A7 predictions being better than InB due to the lack of genetic variability at this stage (Table 4.3). The reasons for the lack of variation at InB could be the small variation in phenology (6 days variation between the most advanced and delayed lines) and the fact that leaves are still accumulating

N at InB, compared to A7 where it is likely that leaf N is being remobilized to the spikes to fill the grains. This makes the case of accounting the variability associated with leaf area and incident radiation of each layer, which affects light scattering in the canopy and influences its N content. Furthermore, the models to predict N content could improve if the number of genotypes studied is increase by adding more genetic variability.

4.6.2 Photosynthesis high-throughput phenotyping

The prediction accuracy for A_{sat} in this study ($R^2 = 0.48$, RMSE = 5.24) is within the range of previous studies in spring bread wheat ($R^2 = 0.49$, RMSE = 3.93; Silva-Pérez et al., 2018), brassica, moricandia and maize ($R^2 = 0.49$, RMSE = 4.98; $R^2 = 0.37$, RMSE = 4.98; $R^2 = 0.62$, RMSE = 3.64, respectively; Heckmann et al., 2017), and tobacco measured above the canopy (450-900 nm and 450-1700 nm) and in the top leaf layer (350-2500 nm) ($R^2 = 0.54$, 0.5, 0.56; RMSE = 7.77, 8.52, 7.04, respectively; Meacham-Hensold et al., 2020). But they were lower compared to reports in tropical trees ($R^2 = 0.74$, RMSE = 2.85; Doughty et al., 2011) and wheat grown under different salinity concentrations ($R^2 = 0.73$, RMSE = 2.25; El-Hendawy et al., 2019). Including different layers of the canopy to our models improved the accuracy of the models compared to only predicting the top layer ($R^2 = 0.11$, RMSE = 4.96, Figure 4.1). This solidifies the importance of accounting for the variability associated with leaf area, incident radiation levels and N content in the canopy, which affects light scattering within the canopy thus influencing top, middle and bottom A_{sat} rates.

The variation of A_{sat} within canopy layers can be explained by genetic variation of canopy architecture found in LAI and SLA (Table 4.2), as light penetrating in areas of the canopy where leaves are smaller (and usually erect) will generate differences in light quality and quantity in the bottom layers of the canopy where large amounts of diffuse radiation and decreased red:far red and blue:red ratios compared to the top layers are found (Burgess et al., 2021).

Stomatal conductance has been predicted previously only in wheat (Silva-Pérez et al., 2018; El-Hendawy et al., 2019; Furbank et al., 2021). In spring wheat elite and landrace cultivars grown in Northwest Mexico, prediction accuracies for *gs* were the lowest for a set of traits studied ($R^2 = 0.34$, RMSE = 0.15) and had the largest associated prediction error (Silva-Pérez et al., 2018). In salt sensitive and tolerant genotypes El-Hendawy et al., (2019) found very high associations between observations and predictions of *gs* between genotypes, growing seasons and salt tolerance treatments ($R^2 = 0.75$). Furbank et al., (2021) tested different methods to predict photosynthetic traits and for *gs* they found a performance of $R^2 = 0.42$ in flag leaves using PLSR models. In our study, *gs* predictions were weaker than A_{sat} predictions ($R^2 = 0.36$, RMSE = 0.14; Table 4.1), and assessing this through the different layers of the canopy can help us to understand why that is the case.

Our layer approach shows that there is higher prediction accuracy in the middle layer of the canopy, compared to the top and bottom layers, this could be explained by the environmental factors affecting *gs*, such as stomatal responses to sun flecks at the top of the canopy, the temperature and vapor pressure deficit differential within the canopy layers, wind speed affecting the boundary layer especially at the top, relative humidity, leaf water content and CO_2 depletion in

sunny days. Hence, the lack of studies predicting *gs* under field conditions and future studies should consider the influence of the abovementioned environmental factors when building predictive models, a combination between PLSR and thermography or the use of deep learning methods (Figure 4.9).

Chlorophyll content has been used as an important trait to assess photosynthetic capacity, the ability of canopies to intercept light and the time wheat can maintain photosynthetically active tissues during the crop cycle. SPAD measurements have become one of the standard proxies to estimate chlorophyll content in the field. Our predictions for SPAD values were lower than ones reported in a previous study measuring elite and landrace bread wheat cultivars growing under yield potential conditions in the same study site ($R^2 = 0.63$ vs $R^2 = 0.82$, in flag leaves) (Silva-Pérez et al., 2018). In general, the predictions of chlorophyll content ranked very high in terms of accuracy (R^2, RMSE) in this study compared to other traits a similar trend has been found for tobacco (Meacham-Hensold et al., 2020) and tropical tree species (Doughty et al., 2011).

4.6.3 Speeding up physiological breeding

The use of HTP methods for physiological breeding has increased in popularity, particularly the use of field spectroradiometers, hyperspectral cameras mounted on UAVs or modified IRGAs which are deployed in glasshouses and field trials in conjunction with commercial IRGAs. The use of these technologies can reduce dramatically the measurement time, for example, for A_{sat} measurements take ~15-25 min per leaf using a commercial IRGA compared to 1 min when collecting leaf spectral data (Heckmann et al., 2017), and using custom IRGAs

allowed the collection of A_{sat} 4-7 times faster than commercial IRGAs (Salter et al., 2018). The use of HTTP in this study allowed us to screen ~50 plots for flag, second and third leaves reflectance in ~1 hour compared to only 10 plots using two commercial IRGAs during 6 hours of field measurements in a day, thus increasing our phenotyping capacity 30-fold. Coupling approaches like the one used in our study based on hyperspectral data combined with the modelling of performance physiological traits such as biomass and RUE (Robles-Zazueta et al., 2021) can boost the phenotyping capacity in large breeding trials, increase our understanding of the source-sink relationship and help with the selection of genotypes with higher biomass, RUE and yield.

The relationship found between canopy assimilation predictions and RUE observations, could be used for screening RUE in breeding programs and coupled with the previous results from Robles-Zazueta et al., (2021) RUE could be screened with up to 70% accuracy using vegetation indices. The predictions presented in this study could be used to screen lines for extreme high and low RUE rates as the positive relationship found between RUE and canopy assimilation predictions indicate that the higher predicted values, we expect to find higher RUE genotypes.
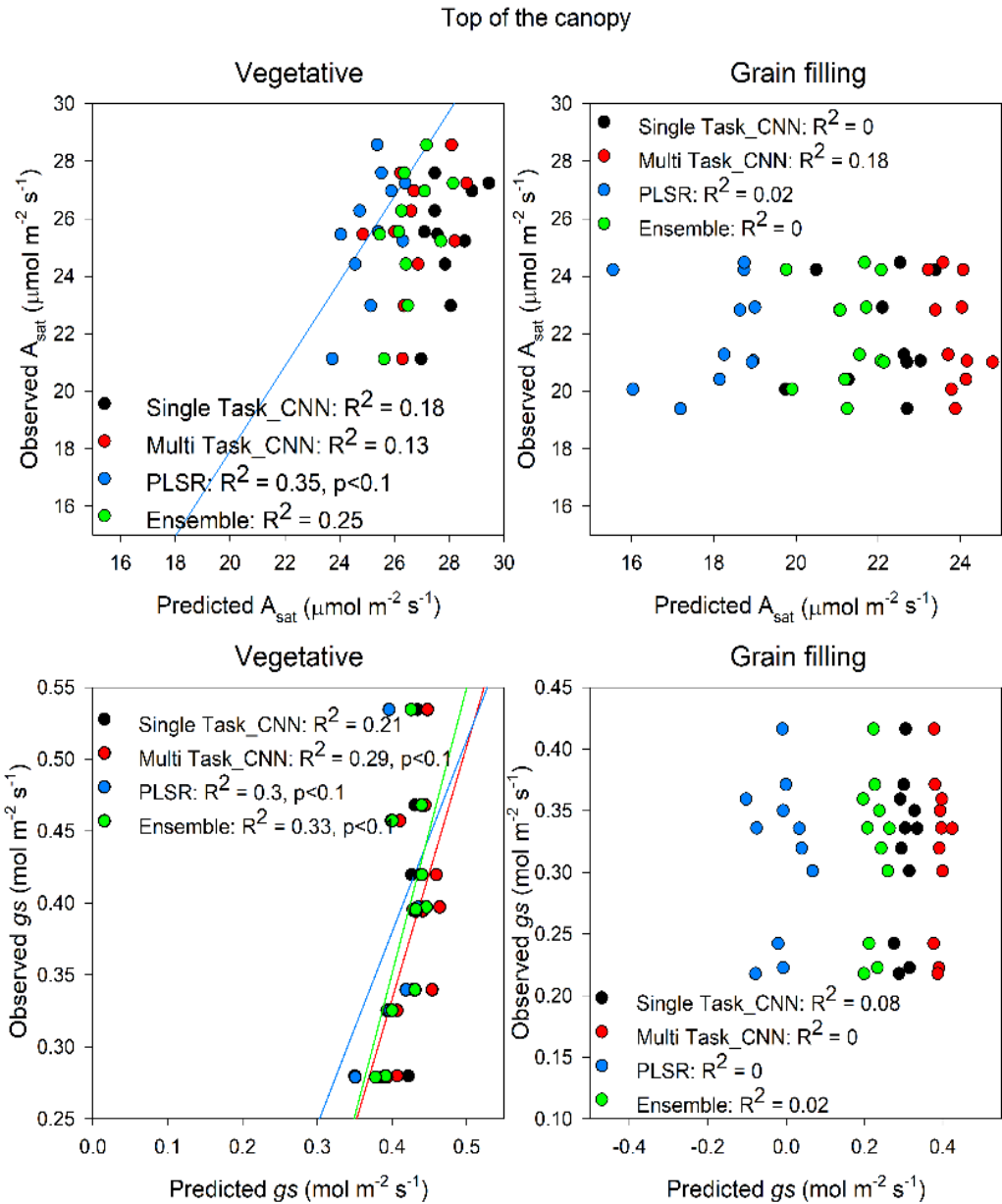
Figure 4.9. Observations of Asat and gs compared to the predictions from the models developed in Furbank et al., 2021. Measurements from flag leaves were compared to predictions made with flag leaf reflectance from the vegetative and grain filling periods. The modelling was done using the web tool Wheat Physiology Predictor (https://plantpredict.shinyapps.io/PredictionShiny/). We selected the different methods available in the tool to compare the prediction ability. Methods included single task convolutional neural network (black dots), multi-task convolutional neural network (red dots), partial least square regression (blue dots) and an ensemble of the three models (green dots). Lines represent the linear regression when relationships between ground truth data and predictions were statistically significant.

4.7 Conclusions

This is the first study that predicts physiological traits in different layers of the canopy by building predictive models with hyperspectral data using PLSR in wheat growing under field conditions. We showed that using measurements from different canopy layers improves the accuracy of the models. These models can be used to study the variation caused by different environmental conditions within the canopy and the effect of phenology. Our models were built using an extensive dataset from three field campaigns, which provides them robustness, enabling their application in future field breeding and pre-breeding trials. Furthermore, this modelling approach delivered fair estimations of A_{sat} and gs that can be incorporated in breeding pipelines. Using hyperspectral data will allow the alleviation of the phenotyping bottleneck and if this approach is coupled to faster phenotyping platforms the probabilities to screen genotypes for higher yield will increase.

Chapter 5 Disentangling the physiological constraints of radiation use efficiency in wheat

Carlos A. Robles-Zazueta[1,2*], Gemma Molero[2,3], Matthew P. Reynolds[2], Erik H. Murchie[1*]

[1]Division of Plant and Crop Sciences, School of Biosciences, University of Nottingham, Sutton Bonington Campus, Leicestershire, LE12 5RD, United Kingdom.

[2]Global Wheat Program, International Maize and Wheat Improvement Center (CIMMYT), carretera Mexico-Veracruz km 45, El Batan, Texcoco, Mexico. CP 56237.

[3]Current address: KWS Momont Recherche, 7 rue de Martinval, 59246 Mons-en-Pevele, France.

Authors for correspondence: carlos.robleszazueta@nottingham.ac.uk;

erik.murchie@nottingham.ac.uk

Abstract

There is clear consensus in the physiological and breeding communities that improving RUE will be key to boost wheat yield. In the 44 years of previous RUE research little has been explored on the role of root traits and its interaction with aboveground accumulation, RUE and yield. Roots as heterotrophic tissues have a complex relationship with RUE since they consume fixed carbon but in return the shoot obtains water and nutrients, influencing aboveground physiological processes through complex signalling from the soil-plant continuum. In this study above- and belowground traits related to RUE and yield were studied to identify the main interactions between roots and aboveground RUE. Strong positive associations were found between above and belowground biomass accumulation ($R^2 = 0.91$, p<0.001), and RUE and root biomass ($R^2 = 0.85$, p<0.001) during the vegetative period. On the other hand, negative links were found between yield components and root biomass accumulation, especially at GS65 with HI ($R^2 = 0.5$, p<0.05). We hypothesize that two mechanisms are present in wheat: synergy and cooperation during vegetative stages and competition from roots and shoots from grain filling towards physiological maturity which suggests that root biomass accumulation will depend mostly on phenology and environmental conditions, rather than genetic variability. Finally, our results suggests that g_{smax} or SLA could be used as proxies in the field to estimate belowground biomass in a high-throughput context.

Keywords: *Radiation use efficiency, aboveground biomass, belowground biomass, yield, RUE_below*

5.1 Introduction

Staple crop yield improvement will be essential to fulfil food security and the avenues to increase yields, especially in cereals have been identified to be closely related to the efficiency at which plants can convert radiation into biomass (i.e. radiation use efficiency, RUE) (Horton 2000; Reynolds et al., 2000b) which is a physiological trait that is closely aligned with leaf photosynthesis, respiration and net carbon assimilation (Posch et al., 2019; Joynson et al., 2021).

5.1.1 Brief history of radiation use efficiency research

RUE is a physiological trait that was brought to crop science attention 44 years ago in the seminal work from Monteith (1977). In his work, Professor Monteith established the theoretical background for the study of the relationship between biomass accumulation and intercepted solar radiation in crops and concluded that in average crops grown in the absence of abiotic stresses will have a RUE of ~1.4 g MJ^{-1}. After developing the theoretical and methodological principle for measurement, the crop science and ecology communities started to pay attention to this newly defined trait with potential to improve yield.

Gallagher and Biscoe (1978) measured aboveground biomass in barley and wheat and they found higher RUE values (2.2 g MJ^{-1}) than those proposed by Monteith and they emphasized the link between full canopy coverage and large leaf area index (LAI) for high RUE rates. Later efforts were made to correct previous assumptions that C_3 and C_4 crop growth rates were similar, and it was discovered that C_4 plants have a higher relative growth rate than C_3 species (Monteith, 1978). After these theoretical works, research was focused in

understanding what were the interactions of light interception with abiotic factors such as irrigation and nitrogen (N) fertilisation rates (Whitfield and Smith, 1989), light quality and [CO_2] (Bugbee and Salisbury, 1988), the effects of shading and N distribution in wheat canopies over grain number and yield (Abbate et al., 1995), the response of sink traits and RUE to different plant densities (Whaley et al., 2000) or the exploration of source and sink limitations to RUE in wheat grown under yield potential conditions (Reynolds et al., 2007).

Then research started to focus on modelling RUE at leaf level by means of remote sensing, especially the development of proxy measurements for photosynthesis and light "conversion". Among these the photochemical reflectance index (PRI) received particular attention due to its close relationship with leaf pigment composition and chlorophyll fluorescence transitions from high to low light conditions or vice versa (Peñuelas et al., 1995) and then coupling different spatial scales (leaf-canopy-ecosystem) to increase the reach of the predictions to different ecosystems (Garbulsky et al., 2011; Peñuelas et al., 2011). RUE research has focused in increasing the high throughput of its measurement in the field, as manual biomass harvests and ceptometer measurements are expensive and time consuming, efforts have been done to predict its components i.e. biomass (Babar et al., 2006; Prasad et al., 2009), intercepted photosynthetically active radiation (PAR) through normalised differenced vegetation index (NDVI) (Tattaris et al., 2016).

More recent studies have used 3D light tracing modelling to predict RUE in maize grown in controlled conditions (Cabrera-Bosquet et al., 2016), used UAV RGB imagery to predict RUE in field-grown maize (Tewes and Schellberg, 2018) and using a combination of vegetation indices related to chlorophyll, water

146

content and canopy greenness predictions of RUE in wheat grown in the field were made (Robles-Zazueta et al., 2021).

In the years of RUE-related research, very little information has been produced about the effect root physiology and belowground biomass accumulation has on the efficiency of converting radiation into biomass aboveground. This is somewhat curious since roots as heterotrophic tissue have an important contribution to make to RUE even if this relationship is complex and little understood. They receive and consume fixed carbon but exchange more diverse forms of currency: nutrients and water. They also influence aboveground growth through complex signalling depending on soil conditions (i.e. low water, N or P content) as well as track soil compaction (Pandey et al., 2021). Roots are being recognized as key players in yield formation and the identification of traits that will aid crops to adapt to climate change (Ahmadi et al., 2014) and new aspects of root physiology needs to be accounted for example the role of root exudates in the remobilization of nutrients such as P (Wen et al., 2021).

Some clues suggests that root biomass accumulation might play a key role in the mechanisms behind RUE decreasing from the vegetative to the grain filling period, as recent evidence suggests that there are not significant reductions in source size (Molero et al., 2019) or canopy greenness during early grain filling (Robles-Zazueta et al., 2021). In the period between these two growth stages under yield potential conditions there is not a clear explanation of the mechanisms involved in RUE reduction. To fully understand the components of RUE we must dig belowground to look for answers among the root systems.

5.1.2 Root phenotyping for wheat improvement

The study of roots for physiology, ecology, agronomy or breeding purposes has been largely constrained by the challenges of measuring processes such as growth, nutrient acquisition and remobilisation in the soil environment. This is further limited by the difficulty of measuring belowground traits under field conditions. Many of the advances in basic root biology and phenotyping have come from studying roots outside the soil environment (Morris et al., 2017; Pound et al., 2013; Tracy et al., 2010; 2011). The fact that root phenology is not coupled to shoot phenology means that is harder to accurately measure metabolic processes such as N, P or water uptake with soil conditions varying in matter of hours after dry-wetting events due to rain or irrigation (Freschet et al., 2021). Regardless of the difficulty of root research, advances in physiology, breeding and phenotyping have been made to address which traits should be targeted to improve resilience to abiotic stress caused by climate change (Ober et al., 2021).

Previous studies have focused on modelling the capture of water and N by roots in wheat grown in the UK (King et al., 2003) or the effects that faster growing root systems will have in improving Australian wheat yields by increasing them ~0.4 tonnes ha^{-1} using the Agricultural Production Systems sIMulator (APSIM) (Lilley and Kirkegaard, 2011). Other research has focused on the relation between different root architecture traits, such as plate spread, depth, dry weight root biomass and anchorage strength with lodging and its implications for yield improvement (Pinera-Chavez et al., 2016a; Pinera-Chavez et al., 2016b; Dreccer et al., 2020) or the strategies roots use to penetrate deeper in the soils with the implications of resource acquisition through changing their trajectory by sensing soil pores (Atkinson et al., 2020). Furthermore, studies have explored the

relation between HI, chlorophyll content and canopy greenness with total root length (Wasson et al., 2014), the relationship between canopy temperature and belowground dry biomass under heat stress conditions (Lopes and Reynolds, 2010) and only one study has made comprehensive measurements for root traits interacting with shoot traits such as biomass, yield, flowering time and its interaction with environmental conditions (Severini et al., 2020).

Despite the previous efforts to integrate root phenotyping into wheat pre-breeding platforms, there is a lack of information that connects belowground traits such as root dry biomass or the conversion efficiency of PAR interception into root biomass, a concept we introduce in this chapter as "RUE_below" with photosynthetic traits such as light-saturated photosynthetic rates (A_{sat}), maximum stomatal conductance (g_{smax}), maximum velocity of Rubisco carboxylation (V_{cmax}), electron transport rate (J_{max}), triose phosphate utilisation (TPU) or agronomic traits such as harvest index (HI), aboveground biomass accumulation, RUE and yield.

5.2 Objectives

The objectives of this study were to study root biomass accumulation and its relationship with physiological and agronomic traits to improve our understanding of the link between root and shoot biomass accumulation and the efficiency of PAR conversion in the context of yield improvement; and explore whether the information produced under glasshouse conditions can be extrapolated to information collected in field trials.

5.3 Materials and methods

Eight spring bread wheat genotypes from the Photosynthesis Respiration Tails (PS Tails) (Table 5.1) panel from the International Maize and Wheat Improvement Center (CIMMYT) were grown at University of Nottingham Sutton Bonington Campus glasshouse, in Leicestershire, United Kingdom. The genotypes were studied for two crop cycles during Summer and Autumn 2018 and Summer 2019.

5.3.1 Experimental design

A randomised complete block design with five repetitions per genotype was used. Sowing date was July 31st 2018, emergence date August 6th 2018, potting date August 21st 2018 and harvest date was December 21st 2018 with one plant grown in each 2l pot. Mean temperature in the glasshouse was 17.78 °C, mean solar radiation was 4.61 MJ m^{-2} during this study. Around 700 µmol m^{-2} s^{-1} of artificial light was supplied for 16 h a day during the experiment. The main tiller of each pot was marked in tillering (GS21) in order to perform the aboveground physiological measurements.

Irrigation was applied using an automated dripping system based on tensiometers which sensed when the pots started to get dry. Plants were grown under optimal conditions in John Innes #2 soil compost with pests and weed control, and fertilisation to avoid any biotic or abiotic limitations to yield. Fertilisation was applied in the form of urea at stem elongation (80 kg N ha^{-1}) and at initiation of booting (80 kg N ha^{-1}). The square design edge rows were

wheat variety Paragon in order to reduce border effects and minimise any gradient of heat in the glasshouse.

Phenological stages were scored visually according to the Zadoks growth scale for cereals (Zadoks et al., 1974). Growth stages recorded were initiation of booting (GS41), anthesis (GS65) and physiological maturity (GS87). These growth stages are critical for crop development, as the maximum canopy expansion happens at GS41, the start of the grain filling period (GS65) and grain ripening (GS87) (Table 5.1).

5.3.2 Canopy architecture

Canopy height was measured in GS65 and GS87 in the main tiller in each pot from the base of the tiller to the tip of the spike using a measuring tape. Leaf width and length of the flag, second and third leaves were measured at GS65 with a ruler, as well as leaf distance from the stem to the tip of the leaves. Leaf angles with respect to the ligule and leaf curvature (place where a leaf started to bend) were measured using a protractor. Spike, awn length, peduncle and the length of internodes two, three and four were measured in the main shoot using a ruler.

At GS65 two replicates of each genotype were selected for biomass partitioning and plant organs were separated in stem, leaves and spikes. After measuring areas with a planimeter (LI 3100C, Licor Biosciences, Lincoln, NE, USA) samples were dried in an oven for 2 days at 70°C, weight and leaf area data were used to calculate the leaf area index (LAI) as follows:

$$LAI = \frac{Green\ leaf\ lamina\ area}{\#\ stems\ m^2} \qquad \text{eq. (1)}$$

151

5.3.3 Source

A second experiment was made in the summer of 2019 with the same genotypes studied in the 2018 experiment grown under optimal conditions with the same experimental design. Sowing date was June 11th 2019, harvest of biomass at GS41 was done in July 20th 2019 and biomass harvests at GS65 in July 29th 2019. The objective of the experiment was to make destructive sampling of above and belowground biomass at GS41 and GS65. Aboveground biomass harvests were done in all the shoots of the 2l pots and belowground biomass was collected after finishing aboveground harvests in all the growth stages in five replicates per genotype. The samples were rinsed to separate roots from soil and then sieved to keep only the roots. Then samples were dried in an oven for 2 days at 70°C, calculations for above and belowground biomass were made as follows:

$$\text{Above and belowground biomass} = \frac{Dry\ weight\ biomass\ (g)}{Pot\ area\ (m^2)} \qquad \text{eq. (2)}$$

Radiation use efficiency (RUE) from above and belowground was estimated according to Robles-Zazueta et al., (2021). Incoming solar radiation collected from a meteorological station on campus was used to estimate the accumulated PAR throughout the growth cycle using multiplying the incoming radiation by 0.45 to estimate PAR (MJ m^{-2}), then the value of the linear regression between biomass accumulation and PAR was used to estimate RUE_below and RUE_above as follows:

$$RUE\_preGF\ (above\ and\ below) = \frac{(BM\ GS65 - BM\ GS41)}{(Acc\ IPAR\ GS65 - Acc\ IPAR\ GS41)} \qquad \text{eq. (3)}$$

$$RUE\_GF\ (above\ and\ below) = \frac{(BM\ GS65 - BM\ GS87)}{(Acc\ IPAR\ GS65 - Acc\ IPAR\ GS87)} \qquad \text{eq. (4)}$$

$$RUE\_Total\ (above\ and\ below) = \frac{(BM\ GS87 - BM\ GS41)}{(Acc\ IPAR\ GS87 - Acc\ IPAR\ GS41)} \qquad \text{eq. (5)}$$

Where BM GS41, BM GS65 and BM GS87 are biomass harvested at initiation of booting, anthesis and physiological maturity, respectively. Acc IPAR GS41, Acc IPAR GS65 and Acc IPAR GS87 are the accumulated intercepted PAR at initiation of booting, anthesis and physiological maturity, respectively.

Gas exchange traits were measured at GS41 and GS65 using an infrared gas analyser (IRGA) (Licor 6400 XT, Licor Biosciences, Lincoln, NE, USA). Light and CO_2 response curves were measured on the flag leaves of five replicates following phenotyping protocols (Evans and Santiago, 2014) and V_{cmax}, J_{max} and TPU were calculated using the R package plantecophys (Duursma, 2015). Measurements were carried between 10-4 pm to minimise stomatal limitation. Leaf chlorophyll content was measured using a SPAD-502 meter (Konika Minolta, Japan) as a proxy. Non-photochemical quenching was measured using a MultispeQ (PhotosynQ, East Lansing, MI, USA) which allowed us to do fast measurements of NPQ (NPQt) without the need for dark adaptation in the leaves (Kuhlgert et al., 2016). Finally, stomatal morphology traits were measured to calculate maximum stomatal conductance (g_{smax}) according to Franks and Beerling (2009). Stomatal impressions were collected using transparent nail varnish and when dried, adhesive tape was applied in the medium area of adaxial and abaxial sides of the main shoot flag leaf where the gas exchange measurements were done. Samples were left to dry for 10 minutes and then placed on a slide to be examined and imaged using a microscope (Leica DM 5000 B, Wetzlar, Germany). Stomatal density, stomatal size, pore length, peristomatal groove distance, guard cell width and stomatal pore area were measured in order to estimate g_{smax} as follows:

$$g_{smax} = \frac{(d \; x \; D \; x \; a_{max})}{v[l+(\frac{\pi}{2}) \; x \; \sqrt{\frac{a_{max}}{\pi}}]}$$ eq. (6)

Where d is the diffusivity of water in air ($m^2 \; s^{-1}$, at 25 °C), D is the stomatal density of the measured leaf surface (mm^2), l is the pore depth (µm) estimated as half the mean guard cell width. Amax is the maximum stomatal pore area (μm^2) which is calculated as the area of a circle with the diameter corresponding to the pore length, v is the molar volume of air ($m^3 \; mol^{-1}$ at 25 °C) and µ is the mathematical constant taken as 3.1416 (Franks and Beerling, 2009). Stomatal density was calculated using the following equation:

$$D = \frac{Number \; of \; stomata}{mm^2}$$ eq. (7)

5.3.4 Sink (reproductive) traits

When the genotypes reached GS87 in the 2018 experiment, all the shoots from each replicate were harvested from each pot and dried in an oven at 70 °C for 48 hours. Then the spikes were threshed to separate the grains from the rest of biomass and the harvest index was calculated as follows:

$$Harvest \; index \; (HI) = \frac{Grain \; dry \; weight}{Biomass \; dry \; weight}$$ eq. (8)

Yield was sampled using a manual harvest machine, and a subsample was collected to be processed and calculate the thousand grain weight (TGW), number of grains per spike (GSP) and grains m^{-2} (GM2) using a seed counter, grain weight per spike (GWSP) and the number of spikes m^{-2} (SM2) were calculated afterwards. Yield was calculated as follows:

$$Yield = \frac{Grain \; dry \; weight_{\# \; shoots \; in \; the \; pot}}{Pot \; area}$$ eq. (9)

Table 5.1. Reference ID (#), cross name, average days to initiation of booting (DTGS41), days to anthesis (GS65), days to physiological maturity (GS87), intercepted PAR (MJ) and thermal time (°C days) measured during the growth cycle for the 8 spring bread wheat genotypes studied. H^2 = Broad sense heritability, G = Genotypic differences.

#	Cross name	DGS41 (days)	DGS65 (days)	DGS87 (days)	PARGS41 (MJ)	PARGS65 (MJ)	PARGS87 (MJ)	TTGS41 (°C days)	TTGS65 (°C days)	TTGS87 (°C days)
1	W15.92/4/PASTOR//HXL7573/2*BAU/3/WBLL1	51	72	127	276.57	353.12	445.54	1020.8	1371.76	2263.83
2	KUKRI	48	70	125	261.43	346.45	444.29	959.38	1328.7	2241.61
3	MUNAL #1	49	70	125	262.78	348.38	444	973.49	1338.58	2238.19
4	CHEWINK #1	47	65	127	254.83	331.86	446.24	932.44	1243.95	2277.19
5	SOKOLL//PUB94.15.1.12/WBLL1	49	67	129	265.3	338.15	447.4	974.31	1285.48	2298.35
6	PUB94.15.1.12/FRTL/5/CROC_1/AE.SQUARROSA (205)//BORL95/3/PRL/SARA//TSI/VEE#5/4/FRET2	48	68	127	259.79	340.92	446.11	957.26	1300.63	2277.86
7	C80.1/3*QT4118//KAUZ/RAYON/3/2*TRCH/7/CMH79A.955/4/AGA/3/4*SN64/CNO67//INIA66/5/NAC/6/RIALTO/8/WBLL1*2/KURUKU	50	71	128	266.83	350.31	446.86	989.72	1345.47	2290.89
8	QUAIU*2/KINDE	52	79	130	278.33	374.17	448.89	1028.57	1489.34	2325.66
	Mean	52	74	127	1021.57	1400.51	2276.7	275.15	356.41	446.16
	H^2	0.96	0.93	0	0.96	0.93	0	0.95	0.9	0
	G	***	***	ns	***	***	ns	***	***	ns

5.4 Results

5.4.1 Plant architecture

Significant height differences were found at GS65 (p<0.001) but not at GS87. Shoot architecture was similar in all the genotypes as evidenced by internodes and peduncle length, however, differences were found in the number of shoots per plant (p<0.01) (Table 5.2). Spike length varied from 9.9-10.78 cm and highly significant differences were found between the genotypes studied (p<0.001) (Table 5.2). Mixed results were found for leaf architecture traits, on one side no statistical differences were found for LAI, flag and third leaves angles, and leaves curvatures. On the other hand, differences were found across leaf layers in the distance from stem to tip of the leaves, length and width (Table 5.2).

5.5.2 Above-, belowground biomass accumulation and radiation use efficiency

Statistically significant differences were found before (p<0.001) and during grain filling (p<0.05) but no differences were found when integrating the whole growth cycle for RUE aboveground (Table 5.2). In general, RUE aboveground is usually higher in glasshouse studies than in field studies due to the larger availability of diffuse radiation product of light scattering in the glasshouse structure and a lower competition for light due to lower plant densities compared to the field, hence a greater amount of light intercepted per plant.

For RUE_above, the highest rates were found during the grain filling stage, while in RUE_below the highest rates were found when integrating the whole growth cycle and the lowest values were found during the vegetative period both

for above and belowground (Figure 5.1). Similar to RUE_above, statistically significant differences were found before and during grain filling (p<0.01) for RUE_above, although H^2 in this trait was lower compared to its above counterpart (Table 5.2), and with the exception of genotype 2 and 7, all the cultivars studied showed higher RUE_below when integrating the growth cycle (Figure 5.1). For aboveground biomass statistically significant differences were found both at GS41 and GS65 (p<0.001) as well as for belowground biomass accumulation in the same growth stages (p<0.01) (Table 5.2).

Table 5.2. Agronomic traits measured in this study. Data was collected for 8 genotypes, which were studied extensively under field conditions in Robles-Zazueta et al., 2021. sd: standard deviation, LSD: Least significant differences, CV: Coefficient of variation, H^2: Broad sense heritability, G: Genotypic differences.

Trait	Minimum	Mean (sd)	Maximum	LSD	CV	H^2	G
Yield	597.44	750.5 (253.79)	920.46	328.45	33.97	0	ns
HI	0.39	0.46 (0.08)	0.52	0.01	16.11	0.51	ms
GSP	6.75	11.43 (4.42)	17.72	11.82	55.73	0.38	ns
GWSP	2.04	2.45 (0.65)	2.68	0.88	27.9	0	ns
GM2	10415.58	12691.55 (4507.08)	15621.6	6556.13	34.49	0	ns
SM2	233.4	333.36 (107.42)	433.4	144.66	33.68	0.63	*
Height_A (cm)	67.76	69.89 (6.93)	78.18	9.26	10.28	0.87	***
Height_PM (cm)	81.06	82.11 (6.35)	87.68	9.36	8.85	0.28	ns
Internode 2 (cm)	17.72	18.65 (2.05)	19.76	2.98	12.41	0	ns
Internode 3 (cm)	11.16	13.13 (2.8)	14.32	3.9	23.07	0	ns
Internode 4 (cm)	7.18	8.36 (2.86)	9.86	4.03	37.39	0	ns
Peduncle length (cm)	31.94	33.49 (4.26)	37.52	7.39	17.13	0.03	ns
Spike length (cm)	9.9	10.83 (1.33)	10.78	1.96	14.03	0.86	***
Awn length (cm)	5.92	6.36 (0.9)	6.66	1.19	14.52	0	ns
Shoots_GS65 (# m^{-2})	333.2	459.29 (103.23)	533.4	153.34	25.92	0.7	**
LAI_GS65	4.05	4.97 (1.92)	5.97	2.37	36.35	0	ns
Angle_GS65 (Top) (°)	59	72.24 (33.17)	99.2	42.03	45.16	0.55	ms
Angle_GS65 (Middle) (°)	40.4	52.69 (22.71)	95	30.49	44.91	0.68	*
Angle_GS65 (Bottom) (°)	37	51.02 (19.5)	68.6	33.74	51.33	0.11	ns
Curv_GS65 (Top) (°)	51.8	70.76 (37)	91	48.14	52.81	0.15	ns
Curv_GS65 (Middle) (°)	47.7	58.31 (23.21)	76.6	33.71	44.87	0	ns
Curv_GS65 (Bottom) (°)	48.4	59.13 (20.22)	75.4	32.19	42.26	0	ns
Diststemtip (Top) (cm)	20.28	27.04 (4.88)	28.92	7.29	20.92	0.91	***

Diststemtip (Middle) (cm)	19.44	25.58 (4.87)	26.94	8.9	27.01	0.73	**
Diststemtip (Bottom) (cm)	19.94	23.34 (4.32)	24.76	6.43	21.37	0.44	ns
RUE_above_preGF (g MJ^{-1})	1.44	1.75 (0.4)	2.41	0.46	18.34	0.78	***
RUE_above_GF (g MJ^{-1})	2.9	3.95 (1.08)	4.95	1.6	26.88	0.52	*
RUE_above_Total (g MJ^{-1})	1.91	2.77 (0.89)	3.59	1.3	36.59	0.3	ns
RUE_below_preGF (g MJ^{-1})	0.09	0.11 (0.03)	0.16	0.04	26.17	0.68	**
RUE_ below _GF (g MJ^{-1})	0.11	0.12 (0.03)	0.14	0.05	28.15	0	**
RUE_below_Total (g MJ^{-1})	0.08	0.14 (0.11)	0.21	0.15	86.62	0	ns
Root:Shoot_GS41	0.05	0.07 (0.01)	0.08	0.02	18.74	0.72	*
Root:Shoot_GS65	0.05	0.06 (0.01)	0.07	0.015	18.33	0.13	ns
Root:Shoot_GS87	0.03	0.05 (0.02)	0.09	0.06	87.36	0	ns
AGBM_GS41 (g m^{-2})	403.73	477.17 (83.47)	642.61	115.33	16.8	0.83	***
AGBM_GS65 (g m^{-2})	493.08	829.5 (34.18)	776.83	266.89	24.55	0.98	***
AGBM_GS87 (g m^{-2})	867.85	1250.89 (402.99)	1622.43	586.46	36.39	0.32	ns
BGBM_GS41 (g m^{-2})	24.28	30.56 (7.34)	43.56	11.01	25.05	0.72	**
BGBM_GS65 (g m^{-2})	29.97	42.47 (10.39)	64.89	16.41	26.85	0.69	**
BGBM_GS87 (g m^{-2})	33.75	60.95 (51.09)	95.22	67.68	86.19	0	ns
RSGP (%)	14.28	16.68 (4.02)	21.24	5.81	27.02	0.17	ns
CGR_PreGF (g m^{-2} day^{-1})	3.63	5.26 (1.33)	6.09	1.99	28.06	0.89	***
CGR_GF (g m^{-2} day^{-1})	13.89	17.07 (7.99)	24.42	11.4	50.2	0	ns
CGR_Total (g m^{-2} day^{-1})	6.79	9.85 (3.23)	12.85	4.77	37.48	0.26	ns
SLA_GS65 (m^2 kg^{-1})	13.79	29.31 (17.02)	44.12	25.32	67.05	0.13	ns

Abbreviations: HI: harvest index, GSP: Grains per spike, GWSP: Grain weight per spike, GM2: Grains m^{-2}, SM2: Spikes m^{-2}, Curv: Leaf curvature, Diststemtip: Distance from stem to tip of the leaf, LAI: Leaf area index, Root:Shoot: Root to shoot ratio, AGBM: Aboveground biomass, BGBM: Belowground biomass, RSGP: Rapid spike growth period, CGR: Crop growth rate, SLA: Specific leaf area, DT: Days to.
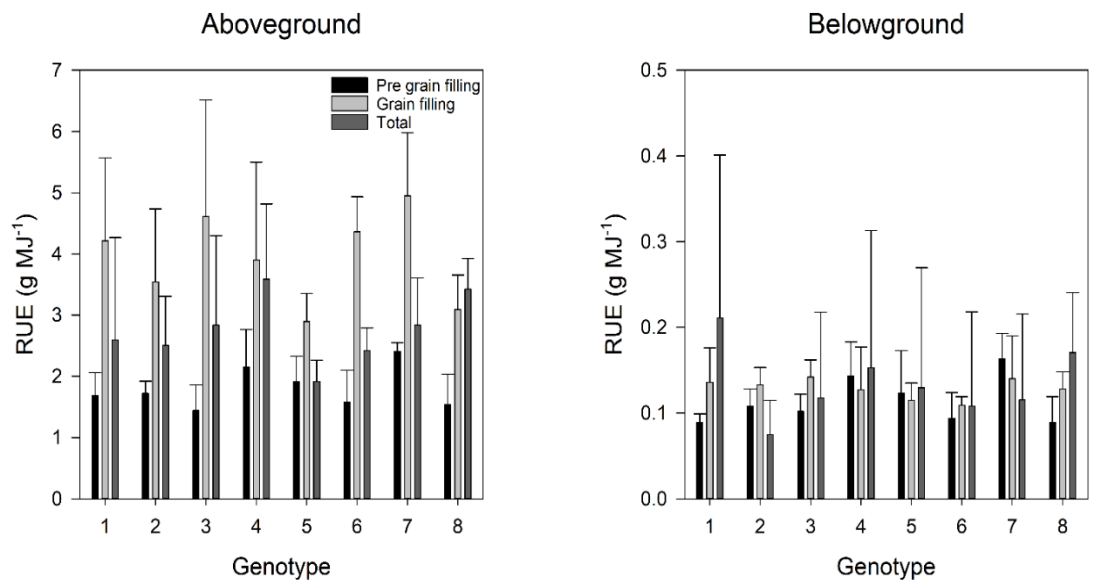
Figure 5.1. Radiation use efficiency measured above and belowground. Measurements were made during the pre grain filling stage (black bars), grain filling (light grey) and considering the whole crop cycle (dark grey). Data are mean ± standard error.

Heritability in the belowground traits was high for both stages ($H^2 = 0.72$, 0.69, respectively) which increases the prospect of incorporating these traits into pre-breeding pipelines in the near future. The ratio of below to aboveground biomass (Root:Shoot) was only statistically significant at GS41 ($p<0.05$). This ratio was maintained during the vegetative and grain filling period but was drastically reduced at GS87 (Figure 5.2), which implies that once the plant has sufficient root biomass in the vegetative and grain filling periods to acquire resources and provide the shoot with mechanical stability against lodging, efforts are shifted to produce as much aboveground biomass in order for spikes to have enough access to assimilates to fill the grains.
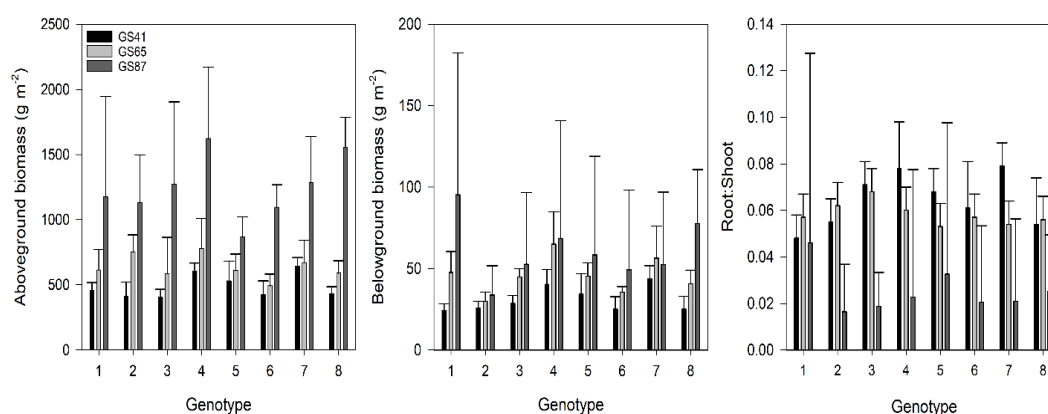
Figure 5.2. Aboveground and belowground biomass measured at anthesis (black bars) and physiological maturity (grey bars), and root shoot ratios of the studied genotypes. Data are mean ± standard deviation.

5.4.3 Leaf photosynthesis

The photosynthetic traits did not show genetic variation in general at GS41, except for *gs* ($p<0.05$), transpiration (E) ($p<0.05$), light compensation and saturation points (LCP, LSP) ($p<0.05$, $p<0.01$, respectively). On the other hand, at GS65 statistically significant genotypic differences were found for A_{max}, A_{sat},

J_{max}, LUE, $\Phi PSII$ (p<0.01), *gs* (p<0.001), E, LCP and LSP (p<0.05) (Table 5.3). A_{sat} ranged from 25.22-28.81 μmol m^{-2} s^{-1} at GS41 and 25.75-30.5 μmol m^{-2} s^{-1} at GS65, while A_{max} had greater values, specially at GS65 with a range from 29.59-37.8 μmol m^{-2} s^{-1}, and no statistical differences were found for V_{cmax} or dark respiration (R_d) at neither growth stages (Table 5.3).

The largest V_{cmax} and J_{max} were found in genotype 1 (Figure 3 and 4), both for GS41 and GS65 but this did not translate into higher yield or HI, whilst belowground biomass at GS87 was the highest for this genotype, suggesting that higher V_{cmax} and J_{max} rates could be associated to larger biomass accumulation during the crop cycle, with marginally significant phenotypic correlations found for these traits (Table 5.5).

Table 5.3. Photosynthetic traits measured at initiation of booting and anthesis. LSD: least significant differences, CV: coefficient of variation, H^2: broad sense heritability, G: genotypic differences, GS_41: Initiation of booting, GS_65: Anthesis.

Trait	Minimum	Mean (sd)	Maximum	LSD	CV	H^2	G
A_{sat}_GS41 (μmol m^{-2} s^{-1})	25.22	28.1 (3.78)	28.81	4.76	12.91	0.22	ms
A_{sat}_GS65 (μmol m^{-2} s^{-1})	25.75	27.01 (3.86)	30.5	5.79	15.64	0.73	**
A_{max}_GS41 (μmol m^{-2} s^{-1})	26.9	32.38 (5.31)	34.3	6.64	15.65	0.53	ns
A_{max}_GS65 (μmol m^{-2} s^{-1})	29.59	32.17 (5.02)	37.8	7.53	17.08	0.74	**
V_{cmax}_GS41 (μmol m^{-2} s^{-1})	137.41	151.29 (34.98)	186.77	48.77	24.19	0.43	ns
V_{cmax}_GS65 (μmol m^{-2} s^{-1})	126.08	137.47 (24.18)	166.81	40.89	21.72	0.46	ms
J_{max}_GS41 (μmol m^{-2} s^{-1})	227.31	241.84 (30.07)	271.43	44.55	13.82	0.01	ns
J_{max}_GS65 (μmol m^{-2} s^{-1})	210.36	226.18 (23.94)	256.57	38.93	12.57	0.74	**
R_d_GS41 (μmol m^{-2} s^{-1})	1.14	1.7 (0.48)	2.06	0.64	28.87	0.51	ms
R_d_GS65 (μmol m^{-2} s^{-1})	1.05	1.36 (0.45)	1.67	0.67	36.11	0.05	ns
gs_GS41 (mol m^{-2} s^{-1})	0.31	0.44 (0.16)	0.47	0.19	33.18	0.64	*
gs_GS65 (mol m^{-2} s^{-1})	0.33	0.43 (0.13)	0.6	0.18	31.38	0.79	***
g_{smax}_GS65 (mol m^{-2} s^{-1})	1.46	1.94 (0.25)	2.01	0.43	14.83	0.5	ns
E_GS41 (mmol m^{-2} s^{-1})	3.83	5.22 (1.31)	6.42	1.95	28.53	0.66	*
E_GS65 (mmol m^{-2} s^{-1})	4.22	5.09 (1.51)	6.62	2.09	31.32	0.66	*
LCP_GS41 (μmol m^{-2} s^{-1})	18.63	23.79 (6.98)	30.01	8.86	28.4	0.58	*
LCP_GS65 (μmol m^{-2} s^{-1})	15.9	18.49 (5.29)	21.21	7.91	31.23	0	ns
LSP_GS41 (μmol m^{-2} s^{-1})	462.53	731.62 (214.97)	908.03	296.74	30.94	0.76	**
LSP_GS65 (μmol m^{-2} s^{-1})	660.72	832.13 (241.86)	1150.63	334.32	29.34	0.62	*
TPU_GS41 (μmol m^{-2} s^{-1})	14.04	14.86 (1.74)	16.28	2.64	13.12	0	ns
TPU_GS65 (μmol m^{-2} s^{-1})	13.89	14.65 (1.12)	16.07	2.41	9.42	0.29	ns
iWUE_GS41 (μmol CO_2 mmol m^{-2} s^{-1} H_2O)	70.08	74.99 (27.85)	95.14	40.65	41.36	0	ns
iWUE_GS65 (μmol CO_2 mmol m^{-2} s^{-1} H_2O)	51.91	67.7 (15.92)	91.94	26.05	28.01	0.56	ms
WUE_GS41 (μmol CO_2 mol m^{-2} s^{-1} H_2O)	4.68	5.9 (1.66)	8.15	2.78	35.97	0.32	ns
WUE_GS65 (μmol CO_2 mol m^{-2} s^{-1} H_2O)	4.79	5.59 (1.13)	7.3	1.89	24.75	0.36	ns
LUE_GS41 (g C mol^{-1} photons)	0.16	0.19 (0.03)	0.21	0.04	15.67	0.53	ms
LUE_GS65 (g C mol^{-1} photons)	0.18	0.19 (0.03)	0.23	0.05	17.06	0.74	**
NPQt_GS41	0.89	1.11 (0.22)	1.27	0.31	21.45	0.47	ms
NPQt_GS65	0.63	0.74 (0.12)	0.83	0.17	18.3	0.09	ns
Fv'/Fm'_GS41	0.43	0.45 (0.04)	0.47	0.04	7.49	0.11	ns
Fv'/Fm'_GS65	0.48	0.5 (0.03)	0.52	0.05	8.12	0	ns
ΦPSII_GS41	0.16	0.18 (0.03)	0.19	0.04	16.85	0	ns
ΦPSII_GS65	0.16	0.16 (0.03)	0.19	0.04	18.51	0.73	**
SPAD_GS41	42.19	43.52 (1.74)	44.58	2.3	4.11	0	ns
SPAD_GS65	38.85	43.6 (4.36)	46.28	6.18	11	0.34	ns
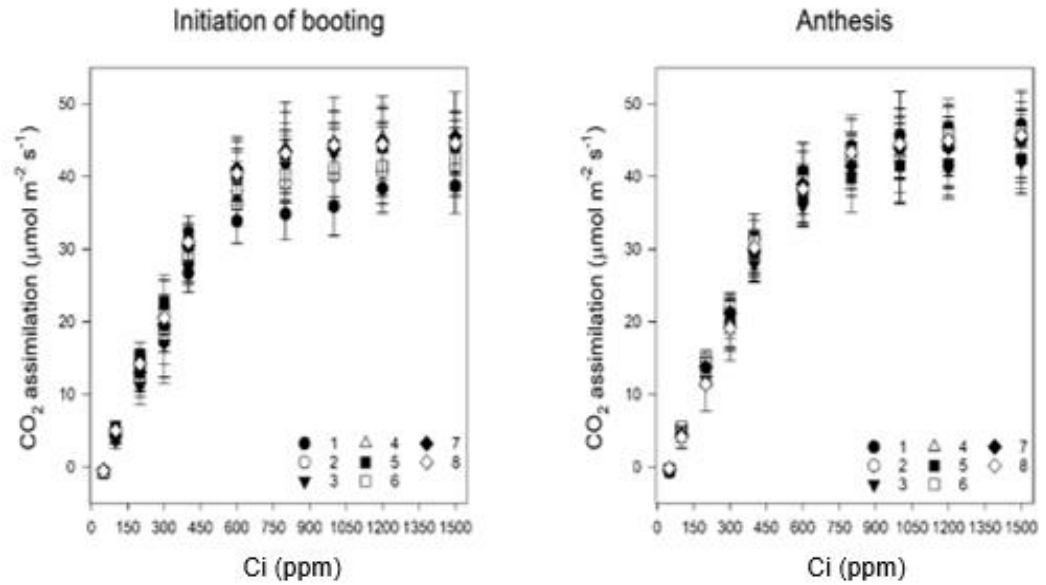
Figure 5.3. CO_2 response curves (A/Ci) measured at GS41 and GS65. Different symbols represent the genotypes studied. Data are mean ± standard deviation.

In the case of the stomatal traits' differences were found in abaxial stomatal density ($p<0.01$) as well as the peristomatal groove distance ($p<0.001$), pore area ($p<0.01$) and g_{smax} ($p<0.05$) and the same traits with exception of stomatal density which also showed the lowest heritability ($H^2 = 0$) for adaxial traits (Table 4). The stomatal traits were the photosynthetic traits with the highest H^2 in this study, this highlights the value of screening gs traits to be added to phenotyping programs coupling these measurements with high-throughput platforms if they correlate with traits related to yield improvement (Table 5.4).
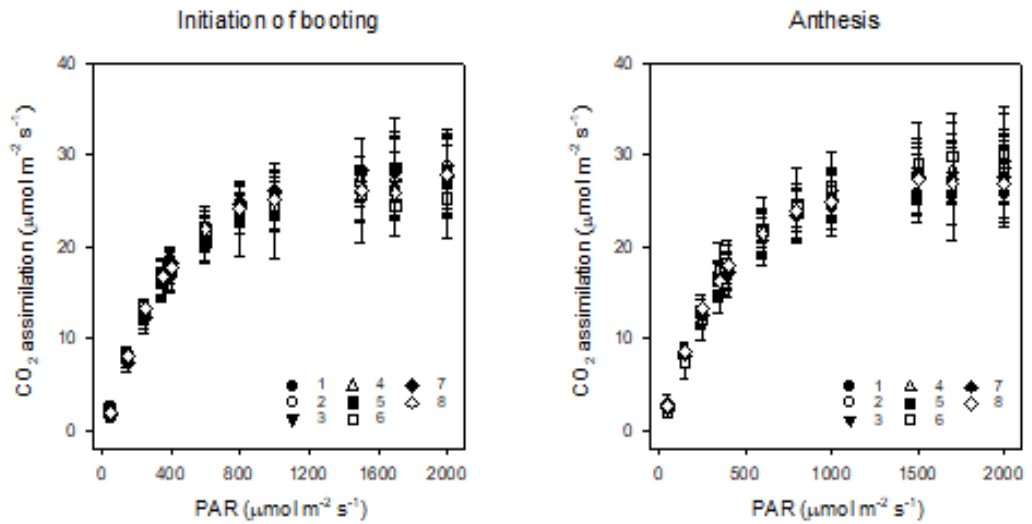
Figure 5.4. Light response curves (A/Q) measured at GS41 and GS65. Different symbols represent the genotypes studied. Data are mean ± standard deviation.

5.4.4 Uncovering the link between below and aboveground biomass accumulation

Negative statistically significant relationships were found between HI and belowground biomass accumulation at GS65 and GS87 ($p < 0.05$, $p < 0.1$, respectively) (Figure 5.5), as well as GSP and RUE_below_preGF suggesting a trade-off between grain yield partitioning components and the accumulation of root biomass at both vegetative and grain filling stages (Table 5.5). Furthermore, strong positive relationships were found between aboveground biomass at GS41 with belowground biomass at GS41 ($p < 0.001$) and GS65 ($p < 0.01$) (Figure 5.5). In the case of RUE, positive associations were found with root biomass at GS41 ($p < 0.001$) and GS65 ($p < 0.05$) indicating a synergy between the shoot and roots during the vegetative stage (Figure 5.5).

Table 5.4. Stomatal traits measured at GS65. sd: standard deviation, LSD: Least significant differences, CV: Coefficient of variation, H^2: Broad sense heritability, G: Genotypic differences, g_{smax}: maximal stomatal conductance.

Trait	Minimum	Mean (sd)	Maximum	LSD	CV	H^2	G
Adaxial							
Stomatal density (# mm^{-2})	67.5	71.19 (8.98)	76.42	13.77	14.05	0	ns
Stomatal size (µm)	241	411.71 (82.65)	477.38	136.28	22.65	0.54	ms
Pore length (µm)	25.63	31.9 (4.06)	36.73	6.63	14.22	0.74	*
Peristomatal groove distance (µm)	15.35	22.84 (2.1)	26.6	3.84	11.52	0.88	***
Guard cell width (µm)	4.84	6.66 (0.86)	8.93	2.48	25.46	0.27	ns
Stomatal pore area (µm^{-2})	317.68	581.03 (98.33)	686.83	169.91	20.01	0.84	**
g_{smax} (mol m^{-2} s^{-1})	1.49	2.06 (0.3)	2.34	0.61	18.72	0.78	*
Bottom							
Stomatal density (# mm^{-2})	49.98	61.61 (8.59)	74.25	11.39	13.65	0.73	**
Stomatal size (µm)	175.76	426.21 (71.83)	515.17	154.39	23.8	0.34	ns
Pore length (µm)	22.15	30.63 (3.92)	34.99	6.63	14.22	0.45	ns
Peristomatal groove distance (µm)	14.86	24.37 (2.05)	27.26	3.75	10.11	0.91	***
Guard cell width (µm)	4.18	6.85 (0.71)	7.61	1.65	15.81	0.45	ms
Stomatal pore area (µm^{-2})	246.52	597.04 (99.82)	744.26	178.29	19.63	0.83	**
g_{smax} (mol m^{-2} s^{-1})	1.16	1.78 (0.22)	2.14	0.42	14.81	0.68	*
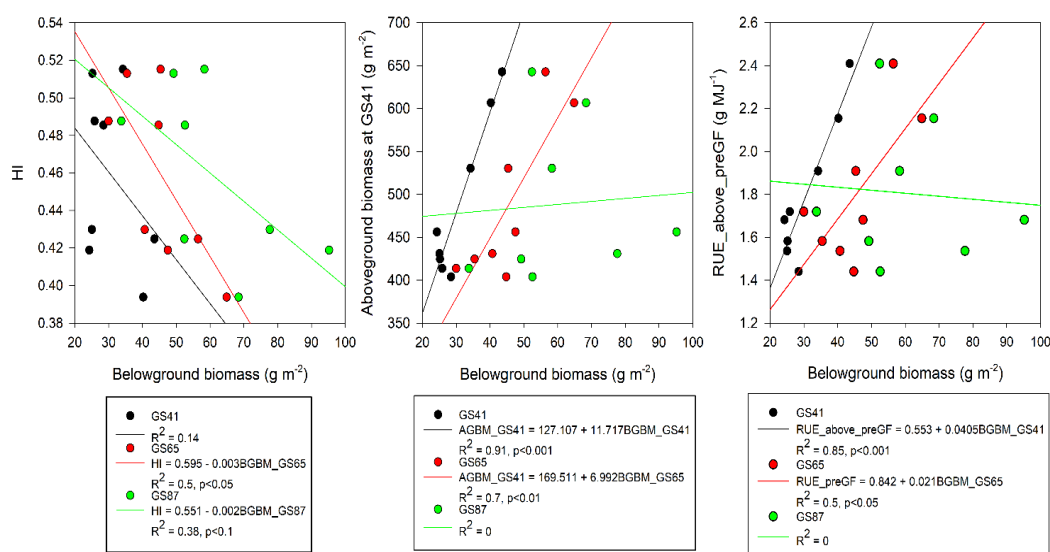
Figure 5.5. Relation between HI (left panel), aboveground biomass at initiation of booting (middle panel) and RUE aboveground at vegetative period (right panel) with belowground biomass accumulation at initiation of booting (black dots), anthesis (red dots) and physiological maturity (green dots).

Statistically significant relations were found between A_{sat} ($p<0.01$) and *gs* ($p<0.05$) at GS41 with the Root:Shoot ratio at GS65 meaning larger photosynthetic rates from the vegetative period may serve as stores of carbon assimilates for future plant growth and are beneficial for larger root and shoot accumulation in the later grain filling period.

Table 5.5. Phenotypic correlations between belowground traits and aboveground traits measured under controlled environmental conditions. Statistical significance is represented as follows: in bold * = p<0.05, in bold ** = p<0.01, *** = p<0.001, in italic = 0.1>p>0.05.

Trait	BGBM GS41	BGBM GS65	BGBM GS87	RUE_below preGF	RUE_below GF	RUE_below Total	Root:Shoot GS41	Root:Shoot GS65	Root:Shoot GS87
Yield (g m^{-2})	-0.01	0.24	0.23	0.09	0.28	-0.34	-0.08	0.2	0.23
HI	-0.38	***-0.71**	*-0.61*	-0.11	0.24	-0.5	-0.15	-0.19	****-0.83**
GM2 (grains m^{-2})	0	0.19	-0.07	0.22	0.56	-0.37	-0.05	-0.08	-0.06
GSP (# grains)	-0.41	-0.33	0.45	***-0.72**	-0.51	***0.77**	-0.38	-0.06	0.45
GWSP (g spike^{-1})	-0.29	-0.4	-0.07	-0.38	0.1	0.34	-0.21	0.38	-0.06
LAI	***0.67**	0.32	*-0.66*	***0.77**	0.36	***-0.78**	***0.73**	0.41	*-0.65*
SLA (m^2 kg^{-1})	*0.57*	0.23	*-0.66*	***0.73**	0.17	-0.56	*0.62*	0.06	*-0.65*
Height_GS65 (cm)	0.29	0.34	-0.13	0.36	0.07	-0.23	0.3	-0.25	-0.13
Height_GS87 (cm)	0.35	*0.63*	0.33	0.24	0.03	0.04	0.32	0.08	0.34
FLAngle (°)	-0.09	-0.14	0.08	-0.27	-0.23	*0.62*	-0.05	-0.09	0.09
SLAngle (°)	0.33	0.51	0.18	0.26	-0.05	0.04	0.28	-0.3	0.19
TLAngle (°)	0.23	0.15	-0.19	0.31	-0.16	0.03	0.19	***-0.75**	-0.18
FLCurv (°)	0.03	-0.2	-0.52	0.08	0.14	***-0.69**	0.15	-0.04	-0.53
SLCurv (°)	0.09	0.13	0	0	-0.14	0	0.11	-0.5	0
TLCurv (°)	0.16	0.22	-0.26	0.44	0.34	-0.46	0.12	-0.35	-0.26
DiststemtipFL (cm)	*-0.57*	-0.29	0.33	*-0.59*	0.28	*0.62*	*-0.57*	0.11	0.34
DiststemtipSL (cm)	-0.24	0.12	0.25	-0.1	0.36	0.15	-0.32	-0.29	0.27
DiststemtipTL (cm)	-0.49	***-0.67**	-0.34	-0.45	-0.15	-0.1	-0.42	***-0.79**	-0.35
AGBM_GS41 (g m^{-2})	*****0.95**	****0.84**	0.07	***0.74**	-0.47	0.03	*****0.93**	0.09	0.08
AGBM_GS65 (g m^{-2})	-0.09	0.08	0.23	-0.32	-0.05	0.21	-0.04	-0.06	0.23
AGBM_GS87 (g m^{-2})	0.22	0.5	0.33	0.22	0.21	-0.23	0.14	0.35	0.33

RUE_above_preGF (g MJ^{-1})	***0.92	*0.7	-0.08	*0.68	-0.46	-0.05	***0.95	0.13	-0.08
RUE_above_GF (g MJ^{-1})	0.26	-0.11	0.36	0.3	-0.18	0.28	0.46	-0.11	-0.06
RUE_above_Total (g MJ^{-1})	0.21	0.49	0.32	0.23	0.23	-0.24	0.14	0.36	0.32
Asat_GS41 (µmol m^{-2} s^{-1})	0.06	0.14	0.07	-0.04	0.49	-0.02	0.11	**0.88	0.08
Asat_GS65 (µmol m^{-2} s^{-1})	0.22	-0.06	*-0.57*	0.48	0.05	-0.4	0.2	*-0.63*	-0.56
gs_GS41 (mol m^{-2} s^{-1})	0.44	0.2	-0.34	0.46	0.37	-0.33	0.47	*0.69	-0.33
gs_GS65 (mol m^{-2} s^{-1})	0.35	0.06	-0.48	*0.57*	-0.12	-0.34	0.31	*-0.61*	-0.48
Rd_GS41 (µmol m^{-2} s^{-1})	0.39	0.27	-0.22	0.45	0.4	-0.41	0.38	0.55	-0.22
Rd_GS65 (µmol m^{-2} s^{-1})	0.45	-0.11	*-0.57*	0.33	-0.49	0.43	0.53	-0.3	*-0.58*
Vcmax_GS41 (µmol m^{-2} s^{-1})	0.04	0.48	*0.59*	-0.04	-0.11	0.53	-0.04	-0.23	*0.59*
Vcmax_GS65 (µmol m^{-2} s^{-1})	-0.53	-0.49	-0.01	*-0.6*	0.3	-0.02	-0.46	0.18	-0.01
Jmax_GS41 (µmol m^{-2} s^{-1})	-0.28	0.21	*0.83	-0.51	-0.2	*0.6*	-0.34	0.1	*0.82
Jmax_GS65 (µmol m^{-2} s^{-1})	*-0.67	*-0.64*	-0.01	*-0.76	0.07	0.28	-0.6	-0.27	0
TPU_GS41 (µmol m^{-2} s^{-1})	-0.45	-0.1	*0.72	*-0.73	-0.25	*0.59*	-0.46	0.25	*0.71
TPU_GS65 (µmol m^{-2} s^{-1})	*-0.58*	*-0.57*	-0.07	*-0.59*	-0.16	0.17	-0.53	*-0.75	-0.07
g_{smax}_GS65 (mol m^{-2} s^{-1})	0.12	0.48	0.55	0.25	-0.17	0.33	-0.08	-0.37	0.55
NPQt_GS41	-0.33	-0.38	-0.37	-0.16	0.56	-0.36	-0.23	0.37	-0.37
NPQt_GS65	-0.11	0.15	0.09	0.18	0.52	-0.4	-0.19	0.23	0.09
SPAD_GS41	0.16	0.49	*0.68	-0.11	-0.56	*0.64*	0.09	-0.3	*0.68
SPAD_GS65	0.24	0.53	0.22	0.26	0.56	-0.03	0.22	*0.75	0.23

5.5 Discussion

In this study, a comprehensive analysis between aboveground traits and belowground agronomic traits was made to understand which are the main controls of above and belowground biomass accumulation as well as the effects of this interaction on wheat RUE. Our main results showed negative associations between HI, GSP and belowground biomass accumulation and RUE_below which suggests a trade-off between some yield components involved with partitioning to grains and root biomass especially during grain filling. On the other hand, a strong link between above and belowground biomass in the vegetative period was found this suggests a coordination between above and below plant processes to boost growth towards grain filling.

5.5.1 Below- and aboveground trait interactions

Previous studies have asserted the benefits for improving root traits such as elongation, depth, distribution, xylem vessel diameter, root:shoot biomass ratio in water-limited environments to improve water acquisition and alleviate shoot stress particularly in grain filling (Lilley and Kirkegaard, 2011), as well as angle of seminal roots, root plate spread and anchorage strength under yield potential conditions in order to make plants more responsive to N and P fertilization and provide the shoot with a greater structural strength against lodging (Pinera-Chavez et al., 2016a; Dreccer et al., 2020). However, to date no studies have suggested a connection between root traits (e.g. root biomass dry weight) and RUE.

Our results suggest there are two main mechanisms for biomass accumulation and resource acquisition in wheat. The first mechanism comes from the positive correlations between above- and belowground biomass during the vegetative period which imply that far from acting in competition, these systems are adapted to operate synergistically in the context of leaf and root economic spectrums and the plant form and function spectrum (Díaz et al., 2016). Wheat as an annual crop follows the trend of "fast-slow" trade-off between highly metabolic cost traits such as high leaf or root N concentrations with those associated with tissue investment for the long run such as stem and root density, leaf mass area (LMA) or specific root length (SRL), therefore it is expected to have high N concentrations in roots and leaves of plants with positive associations between above and belowground   biomass in order to keep the growing demands (Weigelt et al., 2021). This indicates that at the vegetative stage, a wheat plant with higher biomass and LAI will benefit from a larger radicular system thanks to the possibility to acquire more water, N and P from soils to sustain fast growth, and vice versa a larger shoot benefits the root system by providing more access to photoassimilates to meet their metabolic and growth needs. It is also possible that a fast-growing root system helps to prevent sink limitation of shoot growth. Secondly, during grain filling and towards physiological maturity there is a detrimental cost for the plant to have larger root systems as these become antagonising with the shoot and the strength of the reproductive organs as a dominant sink (Simpson et al., 2020), competing for nutrients and water and having a negative effect on yield, HI and GM2.

5.5.2 Could belowground biomass explain the variability of aboveground RUE?

Root metabolism has been assessed in different ecosystems and has been found to have a large impact in aboveground carbon use, biomass accumulation, resource use efficiencies (water, N) and it shows seasonal patterns influenced by phenology.

In our study wheat was grown under yield potential conditions, where irrigation, fertilisation and pest control are optimised, therefore a trend was found where RUE_above increased from the vegetative to the grain filling period and likewise RUE_below showed the same trend. These results are contrasting to what has been found for the same genotypes grown under field conditions. It has been found that RUE_above diminishes from vegetative to grain filling period, even though plants have optimum LAI and their leaves and spikes are still photosynthetically active (Molero et al., 2019; Robles-Zazueta et al., 2021). A previous study in wheat has found that root traits such as respiration and root:shoot ratio were closely related to the plant water status. Furthermore, the reduction in root respiration rates and root biomass accumulation was key for wheat plants to cope drought stress, and implied that genetic expression of root traits is influenced more by the environment rather than genotypic diversity (Hong and Feng, 2005).

This phenomenon could influence the allocation of resources aboveground and the resource use efficiency especially radiation and N. We hypothesize that under field conditions the relatively greater water stress that wheat is subject during grain filling could make the plant to resort for surviving strategies including the reduction of the root:shoot ratio in order to cope with drought or

heat stresses making the plant less responsive to the availability to certain resources including light or N, and focus their attention in water to avoid spike sterility therefore causing a reduction in RUE from the vegetative to grain filling period. This could be supported by the theory of plant resource allocation which states that plants maximize their growth based on N availability in the soil, and it is known that under heat or drought stress less N becomes available due to reduced soil moisture which affects N remobilization, roots are less likely to utilise it therefore reducing root:shoot ratios (Agren and Franklin, 2003), and these abiotic stresses will increase leaf respiration reducing biomass accumulation (Vose and Ryan, 2002).

5.5.3 Glasshouse studies to support root field phenotyping

Even though glasshouse studies should be approached with caution when it comes to comparison with field studies (Poorter et al., 2016), especially for phenotyping or breeding purposes, the slow throughput of field root phenotyping compared to shoot phenotyping (Severini et al., 2020) makes the studies of roots in the glasshouse a feasible option to find traits to explore under field conditions (Atkinson et al., 2019). We explored whether the root biomass traits studied here could be extrapolated with physiological traits from field studies in the same eight genotypes and found negative statistical relationships between yield and RUE_below, specific leaf area (SLA) with belowground biomass and gs both at GS41 and GS65 with several root traits (Table 5.6). This would support the results found at physiological maturity when shoots and roots become antagonists (yield, SLA) and how stomata could coordinate with roots through signalling to reduce water losses. Moreover, these traits could be used to predict

root biomass traits with related aboveground by means of high-throughput phenotyping of maximum stomatal conductance (Gibbs et al., 2021) or through the prediction of SLA in field trials as presented in chapter 4 of this thesis.

5.6 Conclusions

In this study above- and belowground traits related to RUE were studied in order to understand which traits control it. Our results suggest that there is synergy between shoot and root systems during vegetative stages and then shifts to antagonistic relationship from grain filling towards maturity as evidenced by the negative relationship found between yield components and belowground traits. Furthermore, we explored the possibility of implementing root traits in the field by analysing its relationship with physiological traits under field conditions and traits such as gs and SLA could be used to study root traits in the field indirectly by means of high-throughput phenotyping.

Chapter 6 General discussion

Based on our results we can conclude that predicting RUE with models built with canopy reflectance is better than using different sensors or measurements at leaf level thanks to the faster phenotyping capabilities of using only one sensor and the similar prediction accuracy from both approaches applied in Chapter 2. Furthermore, due to the influence of canopy architecture, light saturated photosynthesis in the middle and bottom layer of the canopy we found an association between RUE and yield (Chapter 3) which can be exploited by considering the genotypic variation of CIMMYT germplasms in the future to improve wheat yield.

Our hypothesis of Chapter 4 stated that models derived from rapid measurements of multiple canopy layers will be better than models built with individual leaf layers. In fact, our hypothesis was true especially for photosynthetic traits where we found that using top, middle and bottom layers improved the accuracy and reduced the error in the models. Likewise, it is noteworthy to mention that these models can be improved by increasing the genotypic variability of the dataset or adding data collected in different environments or locations.

Finally in Chapter 5 we explored the relationship between shoot and root physiology and how they were affecting RUE. Our hypothesis was proven correct as we found that greater root biomass accumulation was coupled with smaller aboveground biomass accumulation and smaller HI. Therefore we concluded that to improve yield considering roots and shoots there needs to be a fine tuning of physiological traits that could become antagonistic to avoid penalising yield.

6.1 Importance of growth analysis for wheat yield improvement

Throughout the chapters of this thesis, the importance of increasing wheat yield by improving photosynthetic rates in different leaf layers to upgrade canopy photosynthesis has been stated. The key physiological trait linking yield with photosynthesis and biomass accumulation is RUE. But this trait generally includes labour and resource intensive manual measurements of biomass and light interception in the field that needs to be sampled at least in two periods of time during the growth cycle. In addition, there are methodological inconsistencies on how RUE is measured and this depends if its calculations are based on intercepted photosynthetically active radiation with data from a ceptometer or if its only calculated using incoming solar radiation (Bonhomme, 2000). This issue should be addressed in future modelling studies to improve the accuracy of RUE models.

Most of the recent studies that study traits that could be key for yield improvement in wheat and other crops with emphasis on photosynthetic traits have focused their efforts on newly developed phenotyping methods, increasing the high-throughput of measurements such as A_{sat}, gs, light intercepted, F_v'/F_m', NPQ or g_{smax} (Gibbs et al., 2021; McAusland et al., 2019 Salter et al., 2020; Silva-Pérez et al., 2018; Townsend et al., 2018). But these previous studies have not considered RUE and/or yield in their studies, therefore without the empirical evidence of the thought to be straightforward relationship between photosynthesis and yield, breeding programmes will hardly give priority to photosynthetic traits in their phenotyping pipelines.

Another trait with high importance in breeding programmes is aboveground biomass. Previous studies have identified it as a key trait in the finding of new

high yielding cultivars (Aisawi et al., 2015; Molero et al., 2019; Joynson et al., 2021). Aboveground biomass is used to estimate RUE, therefore we should not stop collecting ground truth data when possible, even if HTP methods are available to predict it in different growth stages (Babar et al., 2006; Prasad et al., 2009; Tewes and Schellberg, 2018; Robles-Zazueta et al., 2021). In chapter 2 of this thesis, RUE was predicted with 53%, 61% and 69% accuracy in the vegetative stage, grain filling stage and whole crop cycle, respectively using vegetation indices related to water and chlorophyll content in the leaves as well as canopy light interception. Despite the good results from the models, we concluded that measurements of aboveground biomass should not be replaced entirely by HTP methods and highlighted that if we want to increase our understanding of the link between photosynthesis and yield, growth analysis is an important piece of the puzzle (Robles-Zazueta et al., 2021), especially because this relationship might be environment or location specific.

The method developed in this thesis could also be used to screen genotypes for high biomass and RUE in wheat populations that could be tolerant to heat, drought, or nutrient stresses. Although we recognize that aboveground biomass and RUE are influenced by the latitude where wheat is grown as it has been proven that cloud cover affects the amount of incident radiation as it increases the amount of diffuse radiation plants receive as well as altering the R:FR especially in the lower parts of the canopy. These abiotic changes also depend in the structural composition of the canopy, influenced by architecture (i.e. LAI, leaf angles and orientation) (Durand et al., 2021).

Additionally, the managing conditions will have an effect on canopy architecture which will be key for radiation interception, therefore limitations of N, P will

affect RUE negatively (Sinclair and Vadez, 2002) as well as water limitations. Thus, the next steps should be towards the parameterization of predictive models for resource limited environments including genotypic variability from different parts of the world to test how RUE of wheat responds to different abiotic stresses. Building models that can work on any environment should be a priority for the phenotyping community in order to simplify work in the field and reduce the phenotyping bottleneck of biomass and RUE in the field.

6.2 Are sunlit leaves from top of the canopy enough to represent whole canopy processes?

Leaf photosynthesis is the primary source of carbohydrates for wheat in most part of the growth cycle. The question is, if the main path for plants to grow is photosynthesis, why we have not found clear evidence of the relation between wheat growth (i.e. biomass accumulation, RUE), wheat yield and photosynthesis?

Previous studies addressing this relationship (Table 3.1, Chapter 3) have mostly focused on spot measurements (A_{sat}) under light saturating conditions at the top layer of the canopy (usually flag leaves). The justification for this was that in the past some studies found associations between flag leaf photosynthesis and yield (Fischer et al., 1998; Reynolds et al., 2000). However recent modelling studies have identified the importance of bottom layers of the canopy in boosting biomass accumulation, and possibly yield in wheat (Townsend et al., 2018; Salter et al., 2020) and rice (Foo et al., 2020).

The genotypes studied in this work had middle and bottom layer photosynthesis explaining larger yield variability than top of the canopy photosynthesis in the vegetative stage, which implies that photosynthetic productivity in wheat can be a product of canopies acclimating to low light conditions (<1000 µmol m^{-2} s^{-1}) as light intercepted in the middle and bottom layer can be diminished by 20% and 77% compared to the top layer, respectively. There is evidence in the literature that the efficient exploitation of high light periods can increase plant biomass up to 20% in tobacco (Kromdijk et al., 2016) and slow induction transitions from low to high light in wheat can reduce up to 21% of maximum CO_2 assimilation in wheat (Taylor and Long, 2017) indicating the importance of canopy architecture. Recent studies have emphasized the role canopy architecture for improved canopy photosynthesis by modifying leaf angles to improve the light interception and extinction coefficient (Mantilla-Perez et al., 2017; 2020) for the end-goal of higher aboveground biomass and yield varieties (Richards et al., 2019).

Modifications in canopy architecture will be needed to increase light penetration in the middle and bottom layer of wheat canopies to utilize sun flecks to boost yield, and modelling suggests that breeding for erect wheat canopies will be the best option to exploit dynamic light events such as sunflecks (Burgess et al., 2021). We suggest that breeders start considering a new wheat ideotype with erect flag leaves to increase light penetration towards lower canopy layers with a reduced peduncle length and increased third and fourth internodes length to optimise canopy architecture without yield by reducing the risk of lodging.

Future studies need to consider wheat populations studied in different environmental conditions (i.e. yield potential, heat, drought and nutrient stress)

as well as increase the extent of the study of photosynthetic organs, which has mostly been directed to the flag leaf and spikes (Molero and Reynolds, 2020), to include different leaf layers plus the spikes and stems (Araus et al., 2021; Simkin et al., 2020; Chapter 3). If we increase our understanding of these organ photosynthetic rates, we can picture which abiotic factors might have a larger effect on photosynthesis at the top, middle and bottom layers of the canopy. Finally, besides steady state photosynthesis, recent studies have found evidence of genetic variation in photosynthetic rates of leaves exposed to changes from low to high light (i.e. photosynthetic induction) which can pave the way for the improvement of maximum photosynthetic rates integrated in the whole crop cycle (Acevedo-Siaca et al., 2021; Faralli and Lawson, 2019; McAusland et al., 2020) as plant canopies are subjected to variation of light intensity during scales that goes from seconds to months, and it will be important to consider developing high-throughput phenotyping techniques to account for this variation in the field and study canopy photosynthesis to understand which are the manipulations that need to be done to improve yield without compromising source-sink balance.

6.3 Upscaling physiological traits from leaves to canopies

Using HTP to phenotype complex traits such as gas exchange has become the norm in wheat field phenotyping as mentioned in Chapter 1 and 4. The use of optical remote sensing tools (spectroradiometers, multi and hyperspectral cameras mounted on UAVs) has reduced the phenotyping bottleneck to some extent. However, most of this phenotyping technology has been used to measure just the top layer of the canopy in the field and in glasshouses/growth chambers.

We showed that including the middle and bottom layer of the canopy improved the prediction of photosynthetic, biophysical and biochemical traits. Our photosynthetic prediction accuracy compared to previous studies from wheat (Silva-Pérez et al., 2018; Furbank et al., 2021), having the added value of prediction for high and low extreme rates by including the three layers and considering the effects of phenological variability.

The results presented in Chapter 4, will allow the faster phenotyping of photosynthetic traits at different canopy layers in vegetative and reproductive stages in wheat, and can potentially be used in other cereals such as barley, maize or rice. PLSR predictions could be coupled with whole canopy photosynthesis IRGA measurements (Song et al., 2016) that includes stems and spikes in order to model canopy photosynthesis including those organs as well.

Moreover, the phenotyping capacity in the field was increased up to 30 times more than conventional phenotyping methods for gas exchange, thus justifying the use of PLSR models based on leaf reflectance that can work in different years and phenological stages. The next frontier will be to have models that can predict physiological traits based on plant functional groups (i.e. models for cereals, legumes, trees, or dividing them by C3/C4 models).

6.4 Roots: the latest frontier for RUE and yield improvement

Roots are an important system within a plant. In wheat their importance has been looked through the lens of resource acquisition (i.e. water and nitrogen) and lodging. Virtually no studies have explored the relation between root biomass

accumulation with RUE and yield. The results from Chapter 5, indicate that there is synergy from the below and aboveground parts of the plant at the vegetative stage and a competition relationship from grain filling onwards. Physiologically speaking, traits such as stomatal conductance (Gibbs et al., 2021) and specific leaf area (PLSR models, Chapter 4) could be used as proxies to predict root biomass accumulation in the field by training models collecting ground truth data and associate those results with traits related to shoot architecture or gas exchange.

Wheat genotypes with more belowground biomass can acquire more water, N and P from soils to sustain peaks of rapid growth and store nutrients in the long run. Furthermore, plants with high aboveground biomass and large LAI will benefit from larger radicular systems for anchorage, therefore belowground traits show that they need to be considered in breeding programs if a boost in yield is the goal in the near future.

Future studies should consider measurements of root respiration coupled to canopy photosynthesis as this C flux is an important source of energy loss (Posch et al., 2019) in wheat as well as a stress coping mechanism especially under drought (Hong and Feng, 2005).

Ultimately, increased atmospheric CO_2 and higher air and soil temperature will diminish the allocation of root biomass, as these abiotic stresses have been found to reduce photosynthesis and aboveground biomass accumulation (Ainsworth and Long, 2021) creating source-sink imbalances that could create issues for the plant, including increasing the risk of lodging, reducing the acquisition of resources such as N, P or water, increasing soil and root respiration and have an

antagonistic effect with photosynthesis, therefore having a negative impact on RUE. For this reason, it will be paramount to find wheat genotypes that have radicular systems that can cope with these changes without compromising the function of the shoot.

6.5 Conclusions

Global population is set to reach 10 billion by 2050, and one of the greatest challenges humanity will face in the 21st Century is the improvement of staple crop yields. It has been asserted that photosynthesis is the key trait to meet this goal, but other essential physiological measurements are needed to understand the link between photosynthesis and yield, i.e. biomass accumulation and RUE. These traits are labour intensive and their measurement is prone to errors in the field so improving its prediction by means of high-throughput phenotyping is the ultimate goal of breeding programmes, as well as the creation of combined models from heat, drought and yield potential trials that can predict RUE, biomass and other traits to be used in different wheat megaenvironments to find new genotypes with higher yield.

References

Abbate PE, Andrade FH, Culot JP. 1995. The effects of radiation and nitrogen on number of grains in wheat. The Journal of Agricultural Science 124, 351–360.

Acevedo-Siaca LG, Coe R, Quick WP, Long SP. 2021. Variation between rice accessions in photosynthetic induction in flag leaves and underlying mechanisms. Journal of Experimental Botany 72, 1282-1294.

Acreche M, Briceno-Felix G, Martin-Sanchez JA, Slafer GA. 2009. Radiation interception and use efficiency as affected by breeding in Mediterranean wheat. Field Crops Research 110, 91–97.

Ågren GI, Franklin O. 2003. Root:shoot ratios, optimization and nitrogen productivity. Annals of Botany 92, 795–800.

Ainsworth EA, Leakey ADB, Ort DR, Long SP. 2008. FACE-ing the facts: inconsistencies and interdependence among field, chamber and modelling studies of elevated $[CO_2]$ impacts on crop yield and food supply. New Phytologist 179, 5–9.

Ainsworth EA, Long SP. 2005. What have we learned from 15 years of free-air CO_2 enrichment (FACE)? A meta-analytic review of the responses of photosynthesis, canopy properties and plant production to rising CO_2. New Phytologist 2, 351–372.

Ainsworth EA, Long SP. 2021. 30 years of free-air carbon dioxide enrichment (FACE): What have we learned about future crop productivity and its potential for adaptation? Global Change Biology 27, 27–49.

Aisawi KAB, Reynolds MP, Singh RP, Foulkes MJ. 2015. The physiological basis of the genetic progress in yield potential of CIMMYT spring wheat cultivars from 1966 to 2009. Crop Science 55, 1749-1764.

Alvarado G, Rodríguez FM, Pacheco A, Burgueño J, Crossa J, Vargas M, Pérez-Rodríguez P, López-Cruz MA. 2020. META-R: A software to analyze data from multi-environment plant breeding trials. The Crop Journal 8, 745–756.

Amthor JS. 2010. From sunlight to phytomass: On the potential efficiency of converting solar radiation to phyto-energy. New Phytologist 188, 939–959.

Araus JL, Cairns JE. 2014. Field high-throughput phenotyping: The new crop breeding frontier. Trends in Plant Science 19, 52–61.

Araus JL, Kefauver SC, Zaman-Allah M, Olsen MS, Cairns JE. 2018. Translating High-Throughput Phenotyping into Genetic Gain. Trends in Plant Science 23, 451–466.

Araus JL, Sanchez-Bragado R, Vicente R. 2021. Improving crop yield and resilience through optimization of photosynthesis: panacea or pipe dream? Journal of Experimental Botany 72, 3936–3955.

Araus JL, Slafer GA, Reynolds MP, Royo C. 2002. Plant breeding and drought in C3 cereals: What should we breed for? Annals of Botany 89, 925–940.

Asseng S, Ewert F, Martre P, Rötter RP, Lobell DB, Cammarano D, Kimball BA, Ottman MJ, Wall GW, White JW, Reynolds MP, Alderman PD, Prasad PVV, Aggarwal PK, Anothai J, Basso B, Biernath C, Challinor AJ, De Sanctis G, Doltra J, Fereres E, Garcia-Vila M, Gayler S, Hoogenboom G, Hunt LA, Izaurralde RC, Jabloun M, Jones CD, Kersebaum KC, Koehler AK, Müller C, Kumar SN, Nendel C, O'Leary G, Olesen JE, Palosuo T, Priesack E, Rezaei EE, Ruane AC, Semenov MA, Shcherbak I, Stöckle C, Stratonovitch P, Streck T, Supit I, Tao F, Thorburn PJ, Waha K, Wang E, Wallach D, Wolf J, Zhao Z, Zhu Y. 2015. Rising temperatures reduce global wheat production. Nature Climate Change 5, 143–147.

Asseng S, Foster I, Turner NC. 2011. The impact of temperature variability on wheat yields. Global Change Biology 17, 997–1012.

Atkinson JA, Hawkesford MJ, Whalley WR, Zhou H, Mooney SJ. 2020. Soil strength influences wheat root interactions with soil macropores. Plant Cell and Environment 43, 235–245.

Atkinson JA, Pound MP, Bennett MJ, Wells DM. 2019. Uncovering the hidden half of plants using new advances in root phenotyping. Current Opinion in Biotechnology 55, 1–8.

Babar MA, Reynolds MP, Van Ginkel M, Klatt AR, Raun WR, Stone ML. 2006a. Spectral reflectance to estimate genetic variation for in-season biomass, leaf chlorophyll, and canopy temperature in wheat. Crop Science 46, 1046–1057.

Babar MA, Reynolds MP, Van Ginkel M, Klatt AR, Raun WR, Stone ML. 2006b. Spectral reflectance indices as a potential indirect selection criteria for wheat yield under irrigation. Crop Science 46, 578–588.

Bailey-Serres J, Parker JE, Ainsworth EA, Oldroyd GED, Schroeder JI. 2019. Genetic strategies for improving crop yields. Nature 575, 109–118.

Baker NR. 2008. Chlorophyll fluorescence: a probe of photosynthesis in vivo. Annual Review of Plant Biology 59, 89–113.

Baldocchi DD. 2003. Assessing the eddy covariance technique for evaluating carbon dioxide exchange rates of ecosystems: past, present and future. Global Change Biology 9, 479–492.

Baldocchi DD. 2014. Measuring fluxes of trace gases and energy between ecosystems and the atmosphere - the state and future of the eddy covariance method. Global Change Biology 20, 3600–3609.

Barbour MM, Kaiser BN. 2016. The response of mesophyll conductance to nitrogen and water availability differs between wheat genotypes. Plant Science 251, 119–127.

Basler G, Küken A, Fernie AR, Nikoloski Z. 2016. Photorespiratory bypasses lead to increased growth in Arabidopsis thaliana: are predictions consistent with experimental evidence? Frontiers in Bioengineering and Biotechnology 4, 31.

Bendig J, Bolten A, Bareth G. 2012. Introducing a low-cost mini-UAV for thermal- and multispectral-imaging. International Archives of the Photogrammetry, Remote Sensing and Spatial Information Sciences 39, 345–349.

Blackburn GA. 1998. Quantifying chlorophylls and carotenoids at leaf and canopy scales: An evaluation of some hyperspectral approaches. Remote Sensing of Environment 66, 273–285.

Blackburn GA. 2007. Hyperspectral remote sensing of plant pigments. Journal of Experimental Botany 58, 855–867.

Bobik K, Burch-Smith TM. 2015. Chloroplast signalling within, between and beyond cells. Frontiers in Plant Science 6, 781.

Bonhomme, R. 2000. Beware of comparing RUE values calculated from PAR vs solar radiation or absorbed vs intercepted radiation. Field Crops Research 68, 247-252.

Broge NH, Mortensen J V. 2002. Deriving green crop area index and canopy chlorophyll density of winter wheat from spectral reflectance data. Remote Sensing of Environment 81, 45–57.

Bugbee BG, Salisbury FB. 1988. Exploring the limits of crop productivity. Plant Physiology 88, 869–878.

Burgess AJ, Durand M, Gibbs JA, Retkute R, Robson TM, Murchie EH. 2021. The effect of canopy architecture on the patterning of 'windflecks' within a wheat canopy. Plant, Cell and Environment 44, 3524-3537.

Burgess AJ, Gibbs JA, Murchie EH. 2019. A canopy conundrum: can wind-induced movement help to increase crop productivity by relieving photosynthetic limitations? Journal of Experimental Botany 70, 2371-2380.

Burgess AJ, Retkute R, Herman T, Murchie EH. 2017a. Exploring relationships between canopy architecture, light distribution, and photosynthesis in contrasting rice genotypes using 3D canopy reconstruction. Frontiers in Plant Science 8, 734.

Burgess AJ, Retkute R, Pound MP, Foulkes J, Preston SP, Jensen OE, Pridmore TP, Murchie EH. 2015. High-resolution three-dimensional structural data quantify the impact of photoinhibition on long-term carbon gain in wheat canopies in the field. Plant Physiology 169, 1192–1204.

Burgess AJ, Retkute R, Pound MP, Mayes S, Murchie EH. 2017b. Image-based 3D canopy reconstruction to determine potential productivity in complex multi-species crop systems. Annals of Botany 119, 517–532.

Burgess AJ, Retkute R, Preston SP, Jensen OE, Pound MP, Pridmore TP, Murchie EH. 2016. The 4-dimensional plant: Effects of wind-induced canopy movement on light fluctuations and photosynthesis. Frontiers in Plant Science 7, 1392.

Burnett AC, Serbin SP, Rogers A. 2021. Source:sink imbalance detected with leaf- and canopy-level spectroscopy in a field-grown crop. Plant, Cell and Environment 44, 2466–2479.

Cabrera-Bosquet L, Crossa J, von Zitzewitz J, Serret MD, Araus JL. 2012. High-throughput phenotyping and genomic selection: the frontiers of crop breeding converge. Journal of Integrative Plant Biology 54, 312–320.

Cabrera-Bosquet L, Fournier C, Brichet N, Welcker C, Suard B, Tardieu F. 2016. High-throughput estimation of incident light, light interception and radiation-use efficiency of thousands of plants in a phenotyping platform. New Phytologist 212, 269–281.

Cabrera-Bosquet L, Molero G, Stellacci A, Bort J, Nogues S, Araus JL. 2011. NDVI as a potential tool for predicting biomass, plant nitrogen content and growth in wheat genotypes subjected to different water and nitrogen conditions. Cereal Research Communications 39, 147–159.

Calderini DF, Dreccer MF, Slafer GA. 1997. Consequences of breeding on biomass, radiation interception and radiation-use efficiency in wheat. Field Crops Research 52, 271–281.

Carmo-Silva E, Andralojc PJ, Scales JC, Driever SM, Mead A, Lawson T, Raines CA, Parry MAJ. 2017. Phenotyping of field-grown wheat in the UK highlights contribution of light response of photosynthesis and flag leaf longevity to grain yield. Journal of Experimental Botany 68, 3473–3486.

Casadebaig P, Zheng B, Chapman S, Huth N, Faivre R, Chenu K. 2016. Assessment of the potential impacts of wheat plant traits across environments by combining crop modelling and global sensitivity analysis. PloS one 11, e0146385.

Chappelle EW, Kim MS, McMurtrey JE. 1992. Ratio analysis of reflectance spectra (RARS): An algorithm for the remote estimation of the concentrations

of chlorophyll A, chlorophyll B, and carotenoids in soybean leaves. Remote Sensing of Environment 39, 239–247.

Chen J, Cao F, Li H, Shan S, Tao Z, Lei T, Liu Y, Xiao Z, Zou Y, Huang M, Abou-Elwafa SF. 2020. Genotypic variation in the grain photosynthetic contribution to grain filling in rice. Journal of Plant Physiology 253, 153269.

Chen X, Hao MD. 2015. Low contribution of photosynthesis and water-use efficiency to improvement of grain yield in Chinese wheat. Photosynthetica 53, 519–526.

Chytyk CJ, Hucl PJ, Gray GR. 2011. Leaf photosynthetic properties and biomass accumulation of selected western Canadian spring wheat cultivars. Canadian Journal of Plant Science 91, 305–314.

Coast O, Shah S, Ivakov A, Gaju O, Wilson PB, Posch BC, Bryant CJ, Negrini ACA, Evans JR, Condon AG, Silva-Pérez V, Reynolds MP, Pogson BJ, Millar AH, Furbank RT, Atkin OK. 2019. Predicting dark respiration rates of wheat leaves from hyperspectral reflectance. Plant, Cell and Environment 42, 2133-2150.

Dalal J, Lopez H, Vasani NB, Hu Z, Swift JE, Yalamanchili R, Dvora M, Lin X, Xie D, Qu R, Sederoff HW. 2015. A photorespiratory bypass increases plant growth and seed yield in biofuel crop Cameliana sativa. Biotechnology for Biofuels 8, 175.

DaMatta FM, Grandis A, Arenque BC, Buckeridge MS. 2010. Impacts of climate changes on crop physiology and food quality. Food Research International 43, 1814–1823.

Daughtry CST, Walthall CL, Kim MS, De Colstoun EB, McMurtrey III JE. 2000. Estimating corn leaf chlorophyll concentration from leaf and canopy reflectance. Remote Sensing of Environment 74, 229–239.

De Pury DGG, Farquhar GD. 1997. Simple scaling of photosynthesis from leaves to canopies without the errors of big-leaf models. Plant, Cell and Environment 20, 537–557.

Díaz S, Kattge J, Cornelissen JHC, Wright IJ, Lavorel S, Dray S, Reu B, Kleyer M, Wirth C, Colin Prentice I, Garnier E, Bönisch G, Westoby M, Poorter H, Reich PB, Moles AT, Dickie J, Gillison AN, Zanne AE, Chave J, Joseph Wright S, Sheremet Ev SN, Jactel H, Baraloto C, Cerabolini B, Pierce S, Shipley B, Kirkup D, Casanoves F, Joswig JS, Günther A, Falczuk V, Rüger N, Mahecha MD, Gorné LD. 2016. The global spectrum of plant form and function. Nature 529, 167–171.

Doughty CE, Asner GP, Martin RE. 2011. Predicting tropical plant physiology from leaf and canopy spectroscopy. Oecologia 165, 289–299.

Dreccer MF, Condon AG, Macdonald B, Rebetzke GJ, Awasi M-A, Borgognone MG, Peake A, Pinera-Chavez FJ, Hundt A, Jackway P, McIntyre CL. 2020. Genotypic variation for lodging tolerance in spring wheat: wider and deeper root plates, a feature of low lodging, high yielding germplasm. Field Crops Research 258, 1–16.

Driedonks N, Rieu I, Vriezen WH. 2016. Breeding for plant heat tolerance at vegetative and reproductive stages. Plant Reproduction 29, 67–79.

Driever SM, Lawson T, Andralojc PJ, Raines CA, Parry MAJ. 2014. Natural variation in photosynthetic capacity, growth, and yield in 64 field-grown wheat genotypes. Journal of Experimental Botany 65, 4959–4973.

Driever SM, Simkin AJ, Alotaibi S, Fisk SJ, Madgwick PJ, Sparks CA, Jones HD, Lawson T, Parry MAJ, Raines CA. 2017. Increased SBPase activity improves photosynthesis and grain yield in wheat grown in greenhouse conditions. Philosophical Transactions of the Royal Society B: Biological Sciences 372, 20160384.

Duan T, Chapman SC, Guo Y, Zheng B. 2017. Dynamic monitoring of NDVI in wheat agronomy and breeding trials using an unmanned aerial vehicle. Field Crops Research 210, 71–80.

Durand M, Murchie EH, Lindfors AV, Urban O, Aphalo PJ, Robson TM. 2021. Diffuse solar radiation and canopy photosynthesis in a changing environment. Agricultural and Forest Meteorology 311, 108684.

Duursma RA .2015. Plantecophys - An R package for analysing and modelling leaf gas exchange data. PloS one 10, e0143346.

Duveiller G, Cescatti A. 2016. Spatially downscaling sun-induced chlorophyll fluorescence leads to an improved temporal correlation with gross primary productivity. Remote Sensing of Environment 182, 72–89.

Ecarnot M, Compan F, Roumet P. 2013. Assessing leaf nitrogen content and leaf mass per unit area of wheat in the field throughout plant cycle with a portable spectrometer. Field Crops Research 140, 44–50.

Elazab A, Moraga F, del Pozo A. 2021. Photosynthetic organs contributions to grain yield genetic gains in Chilean winter wheat. Agronomy Journal 113, 5006-5026.

El-Hendawy S, Al-Suhaibani N, Alotaibi M, Hassan W, Elsayed S, Tahir MU, Mohamed AI, Schmidhalter U. 2019. Estimating growth and photosynthetic properties of wheat grown in simulated saline field conditions using hyperspectral reflectance sensing and multivariate analysis. Scientific Reports 9, 1–15.

El-Sharkawy MA, Cock JH, Lynam JK, del Pilar Hernández A, Cadavid LF. 1990. Relationships between biomass, root-yield and single-leaf photosynthesis in field-grown cassava. Field Crops Research 25, 183–201.

Ely KS, Burnett AC, Lieberman-Cribbin W, Serbin SP, Rogers A. 2019. Spectroscopy can predict key leaf traits associated with source-sink balance and carbon-nitrogen status. Journal of Experimental Botany 70, 1789–1799.

Evans J, Santiago L. 2014. PrometheusWiki Gold Leaf Protocol: gas exchange using LI-COR 6400. Functional Plant Biology 41, 223–226.

Evans J. 1993. Photosynthetic acclimation and nitrogen partitioning within a lucerne canopy. I Canopy characteristics. Australian Journal of Plant Physiology 20, 55–67.

Evans JR, Lawson T. 2020. From green to gold: Agricultural revolution for food security. Journal of Experimental Botany 71, 2211–2215.

Faralli M, Lawson T. 2019. Natural genetic variation in photosynthesis: an untapped resource to increase crop yield potential? Plant Journal 101, 518–528.

Farquhar GD, von Caemmerer S, Berry JA. 1980. A biochemical model of photosynthetic CO_2 assimilation in leaves of C3 species. Planta 149, 78–90.

Farquhar GD, von Caemmerer S, Berry JA. 2001. Models of photosynthesis. Plant Physiology 125, 42–45.

Farquhar GD. 1989. Models of integrated photosynthesis of cells and leaves. Philosophical Transactions of the Royal Society of London 323, 357–367.

Fiorani F, Schurr U. 2013. Future scenarios for plant phenotyping. Annual Review of Plant Biology 64, 267–291.

Fischer RA, Rees D, Sayre KD, Lu ZM, Condon AG, Larque Saavedra A. 1998. Wheat yield progress associated with higher stomatal conductance and photosynthetic rate, and cooler canopies. Crop Science 38, 1467–1475.

Flexas J, Loreto F, Medrano H. 2012. Terrestrial photosynthesis in a changing environment. A molecular, physiological and ecological approach. Cambridge University Press. 723 pp.

Flood PJ, Kruijer W, Schnabel SK, Schoor R Van Der, Jalink H, Snel JFH, Harbinson J, Aarts MGM. 2016. Phenomics for photosynthesis, growth and reflectance in Arabidopsis thaliana reveals circadian and long - term fluctuations in heritability. Plant Methods 12, 1–14.

Foley JA, Ramankutty N, Brauman KA, Cassidy ES, Gerber JS, Johnston M, Mueller ND, O'Connell C, Ray DK, West PC, Balzer C, Bennett EM, Carpenter SR, Hill J, Monfreda C, Polasky S, Rockström J, Sheehan J, Siebert S, Tilman D, Zaks DPM. 2011. Solutions for a cultivated planet. Nature 478, 337–342.

Foo CC, Burgess AJ, Retkute R, Tree-Intong P, Ruban A V, Murchie EH. 2020. Photoprotective energy dissipation is greater in the lower, not the upper, regions of a rice canopy: a 3D analysis. Journal of Experimental Botany 71, 7382–7392.

Food and Agriculture Organization of the United Nations. (2020). FAOSTAT Database. Rome, Italy: FAO. Retrieved October 29th, 2020 from http://www.fao.org/faostat/en/#data/QC

Food and Agriculture Organization of the United Nations. (2021). FAOSTAT Database. Rome, Italy: FAO. Retrieved August 12th, 2021 from http://www.fao.org/faostat/en/#data/QC

Foulkes MJ, Slafer GA, Davies WJ, Berry PM, Sylvester-Bradley R, Martre P, Calderini DF, Griffiths S, Reynolds MP. 2011. Raising yield potential of wheat. III. Optimizing partitioning to grain while maintaining lodging resistance. Journal of Experimental Botany 62, 469–486.

Foulkes, MJ, Murchie EH. 2011. Optimising canopy physiology traits to improve the nutrient-utilization efficiency of crops. In: The Molecular Basis of Nutrient Use Efficiency in Crops. Eds: Hawkesford, M. J. and Barraclough, P. B. Wiley-Blackwell, 65-82.

Franks PJ, Beerling DJ. 2009. Maximum leaf conductance driven by CO_2 effects on stomatal size and density over geologic time. Proceedings of the National Academy of Sciences 106, 10343-10347.

Freschet GT, Pages L, Iversen CM, Comas LH, Rewald B, Roumet C, Zadworny M, Poorter H, Postma JA, Adams TS, Bagniewska-Zadworna A, Bengough AG, Blancaflor EB, Brunner I, Cornelissen JHC, Garnier E, Gessler A, Hobbie SE, Meier IC, Mommer L, Picon-Cochard C, Rose L, Ryser P, Scherer-Lorenzen M, Soudzilovskaia NA, Stokes A, Sun T, Valverde-Barrantes OJ, Weemstra M, Weigelt A, Wurzburger N, York LM, Batterman SA, Gomes de Moraes M, Janecek S, Lambers H, Salmon V, Tharayil N, McCormack ML. 2021. A starting guide to root ecology: strengthening ecological concepts and standardising root classification, sampling, processing and trait measurements. New Phytologist 232, 973–1122.

Fu L, Govindjee, Tan J, Guo Y. 2020. Development of a minimized model structure and a feedback control framework for regulating photosynthetic activities. Photosynthesis Research 146, 213-225.

Fu P, Meacham-Hensold K, Guan K, Wu J, Bernacchi C. 2020. Estimating photosynthetic traits from reflectance spectra: A synthesis of spectral indices, numerical inversion, and partial least square regression. Plant, Cell and Environment 43, 1241-1258.

Furbank RT, Jimenez-Berni JA, George-Jaeggli B, Potgieter AB, Deery DM. 2019. Field crop phenomics: enabling breeding for radiation use efficiency and biomass in cereal crops. New Phytologist 223, 1714–1727.

Furbank RT, Sharwood R, Estavillo GM, Silva-Pérez V, Condon AG. 2020. Photons to food: Genetic improvement of cereal crop photosynthesis. Journal of Experimental Botany 71, 2226–2238.

Furbank RT, Silva-Pérez V, Evans JR, Condon AG, Estavillo GM, Wennan, H, Newman S, Poiré R, Hall A, Zhen H. 2021. Wheat physiology predictor: predicting physiological traits in wheat from hyperspectral reflectance measurements using deep learning. Plant Methods 17, 1-15.

Furbank RT, Tester M. 2011. Phenomics - technologies to relieve the phenotyping bottleneck. Trends in Plant Science 16, 635–644.

Gaju O, DeSilva J, Carvalho P, Hawkesford MJ, Griffiths S, Greenland A, Foulkes MJ. 2016. Leaf photosynthesis and associations with grain yield, biomass and nitrogen-use efficiency in landraces, synthetic-derived lines and cultivars in wheat. Field Crops Research 193, 1–15.

Galán RJ, Bernal-Vasquez AM, Jebsen C, Piepho HP, Thorwarth P, Steffan P, Gordillo A, Miedaner T. 2020. Hyperspectral reflectance data and agronomic traits can predict biomass yield in winter rye hybrids. Bioenergy Research 13, 168–182.

Gallagher JN, Biscoe PV. 1978. Radiation absorption, growth and yield of cereals. The Journal of Agricultural Science 91, 47–60.

Galloway JN, Townsend AR, Erisman JW, Bekunda M, Cai Z, Freney JR, Martinelli LA, Seitzinger SP, Sutton MA. 2008. Transformation of the nitrogen cycle: recent trends, questions, and potential solutions. Science 320, 889–893.

Gamon JA, Field CB, Goulden ML, Griffin KL, Hartley AE, Joel G, Peñuelas J, Valentini R. 1995. Relationships between NDVI, canopy structure, and photosynthesis in three Californian vegetation types. Ecological Applications 5, 28–41.

Gamon JA, Serrano L, Surfus JS. 1997. The photochemical reflectance index: An optical indicator of photosynthetic radiation use efficiency across species, functional types, and nutrient levels. Oecologia 112, 492–501.

Gamon JA, Somers B, Malenovský Z, Middleton EM, Rascher U, Schaepman ME. 2019. Assessing Vegetation Function with Imaging Spectroscopy. Surveys in Geophysics 40, 489–513.

Gao BC. 1996. NDWI—A normalized difference water index for remote sensing of vegetation liquid water from space. Remote Sensing of Environment 58, 257-266.

Gara TW, Skidmore AK, Darvishzadeh R, Wang T. 2019. Leaf to canopy upscaling approach affects the estimation of canopy traits. GIScience and Remote Sensing 56, 554–575.

Garatuza-Payan J, Argentel-Martinez L, Yepez EA, Arredondo T. 2018. Initial response of phenology and yield components of wheat (*Triticum durum* L., CIRNO C2008) under experimental warming field conditions in the Yaqui Valley. PeerJ 6, e5064.

Garbulsky MF, Peñuelas J, Gamon J, Inoue Y, Filella I (2011) The photochemical reflectance index (PRI) and the remote sensing of leaf, canopy and ecosystem radiation use efficiencies. A review and meta-analysis. Remote Sensing of Environment 115, 281–297.

Gent MP. 1995. Canopy light interception, gas exchange, and biomass in reduced height isolines of winter wheat. Crop Science 35, 1636–1642.

Gibbs JA, McAusland L, Robles-Zazueta CA, Murchie EH, Burgess AJ. 2021. A deep learning method for fully automatic stomatal morphometry and maximal conductance estimation. Frontiers in Plant Science 12, 780180.

Gitelson AA, Merzlyak MN. 1996. Signature analysis of leaf reflectance spectra: algorithm development for remote sensing of chlorophyll. Journal of Plant Physiology 14, 494-500.

Gnyp ML, Miao Y, Yuan F, Ustin SL, Yu K, Yao Y, Huang S, Bareth G. 2014. Hyperspectral canopy sensing of paddy rice aboveground biomass at different growth stages. Field Crops Research 155, 42–55.

Gonzalez-Navarro OE, Griffiths S, Molero G, Reynolds MP, Slafer GA. 2016. Field Crops Research Variation in developmental patterns among elite wheat lines and relationships with yield, yield components and spike fertility. Field Crops Research 196, 294–304.

Guo J, Trotter CM. 2004. Estimating photosynthetic light-use efficiency using the photochemical reflectance index: Variations among species. Functional Plant Biology 31, 255–265.

Gutierrez M, Reynolds MP, Klatt AR. 2010. Association of water spectral indices with plant and soil water relations in contrasting wheat genotypes. Journal of Experimental Botany 61, 3291–3303.

Gutiérrez-Rodríguez M, Reynolds M, Larqué-Saavedra A. 2000. Photosynthesis of wheat in a warm, irrigated environment II. Traits associated with genetic gains in yield. Field Crops Research 66, 51–62.

Haboudane D, Miller JR, Tremblay N, Zarco-Tejada PJ, Dextraze L. 2002. Integrated narrow-band vegetation indices for prediction of crop chlorophyll content for application to precision agriculture. Remote Sensing of Environment 81, 416-426.

Haboudane D, Tremblay N, Miller JR, Vigneault P. 2008. Remote estimation of crop chlorophyll content using spectral indices derived from hyperspectral data. IEEE Geoscience and Remote Sensing 46, 423–437.

Hämmerle M, Höfle B. 2016. Direct derivation of maize plant and crop height from low - cost time - of - flight camera measurements. Plant Methods, 1–13.

Hatfield JL, Prueger JH. 2010. Value of using different vegetative indices to quantify agricultural crop characteristics at different growth stages under varying management practices. Remote Sensing 2, 562–578.

Heckmann D, Schlüter U, Weber APM. 2017. Machine learning techniques for predicting crop photosynthetic capacity from leaf reflectance spectra. Molecular Plant 10, 878–890.

Hikosaka K. 2016. Optimality of nitrogen distribution among leaves in plant canopies. Journal of Plant Research 129, 299–311.

Hinojo-Hinojo C, Goulden ML. 2020. Plant traits help explain the tight relationship between vegetation indices and gross primary production. Remote Sensing 12, 1–18.

Hirose T. 2005. Development of the Monsi-Saeki theory on canopy structure and function. Annals of Botany 95, 483–494.

Hong SL, Feng ML. 2005. Root respiration, photosynthesis and grain yield of two spring wheat in response to soil drying. Plant Growth Regulation 46, 233–240.

Horton P. 2000. Prospects for crop improvement through the genetic manipulation of photosynthesis: morphological and biochemical aspects of light capture. Journal of Experimental Botany 51, 475–485.

Hoyaux J, Moureaux C, Tourneur D, Bodson B, Aubinet M. 2008. Extrapolating gross primary productivity from leaf to canopy scale in a winter wheat crop. Agricultural and Forest Meteorology 148, 668–679.

Huang M, Shan S, Zhou X, Chen J, Cao F, Jiang L, Zou Y. 2016. Leaf photosynthetic performance related to higher radiation use efficiency and grain yield in hybrid rice. Field Crops Research 193, 87–93.

Hubbart S, Smillie IRA, Heatley M, Swarup R, Foo CC, Zhao L, Murchie EH. 2018. Enhanced thylakoid photoprotection can increase yield and canopy radiation use efficiency in rice. Communications Biology 1, 1–12.

Huete A, Didan K, Miura T, Rodriguez E., Gao X, Ferreira L. 2002. Overview of the radiometric and biophysical performance of the MODIS vegetation indices. Remote Sensing of Environment 83, 195–213.

Huete A. 1988. A soil-adjusted vegetation index (SAVI). Remote Sensing of Environment 25, 295-309.

Impa SM, Sunoj VSJ, Krassovskaya I, Bheemanahalli R, Obata T, Jagadish SVK. 2019. Carbon balance and source-sink metabolic changes in winter wheat exposed to high night-time temperature. Plant Cell and Environment 42, 1233–1246.

Intergovernmental Panel on Climate Change (IPCC). 2014. Summary for Policymakers. Geneva, Switzerland.

Jägermeyr J, Müller C, Ruane AC, Elliott J, Balkovic J, Castillo O, Faye B, Foster I, Folberth C, Franke JA, Fuchs K, Guarin JR, Heinke J, Hoogenboom G, Iizumi T, Jain AK, Kelly D, Khabarov N, Lange S, Lin TS, Liu W, Mialyk O, Minoli S, Moyer EJ, Okada M, Phillips M, Porter C, Rabin SS, Scheer C, Schneider JM, Schyns JF, Skalsky R, Smerald A, Stella T, Stephens H, Webber H, Zabel F, Rosenzweig C. 2021. Climate impacts on global agriculture emerge earlier in new generation of climate and crop models. Nature Food 2, 873–885.

Jiang GM, Sun JZ, Liu HQ, Qu CM, Wang KJ, Guo RJ, Bai KZ, Gao LM, Kuang TY. 2003. Changes in the rate of photosynthesis accompanying the yield increase in wheat cultivars released in the past 50 years. Journal of Plant Research 116, 347–354.

Joynson R, Molero G, Coombes B, Gardiner LJ, Rivera-Amado C, Piñera-Chávez FJ, Evans JR, Furbank RT, Reynolds MP, Hall A. 2021. Uncovering candidate genes involved in photosynthetic capacity using unexplored genetic variation in spring wheat. Plant Biotechnology Journal 19, 1537-1552.

Keenan TF, Luo X, De Kauwe MG, Medlyn BE, Prentice IC, Stocker BD, Smith NG, Terrer C, Wang H, Zhang Y, Zhou S. 2021. A constraint on historic growth in global photosynthesis due to increasing CO_2. Nature 600, 253-258.

Kimball BA. 2016. Crop responses to elevated CO_2 and interactions. Current Opinion in Plant Biology 31, 36–43.

King J, Gay A, Sylvester-Bradley R, Bingham I, Foulkes J, Gregory P, Robinson D. 2003. Modelling cereal root systems for water and nitrogen capture: Towards an economic optimum. Annals of Botany 91, 383–390.

Kromdijk J, Glowacka K, Leonelli L, Gabilly ST, Iwai M, Niyogi KK, Long SP. 2016. Improving photosynthesis and crop productivity by accelerating recovery from photoprotection. Science 354, 857–861.

Kromdijk J, Long SP. 2016. One crop breeding cycle from starvation? How engineering crop photosynthesis for rising CO_2 and temperature could be one important route to alleviation. Proceedings of the Royal Society B 283, 20152578.

Kuhlgert S, Austic G, Zegarac R, Osei-Bonsu I, Hoh D, Chilvers MI, Roth MG, Bi K, TerAvest D, Weebadde P, Kramer DM. 2016. MultispeQ Beta: a tool for large-scale plant phenotyping connected to the open PhotosynQ network. Royal Society Open Science 3, 160592.

Lambers H, Chapin FS III, Pons TL. 2008. Plant physiological ecology. Second edition. Springer. 605 pp.

Langridge P, Reynolds M. 2021. Breeding for drought and heat tolerance in wheat. Theoretical and Applied Genetics 134, 1753–1769.

Lawson T, Blatt MR. 2014. Stomatal size, speed, and responsiveness impact on photosynthesis and water use efficiency. Plant Physiology 164, 1556-1570.

Lawson T, Kramer DM, Raines CA. 2012. Improving yield by exploiting mechanisms underlying natural variation of photosynthesis. Current Opinion in Biotechnology 23, 215–220.

Lemaire G, Oosterom E van, Sheehy J, Jeuffroy MH, Massignam A, Rossato L. 2007. Is crop N demand more closely related to dry matter accumulation or leaf area expansion during vegetative growth? Field Crops Research 100, 91–106.

Li F, Miao Y, Hennig SD, Gnyp ML, Chen X, Jia L, Bareth G. 2010. Evaluating hyperspectral vegetation indices for estimating nitrogen concentration of winter wheat at different growth stages. Precision Agriculture 11, 335–357.

Lilley JM, Kirkegaard JA. 2011. Benefits of increased soil exploration by wheat roots. Field Crops Research 122, 118–130.

Lilley JM, Kirkegaard JA. 2016. Farming system context drives the value of deep wheat roots in semi-arid environments. Journal of Experimental Botany 67, 3665–3681.

Liu L, Peng D, Hu Y, Jiao Q. 2013. A novel in Situ FPAR measurement method for low canopy vegetation based on a digital camera and reference panel. Remote Sensing 5, 274–281.

Lobell DB, Asner GP, Ortiz-Monasterio JI, Benning TL. 2003. Remote sensing of regional crop production in the Yaqui Valley, Mexico: estimates and uncertainties. Agriculture, Ecosystems and Environment 94, 205–220.

Lobell DB, Cassman KG, Field CB. 2009. Crop yield gaps: their importance, magnitudes, and causes. Annual Review of Environment and Resources 34, 179–204.

Long SP, Ainsworth EA, Leakey ADB, Ort DR. 2006. Food for thought: lower-than-expected crop yield stimulation with rising CO_2 concentrations. Science 312, 1918–1921.

Long SP, Ainsworth EA, Rogers A, Ort DR. 2004. Rising atmospheric carbon dioxide: plants FACE the future. Annual Review of Plant Biology 55, 591–628.

Long SP, Marshall-Colon A, Zhu XG. 2015. Meeting the global food demand of the future by engineering crop photosynthesis and yield potential. Cell 161, 56–66.

Long SP, Zhu XG, Naidu SL, Ort DR. 2006. Can improvement in photosynthesis increase crop yields? Plant, Cell and Environment 29, 315–330.

Lopes MS, Reynolds MP. 2010. Partitioning of assimilates to deeper roots is associated with cooler canopies and increased yield under drought in wheat. Functional Plant Biology 37, 147–156.

Lopes MS, Reynolds MP. 2012. Stay-green in spring wheat can be determined by spectral reflectance measurements (normalized difference vegetation index) independently from phenology. Journal of Experimental Botany 63, 3789–3798.

Lu Z, Percy RG, Qualset CO, Zeiger E. 1998. Stomatal conductance predicts yields in irrigated Pima cotton and bread wheat grown at high temperatures. Journal of Experimental Botany 49, 453–460.

Mahner M, Kary M. 1997. What exactly are genomes, genotypes and phenotypes? And what about phenomes? Journal of Theoretical Biology 186, 55–63.

Malenovský Z, Mishra KB, Zemek F, Rascher U, Nedbal L. 2009. Scientific and technical challenges in remote sensing of plant canopy reflectance and fluorescence. Journal of Experimental Botany 60, 2987–3004.

Mantilla-Perez MB, Fernandez-Salas MG. 2017. Differential manipulation of leaf angle throughout the canopy: current status and prospects. Journal of Experimental Botany 68, 5699-5717.

Mantilla-Perez MB, Bao Y, Tang L, Schnable PS, Salas-Fernandez MG. 2020. Toward "Smart canopy" sorghum: Discovery of the genetic control of leaf angle across layers. Plant Physiology 184, 1927-1940.

Marshall M, Thenkabail P. 2015. Developing in situ non-destructive estimates of crop biomass to address issues of scale in remote sensing. Remote Sensing 7, 808–835.

McAusland L, Atkinson JA, Lawson T, Murchie EH. 2019. High throughput procedure utilising chlorophyll fluorescence imaging to phenotype dynamic photosynthesis and photoprotection in leaves under controlled gaseous conditions. Plant Methods 15, 1-15.

McAusland L, Davey PA, Kanwal N, Baker NR, Lawson T. 2013. A novel system for spatial and temporal imaging of intrinsic plant water use efficiency. Journal of Experimental Botany 64, 4993-5007.

McAusland L, Vialet-Chabrand S, Jauregui I, Burridge A, Hubbart-Edwards S, Fryer MJ, King IP, King J, Pyke K, Edwards KJ, Carmo-Silva E, Lawson T, Murchie EH. 2020. Variation in key leaf photosynthetic traits across wheat wild relatives is accession dependent not species dependent. New Phytologist 228, 1767-1780.

Meacham-Hensold K, Fu P, Wu J, Serbin S, Montes CM, Ainsworth E., Guan K, Dracup E, Pederson T, Driever S, Bernacchi C. 2020. Plot-level rapid screening for photosynthetic parameters using proximal hyperspectral imaging. Journal of Experimental Botany 71, 2312-2338.

Meroni M, Rossini M, Guanter L, Alonso L, Rascher U, Colombo R, Moreno J. 2009. Remote sensing of solar-induced chlorophyll fluorescence: Review of methods and applications. Remote Sensing of Environment 113, 2037–2051.

Mevik B, Wehrens R. 2007. The pls package: Principal component and partial least squares regression in R. Journal of Statistical Software 18, 1–23.

Molero G, Joynson R, Pinera-Chavez FJ, Gardiner LJ, Rivera-Amado C, Hall A, Reynolds MP. 2019. Elucidating the genetic basis of biomass accumulation and radiation use efficiency in spring wheat and its role in yield potential. Plant Biotechnology Journal 17, 1276–1288.

Molero G, Reynolds MP. 2020. Spike photosynthesis measured at high throughput indicates genetic variation independent of flag leaf photosynthesis. Field Crops Research 255, 107866.

Monteith JL. 1977. Climate and the efficiency of crop production in Britain. Philosophical Transactions of the Royal Society B: Biological Sciences 281, 277–294.

Monteith JL. 1978. Reassessment of maximum growth rates for C_3 and C_4 crops. Experimental Agriculture 14, 1–5.

Montesinos-López OA, Montesinos-López A, Crossa J, de los Campos G, Alvarado G, Suchismita M, Rutkoski J, Pérez LG, Burgueño J. 2017. Predicting grain yield using canopy hyperspectral reflectance in wheat breeding data. Plant Methods 13, 1–23.

Moraga F, Alcaíno M, Matus I, Castillo D, del Pozo A. 2022. Leaf and canopy traits associated with stay-green expression are closely related to yield components of wheat genotypes with contrasting tolerance to water stress. Plants 11, 292.

Moreau D, Allard V, Gaju O, le Gouis J, Foulkes MJ, Martre P. 2012. Acclimation of leaf nitrogen to vertical light gradient at anthesis in wheat is a whole-plant process that scales with the size of the canopy. Plant Physiology 160, 1479–1490.

Morris EC, Griffiths M, Golebiowska A, Mairhofer S, Burr-Hersey J, Goh T, von Wangenheim D, Atkinson B, Sturrock CJ, Lynch JP, Vissenberg K, Ritz K, Wells DM, Mooney SJ, Bennett MJ. 2017. Shaping 3D root system architecture. Current Biology 27, 919-930.

Müller-Linow M, Pinto-Espinosa F, Scharr H, Rascher U. 2015. The leaf angle distribution of natural plant populations: assessing the canopy with a novel software tool. Plant Methods 11, 1-16.

Murchie EH, Kefauver S, Araus JL, Muller O, Rascher U, Flood PJ, Lawson T. 2018. Measuring the dynamic photosynthome. Annals of Botany 122, 207–220.

Murchie EH, Lawson T. 2013. Chlorophyll fluorescence analysis: A guide to good practice and understanding some new applications. Journal of Experimental Botany 64, 3983–3998.

Murchie EH, Niyogi KK. 2011. Manipulation of photoprotection to improve plant photosynthesis. Plant Physiology 155, 86–92.

Murchie EH, Pinto M, Horton P. 2009. Agriculture and the new challenges for photosynthesis research. New Phytologist 181, 532–552.

Murchie EH, Reynolds MP. 2013. Crop radiation capture and use efficiency (P Christou, R Savin, BA Costa-Pierce, I Misztal, and CBA Whitelaw, Eds.). Sustainable Food Production, 591–614.

Murchie EH, Ruban AV. 2020. Dynamic non-photochemical quenching in plants: from molecular mechanism to productivity. The Plant Journal 101, 885–896.

Murchie EH. 2017. Safety conscious or living dangerously: what is the 'right' level of plant photoprotection for fitness and productivity? Plant, Cell and Environment 40, 1239–1242.

Niinemets Ü. 2010. A review of light interception in plant stands from leaf to canopy in different plant functional types and in species with varying shade tolerance. Ecological Research 25, 693–714.

Nobel PS. 2009. Physicochemical and environmental plant physiology. Fourth edition. Elsevier. 582 pp.

O'Leary GJ, Christy B, Nuttall J, Huth N. 2015. Response of wheat growth, grain yield and water use to elevated CO_2 under a Free-Air CO_2 Enrichment (FACE) experiment and modelling in a semi-arid environment. Global Change Biology 21, 2670–2686.

Ober ES, Alahmad S, Cockram J, Forestan C, Hickey LT, Kant J, Maccaferri M, Marr E, Milner M, Pinto F, Rambla C, Reynolds M, Salvi S, Sciara G, Snowdon RJ, Thomelin P, Tuberosa R, Uuay C, Voss-Fels KP, Wallington E, Watt M. 2021. Wheat root systems as a breeding target for climate resilience. Theoretical and Applied Genetics 134, 1645-1662.

Ollinger SV. 2011. Sources of variability in canopy reflectance and the convergent properties of plants. New Phytologist 189, 375–394.

Ort DR, Merchant SS, Alric J, Barkan A, Blankenship RE, Bock R, Croce R, Hanson MR, Hibberd JM, Long SP, Moore TA, Moroney J, Niyogi KK, Parry MAJ, Peralta-Yahya PP, Prince RC, Redding KE, Spalding MH, van Wijk KJ, Vermaas WFJ, von Caemmerer S, Weber APM, Yeates TO, Yuan JS, Zhu XG. 2015. Redisigning photosynthesis to sustainably meet global food and bioenergy demand. Proceedings of the National Academy of Sciences 112, 8529-8536.

Pandey BK, Huang G, Bhosale R, Hartman S, Sturrock CJ, Martin LJOC, Karady M, Voesenek LACJ, Ljung K, Lynch JP, Brown KM, Whalley WR, Mooney SJ, Zhang D, Bennett M. 2021. Plant roots sense soil compaction through restricted ethylene diffusion. Science 371, 276-280.

Pang J, Palta JA, Rebetzke GJ, Milroy SP. 2014. Wheat genotypes with high early vigour accumulate more nitrogen and have higher photosynthetic nitrogen use efficiency during early growth. Functional Plant Biology 41, 215–222.

Parazoo NC, Bowman K, Fisher JB, Frankenberg C, Jones DBA, Cescatti A, Pérez-Priego O, Wohlfahrt G, Montagnani L. 2014. Terrestrial gross primary

production inferred from satellite fluorescence and vegetation models. Global Change Biology 20, 3103–3121.

Parry MAJ, Reynolds M, Salvucci ME, Raines C, Andralojc PJ, Zhu XG, Price GD, Condon AG, Furbank RT. 2011. Raising yield potential of wheat. II. Increasing photosynthetic capacity and efficiency. Journal of Experimental Botany 62, 453–467.

Pask A, Pietragalla J, Mullan D, Reynolds MP. 2013. Physiological breeding II: a field guide to wheat phenotyping (AJ Pask, J Pietragalla, D Mullan, and MP Reynolds, Eds.). Mexico, D.F.: CIMMYT.

Pauli D, Chapman SC, Bart R, Topp CN, Lawrence-Dill CJ, Poland J, Gore MA. 2016. The quest for understanding phenotypic variation via integrated approaches in the field environment. Plant Physiology 172, 622–634.

Paulus S, Schumann H, Kuhlmann H, Léon J. 2014. High-precision laser scanning system for capturing 3D plant architecture and analysing growth of cereal plants. Biosystems Engineering 121, 1–11.

Pearcy RW. 1990. Photosynthesis in plant life. Annual Review of Plant Physiology and Plant Molecular Biology 41, 421–453.

Peng S, Krieg DR, Girma FS. 1991. Leaf photosynthetic rate is correlated with biomass and grain production in grain sorghum lines. Photosynthesis Research 28, 1–7.

Pennacchi JP, Carmo-Silva E, Andralojc PJ, Feuerhelm D, Powers SJ, Parry MAJ. 2018. Dissecting wheat grain yield drivers in a mapping population in the UK. Agronomy 8, 94.

Peñuelas J, Baret F, Filella I. 1995. Semi-empirical indices to assess carotenoids/chlorophyll a ratio from leaf spectral reflectance. Photosynthetica 31, 221-230.

Peñuelas J, Filella I, Gamon JA. 1995. Assessment of photosynthetic radiation-use efficiency with spectral reflectance. New Phytologist 131, 291-296.

Peñuelas J, Gamon JA, Fredeen AL, Merino J, Field CB. 1994. Reflectance indices associated with physiological changes in nitrogen- and water-limited sunflower leaves. Remote Sensing of Environment 48, 135-146.

Peñuelas J, Garbulsky MF, Filella I. 2011. Photochemical reflectance index (PRI) and remote sensing of plant CO_2 uptake. New Phytologist 191, 596–599.

Peñuelas J, Pinol J, Ogaya R, Filella I. 1997. Estimation of plant water concentration by the reflectance Water Index WI (R900/R970). International Journal of Remote Sensing 18, 2869–2875.

Peterhansel C, Blume C, Offermann S. 2013. Photorespiratory bypasses: how can they work? Journal of Experimental Botany 64, 709-715.

Pinera-Chavez FJ, Berry PM, Foulkes MJ, Jesson MA, Reynolds MP. 2016a. Avoiding lodging in irrigated spring wheat. I. Stem and root structural requirements. Field Crops Research 196, 325–336.

Pinera-Chavez FJ, Berry PM, Foulkes MJ, Molero G, Reynolds MP. 2016b. Avoiding lodging in irrigated spring wheat. II. Genetic variation of stem and root structural properties. Field Crops Research 196, 64–74.

Pinto F, Damm A, Schickling A, Panigada C, Cogliati S, Müller-Linow M, Balvora A, Rascher U. 2016. Sun-induced chlorophyll fluorescence from high-resolution imaging spectroscopy data to quantify spatio-temporal patterns of photosynthetic function in crop canopies. Plant, Cell and Environment 39, 1500–1512.

Pinto F, Müller-Linow M, Schickling A, Cendrero-Mateo MP, Ballvora A, Rascher U. 2017. Multiangular observation of canopy sun-induced chlorophyll fluorescence by combining imaging spectroscopy and stereoscopy. Remote Sensing 9, 1–21.

Pinto RS, Lopes MS, Collins NC, Reynolds MP. 2016. Modelling and genetic dissection of staygreen under heat stress. Theoretical and Applied Genetics 129, 2055–2074.

Pinto RS, Molero G, Reynolds MP. 2017. Identification of heat tolerant wheat lines showing genetic variation in leaf respiration and other physiological traits. Euphytica 213, 1-15.

Pogson BJ, Ganguly D, Albrecht-Borth V. 2015. Insights into chlorophyll biogenesis and development. Biochimica et Biophysica Acta 1847, 1017-1024.

Poland J, Endelman J, Dawson J, Rutkoski J, Wu S, Manes Y, Dreisigacker S, Crossa J, S-Villeda H, Sorrells M, Jannink JL. 2012. Genomic selection in wheat breeding using genotyping-by-sequencing. The Plant Genome 5, 103–113.

Poorter H, Fiorani F, Pieruschka R, Putten WH Van Der, Kleyer M, Schurr U. 2016. Pampered inside, pestered outside? Differences and similarities between plants growing in controlled conditions and in the field. New Phytologist 212, 838–855.

Porcar-Castell A, Palmroth S. 2012. Modelling photosynthesis in highly dynamic environments: The case of sun flecks. Tree Physiology 32, 1062–1065.

Porter JR, Xie L, Challinor AJ, et al., 2014. Food security and food production systems. Climate change impacts 2014: Impacts, adaptation and vulnerability. Part A: Global and sectoral aspects. Contribution of working group II to the Fifth Assessment Report of the Intergovernmental Panel on Climate Change. Cambridge University Press, Cambridge, 485–533.

Posch BC, Kariyawasam BC, Bramley H, Coast O, Richards RA, Reynolds MP, Trethowan R, Atkin OK. 2019. Exploring high temperature responses of photosynthesis and respiration to improve heat tolerance in wheat. Journal of Experimental Botany 70, 5051–5069.

Pound MP, Atkinson JA, Townsend AJ, Wilson MH, Griffiths M, Jackson AS, Bulat A, Tzimiropoulos G, Wells DM, Murchie EH, Pridmore TP, French AP. 2017. Deep machine learning provides state-of-the-art performance in image-based plant phenotyping. GigaScience 6, 1-10.

Pound MP, French AP, Atkison JA, Wells DM, Bennett MJ, Pridmore T. 2013. RootNav: Navigating images of complex root architectures. Plant Physiology 162, 1802-1814.

Prasad B, Babar MA, Carver BF, Raun WR, Klatt AR. 2009. Association of biomass production and canopy spectral reflectance indices in winter wheat. Canadian Journal of Plant Science 89, 485–496.

Prins A, Orr DJ, Andralojc PJ, Reynolds MP, Carmo-Silva E, Parry MAJ. 2016. Rubisco catalytic properties of wild and domesticated relatives provide scope for improving wheat photosynthesis. Journal of Experimental Botany 67, 1827–1838.

Qi J, Chehbouni A, Huete AR, Kerr YH, Sorooshian S. 1994. A modified soil adjusted vegetation index. Remote Sensing of Environment 48, 119–126.

Quintero A, Molero G, Reynolds MP, Calderini DF. 2018. Trade-off between grain weight and grain number in wheat depends on GxE interaction: A case study of an elite CIMMYT panel (CIMCOG). European Journal of Agronomy 92, 17–29.

R Core Team. 2016. R: A language and environment for statistical computing. R Foundation for Statistical Computing, Vienna, Austria. URL http://www.R-project.org/.

Rajaram S, van Ginkel M, Fischer R. 1993. CIMMYT wheat breeding mega-environments (ME). 8th International Wheat Genetics Symposium, 1101–1106.

Ray DK, Mueller ND, West PC, Foley JA. 2013. Yield trends are insufficient to double global crop production by 2050. PloS one 8, e66428.

Ray DK, Ramankutty N, Mueller ND, West PC, Foley JA. 2012. Recent patterns of crop yield growth and stagnation. Nature Communications 3, 1-7.

Reichstein M, Bahn M, Ciais P, Frank D, Mahecha MD, Seneviratne SI, Zscheischler J, Beer C, Buchmann N, Frank DC, Papale D, Rammig A, Smith P, Thonicke K, van der Velde M, Vicca S, Walz A, Wattenbach M. 2013. Climate extremes and the carbon cycle. Nature 500, 287–295.

Retkute R, Smith-Unna SE, Smith RW, Burgess AJ, Jensen OE, Johnson GN, Preston SP, Murchie EH. 2015. Exploiting heterogeneous environments: Does photosynthetic acclimation optimize carbon gain in fluctuating light? Journal of Experimental Botany 66, 2437–2447.

Reynolds M, Calderini D, Condon A, Vargas M. 2007. Association of source/sink traits with yield, biomass and radiation use efficiency among random sister lines from three wheat crosses. The Journal of Agricultural Science 145, 3.

Reynolds M, Chapman S, Crespo-Herrera L, Molero G, Mondal S, Pequeno DNL, Pinto F, Pinera-Chavez FJ, Poland J, Rivera-Amado C, Saint-Pierre C, Sukumaran S. 2020. Breeder friendly phenotyping. Plant Science 295, 110396.

Reynolds M, Foulkes J, Furbank R, Griffiths S, King J, Murchie E, Parry M, Slafer G. 2012. Achieving yield gains in wheat. Plant, Cell and Environment 35, 1799–1823.

Reynolds M, Foulkes MJ, Slafer GA, Berry P, Parry MAJ, Snape JW, Angus WJ. 2009. Raising yield potential in wheat. Journal of Experimental Botany 60, 1899–1918.

Reynolds M, Langridge P. 2016. Physiological breeding. Current Opinion in Plant Biology 31, 162–171.

Reynolds MP, Balota M, Delgado MIB, Amani I, Fischer RA. 1994. Physiological and morphological traits associated with spring wheat yield under hot, irrigated conditions. Australian Journal of Plant Physiology 21, 717–730.

Reynolds MP, Borlaug NE. 2006. Impacts of breeding on international collaborative wheat improvement. The Journal of Agricultural Science 144, 3–17.

Reynolds MP, Delgado B. MI, Gutiérrez-Rodríguez M, Larqué-Saavedra A. 2000a. Photosynthesis of wheat in a warm, irrigated environment I: Genetic diversity and crop productivity. Field Crops Research 66, 37–50.

Reynolds MP, Pellegrineschi A, Skovmand B. 2005. Sink-limitation to yield and biomass: a summary of some investigations in spring wheat. Annals of Applied Biology 146, 39–49.

Reynolds MP, van Ginkel M, Ribaut JM. 2000b. Avenues for genetic modification of radiation use efficiency in wheat. Journal of Experimental Botany 51, 459–473.

Richards RA, Cavanagh CR, Riffkin P. 2019. Selection for erect canopy architecture can increase yield and biomass of spring wheat. Field Crops Research 244, 107649.

Richards RA. 2000. Selectable traits to increase crop photosynthesis and yield of grain crops. Journal of Experimental Botany 51, 447–458.

Rivera-Amado C, Molero G, Trujillo-Negrellos E, Reynolds M, Foulkes J. 2020. Estimating organ contribution to grain filling and potential for source upregulation in wheat cultivars with a contrasting source – sink balance. Agronomy 10, 1–21.

Robles-Zazueta CA, Molero G, Pinto F, Foulkes MJ, Reynolds MP, Murchie EH. 2021. Field-based remote sensing models predict radiation use efficiency in wheat. Journal of Experimental Botany 72, 3756–3773.

Robles-Zazueta CA, Pinto F, Molero G, Foulkes MJ, Reynolds MP, Murchie EH. 2022. Prediction of photosynthetic, biophysical and biochemical traits in wheat canopies to reduce the phenotyping bottleneck. Frontiers in Plant Science 13, 828451.

Roitsch T, Cabrera-Bosquet L, Fournier A, Ghamkhar K, Jiménez-Berni J, Pinto F, Ober ES. 2019. New sensors and data-driven approaches—A path to next generation phenomics. Plant Science 282, 2–10.

Sadeghi-Tehran P, Sabermanesh K, Virlet N, Hawkesford MJ. 2017. Automated method to determine two critical growth stages of wheat: Heading and flowering. Frontiers in Plant Science 8, 252.

Sage RF, Sage TL, Kocacinar F. 2012. Photorespiration and the evolution of C_4 photosynthesis. Annual Review of Plant Biology 63, 19–47.

Sage RF, Stata M. 2015. Photosynthetic diversity meets biodiversity: The C_4 plant example. Journal of Plant Physiology 172, 104–119.

Saint Pierre C, Trethowan R, Reynolds M. 2010. Stem solidness and its relationship to water-soluble carbohydrates: association with wheat yield under water deficit. Functional Plant Biology 37, 166-174.

Sakai H, Hasegawa T, Kobayashi K. 2006. Enhancement of rice canopy carbon gain by elevated CO_2 is sensitive to growth stage and leaf nitrogen concentration. New Phytologist 170, 321–332.

Salter WT, Gilbert ME, Buckley TN. 2018. A multiplexed gas exchange system for increased throughput of photosynthetic capacity measurements. Plant Methods 14, 1–12.

Salter WT, Merchant A, Trethowan RM, Richards RA, Buckley TN. 2020. Wide variation in the suboptimal distribution of photosynthetic capacity in relation to light across genotypes of wheat. AoB PLANTS 12, 1–11.

Sanchez-Bragado R, Elazab A, Zhou B, Serret MD, Bort J, Nieto-Taladriz MT, Araus JL. 2014. Contribution of the ear and the flag leaf to grain filling in durum wheat inferred from the carbon isotope signature: Genotypic and growing conditions effects. Journal of Integrative Plant Biology 56, 444–454.

Sanchez-Bragado R, Vicente R, Molero G, Serret MD, Maydup ML, Araus J.L. 2020. New avenues for increasing yield and stability in C_3 cereals: exploring ear photosynthesis. Current Opinion in Plant Biology 56, 223–234.

Sankaran S, Khot LR, Espinoza CZ, Jarolmasjed S, Sathuvalli VR, Vandemark GJ, Miklas PN, Carter AH, Pumphrey MO, Knowles NR, Pavek MJ. 2015. Low-altitude, high-resolution aerial imaging systems for row and field crop phenotyping: A review. European Journal of Agronomy 70, 112–123.

Serbin SP, Dillaway DN, Kruger EL, Townsend PA. 2012. Leaf optical properties reflect variation in photosynthetic metabolism and its sensitivity to temperature. Journal of Experimental Botany 63, 489–502.

Serbin SP, Singh A, McNeil BE, Kingdon CC, Townsend PA. 2014. Spectroscopic determination of leaf morphological and biochemical traits for northern temperate and boreal tree species. Ecological Applications 24, 1651–1669.

Severini AD, Wasson AP, Evans JR, Richards RA, Watt M. 2020. Root phenotypes at maturity in diverse wheat and triticale genotypes grown in three field experiments: Relationships to shoot selection, biomass, grain yield, flowering time, and environment. Field Crops Research 255, 107870.

Sharwood RE. 2017. Engineering chloroplasts to improve Rubisco catalysis: prospects for translating improvements into food and fiber crops. New Phytologist 213, 494–510.

Shen BR, Wang LM, Lin XL, Yao Z, Xu HW, Zhu CH, Teng HY, Cui LL, Liu EE, Zhang JJ, He ZH, Peng XX. 2019. Engineering a new chloroplastic photorespiratory bypass to increase photosynthetic efficiency and productivity in rice. Molecular Plant 12, 199-214.

Sierra-Gonzalez A, Molero G, Rivera-Amado C, Babar MA, Reynolds MP, Foulkes MJ. 2021. Exploring genetic diversity for grain partitioning traits to enhance yield in a high biomass spring wheat panel. Field Crops Research 260, 107979.

Silva-Pérez V, De Faveri J, Molero G, Deery DM, Condon AG, Reynolds MP, Evans JR, Furbank RT. 2020. Genetic variation for photosynthetic capacity and efficiency in spring wheat. Journal of Experimental Botany 71, 2299–2311.

Silva-Pérez V, Molero G, Serbin SP, Condon AG, Reynolds MP, Furbank RT, Evans JR. 2018. Hyperspectral reflectance as a tool to measure biochemical and physiological traits in wheat. Journal of Experimental Botany 69, 483-496.

Simkin AJ, Faralli M, Ramamoorthy S, Lawson T. 2020. Photosynthesis in non-foliar tissues: implications for yield. Plant Journal 101, 1001–1015.

Simpson KJ, Bennett C, Atkinson RRL, Mockford EJ, McKenzie S, Freckleton RP, Thompson K, Rees M, Osborne CP. 2020 C_4 photosynthesis and the economic spectra of leaf and root traits independently influence growth rates in grasses. Journal of Ecology 108, 1899–1909.

Sims DA, Gamon JA. 2002. Relationships between leaf pigment content and spectral reflectance across a wide range of species, leaf structures and developmental stages. Remote Sensing of Environment 81, 337-354.

Sinclair TR, Muchow RC. 1999. Radiation use efficiency. Advances in Agronomy 65, 215–265.

Sinclair TR, Rufty TW, Lewis RS. 2019. Increasing photosynthesis: unlikely solution for world food problem. Trends in Plant Science 24, 1032-1039.

Sinclair TR, Rufty TW. 2012. Nitrogen and water resources commonly limit crop yield increases, not necessarily plant genetics. Global Food Security 1, 94–98.

Sinclair TR, Vadez V. 2002. Physiological traits for crop yield improvement in low N and P environments. Plant and Soil 245, 1-15.

Slafer GA. 2003. Genetic basis of yield as viewed from a crop physiologist's perspective. Annals of Applied Biology 142, 117–128.

Slattery RA, Ainsworth EA, Ort DR. 2013. A meta-analysis of responses of canopy photosynthetic conversion efficiency to environmental factors reveals major causes of yield gap. Journal of Experimental Botany 64, 3723–3733.

Smith RCG, Adams J, Stephens DJ, Hick PT. 1995. Forecasting wheat yield in a Mediterranean-type environment from the NOAA satellite. Australian Journal of Agricultural Research 46, 113–125.

Song Q, Chen D, Long SP, Zhu XG. 2017. A user-friendly means to scale from the biochemistry of photosynthesis to whole crop canopies and production in time and space – development of Java WIMOVAC. Plant, Cell and Environment 40, 51–55.

Song Q, Wang Y, Qu M, Ort DR, Zhu X. 2017. The impact of modifying photosystem antenna size on canopy photosynthetic efficiency. Plant, Cell and Environment, 2946–2957.

Song Q, Xiao H, Xiao X, Zhu XG. 2016. A new canopy photosynthesis and transpiration measurement system (CAPTS) for canopy gas exchange research. Agricultural and Forest Meteorology 217, 101–107.

South PF, Cavanagh AP, Liu HW, Ort DR. 2019. Synthetic glycolate metabolism pathways stimulate crop growth and productivity in the field. Science 363, 1–9.

Steddom K, Heidel G, Jones D, Rush CM. 2003. Remote detection of rhizomania in sugar beets. The American Phytopathological Society 93, 720–726.

Sun Y, Wang X, Wang N, Chen Y, Zhang S. 2014. Changes in the yield and associated photosynthetic traits of dry-land winter wheat (*Triticum aestivum* L.)

from the 1940s to the 2010s in Shaanxi Province of China. Field Crops Research 167, 1–10.

Tardieu F, Cabrera-Bosquet L, Pridmore T, Bennett M. 2017. Plant phenomics, from sensors to knowledge. Current Biology 27, R770–R783.

Tattaris M, Reynolds MP, Chapman SC. 2016. A direct comparison of remote sensing approaches for high-throughput phenotyping in plant breeding. Frontiers in Plant Science 7, 1131.

Taylor SH, Long SP. 2017. Slow induction of photosynthesis on shade to sun transitions in wheat may cost at least 21% of productivity. Philosophical Transactions of the Royal Society B 372, 20160543.

Tester M, Landridge P. 2010. Breeding technologies to increase crop production in a changing world. Science 327, 818–822.

Tewes A, Schellberg J. 2018. Towards remote estimation of radiation use efficiency in maize using UAV-based low-cost camera imagery. Agronomy 8, 1–15.

Thomas H, Ougham H. 2014. The stay-green trait. Journal of Experimental Botany 65, 3889–3900.

Tilman D, Balzer C, Hill J, Befort B. 2011. Global food demand and the sustainable intensification of agriculture. Proceedings of the National Academy of Sciences 108, 20260–20264.

Tindall AJ, Waller J, Greenwood M, Gould PD, Hartwell J, Hall A. 2015. A comparison of high-throughput techniques for assaying circadian rhythms in plants. Plant Methods 11, 1–7.

Townsend AJ, Retkute R, Chinnathambi K, Randall JWP, Foulkes J, Carmo-Silva E, Murchie EH. 2018. Suboptimal acclimation of photosynthesis to light in wheat Canopies. Plant Physiology 176, 1233–1246.

Tracy SR, Black CR, Roberts JA, Mooney SJ. 2011. Soil compaction: a review of past and present techniques for investigating effects on root growth. Journal of the Science of Food and Agriculture 91, 1528-1537.

Tracy SR, Roberts JA, Black CR, McNeill A, Davidson R, Mooney SJ. 2010. The X-factor: visualizing undisturbed root architecture in soils using X-ray computed tomography. Journal of Experimental Botany 61, 311-313.

Trenberth KE, Dai A, Schrier G Van Der, Jones PD, Barichivich J, Briffa KR, Sheffield J. 2014. Global warming and changes in drought. Nature Climate Change 4, 17–22.

Tucker CJ. 1979. Red and photographic infrared linear combinations for monitoring vegetation. Remote Sensing of Environment 8, 127-150.

Turner W, Spector S, Gardiner N, Fladeland M, Sterling E, Steininger M. 2003. Remote sensing for biodiversity science and conservation. Trends in Ecology and Evolution 18, 306–314.

Ustin SL, Gamon JA. 2010. Remote sensing of plant functional types. New Phytologist 186, 795–816.

Valluru R, Reynolds MP, Lafarge T. 2015. Food security through translational biology between wheat and rice. Food and Energy Security 4, 203–218.

Vialet-Chabrand SRM, Matthews JSA, McAusland L, Blatt MR, Griffiths H, Lawson T. 2017. Temporal dynamics of stomatal behaviour: modelling and implications for photosynthesis and water use. Plant Physiology 174, 603-613.

Vose JM, Ryan MG. 2002. Seasonal respiration of foliage, fine roots, and woody tissues in relation to growth, tissue N, and photosynthesis. Global Change Biology 8, 182–193.

Wada M, Carvalho LJCB, Rodrigues GC, Ishii R. 1994. Cultivar differences in leaf photosynthesis and grain yield of wheat under soil water deficit conditions. Japanese Journal of Crop Science 63, 339–344.

Wang E, Brown HE, Rebetzke GJ, Zhao Z, Zheng B, Chapman SC. 2019. Improving process-based crop models to better capture genotype $\times$ environment $\times$ management interactions. Journal of Experimental Botany 70, 2389–2401.

Wasson AP, Rebetzke GJ, Kirkegaard JA, Christopher J, Richards RA, Watt M. 2014. Soil coring at multiple field environments can directly quantify variation

in deep root traits to select wheat genotypes for breeding. Journal of Experimental Botany 65, 6231–6249.

Way DA, Pearcy RW. 2012. Sun flecks in trees and forests: from photosynthetic physiology to global change biology. Tree Physiology 32, 1066-1081.

Weigelt A, Mommer L, Andraczek K, Iversen CM, Bergmann J, Bruelheide H, Fan Y, Freschet T, Guerrero-Ramírez NR, Kattge J, Kuyper TW, Laughlin DC, Meier IC, Plas F Van Der, Poorter H, Roumet C, Ruijven J Van, Valverde-Barrantes OJ, York L, Mccormack ML. 2021. An integrated framework of plant form and function: the belowground perspective. New Phytologist 232, 42–59.

Wen Z, White PJ, Shen J, Lambers H. 2021. Linking root exudation to belowground economic traits for resource acquisition. New Phytologist 223, 1620-1635.

Whaley JM, Sparkes DL, Foulkes MJ, Spink JH, Semere T, Scott RK. 2000. The physiological response of winter wheat to reductions in plant density. Annals of Applied Biology 137, 165–177.

White JW, Andrade-Sanchez P, Gore MA, Bronson KF, Coffelt TA, Conley MM, Feldmann KA, French AN, Heun JT, Hunsaker DJ, Jenks MA, Kimball BA, Roth RL, Strand RJ, Thorp KR, Wall GW, Wang G. 2012. Field-based phenomics for plant genetics research. Field Crops Research 133, 101–112.

Whitfield DM, Smith CJ. 1989 Effects of irrigation and nitrogen on growth, light interception and efficiency of light conversion in wheat. Field Crops Research 20, 279–295.

Wu A, Doherty A, Farquhar GD, Hammer GL. 2018. Simulating daily field crop canopy photosynthesis: An integrated software package. Functional Plant Biology 45, 362–377.

Wu A, Hammer GL, Doherty A, von Caemmerer S, Farquhar GD. 2019. Quantifying impacts of enhancing photosynthesis on crop yield. Nature Plants 5, 380–388.

Wu C, Niu Z, Tang Q, Huang W. 2008. Estimating chlorophyll content from hyperspectral vegetation indices: Modelling and validation. Agricultural and Forest Meteorology 148, 1230–1241.

Wu C, Niu Z, Tang Q, Huang W. 2010. Revised photochemical reflectance index (PRI) for predicting light use efficiency of wheat in a growth cycle: Validation and comparison. International Journal of Remote Sensing 31, 2911–2924.

Xin CP, Tholen D, Devloo V, Zhu XG. 2015. The benefits of photorespiratory bypasses: how can they work? Plant Physiology 167, 574-585.

Xu Y. 2016. Envirotyping for deciphering environmental impacts on crop plants. Theoretical and Applied Genetics 129, 653–673.

Yendrek CR, Tomaz T, Montes CM, Cao Y, Morse AM, Brown PJ, McIntyre LM, Leakey ADB, Ainsworth EA. 2017. High-throughput phenotyping of maize leaf physiological and biochemical traits using hyperspectral reflectance. Plant Physiology 173, 614–626.

Yin X, Struik PC. 2009. C_3 and C_4 photosynthesis models: An overview from the perspective of crop modelling. NJAS - Wageningen Journal of Life Sciences 57, 27–38.

Zadoks JC, Chang TT, Konzak CF. 1974. A decimal code for the growth stages of cereals. Weed Research 14, 415–421.

Zarco-Tejada PJ, Berjon A, Lopez-Lozano R, Miller JR, Martin P, Cachorro V, Gonzalez MR, de Frutos A. 2005. Assessing vineyard condition with hyperspectral indices: Leaf and canopy reflectance simulation in a row-structured discontinuous canopy. Remote Sensing of Environment 99, 271–287.

Zarco-Tejada PJ, Miller JR, Mohammed GH, Noland TL, Sampson PH. 2000. Chlorophyll fluorescence effects on vegetation apparent reflectance: II. Laboratory and airborne canopy-level measurements with hyperspectral data. Remote Sensing of Environment 47, 596–608.

Zarco-Tejada PJ, Miller JR, Noland TL, Mohammed GH, Sampson PH. 2001. Scaling-up and model inversion methods with narrowband optical indices for

chlorophyll content estimation in closed forest canopies with hyperspectral data. IEEE Transactions on Geoscience and Remote Sensing 39, 1491–1507.

Zhang Y, Guanter L, Berry JA, van der Tol C, Yang X, Tang J, Zhang F. 2016. Model-based analysis of the relationship between sun-induced chlorophyll fluorescence and gross primary production for remote sensing applications. Remote Sensing of Environment 187, 145–155.

Zhen S, van Iersel M, Bugbee, B. 2021. Why far-red photons should be included in the definition of photosynthetic photons and the measurement of horticultural fixture efficacy. Frontiers in Plant Science 12, 693445.

Zheng TC, Zhang XK, Yin GH, Wang LN, Han YL, Chen L, Huang F, Tang JW, Xia XC, He ZH. 2011. Genetic gains in grain yield, net photosynthesis and stomatal conductance achieved in Henan Province of China between 1981 and 2008. Field Crops Research 122, 225–233.

Zhou B, Serret MD, Elazab A, Bort Pie J, Araus JL, Aranjuelo I, Sanz-Sáez Á. 2016. Wheat ear carbon assimilation and nitrogen remobilization contribute significantly to grain yield. Journal of Integrative Plant Biology 58, 914–926.

Zhu XG, Long SP, Ort DR. 2008. What is the maximum efficiency with which photosynthesis can convert solar energy into biomass? Current Opinion in Biotechnology 19, 153-159.

Zhu XG, Long SP, Ort DR. 2010. Improving photosynthetic efficiency for greater yield. Annual Review of Plant Biology 61, 235–261.

Zhu XG, Ort DR, Whitmarsh J, Long SP. 2004. The slow reversibility of photosystem II thermal energy dissipation on transfer from high to low light may cause large losses in carbon gain by crop canopies: a theoretical analysis. Journal of Experimental Botany 55, 1167-1175.

Zhu XG, Song Q, Ort DR. 2012. Elements of a dynamic systems model of canopy photosynthesis. Current Opinion in Plant Biology 15, 237–244.